

TESIS DOCTORAL



2023

Análisis y selección de condiciones óptimas de extrusión multimaterial de aleaciones ligeras para aplicaciones aeronáuticas mediante simulación por elementos finitos y métodos de decisión multicriterio

DANIEL FERNÁNDEZ MARTÍN

GRADUADO EN INGENIERÍA AEROESPACIAL Y MÁSTER
UNIVERSITARIO EN INGENIERÍA AVANZADA DE FABRICACIÓN

Programa de Doctorado en Tecnologías Industriales

Directores:

Dra. D^a. Ana María Camacho López
Dr. D. Álvaro Rodríguez Prieto

Agradecimientos

Quiero dar las gracias a mi familia por su apoyo durante estos años, en especial a mi mujer Raquel, mis hijos Diego y Lucía que son los que me aguantan y dan sentido a mis días y a mis padres por su confianza y paciencia.

También quiero mostrar mi agradecimiento a mis directores de tesis D. Álvaro Rodríguez Prieto y Dª. Ana María Camacho López por su soporte durante su desarrollo, destacando la rapidez en la respuesta de las múltiples dudas que me surgieron durante el proceso y su apoyo durante la fase de publicaciones. Haciendo extensivo este agradecimiento al Grupo de Investigación en Producción Industrial e Ingeniería de Fabricación (*Industrial Production and Manufacturing Engineering – IPME*) de la UNED.

Este trabajo se ha desarrollado en el marco del Programa de Doctorado en Tecnologías Industriales de la UNED y ha sido financiado parcialmente por las Ayudas de la Escuela Técnica Superior de Ingenieros Industriales de la UNED en diferentes convocatorias anuales.

Índice

ÍNDICE.....	III
RESUMEN	V
ABSTRACT.....	VI
CAPÍTULO 1. INTRODUCCIÓN.....	1
1.1. NECESIDAD DE LA INVESTIGACIÓN	2
1.2. PROCESO DE COEXTRUSIÓN. APLICACIÓN A COMPONENTES MULTIMATERIAL	3
1.3. ALEACIONES LIGERAS PARA LA INDUSTRIA AERONÁUTICA	5
1.4. SIMULACIÓN DEL PROCESO POR EL MÉTODO DE ELEMENTOS FINITOS.....	5
1.4.1. <i>Daño</i>	6
1.4.2. <i>Desgaste</i>	7
1.4.3. <i>Evolución de la microestructura</i>	7
1.5. MÉTODOS DE DECISIÓN MULTICRITERIO	9
1.6. JUSTIFICACIÓN DE LA UNIDAD TEMÁTICA DE LA TESIS	10
CAPÍTULO 2. HIPÓTESIS Y OBJETIVOS.....	13
2.1. HIPÓTESIS.....	14
2.2. OBJETIVOS	15
CAPÍTULO 3. METODOLOGÍA	17
3.1. MÉTODO DE LOS ELEMENTOS FINITOS (MEF)	18
3.2. DISEÑO DE EXPERIMENTOS Y ANÁLISIS DE LA VARIANZA	22
3.3. MÉTODOS DE DECISIÓN MULTICRITERIO (MCDM).....	23
CAPÍTULO 4. PUBLICACIONES.....	25
4.1. EFFECT OF PROCESS PARAMETERS AND DEFINITION OF FAVOURABLE CONDITIONS IN MULTIMATERIAL EXTRUSION OF BIMETALLIC AZ31B-Ti6Al4V BILLETS	27
4.1.1. <i>Datos de la publicación y factor de impacto</i>	27
4.1.2. <i>Resumen y copia de la publicación</i>	27
4.1.3. <i>Resumen de las aportaciones</i>	28
4.2. ANALYSIS OF AZ31B -Ti6Al4V BIMETALLIC EXTRUSION BY NUMERICAL SIMULATION AND TAGUCHI METHOD	49
4.2.1. <i>Datos de la publicación y factor de impacto</i>	49
4.2.2. <i>Resumen y copia de la publicación</i>	49
4.2.3. <i>Resumen de las aportaciones</i>	50
4.3. SELECTION OF DIE MATERIAL AND ITS IMPACT ON THE MULTIMATERIAL EXTRUSION OF BIMETALLIC AZ31B-Ti6Al4V COMPONENTS FOR AERONAUTICAL APPLICATIONS	61
4.3.1. <i>Datos de la publicación y factor de impacto</i>	61
4.3.2. <i>Resumen y copia de la publicación</i>	61
4.3.3. <i>Resumen de las aportaciones</i>	63
4.4. OPTIMAL PARAMETERS SELECTION IN ADVANCED MULTIMETALLIC CO-EXTRUSION BASED ON INDEPENDENT MCDM ANALYTICAL APPROACHES AND NUMERICAL SIMULATION	95
4.4.1. <i>Datos de la publicación y factor de impacto</i>	95
4.4.2. <i>Resumen y copia de la publicación</i>	95
4.4.3. <i>Resumen de las aportaciones</i>	96
CAPÍTULO 5. CONCLUSIONES Y DESARROLLOS FUTUROS	135

5.1. CONCLUSIONES GENERALES	136
5.2. CONCLUSIONES PARTICULARES	137
5.3. DESARROLLOS FUTUROS	139
CAPÍTULO 6. OTRAS APORTACIONES CIENTÍFICAS DERIVADAS DE LA TESIS DOCTORAL	141
6.1. CONTRIBUCIONES EN CONGRESOS INTERNACIONALES.....	142
CAPÍTULO 7. REFERENCIAS.....	143
APÉNDICES.....	151
APÉNDICE A. INDICIOS DE CALIDAD DEL ARTÍCULO “EFFECT OF PROCESS PARAMETERS AND DEFINITION OF FAVORABLE CONDITIONS IN MULTIMATERIAL EXTRUSION OF BIMETALLIC AZ31B-Ti6Al4V BILLETS”	152
APÉNDICE B. INDICIOS DE CALIDAD DEL ARTÍCULO “ANALYSIS OF AZ31B-Ti6Al4V BIMETALLIC EXTRUSION BY NUMERICAL SIMULATION AND TAGUCHI METHOD”	155
APÉNDICE C. INDICIOS DE CALIDAD DEL ARTÍCULO “SELECTION OF DIE MATERIAL AND ITS IMPACT ON THE MULTIMATERIAL EXTRUSION OF BIMETALLIC AZ31B-Ti6Al4V COMPONENTS FOR AERONAUTICAL APPLICATIONS”	156
APÉNDICE D. INDICIOS DE CALIDAD DEL ARTÍCULO “OPTIMAL PARAMETERS SELECTION IN ADVANCED MULTIMETALLIC CO-EXTRUSION BASED ON INDEPENDENT MCDM ANALYTICAL APPROACHES AND NUMERICAL SIMULATION”	159
APÉNDICE E. EXTRACTO DEL LIBRO DE RESÚMENES DEL “9TH MANUFACTURING ENGINEERING SOCIETY INTERNATIONAL CONFERENCE (MESIC’09)”	162
APÉNDICE F. EXTRACTO DEL LIBRO DE RESÚMENES DEL “4TH INTERNATIONAL CONFERENCE ON MATERIALS DESIGN AND APPLICATIONS (MDA2022).”	165

Resumen

Con el auge de la Industria 4.0, las empresas están invirtiendo cada vez más en tecnologías de simulación para evitar la tradicional metodología de prueba y error empleada en el desarrollo de nuevos productos, con la intención de reducir costes, haciéndolas más competitivas y sostenibles en lo que a la producción se refiere. Por otra parte, el desarrollo de piezas multimaterial ha cobrado relevancia durante los últimos años debido a las posibilidades de adaptar las propiedades mecánicas de cada material a los requisitos específicos de servicio del componente. Así, al combinar diferentes materiales, es posible lograr una reducción de peso, mejorar la rigidez y la resistencia mecánica, entre otras propiedades. Esto es de especial relevancia en la industria aeroespacial, donde la reducción de peso en los componentes es un factor clave para aumentar la carga útil en aviones y satélites, generando un ahorro de combustible y reduciendo el impacto ambiental, sin comprometer, por ello, la respuesta de los materiales a las solicitudes mecánicas, térmicas y de fatiga, durante su vida útil. Debido a esto, las tecnologías industriales para procesos avanzados de conformado multimaterial se han identificado como un área crítica de investigación y desarrollo. En esta Tesis Doctoral se acomete el estudio de un proceso de coextrusión para obtener cilindros bimetálicos combinando dos aleaciones ligeras de especial interés en la industria aeronáutica como son la de titanio Ti₆Al₄V y la de magnesio AZ31B. Este es un proceso termo-mecánico muy complejo debido a la combinación de deformación plástica y difusión en la intercara entre ambos materiales debido a la presión y temperaturas generadas; así como, por el distinto comportamiento plástico de cada uno de sus componentes. Por este motivo, se han desarrollado modelos de elementos finitos que incorporan criterios para representar el daño inducido en las piezas extruidas (*Latham - Cockcroft*), el desgaste (*Archard*) de las matrices y la recristalización dinámica (*Johnson – Mehl – Avrami - Kolmogorov*) para evaluar la microestructura resultante y el tamaño de grano, el cual tendrá un efecto muy importante en el aumento de la resistencia y ductilidad de la pieza final. Así mismo, se ha demostrado que la simulación por elementos finitos combinada con técnicas estadísticas de Diseño de Experimentos (DoE, por sus siglas en inglés), análisis de la varianza (ANOVA) y la aplicación de métodos de decisión multicriterio (MCDM) puede ser utilizada como herramienta predictiva para seleccionar los parámetros óptimos del proceso en función de diferentes criterios, mejorando las características funcionales de la pieza final y/o minimizando las fuerzas requeridas y el desgaste de la pieza. Esta metodología puede ser extendida a otros procesos de

conformado por deformación plástica y contribuir de manera significativa a la reducción en tiempo y costes en la fabricación de nuevos componentes, así como a la sostenibilidad del proceso y su impacto en el medio ambiente debido a la reducción de piezas rechazadas durante la fase de puesta a punto.

Abstract

With the rise of Industry 4.0, companies are investing more and more in simulation technologies to avoid the traditional trial and error methodology used in the development of new products, with the intention of reducing costs that make them more competitive and sustainable in terms of production. On the other hand, the development of multimaterial parts has gained relevance in recent years due to the possibilities of adapting the mechanical properties of each material to the specific in-service requirements of the component. Thus, by combining different materials, it is possible to reduce weight, improve stiffness and mechanical resistance, among other properties. This is especially important in the aerospace industry, where weight reduction in components is a key factor to increase the payload in aircraft and satellites, saving fuel and reducing environmental impact, without compromising the requirements due to mechanical, thermal and fatigue that these parts must endure during their on-service life. Because of this, industrial technologies for advanced multimaterial forming processes have been identified as a critical area of research and development. In this Doctoral Thesis, the study of a coextrusion process to obtain bimetallic cylinders is approached by combining two light alloys of special interest in the aerospace industry such as titanium Ti₆Al₄V and magnesium AZ31B. Since this is a very complex thermo-mechanical process because of the combination of plastic deformation and diffusion at the interface of both materials due to the pressure and temperatures generated, as well as the different plastic behaviour of each of its components. For these reasons, finite element models have been developed that incorporate various models and criteria to represent damage (Latham – Cockcroft), wear (Archard) and dynamic recrystallization model (Johnson – Mehl – Avrami – Kolmogorov) to evaluate the resulting microstructure and grain size, which will have a very important effect on increasing the resistance and ductility of the final part. It has been shown that finite element simulation combined with statistical techniques of Design of Experiments (DoE), analysis of variance (ANOVA), as well as its application through multicriteria decision making methods (MCDM) can be used as a predictive model to select the optimal parameters of the process based on

different criteria such as the functional characteristics of the final part, the minimization of the forces required or the wear of the part. This methodology can be extended to other forming processes and contribute significantly to the reduction in time and costs in the manufacture of new components, as well as to the sustainability of the process and its impact on the environment due to the reduction of parts rejected during the make-ready stage.

Capítulo 1. Introducción

1.1. Necesidad de la investigación

Las tecnologías de fabricación multmaterial para la producción de elementos estructurales han ganado relevancia durante los últimos años [1, 2] debido a un superior rendimiento en servicio y a un peso menor en comparación con su equivalente usando un único material. Trabajar con múltiples materiales permite a los diseñadores combinar las propiedades mecánicas de cada material con los requisitos de servicio específicos del componente. La reducción del peso de las piezas finales es una de las características más relevantes a la hora de utilizar estos materiales avanzados, factor clave en industrias como la aeroespacial para aumentar la carga útil en aviones y satélites, ahorrar combustible y reducir el impacto medioambiental.

Dentro de las tecnologías de fabricación multmaterial, las más extendidas en la industria aeronáutica utilizan materiales compuestos, tanto con matriz termoplástica como termoestable; sin embargo, el conformado de materiales compuestos entraña ciertas dificultades que limitan la aplicabilidad de este tipo de tecnologías. Además, en los últimos años se ha desarrollado la fabricación aditiva [3-5] para reducir los costes de herramientas y fabricar piezas con geometrías que no se pueden conseguir con métodos convencionales. Desafortunadamente, todavía existen limitaciones en el uso de las piezas obtenidas por estos métodos de fabricación, como son las temperaturas de trabajo en los materiales compuestos y su acabado superficial [6], así como sus limitadas propiedades mecánicas y la falta de certificaciones de aeronavegabilidad de la fabricación aditiva para utilizarse como parte de la estructura primaria en aeronaves. Por ello, se hace necesario el desarrollo de otras soluciones que permitan ampliar los campos de aplicación de los materiales para condiciones de servicio cada vez más exigentes.

En este sentido, el conformado multmaterial se presenta como una alternativa factible para el conformado de piezas para el sector aeronáutico. A modo de ejemplo, existen estudios recientes sobre el conformado multmaterial como el de Camacho *et al.* [7], que analizan el efecto de factores de forma y diferentes tolerancias de ajuste sobre el daño dúctil y la microestructura resultante en la acuñación de cilindros bimetálicos, compuestos de un anillo exterior de latón UNS C38500 y núcleo de aleación de aluminio UNS A92011. Otro ejemplo de conformado multmaterial es el presentado en el estudio de Zhang *et al.* [8], donde utilizaron la laminación en caliente para fabricar un compuesto de Al/Mg/Al con una estructura trilaminada. Alcaraz y Sevillano [9] utilizaron cálculos de elementos finitos (FE) para estudiar la

Capítulo 1. Introducción

influencia de algunas variables de extrusión, como la relación de límite elástico entre los dos materiales, la ubicación de las capas, la relación de espesor y el ángulo de matriz en los tubos bimetálicos compuestos por dos diferentes aleaciones. Chenot *et al.* [10] analizaron varios métodos de simulación para el problema de contacto de múltiples cuerpos, como el enfoque clásico de malla múltiple, la técnica de malla única y la formulación de Euler, revisando las formulaciones mecánicas y numéricas y evaluando el tiempo de CPU transcurrido para cada método. Respecto al uso de aleaciones de titanio en procesos de conformado multimaterial tenemos la comparativa realizada por Abdelkader *et al.* [11] entre una lámina bimetálica de titanio y acero de bajo contenido en carbono con una lámina de una sola capa de titanio en un proceso de conformado incremental (single point incremental forming SPIF).

Dentro de los procesos de conformado, la extrusión es uno de los procesos más prometedores de cara a la fabricación de componentes multimaterial. Con respecto a las aleaciones de magnesio en procesos de extrusión multimaterial, existen experiencias como la de Negendanka *et al.* [12], quienes estudiaron la influencia del semi-ángulo de la matriz de extrusión sobre la formación de la capa de difusión para la fabricación de cilindros bimetálicos compuestos de un núcleo de magnesio y un anillo de aluminio, llegando a la conclusión que a valores altos del semi-ángulo, mayor era la presión de contacto, mejorando así la calidad de la capa de difusión.

1.2. Proceso de coextrusión. Aplicación a componentes multimaterial

El proceso de coextrusión metálica es típicamente usado para obtener cilindros bimetálicos. Este es un proceso termo-mecánico complejo debido a la combinación de deformación plástica y difusión en la intercara de ambos materiales debido a la presión y temperaturas generadas. Además, para unir materiales diferentes, este proceso se vuelve más complicado debido a las diferentes características de los materiales a combinar tales como el coeficiente de dilatación térmica o el comportamiento plástico de cada uno de ellos. La mayoría de los estudios sobre procesos de conformado multimaterial se han realizado utilizando aleaciones de aluminio como, por ejemplo, el estudio realizado por Khosravifard *et al.* [13] donde se demostró que la unión en la intercara se puede asociar con la velocidad del flujo del material y la temperatura en el proceso de extrusión de varillas bimetálicas revestidas de Al/Cu. Otro estudio interesante que combina Al y Cu fue el de Lapovok *et al.* [14] sobre la mejora de la interdifusión en la

Capítulo 1. Introducción

fabricación de Cu/Al utilizando métodos de deformación plástica severa (SVD). Berski *et al.* [15] analizaron el estado de tensión-deformación en varillas bimetálicas compuestas de Cu-Al utilizando dos relaciones de extrusión diferentes en una matriz cónica y en una matriz de doble reducción. Kocich *et al.* [16] utilizaron el método de prensado angular de canal de torsión (TCAP) para analizar el comportamiento de deformación de un compuesto revestido de Al/Cu.

Thirumurugan *et al.* [17] realizaron un análisis del efecto de la relación de extrusión manteniendo constantes la temperatura y la velocidad del pistón en un proceso de coextrusión de aleaciones de magnesio ZM21/aluminio CP. Gall *et al.* [18] propusieron una combinación de simulación por el método de elementos finitos (FEM) junto con experimentos para estudiar el comportamiento de las palanquillas bimetálicas Al-Mg durante el proceso de coextrusión. Rong *et al.* [19] analizaron los efectos sobre la microestructura y las propiedades mecánicas de una aleación de Mg-Gd-Zn-Zr fabricada por extrusión térmica diferencial. Además, se han realizado algunos estudios utilizando el proceso de extrusión hidrostática para obtener varillas bimetálicas como el realizado por Osakada *et al.* [20] donde se llevó a cabo un estudio experimental utilizando varillas compuestas de Cu-Al, determinando que se producía una deformación uniforme para relaciones de extrusión bajas, mientras que la varilla de cobre fallaba por tensión a relaciones de extrusión altas. Además, la relación de extrusión crítica aumentaba a medida que disminuía el ángulo de la matriz. Otro estudio que utiliza extrusión hidrostática es el de Lehmann *et al.* [21] quienes analizaron la resistencia mecánica y las propiedades de fractura de compuestos de Al-Mg.

Sin embargo, no hay demasiados estudios que combinen aleaciones ligeras tan distintas como las aleaciones de titanio y magnesio en términos de densidad, resistencia a la tracción, límite elástico y módulo elástico y que, además, son de especial interés en la industria aeroespacial. Behrens *et al.* [22] estudiaron la coextrusión angular lateral (LACE, por sus siglas en inglés) para producir productos semi-acabados de aluminio y acero. Otro estudio empleando el proceso LACE es el realizado por Thürer *et al.* [23] para la fabricación de perfiles huecos reforzados coaxialmente en la aleación de aluminio EN AW-6082 y el acero de cementación AISI5120 20MnCr5, incluyendo los resultados del ensayo de cortante-compresión en los perfiles híbridos para medir la resistencia al cortante de la zona de unión.

1.3. Aleaciones ligeras para la industria aeronáutica

Los metales ligeros y sus aleaciones son materiales de densidad relativamente baja y relaciones de resistencia a peso elevadas siendo el magnesio, el aluminio y el titanio metales ligeros de gran importancia comercial, y sus aleaciones son usadas en la mayoría de aplicaciones industriales. Las aleaciones de magnesio tienen especial interés en la industria aeroespacial debido a su alta relación resistencia-peso [24, 25]. Sin embargo, estas aleaciones también presentan propiedades mecánicas deficientes y problemas de resistencia a la corrosión, lo que es una clara limitación para su desempeño en servicio, tal y como afirman Mordike *et al.* [23]. Además presenta una baja ductilidad, derivada de una estructura cristalina hexagonal compacta (HCP) que no tiene suficiente cantidad de sistemas de deslizamiento activos, lo que provoca que su conformabilidad sea deficiente [26, 27], reduciendo sus aplicaciones potenciales. Existen varias estrategias para mejorar la ductilidad de las aleaciones con base de magnesio, por ejemplo, mediante la introducción de elementos de aleación como las tierras raras que tienen una alta solubilidad en sólidos y un efecto de endurecimiento [28-30] pero, por otro lado, también pueden aumentar la densidad y el costo de las aleaciones de Mg resultantes.

Las aleaciones de titanio también se usan ampliamente en aplicaciones aeroespaciales debido a su alta relación resistencia-peso, gran tenacidad, resistencia a la fatiga a altas temperaturas y buena resistencia a ambientes corrosivos; sin embargo, debido a la alta tensión de fluencia a temperaturas elevadas, estas aleaciones son difíciles de fabricar [31-33], lo que supone un reto tecnológico.

1.4. Simulación del proceso por el método de elementos finitos

La simulación por el método de elementos finitos (MEF) es una parte fundamental de esta Tesis Doctoral ya que permite modelizar y predecir el comportamiento de los procesos de extrusión multimaterial abordados en esta Tesis Doctoral bajo condiciones que son difíciles de implementar de manera experimental, debido a las limitaciones propias de este tipo de instalaciones. Los modelos MEF desarrollados en esta Tesis se han ido modificando para incorporar fenómenos como la recristalización dinámica y mecanismos físicos como el daño o el desgaste, que entrañan cierta dificultad a la hora de ser incorporados a los modelos numéricos, pero que permiten obtener resultados fiables y difícilmente obtenibles mediante

técnicas experimentales en todas las condiciones de trabajo consideradas. Al usar este método se eliminan las restricciones que pudiera haber en cuanto a presupuesto, instalaciones y tiempo de realización, ya que no requiere de gasto en materiales o equipos ni estar sujeto a horarios de trabajo regulado, confiriendo una gran flexibilidad a la hora de planificar tanto el volumen de experimentos como de organización del trabajo.

En esta Tesis se ha abordado el análisis mediante MEF de los siguientes aspectos: daño, desgaste de herramientas y evolución microestructural, tal y como se describe a continuación.

1.4.1. Daño

El daño inducido en las piezas conformadas puede predecirse a través del factor de daño que recibe cada elemento de la malla y se suele usar para detectar zonas críticas y predecir la fractura durante las operaciones de conformado en frío. El factor de daño aumenta conforme el material se deforma y si alcanza un determinado valor crítico puede aparecer fractura. Existen diversos modelos de daño, tales como el Oyane, Ayada, Osakada, Freudenthal, Rice & Tracy entre otros [34]; pero debido a la sencillez y a los pocos datos que se requieren para su cálculo, se utilizará el criterio normalizado de Cockcroft y Latham [35] para evaluar el factor de daño en la pieza extruida. Este criterio se basa en la hipótesis de que la acumulación de daño ocurre sólo cuando al menos uno de los componentes principales de la tensión es de tracción, como se representa en la Ecuación (1).

$$\int_0^{\varepsilon_f} \left(\frac{\sigma_{max}}{\sigma_H} \right) d\varepsilon = C, \quad (1)$$

Donde ε es la deformación plástica equivalente, ε_f es la deformación límite de fractura, σ_{max} es la tensión principal máxima, σ_H es la tensión según la hipótesis de Huber-Mises, y C es el parámetro que suele denominarse constante del material, y su valor se determina experimentalmente.

El daño está asociado a estados tensionales, principalmente por la tensión hidrostática; De acuerdo con el criterio de tensión hidrostática (HSC), “siempre que la tensión hidrostática en un punto de la línea central en la zona de deformación se vuelve cero y es compresiva en otra parte, hay un inicio de fractura que puede conducir al denominado central burst” [36-38], defecto característico y a evitar en los procesos de extrusión.

En esta Tesis Doctoral se analizará el daño inducido en las piezas bimetálicas extruidas, definiendo aquellas condiciones de conformado favorables para la minimización del mismo y

así, permitir la obtención de piezas de mejor calidad que mejoren la vida en servicio de los componentes fabricados a partir de ellas.

1.4.2. Desgaste

El desgaste es la degradación que sufren las superficies de contacto debido a la presión, fricción y temperatura que se generan durante el proceso de conformado y cuya predicción y control son de vital importancia ya que afecta directamente a la vida útil de la matriz. El cálculo del desgaste en la matriz se realiza utilizando el modelo de desgaste de Archard [39-41]. En este modelo, la profundidad de desgaste es directamente proporcional al coeficiente de desgaste (K), la presión de intercara (P) y la velocidad de deslizamiento (v) entre la matriz y el tocho, y es inversamente proporcional a la dureza de la matriz (H), según la Ecuación (2).

$$W = \int K \cdot \frac{P^a \cdot v^b}{H^c} \cdot dt, \quad (2)$$

Donde a , b , c y K son coeficientes calibrados experimentalmente; a , b comúnmente se toman como 1, y $c = 2$ para aceros para herramientas. K se asume 2×10^{-5} es un método para aumentar la resistencia mecánica de un material metálico durante el proceso de conformado.

1.4.3. Evolución de la microestructura

El objetivo principal de este método es obtener una microestructura de material de grano fino que sea más dura y resistente que la de grano grueso [42]. La razón de que se produzca esta mejora es el aumento del área del límite de grano en el material de grano fino produciendo una barrera para el deslizamiento de las dislocaciones ya que éstas tienen que cambiar de dirección (lo que implica un esfuerzo adicional) y debido a la discontinuidad entre los planos de deslizamiento. Por otro lado, el conformado en caliente implica también cambios microestructurales que van a afectar a las propiedades mecánicas de las piezas obtenidas.

Existen varios modelos para modelar los cambios microestructurales durante el proceso termo-mecánico. Algunos de los más comunes son el modelo de dislocación-densidad de *Kocks – Mecking*, el modelo de parámetros de *Zener – Hollomon* y el modelo de recristalización de *Johnson – Mehl – Avrami – Kolmogorov* (JMAK). *Rotella et al.* [43] implementaron en una subrutina de DEFORM3D® las ecuaciones de *Zener – Hollomon* y *Hall-Petch* para predecir el tamaño de grano y la rugosidad superficial al variar la velocidad de corte y el radio de la herramienta en un torno para mecanizar una aleación de aluminio (AA 7075-T651). Un estudio sobre el refinamiento de grano durante el mecanizado de alta velocidad de una aleación de

Capítulo 1. Introducción

Ti₆Al₄V usando el modelo de recristalización JMAK junto con una modificación de las ecuaciones constitutivas de *Johnson – Cook* fue realizado por Xiang *et al.* [44] obteniendo unos resultados en las simulaciones muy semejantes a los obtenidos experimentalmente usando un microscopio de transmisión de electrones. Otro estudio que empleó las ecuaciones de Avrami en un proceso combinado de extrusión directa y extrusión angular de canal igual (ECAP, por sus siglas en inglés) para provocar deformación plástica severa y estudiar el refinamiento de grano en una aleación de magnesio AZ31, fue Ding-fei *et al.* [45]. En este estudio se utiliza el modelo JMAK para modelar la recristalización y estimar el tamaño de grano medio final, siendo la primera vez que se aplica a un proceso de coextrusión multimaterial.

El modelo JMAK se basa en evaluar el porcentaje de fracción de volumen que recristaliza cuando la deformación excede un valor crítico denominado ε_c . Normalmente este valor es una fracción (a_2) de la llamada deformación pico (ε_p) y que es función de la velocidad de deformación ($\dot{\varepsilon}$), temperatura (T), energía de activación (Q_1), constante de los gases (R) y tamaño inicial de grano (d_{g0}) como se muestra en las ecuaciones (3) y (4):

$$\varepsilon_c = a_2 \cdot \varepsilon_c \quad (3)$$

$$\varepsilon_p = a_1 \cdot d_{g0}^{n_1} \cdot \dot{\varepsilon}^{m_1} \cdot \exp\left(\frac{Q_1}{R \cdot T}\right) + C_1 \quad (4)$$

Siendo a_1 , n_1 , m_1 y C_1 coeficientes de Avrami que dependen del material y se obtienen experimentalmente.

Muchas investigaciones han implementado los citados modelos aplicados a un proceso de extrusión; por ejemplo, Yuan *et al.* [46] investigaron la microestructura y las propiedades mecánicas del material Mg-2.6Sm-1.3Gd-0.6Zn-0.5Zr (% en peso) después de un proceso de extrusión en caliente a 400°C con una relación de extrusión de 25:1 y concluyó que la recristalización dinámica tuvo lugar completamente durante el proceso de extrusión y uno de los mecanismos de aumento de la resistencia dominantes fue la estructura de grano fino resultante. Con respecto a la influencia de la velocidad de extrusión en la microestructura y las propiedades mecánicas de la aleación AXM1104, Liu *et al.* [47] estudiaron el efecto en la tensión de fluencia a tracción inicial (YS) y el alargamiento a fractura (EL) cuando la velocidad de extrusión se incrementa de 1 a 7 mm/s. Duan *et al.* [48] realizaron un análisis del impacto de la configuración de la matriz, la temperatura del contenedor y la temperatura de la matriz en la recristalización durante el proceso de extrusión en caliente de aleaciones de aluminio, determinando que la configuración de la matriz tiene una influencia muy fuerte en el

Capítulo 1. Introducción

comportamiento de la recristalización estática (SRX), mientras que la temperatura del contenedor ayuda a controlar la recristalización ya que cuanto mayor es la temperatura de este, menor es la fracción de volumen de recristalización.

Por tanto, otro aspecto de interés que será abordado a lo largo de esta Tesis Doctoral será la determinación de aquellas condiciones de operación en procesos de extrusión bimetálica AZ31B-TI6AL4V que den lugar a microestructuras favorables.

1.5. Métodos de decisión multicriterio

Una selección adecuada de los parámetros de procesado se convierte en una tarea importante para maximizar la productividad y el rendimiento de los procesos. Debido a la complejidad y al número de parámetros involucrados, la optimización multiobjetivo presenta el mejor enfoque para obtener una solución de compromiso para este tipo de problema. Sin embargo, la amplia gama de métodos de toma de decisiones multicriterio (MCDM, por sus siglas en inglés: *multicriteria decision-making methodologies*), cada uno con sus pros y sus contras, hace que su elección sea el primer escollo a superar, más aún cuando se pueden obtener diferentes resultados aplicados a un mismo problema, debido a la forma diferente de determinar los pesos, escalar los objetivos, etc.

El primer método MCDM fue aplicado por Pareto en 1896 [49] con su famoso principio 80/20. Otro ejemplo es el de Saaty en 1977 [50], quien utilizó modelos multicriterio para resolver problemas con objetivos en conflicto. Desde 1980, se han desarrollado y aplicado varios métodos MCDM para respaldar la decisión en diferentes áreas, como la gestión de la cadena de suministro y la selección de contratos [51], la selección del proceso de fabricación [52, 53], la selección de materiales [54, 55], etc.

A partir de la revisión de la literatura es posible encontrar varios ejemplos de aplicación e incluso comparaciones entre MCDM en la optimización de los parámetros del proceso de fabricación [56-58], pero faltan estudios que vayan paso a paso y comparen los diferentes métodos de ponderación [59, 60] con los métodos MCDM y su efecto en los resultados obtenidos. La mayoría de estos estudios se centran en el método TOPSIS como el realizado por Freeman *et al.* [61] aplicado a la elección de un proveedor combinando los métodos de ponderación AHP (Analytic Hierarchy Process) y de entropía con TOPSIS. El estudio llevado a cabo por Vinodh *et al.* [62] para la selección del mejor método de reciclaje de plásticos o, por último, el estudio para la selección de proveedores de material de construcción realizado por

Capítulo 1. Introducción

Chen [63] en el que se emplean otra vez AHP – Entropía como métodos de ponderación junto con TOPSIS como método de decisión.

El empleo de estas herramientas de ayuda a la decisión en casos como el que se aborda en esta Tesis Doctoral es otro elemento novedoso a destacar, ya que no es frecuente encontrar estudios que realicen un análisis que integre los diferentes criterios de selección de condiciones favorables.

1.6. Justificación de la unidad temática de la Tesis

La unidad temática de esta tesis doctoral está centrada en el estudio de los procesos de coextrusión multimaterial y más concretamente en el desarrollo de una metodología que permita seleccionar los valores óptimos de los parámetros del proceso en función de las características que se requieran para la pieza final.

Para ello, se ha optado por la elaboración de una memoria de acuerdo a la modalidad de compendio de publicaciones. Cada uno de los artículos que componen esta memoria están estructurados de tal forma que el modelo numérico se va completando conforme se va avanzando en la investigación, añadiendo nuevas características que permiten acercar más el modelo a la realidad e incluir distintas características de salida de la pieza final.

La estructura seguida para el desarrollo de esta tesis doctoral es la siguiente:

- Desarrollo de un primer modelo “básico” que sólo tiene en cuenta los materiales del anillo y del núcleo y cuyas variables de salida son la fuerza de extrusión y el daño inducido en la pieza final. Este primer modelo es usado para identificar los parámetros más influyentes en las variables de salida definidas en el modelo y cómo afectan a su comportamiento. Todo esto queda recogido en el artículo “Effect of Process Parameters and Definition of Favorable Conditions in MultiMaterial Extrusion of Bimetallic AZ31B–Ti6Al4V Billets” [65].
- Partiendo del modelo básico, el artículo “Analysis of AZ31B - Ti6Al4V bimetallic extrusion by numerical simulation and Taguchi method” [66] cambia el modelo de fricción de Coulomb por el modelo de semi-adherencia de Tresca para ampliar el rango de valores de fricción del proceso. También incorpora la relación de extrusión como parámetro a estudiar en la generación del daño inducido en la pieza, siendo este daño, su distribución y su variación respecto a las variables del proceso el tema central de este artículo.

Capítulo 1. Introducción

- En el artículo “Selection of Die Material and Its Impact on the MultiMaterial Extrusion of Bimetallic AZ31B–Ti6Al4V Components for Aeronautical Applications” [67] explora la necesidad de tener un modelo más complejo en el cual se tenga en cuenta además el tipo de material usado para la matriz de extrusión y nuevamente cómo afecta esta elección a los parámetros de salida del proceso. Siendo otra novedad de este artículo la inclusión del desgaste de la matriz como variable de salida.
- Finalmente, el artículo “Optimal parameters selection in advanced multimetallic co-extrusion based on independent MCDM analytical approaches and numerical simulation” [68] se incorpora al modelo numérico el modelo de recristalización dinámica de Avrami para establecer una relación entre los parámetros del proceso y el tamaño final de grano de la pieza, que cuanto más fino sea mejores propiedades mecánicas presentará. La incorporación de metodologías MCDM responde a la necesidad de establecer la mejor solución de compromiso que incorpore los distintos parámetros de salida del proceso que se han ido incorporando en cada modelo numérico mencionado anteriormente.

Capítulo 1. Introducción

Capítulo 2. Hipótesis y objetivos

2.1. Hipótesis

Esta Tesis Doctoral se basa en la creciente necesidad que tiene la industria en general, y la aeroespacial en particular, de desarrollar componentes que no sólo sean capaces de trabajar en condiciones de alta exigencia sino que, además, sean lo más ligeros posibles. Todo ello dentro del marco de una producción sostenible y un mercado altamente competitivo y cambiante, donde la reducción de los costes, así como la optimización de los procesos productivos, son claves en el desarrollo de nuevos productos. Es por ello que este estudio se centra en el análisis y determinación de condiciones de conformado óptimas en la extrusión bimetálica AZ31B–Ti6Al4V, para obtener un componente multimaterial de la forma más sostenible y efectiva combinando diferentes técnicas como la simulación por elementos finitos, análisis estadístico y métodos de decisión multicriterio.

Las principales hipótesis de este trabajo son las siguientes:

- La extrusión bimetálica AZ31B-Ti6Al4V presenta diversas ventajas con respecto a la extrusión de un solo material, tales como una menor fuerza de extrusión necesaria para llevar a cabo el proceso.
- Se asume que todos los materiales son isotrópicos.
- El ajuste entre anillo y núcleo se realiza por interferencia.
- El daño inducido durante el proceso de coextrusión se reparte entre los dos componentes, de tal forma que el de peores propiedades en términos de resistencia mecánicas, recibe menos daño que el que recibiría en un proceso de extrusión convencional en el que fuera el único componente.
- El material de la matriz influye en el proceso de coextrusión, no sólo a nivel de desgaste de la misma, sino de la fuerza necesaria para llevarlo a cabo e incluso en el modo en el que los diferentes parámetros del proceso influyen en ella.
- El afinamiento de grano debido a procesos de recristalización dinámica durante el procesado influye sustancialmente en las propiedades mecánicas, mejorándolas.
- El empleo de técnicas de simulación por elementos finitos permite el análisis riguroso de los parámetros más relevantes en procesos de extrusión bimetálica AZ31B–Ti6Al4V y su influencia en diferentes variables de salida. La aplicación de la simulación por el método de los elementos finitos es un recurso indispensable para poder llevar a cabo, literalmente, cientos de simulaciones en las cuales se pueda estudiar la influencia de

Capítulo 2. Hipótesis y objetivos

los distintos parámetros del proceso en el resultado final sin coste alguno en material, mano de obra, instalaciones, energía, etc. contribuyendo a un desarrollo más sostenible de la producción.

- La optimización de los parámetros del proceso a través de una metodología híbrida que combina el Diseño de Experimentos (DoE) y métodos estadísticos como por ejemplo el análisis de la varianza (ANOVA) permite determinar qué parámetros son más relevantes en función de las variables de salida que se quieran medir.
- El empleo de metodologías híbridas que combinan métodos de ponderación (AHP....) con métodos de decisión multicriterio puede ayudar a obtener soluciones para una equilibrada selección de parámetros de proceso en función de las características requeridas para la pieza final.

2.2. Objetivos

El objetivo fundamental de esta Tesis Doctoral consiste en el desarrollo de una metodología que permita analizar las condiciones de conformado óptimas en procesos de extrusión multimaterial, combinando la simulación por elementos finitos (teniendo en cuenta diversos criterios de daño, desgaste, evolución microestructural, etc.) con métodos que permitan la selección de parámetros de proceso idóneos y faciliten la toma de decisión.

Los principales objetivos particulares de este trabajo y las publicaciones donde se han alcanzado dichos objetivos son:

- Crear un modelo robusto de coextrusión multimaterial por el método de elementos finitos usando el software comercial DEFORM3D© [64].
- Determinar el modo en que cada uno de los parámetros del proceso afecta a la fuerza de extrusión requerida y al daño que sufre la pieza [65].
- Determinar qué parámetros tienen una mayor influencia en la fuerza de extrusión y el daño sufrido por la pieza mediante el método de análisis de la varianza (ANOVA) [65, 66].
- Evaluar en qué forma influye el material de la matriz en la fuerza de extrusión necesaria para llevar a cabo el proceso, el daño de la pieza resultante y el desgaste sufrido por la matriz [67].

Capítulo 2. Hipótesis y objetivos

- Determinar si el material de la matriz influye en el comportamiento que los parámetros del proceso tienen sobre la fuerza de extrusión y el daño de la pieza obtenidos [67].
- Determinar qué parámetros del proceso tienen mayor influencia en el desgaste de la matriz [67].
- Implementar el modelo de recristalización dinámica al modelo de simulación por elementos finitos [68].
- Evaluar la influencia de los parámetros del proceso de coextrusión en la microestructura resultante, prestando mayor atención en el refinamiento de grano dado su impacto en la mejora de las propiedades mecánicas de la pieza final [68].
- Desarrollar de una metodología de selección de métodos de decisión multicriterio (MCDM) comparando distintos métodos de ponderación [68].
- Aplicar la metodología para la obtención de la combinación óptima de los parámetros del proceso de coextrusión multimaterial que respondan a una solución de compromiso entre la menor fuerza de extrusión requerida, el menor daño sufrido por la pieza, mínimo desgaste de la matriz y el menor tamaño de grano posible [68].

Capítulo 3. Metodología

Capítulo 3. Metodología

En ese capítulo se describen las bases metodológicas que se han usado para el desarrollo de esta Tesis Doctoral. No obstante, el detalle de cada una de las metodologías empleadas, así como el marco teórico en que se fundamentan, se verán descritas en el próximo capítulo.

3.1. Método de los elementos finitos (MEF)

Para el desarrollo de esta Tesis Doctoral se ha optado por la utilización del programa comercial de análisis por elementos finitos DEFORM3D© [64].

En el preprocesador se han modelizado el pistón, el contenedor y los sistemas de sujeción de la matriz como elementos rígidos (no deformables). El anillo y el núcleo se modelizan como elementos plásticos y la matriz como elemento elástico.

Para la reducir el tiempo de computación y el tamaño de los archivos de datos, se aprovecha la característica de simetría axial y sólo se modeliza un cuarto del modelo, haciendo a posteriori el ajuste numérico del mismo.

Las condiciones de contacto entre los distintos objetos se han definido de la siguiente manera:

- Los objetos rígidos y elásticos se consideran “*master*”, es decir, los que producen deformación.
- Los objetos plásticos que son los que van a sufrir esa deformación se definen como “*slave*”.

En este punto, cabe realizar una aclaración. El contacto entre objetos plásticos, anillo y núcleo, tiene que ser también definido, no pudiendo ser ambos “*slave*”. Debido a la suposición de que el ajuste entre el anillo y el núcleo se hace por interferencia el coeficiente de fricción entre ambos materiales toma el valor máximo de 1 y se define, como complemento, las condiciones de “*sticking*” y “*non-separable*” para evitar que las superficies se separen durante la simulación.

El modelo de fricción elegido por Fernández *et al.* [65] en el primer estudio sobre la influencia de los parámetros de extrusión fue el de Coulomb, ya que el coeficiente de fricción máximo usado fue de 0,170 y, de acuerdo con Rowe [69] y Leu *et al.* [70], el límite superior del coeficiente de fricción de Coulomb es de 0,577 para el criterio de Von Mises y 0,500 para el de Tresca. En posteriores estudios, Fernández *et al.* [65-68], el modelo de fricción usado fue el modelo de fricción de Tresca, ya que los coeficientes empleados en las simulaciones superan el límite indicado anteriormente.

La relación de los parámetros principales de simulación está recogida en la tabla 1.

Tabla 1. Parámetros principales del modelo de elementos finitos.

Parámetro	Valor
Número de elementos	7000
Tipo de densidad de la malla	Relativa
Volumen objetivo	Activo en el MEF + mallado
Tipo de simulación	Lagrangiana incremental
Control de incremento de paso (mm/paso)	Constante = 0,06
Profundidad de interferencia	Relativa = 0,7
Coeficiente de transferencia de calor entre anillo y matriz ($\text{N}\cdot\text{°C}^{-1}\cdot\text{s}^{-1}\cdot\text{mm}^{-1}$)	11
Coeficiente de transferencia de calor entre anillo y núcleo ($\text{N}\cdot\text{°C}^{-1}\cdot\text{s}^{-1}\cdot\text{mm}^{-1}$)	11
Coeficiente de transferencia de calor entre cilindro y aire ($\text{N}\cdot\text{°C}^{-1}\cdot\text{s}^{-1}\cdot\text{mm}^{-1}$)	0,02
Coeficiente de transferencia de calor entre cilindro y utilaje ($\text{N}\cdot\text{°C}^{-1}\cdot\text{s}^{-1}\cdot\text{mm}^{-1}$)	5

La aleación Ti₆Al₄V se define mediante las ecuaciones constitutivas de *Johnson – Cook* (4) [71]:

$$\sigma = A \cdot \left(1 + \frac{B}{A} \cdot \varepsilon^n\right) \cdot (1 + C \cdot \ln \dot{\varepsilon}') \cdot (1 - \vartheta'^m) \quad (4)$$

Donde A es el límite elástico del material a temperatura ambiente (T_0), ε es la deformación plástica equivalente, $\dot{\varepsilon}'$ es la velocidad de deformación expresada adimensionalmente mediante una velocidad de deformación de referencia ($\dot{\varepsilon}_0$) según se muestra en la ecuación (5), ϑ' es función de la temperatura ambiente (T_0), temperatura de fusión (T_m) y temperatura de trabajo (T) como se indica en la ecuación (6) y B , C , m y n son parámetros propios del material que tienen un valor fijo.

$$\dot{\varepsilon}' = \frac{\dot{\varepsilon}}{\dot{\varepsilon}_0} \quad (5)$$

$$\vartheta' = \frac{T-T_0}{T_m-T_0} \quad (6)$$

Mientras que la aleación AZ31B se ha modelizado utilizando el modelo exponencial definido por Wen-juan [72] donde existe una relación cuadrática entre la tensión y la deformación verdadera como se indica en la ecuación (7):

$$\sigma = e^{a+b\varepsilon+c\varepsilon^2} \quad (7)$$

Capítulo 3. Metodología

Donde los parámetros a , b y c dependen de la temperatura y de la velocidad de deformación de acuerdo a las ecuaciones (8), (9) y (10):

$$a = X_1 + X_2 \cdot T \quad (8)$$

$$b = X_3 + X_4 \cdot T \quad (9)$$

$$c = X_5 + X_6 \cdot T \quad (10)$$

Donde, a su vez, X_i dependen de la velocidad de deformación, como se muestra en la ecuación (11):

$$X_i = A_i + B_i \cdot \lg \varepsilon \quad (11)$$

Los parámetros A_i y B_i de la ecuación (11) son el resultado de aplicar métodos de regresión lineal obtenidos experimentalmente bajo distintas velocidades de deformación, como se indica en la tabla 2.

Tabla 2. Valores de los parámetros A_i y B_i del modelo de Wen-juan [73].

i	A _i	B _i
1	6,22943	0,03892
2	-0,00292	-0,00004
3	8,57906	-0,47297
4	-0,00801	0,00199
5	-13,9373	0,3525
6	0,01274	-0,00245

Las figuras 1 y 2 muestran las curvas de fluencia para ambos materiales.

Capítulo 3. Metodología

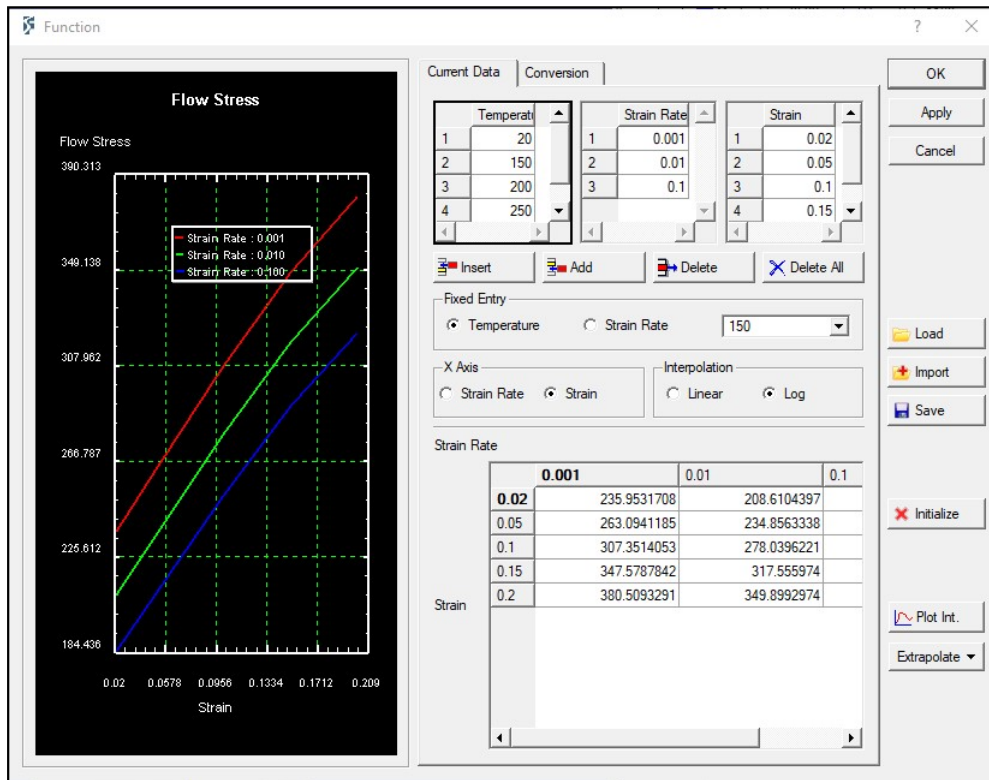


Figura 1. Curvas de fluencia de la aleación AZ31B.

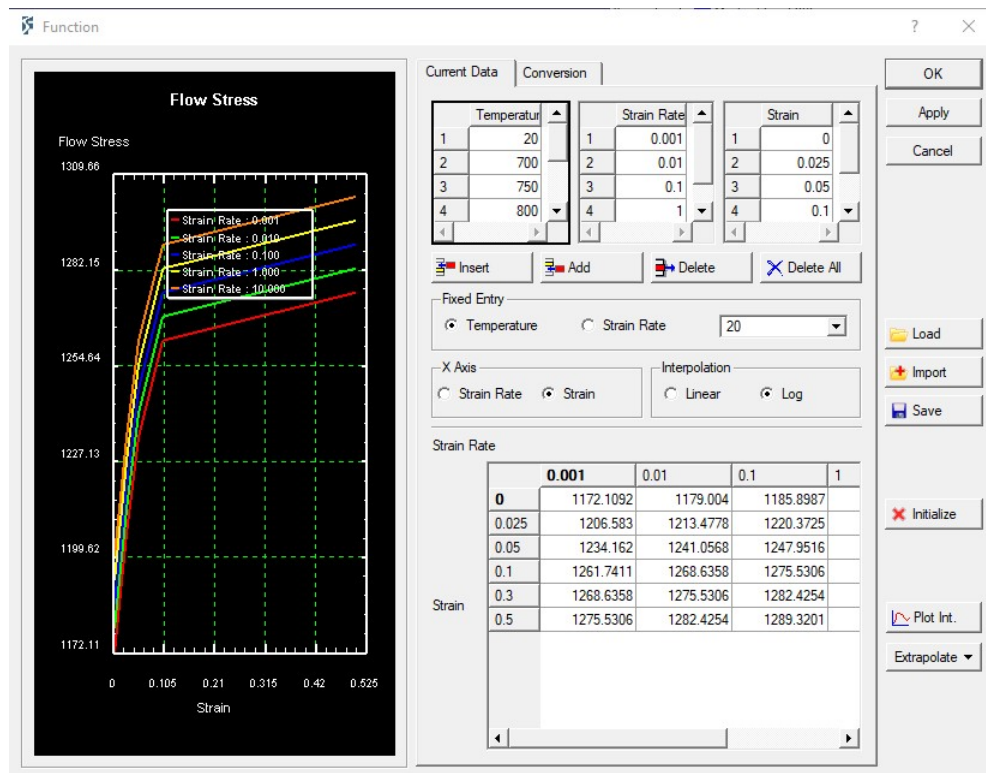


Figura 2. Curvas de fluencia de la aleación Ti₆Al₄V

Capítulo 3. Metodología

Para finalizar, una vez definido el modelo, es necesario validararlo. Para ello, en este trabajo se ha optado por el método semi-empírico de Johnson [73]. Este método es usado normalmente como límite superior para el valor de la fuerza de extrusión en procesos de extrusión directa. Teniendo en cuenta que se trata de un proceso multmaterial, se ha calculado la tensión media de fluencia teniendo en cuenta la fracción de volumen de cada uno de los materiales como se detalla en el estudio realizado por Gisbert *et al.* [74].

3.2. Diseño de experimentos y análisis de la varianza

El DoE es un método estadístico en el cual se busca obtener relaciones causa-efecto por medio de la variación sistemática de los distintos factores que lo componen para medir el efecto que tienen sobre una variable de interés. El DoE establece las pautas relativas al número de factores a tener en cuenta, los niveles dentro de cada factor, cómo se relacionan los factores entre sí, etc. Una de las aplicaciones más comunes de este método es la optimización de procesos productivos, en los que se busca encontrar el valor óptimo de una serie de variables de salida a través del efecto que ciertas variables de entrada tienen sobre ellas.

Un enfoque particular del DoE fue el dado por el estadístico e ingeniero japonés Genichi Taguchi (1924 – 2012) a través del uso de diseños o arreglos ortogonales [75]; esto significa que el diseño está equilibrado, de manera que los niveles de los factores se ponderan equitativamente. Además, están diseñados para que un arreglo específico puede ser utilizado para diferentes números de factores; por ejemplo, un arreglo L8 puede ser utilizado para (2^7) que significa siete factores con dos niveles cada uno, o para $(2^4), (4^1)$ que son cuatro factores con dos niveles más un factor con cuatro niveles.

Por último, tenemos el análisis de la varianza (ANOVA) desarrollado por R.A. Fisher en 1930 [76] que estudia el efecto de los factores del proceso sobre la media de una o más variables de salida, así como los efectos de estos factores sobre la varianza de las variables de salida. Este método ha sido usado durante el desarrollo de esta Tesis Doctoral para evaluar qué parámetros del proceso de coextrusión multmaterial tienen una mayor influencia en las variables de salida, como la fuerza de extrusión o el daño de la pieza final.

3.3. Métodos de decisión multicriterio (MCDM)

Los métodos MCDM se pueden clasificar en dos grupos principales según Hwang y Yoon (1981) [77]: toma de decisiones de atributos múltiples (MADM, por sus siglas en inglés: *multiattribute decision-making*) y toma de decisiones de objetivos múltiples (MODM, por sus siglas en inglés: *multiobjective decision-making*).

Los métodos MADM se utilizan para resolver problemas discretos, mientras que MODM se aplica en la resolución de problemas continuos. Este estudio se centra en MADM.

MADM también se puede agrupar según la información inicial (determinista, estocástica o incierta) o según los grupos de tomadores de decisiones (único o varios grupos), pero las clasificaciones más comunes son las propuestas por Hajkwociz – Collins (2007) [78] y De Brito – Evers (2016) [79]:

- Métodos de puntuación (COPRAS).
- Métodos basados en la distancia (VIKOR y TOPSIS).
- Métodos de comparación por pares (AHP).
- Métodos de utilidad/valor (ARAS)

Cada método tiene sus particularidades, pero todos comparten ciertos pasos. En todos ellos se empieza con una matriz de decisión, en la que se reflejan las alternativas en las columnas y los criterios en las filas. Esta matriz es necesario normalizarla puesto que los criterios pueden tener distinta naturaleza o estar medidos por unidades no comparables entre sí; la forma de calcular esta matriz normalizada puede variar dependiendo del MCDM que se esté empleando. Con la matriz de decisión normalizada se aplican los criterios de ponderación que dan más peso a unos criterios sobre otros, y es a partir de este paso donde cada método diverge de los demás.

La Evaluación de la Relación Aditiva (ARAS, por sus siglas in inglés: *Additive Ratio Assessment*) [80] es un método para seleccionar las mejores alternativas entre las dadas considerando medidas cuantitativas y la teoría de la utilidad que determina la eficiencia relativa por comparación entre las funciones de optimización para cada una de las alternativas.

TOPSIS [81, 82] es el acrónimo para técnica por orden de preferencia por similitud a la solución ideal y es un método MCDM propuesto inicialmente por Hwang y Yoon en 1981 [77]. El concepto detrás de este método es que la mejor opción sería la más cercana a la ideal, y a la vez, la más alejada de la solución anti-ideal, por lo que es necesario calcular la distancia

Capítulo 3. Metodología

euclídea a estas soluciones teniendo en cuenta si lo que se busca es maximizar o minimizar el valor del criterio seleccionado.

El método VIKOR [83, 84] es un MCDM desarrollado originalmente por Serafim Opricovic en 1980 y es un acrónimo del serbio *ViseKriterijumska Optimizacija I Kompromisno Resenje*, que significa Optimización multicriterio y solución de compromiso.

Esta metodología se basa en el mismo concepto que TOPSIS de asumir que una solución de compromiso es aceptable para la resolución de conflictos. Las mayores diferencias con respecto al método TOPSIS son, por una parte la adición de un paso de validación antes de declarar factible la solución de compromiso y, por otra, el cálculo de las solución ideal y anti-ideal, las cuales se basan en obtener las llamadas medidas de utilidad y de arrepentimiento junto a un parámetro v que representa el tipo de votación usada durante el proceso.

La evaluación proporcional compleja (por sus siglas en inglés, COPRAS) es un método MCDM desarrollado por Zavadskas en 1994 [85, 86] que asume dependencias directas y proporcionales de la importancia y el grado de utilidad de las alternativas disponibles bajo la presencia de criterios mutuamente conflictivos. Es un método compensatorio y al igual que ocurre con los métodos TOPSIS y VIKOR, considera también tanto la solución ideal como la ideal-peor para resolver el problema, aunque difiere con ellos en la forma de calcularlas.

Capítulo 4. Publicaciones

Capítulo 4. Publicaciones

Para la realización de esta tesis por compendio de publicaciones, se ha elegido la primera opción descrita en el documento regulador de Tesis por compendio de publicaciones aprobado por el Comité de Dirección de la EIDUNED, en su reunión de 16 de enero de 2017, y por la Comisión de Investigación y Doctorado de la UNED con fecha 21 de febrero de 2017, cumpliéndose así mismo los requisitos exigibles por el Programa de Doctorado en TECNOLOGÍAS INDUSTRIALES en el ANEXO aprobado por la Comisión Académica del programa en reunión celebrada el 8 de abril de 2021:

1.- *El compendio de publicaciones estará formado por un mínimo de tres artículos publicados en revistas científicas cuyo índice de impacto se encuentre incluido en la relación de revistas del Journal of Citation Reports (JCR). Al menos dos de ellos deben estar publicados y el tercero aceptado.*

2.- *Al menos dos de las publicaciones deben estar en el primer cuartil de la citada relación. Para verificar si la revista o editorial en la que se publique el trabajo cumple con los criterios indicados, se tomará en cuenta el año de publicación (o de aceptación del trabajo, si este no fuera publicado todavía) o el año anterior, y se tomará el criterio más favorable para el doctorando.*

3.- *Todos los artículos deben haber sido publicados o aceptados para su publicación, en el periodo de tiempo comprendido entre la fecha de su primera matrícula en la EIDUNED y la de la autorización de defensa pública de la tesis doctoral.*

4.- *El doctorando debe ser el primer firmante de todos los trabajos que presente. En caso contrario es necesario que se justifique debidamente su lugar de firma.*

5.- *Los trabajos realizados en coautoría no podrán ser presentados como parte de otra u otras tesis doctorales. En este sentido, ni podrán integrar más de una tesis en la modalidad de compendio de publicaciones, ni podrán ser utilizados como publicación asociada a otra tesis doctoral presentada en el formato tradicional.*

A continuación, se resume la información principal de cada una de las publicaciones, incluyendo los datos relativos a la publicación y su factor de impacto, así como una copia de cada publicación que constituye este compendio.

4.1. Effect of Process Parameters and Definition of Favourable Conditions in MultiMaterial Extrusion of Bimetallic AZ31B–Ti6Al4V Billets

Los indicios de calidad de este artículo se pueden encontrar en el Apéndice A de esta Tesis Doctoral.

4.1.1. Datos de la publicación y factor de impacto

Título	Effect of Process Parameters and Definition of Favourable Conditions in MultiMaterial Extrusion of Bimetallic AZ31B–Ti6Al4V Billets
Autores	Daniel Fernández; Álvaro Rodríguez-Prieto; Ana María Camacho
Revista	Applied Sciences
ISSN	2076-3417
Editorial	MDPI
País	Switzerland
Volumen	10 (22)
Páginas	8048
Fecha	13 de noviembre de 2020
doi	https://doi.org/10.3390/app10228048
Factor de impacto	2.679 (2020); 5-Year Impact Factor: 2.921 (2021) Q2 (38/91) en “Engineering multidisciplinary”

4.1.2. Resumen y copia de la publicación

En este artículo se estudia un proceso de coextrusión multimaterial con el objetivo de fabricar un cilindro bimetálico formado por un núcleo de aleación de magnesio (AZ31B) recubierto por un anillo externo de aleación de titanio (Ti₆Al₄V) con el objetivo de determinar los parámetros más influyentes y el efecto que tienen cada uno de ellos sobre la fuerza de extrusión y el daño inducido en la pieza durante el proceso. Para ello se ha desarrollado un modelo robusto usando el método de los elementos finitos junto con la metodología de Diseño de Experimentos (DoE) con arreglos ortogonales de Taguchi y el uso de la técnica de análisis de la varianza (ANOVA).

Capítulo 4. Publicaciones

Los resultados obtenidos en las simulaciones muestran que los parámetros que tienen más influencia en la fuerza de extrusión son la fricción del anillo externo de titanio con el contenedor y la altura del cilindro; mientras que los menos influyentes son la temperatura del proceso y la velocidad del troquel. También se concluyó que era posible alcanzar unos valores mínimos para la fuerza de extrusión manteniendo un equilibrio en el daño inducido en la pieza disminuyendo el rozamiento con el contenedor y controlando el diámetro del núcleo. Los resultados se pueden utilizar potencialmente para mejorar la eficiencia de este tipo de proceso de extrusión y la calidad de la pieza extruida que, junto con el uso de materiales ligeros, pueden contribuir a enfoques de producción sostenible.

In this article, a multimaterial co-extrusion process is studied in order to manufacture a bimetallic cylinder formed by a magnesium alloy core (AZ31B) covered by a sleeve made of titanium alloy (Ti6Al4V) in order to determine the most outstanding parameters and the effect that each one of them has on the extrusion force and the damage induced in the part during the process. In order to do this, a robust model has been developed using the finite element method together with the Design of Experiments (DoE) methodology with Taguchi orthogonal arrangements and the use of the analysis of variance (ANOVA) technique. The results obtained in the simulations show that the parameters which have the most influence on the extrusion force are the friction between the titanium external ring with the container and the height of the cylinder; while the least outstanding are the temperature of the process and the ram speed. It was also concluded that it was possible to achieve minimum values for the extrusion force, maintaining a balance in the damage induced in the piece, by reducing friction with the container and controlling the diameter of the core. The results can be used to improve the efficiency of this type of extrusion process and the quality of the extruded part which, together with the use of lightweight materials, can contribute to sustainable production approaches.

4.1.3. Resumen de las aportaciones

En esta publicación el doctorando estuvo a cargo de la definición y desarrollo de los modelos numéricos, la revisión del estado del arte, la metodología empleada y la escritura del artículo. La conceptualización, el análisis formal y la investigación fueron realizadas en conjunto por el doctorando y sus directores de tesis. Por último, las labores de revisión y edición del artículo, administración de recursos del proyecto, supervisión y adquisición de fondos fue llevada a cabo por los directores de tesis.

Article

Effect of Process Parameters and Definition of Favorable Conditions in Multi-Material Extrusion of Bimetallic AZ31B–Ti6Al4V Billets

Daniel Fernández ^{*}, Alvaro Rodríguez-Prieto  and Ana María Camacho 

Department of Manufacturing Engineering, Universidad Nacional de Educación a Distancia (UNED), 28040 Madrid, Spain; alvaro.rodriguez@ind.uned.es (A.R.-P.); amcamacho@ind.uned.es (A.M.C.)

* Correspondence: dfernande146@alumno.uned.es

Received: 18 October 2020; Accepted: 11 November 2020; Published: 13 November 2020



Abstract: This paper investigates the extrusion process to manufacture bimetallic cylinders combining a magnesium alloy core (AZ31B) and a titanium alloy sleeve (Ti6Al4V) of interest in aeronautical applications. A robust finite element model has been developed to determine the most influential parameters and to study the effect of them on the extrusion force and damage induced by means of Design of Experiments (DOE) and Taguchi method. The results show that the most influential parameters in the extrusion forces are the friction between sleeve and container/die and the height of the cylinder; and the less influential ones are the process temperature and ram speed. Moreover, minimum values of forces along with low damage can be reached by favorable interface contact conditions, minimizing the friction at the core-container/die interface, as the main influencing factor; followed by the geometrical dimensions of the billet, being the billet height more important when paying attention to the minimum forces, and being the core diameter when considering the minimum damage as the most important criterion. The results can potentially be used to improve the efficiency of this kind of extrusion process and the quality of the extruded part that, along with the use of lightweight materials, can contribute to sustainable production approaches.

Keywords: metal forming; extrusion; multi-material; bimetallic; AZ31B; Ti6Al4V; finite element method; DOE; force; damage

1. Introduction

Development of multi-material parts has gained relevance during recent years due to the possibilities of adapting the mechanical properties of each material to the specific in-service requirements of the component. Thus, by combining different materials, it is possible to achieve a weight reduction and improve stiffness and strength among other properties; formability can also be improved thanks to the combination of properties. Because of this, the industrial technologies for advanced joining and assembly processes of multi-material have been identified as a critical research and development area of the European Union (EU) Horizon 2020 work program 2018–2020 [1].

In the aerospace industry, the reduction of the weight in the components is a key factor to increase the payload in aircrafts and satellites, saving fuel and reducing the environmental impact. For these reasons, the use of composite materials, such as thermoplastic or thermosetting resins combined with carbon fiber is very well implemented. Currently, additive manufacturing is acquiring more and more importance to reduce tooling costs and manufacture parts with impossible shapes using conventional methods, among other advantages related to the sustainability [2] and design optimization [3]. Additive manufacturing techniques can also be an alternative to conventional processes when design specifications of obsolete parts are difficult to obtain due to a lack of information, such as component drawings or bill of materials, as explained by Rodríguez-Prieto et al. [4].

The problem with these kinds of multi-material components is the limitation in their in-service behavior, as composite materials cannot be used for high temperature requirements. Although additive manufacturing techniques are experiencing very quick improvements, still have poorer surface finishing and lower mechanical properties than parts made by conventional methods due to the layer by layer structure [5], the dimensions of the components to be manufactured are also limited. Furthermore, in the manufacturing of multi-material components by additive manufacturing, other factors, such as materials compatibility, formation of brittle inter-metallic metallurgical structures, residual stresses, and microstructure thermal effects become decisive.

The co-extrusion process is typically used to obtain multi-material cylinders to be used as billets to manufacture components with complex shapes. This is a complex thermo-mechanical process due to the combination of plastic deformation and diffusion in the interface of both materials because of the pressure and temperatures generated. There are several studies about the combination of Mg and Al alloys, such as the one by Negendanka et al. [6], where the influence of the die angle and different combining techniques of Mg–core and Al–sleeve on the diffusion layer formation are investigated. Another example is the work by Thirumurugan et al. [7], where a ZM21 magnesium alloy/CP aluminum was fabricated through direct hot co-extrusion with three different extrusion ratios and constant temperature and ram speed. Gall et al. [8] also studied the co-extrusion of bimetallic Al–Mg billets into hollow profiles by means of experiments and Finite Element Method (FEM) simulation. Lehmann et al. [9] analyzed the mechanical strength and fracture properties of hydrostatic coextruded Al–Mg compounds. Other studies regarding multi-material co-extrusion have been performed using Cu–Al, for example, Lapovok et al. [10] studied the inter-diffusion improvement in the manufacturing of Cu–Al bimetallic tubes using severe plastic deformation methods. Berski et al. [11] analyzed the strain–stress state in bimetallic rods composed by Cu–Al using two different extrusion ratios in conical die and in double reduction die. A study about the deformation behavior of an Al/Cu clad composite by the method of twist channel angular pressing (TCAP) was conducted by Kocich et al. [12]; whereas Rong et al. [13] studied the effects on microstructure and mechanical properties of a Mg–Gd–Zn–Zr alloy manufactured by differential-thermal extrusion. Alcaraz and Sevillano [14] used Finite Element (FE) calculations to study the influence of the different extrusion variables in the bimetallic tubes composed by two different Al alloys. The work of Camacho et al. [15] is another example of a multi-material forming process used in other kind of applications, such as minting. However, only a few studies have explored the behavior of such different metallic alloys in terms of density, tensile strength, yield strength, and elastic modules, such as by Behrens et al. [16], who performed a lateral angular co-extrusion (LACE) to product semi-finished products consisting of aluminum and steel. More information about the LACE process for the production of coaxially reinforced hollow profiles can be found in Thürer et al. [17].

In this study, the direct extrusion of a bimetallic cylinder with a magnesium alloy AZ31B core and a titanium alloy Ti6Al4V sleeve has been analyzed by means of finite element simulation and the design of experiments (DOE) technique; special attention has been paid to the forces required and damage induced in order to determine the most relevant parameters to choose the most efficient operating conditions.

2. Materials and Methods

2.1. Materials, Geometrical Dimensions, and Process Parameters

The bimetallic cylinders used in the simulations have a magnesium alloy UNS M11311 core and a titanium alloy UNS R56400 as sleeve (Figure 1); due to their excellent properties, these alloys are well known in the industry by the nomenclature AZ31B and Ti6Al4V, respectively, so this will be the designation used in the paper from now on.

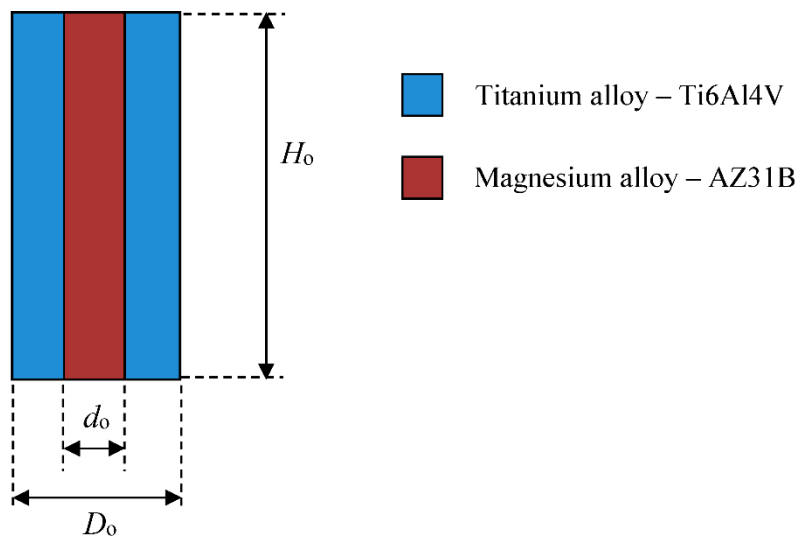


Figure 1. Bimetallic cylinder sketch and initial geometrical dimensions.

The parameters of the extrusion process considered in this work are presented in Figure 2.

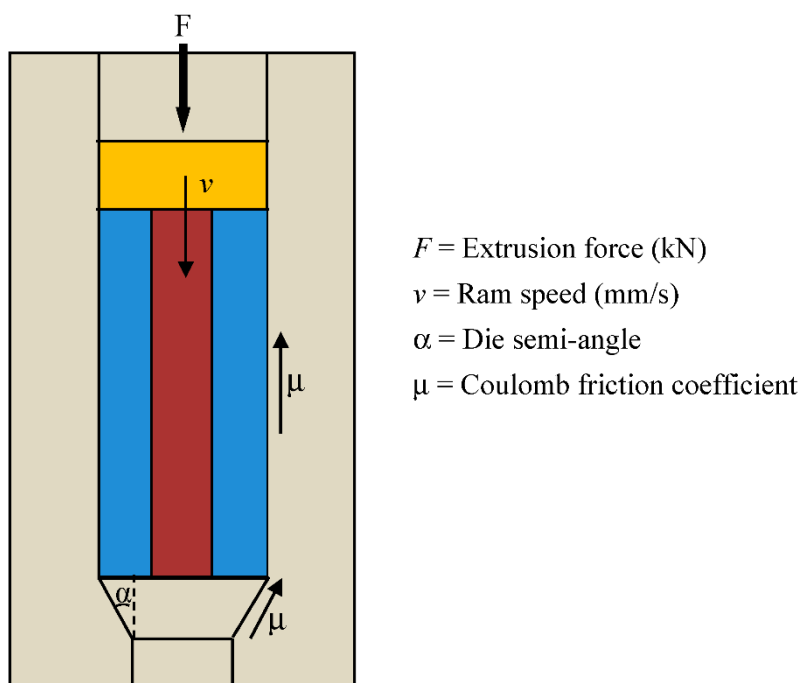


Figure 2. Extrusion process schema.

The chemical composition of both materials are listed in Table 1 [18] and Table 2 [19].

Table 1. Chemical composition of magnesium alloy AZ31B.

Material	Mg (wt.%)	Al (wt.%)	Zn (wt.%)	Mn (wt.%)	Si (wt.%)	Cu (wt.%)	Ca (wt.%)	Fe (wt.%)	Ni (wt.%)
AZ31B	97	2.5–3.5	0.6–1.4	0.20	0.1	0.05	0.04	0.005	0.005

Table 2. Chemical composition of titanium alloy Ti6Al4V.

Material	Ti (wt.%)	Al (wt.%)	V (wt.%)	Fe (wt.%)	C (wt.%)	O (wt.%)	N (wt.%)	H (wt.%)
Ti6Al4V	Bal.	5.5–6.5	3.5–4.5	0.25	0.08	0.13	0.040	0.012

The physical and mechanical properties of both materials are included in Table 3 [18,19] for comparison.

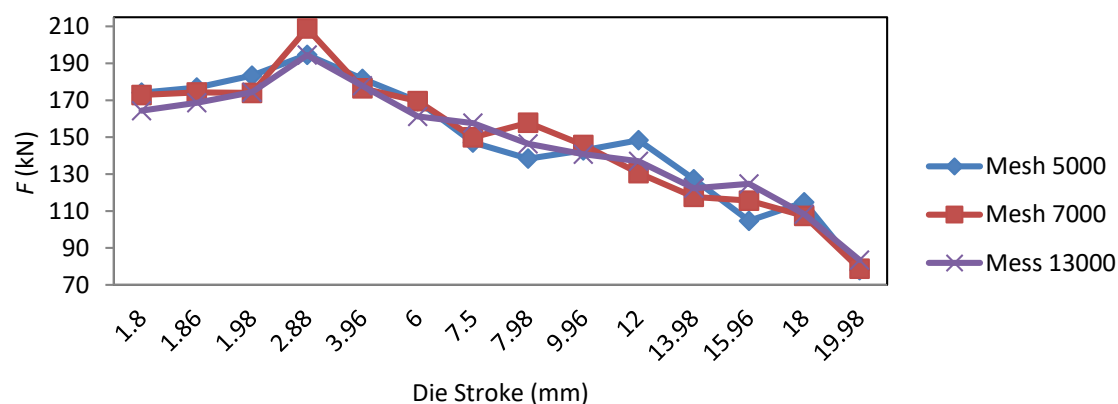
Table 3. Physical and mechanical properties of the magnesium alloy AZ31B and titanium alloy Ti6Al4V.

Property	AZ31B	Ti6Al4V
Density (g/cm ³)	1.74	4.46
Tensile strength (MPa)	260	≥895
Yield strength (MPa)	200	≥828
Elastic modulus (GPa)	44.80	105–120
Poisson's ratio	0.35	0.31

2.2. Finite Element Modeling

Finite element simulations were performed by the commercial finite element program DEFORM 3D. Taking advantage of the axial symmetry of the problem, only a quarter of the process has been modeled in order to reduce the computation time and other computational resources, such as storage needs. The ram and the container were modeled as rigid objects and the bimetallic cylinders were modeled as an assembly between two plastic objects (sleeve and core).

The plastic parts have been meshed using tetrahedral elements. A mesh study has been realized in order to determine the best mesh configuration. Meshes with 5000, 7000, and 13,000 elements have been considered. In Figure 3, the extrusion force results versus the die stroke are shown for different mesh sizes.

**Figure 3.** Extrusion force for different mesh sizes.

Taking into account that the results for the extrusion force using several mesh sizes are quite similar, 7000 elements mesh size is considered the optimum one due to the compromise between the precision reached and the computational time to perform each simulation.

The contact conditions among the different objects have to be defined as well. Rigid objects are considered “master” (the ones who deform) and the plastic objects are considered “slave” (the ones who are deformed). In the case of sleeve and core interaction, where both objects are plastic, titanium alloy is defined as “master” and magnesium alloy as “slave”, according to the properties presented in Table 3. The friction model used in all the simulations is the Coulomb model that, along with the shear friction model, is one of the classical friction models in metal forming analysis [20].

Materials AZ31B and Ti6Al4V were assumed to be isotropic during all the process. The flow curves used for Ti6Al4V are from DEFORM library.

In the case of AZ31B, as there was no reference in DEFORM, an exponential model defined by Wen-Juan [21] was used to define the flow curves, obtaining the results shown in Table 4.

Table 4. AZ31B flow curves values based on Wen-Juan exponential model.

Strain	Stress (MPa)			
	T = 150 °C	T = 200 °C	T = 250 °C	T = 300 °C
Strain rate = 0.001	0.02	112.69	91.54	74.35
	0.05	133.12	107.86	87.40
	0.10	168.45	136.07	109.91
	0.15	202.14	163.00	131.44
	0.20	230.06	185.44	149.47
	0.25	248.31	200.35	161.65
	0.30	254.18	205.56	166.23
				134.43
Strain rate = 0.01	0.02	127.46	105.42	87.19
	0.05	149.13	122.70	100.95
	0.10	186.21	152.12	124.27
	0.15	221.25	179.81	146.14
	0.20	250.18	202.67	164.18
	0.25	269.21	217.81	176.23
	0.30	275.67	223.20	180.72
				146.32
Strain rate = 0.1	0.02	144.17	121.41	102.25
	0.05	167.06	139.58	116.61
	0.10	205.84	170.06	140.50
	0.15	242.17	198.36	162.48
	0.20	272.07	221.51	180.34
	0.25	291.87	236.80	192.13
	0.30	298.99	242.36	196.46
				159.25

Damage factor has been also used in this work as a parameter to evaluate the quality of the extrudate. Damage factor is evaluated in DEFORM using normalized Cockcroft and Latham criterion [22], typically used for predicting damage in metal forming operations [23], due to its simplicity and the accessibility of material data required for its calculation. This criterion considers that the fracture is mainly governed by the maximum principal stress, as it is shown in Equation (1):

$$\int_0^{\varepsilon_f} (\sigma_{max}/\sigma_H) d\varepsilon = C \quad (1)$$

where ε is the equivalent plastic strain, ε_f is the equivalent strain to fracture, σ_{max} is the maximum principal stress, σ_H is the stress according to the Huber–Mises hypothesis and C is a constant depending on the material and experimental determined.

2.3. Finite Element Model Validation

The FE model validation has been performed theoretically comparing the simulations results for the extrusion force with the results using Johnson semi-empirical model [24–26], typically used in this kind of analysis. In this model the deformation is defined in Equation (2):

$$\varepsilon_x = a + b \cdot \ln(r_x) \quad (2)$$

where r_x is the extrusion ratio (A_0/A) and a and b are constants obtained by semi-empirical methods whose values are 0.8 and 1.2, respectively.

The extrusion force is defined in Equation (3):

$$F = A_0 \cdot \sigma_f \left(\varepsilon_x + \frac{2L}{D_0} \right) \quad (3)$$

where A_0 is the initial area, L is the contact length of the container, D_0 is the initial diameter of the billet and σ_f is the average flow stress.

Three simulations have been performed to validate the model. In all the simulations the cylinder had 12 mm of external diameter and 20 mm of height and the final external diameter was 9 mm, therefore the extrusion ratio (r_x) is 1.77. The first simulation is performed using a Ti6Al4V cylinder, the second one using a AZ31B cylinder and the last one using a bimetallic billet with a core of 6 mm diameter.

The extrusion parameters were a die semi-angle of 45° , a friction coefficient of 0.1, a ram speed of 2 mm/s and a temperature of 200°C .

Equation (4) [27] was used to obtain the flow stress for the multi-material cylinder:

$$\sigma_m = \sigma_c \cdot \frac{V_c}{V_c + V_s} + \sigma_s \cdot \frac{V_s}{V_c + V_s} \quad (4)$$

where σ_m is the yield stress for the multi-material part, σ_c is the yield stress for the core, σ_s is the yield stress for the sleeve, V_c is the volume of the core and V_s is the volume of the sleeve.

The comparison results are shown in Figures 4–6.

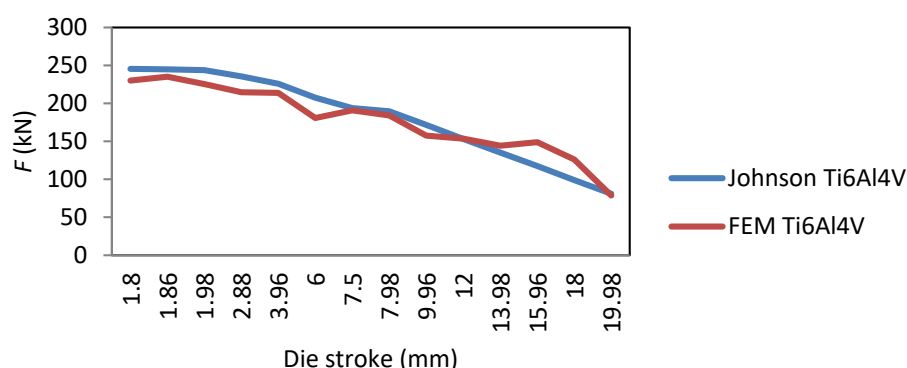


Figure 4. Comparison chart between Johnson and FEM extrusion force for a billet of Ti6Al4V.

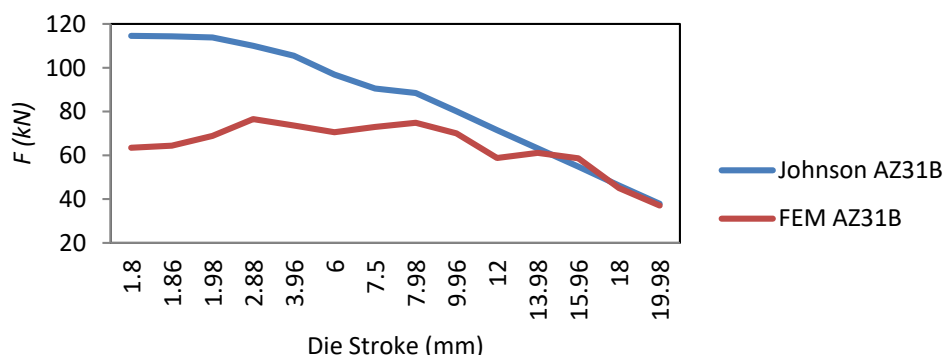


Figure 5. Comparison chart between Johnson and FEM extrusion force for a billet of AZ31B.

After comparing the analytical results with the simulation ones, it can be concluded that the FE model is robust enough to be validated.

2.4. Design of Experiments (DOE)

Once the FE model has been validated, the next step is to define the design of experiment (DOE) methodology [28] to identify and quantify the parameters with a higher influence in the extrusion force and the damage induced in the multi-material extrudate.

In Figure 7, an Ishikawa chart is shown in order to list the possible causes that may affect the extrusion force; where H_0 is the initial height of the billet, D_0 is the initial external diameter of the sleeve and d_0 is the initial diameter of the core.

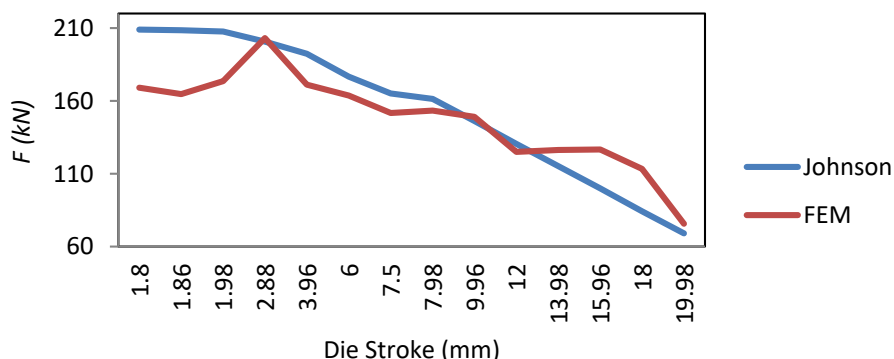


Figure 6. Comparison chart between Johnson and FEM extrusion force for a multi-material billet.

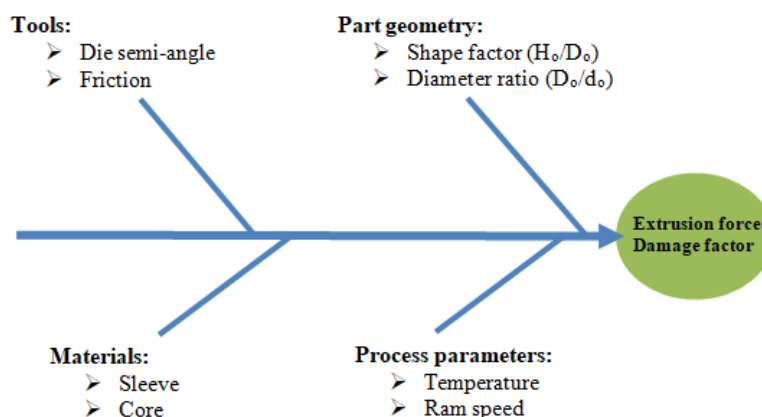


Figure 7. Ishikawa's chart for the analysis of the bimetallic extrusion process.

The values range for each cause/parameter is shown in Table 5:

Table 5. Cause/parameter values distributed by levels.

Variable	Cause/Factor	Units	Level 1	Level 2	Level 3	Level 4	Level 5
X_1	Core diameter	mm	4	5	6	7	8
X_2	Billet height	mm	12	15	20	25	30
X_3	Ram speed	mm/s	1	1.5	2	2.5	3
X_4	Temperature	°C	100	150	200	250	300
X_5	Friction coefficient	N/A	0.030	0.065	0.100	0.135	0.170
X_6	Die semi-angle	°	15	30	45	60	75

The DOE technique consists on the combination of these independent variables by fixing all the values in the center one (level 3), except the variable whose behavior wants to be known. Thus, for each of these combinations, a value for the dependent variables (extrusion force and damage factor) will be obtained.

In Tables 6–11, the combinations of these variables and their influence in the extrusion force are shown. The same procedure has been followed with the independent variable damage factor.

Table 6. Variables combination by varying X_1 (core diameter).

Simulation	X_1 (mm)	X_2 (mm)	X_3 (mm/s)	X_4 (°C)	X_5	X_6 (°)	Extrusion Force (kN)
1	4	20	2	200	0.1	45	249.60
2	5	20	2	200	0.1	45	221.25
3	6	20	2	200	0.1	45	207.46
4	7	20	2	200	0.1	45	183.65
5	8	20	2	200	0.1	45	165.92

Table 7. Variables combination by varying X_2 (billet height).

Simulation	X_1 (mm)	X_2 (mm)	X_3 (mm/s)	X_4 (°C)	X_5	X_6 (°)	Extrusion Force (kN)
1	6	12	2	200	0.1	45	180.29
2	6	16	2	200	0.1	45	186.55
3	6	20	2	200	0.1	45	207.46
4	6	24	2	200	0.1	45	233.23
5	6	28	2	200	0.1	45	278.63

Table 8. Variables combination by varying X_3 (ram speed).

Simulation	X_1 (mm)	X_2 (mm)	X_3 (mm/s)	X_4 (°C)	X_5	X_6 (°)	Extrusion Force (kN)
1	6	20	1	200	0.1	45	221.66
2	6	20	1.5	200	0.1	45	215.94
3	6	20	2	200	0.1	45	207.46
4	6	20	2.5	200	0.1	45	211.10
5	6	20	3	200	0.1	45	208.14

Table 9. Variables combination by varying X_4 (temperature).

Simulation	X_1 (mm)	X_2 (mm)	X_3 (mm/s)	X_4 (°C)	X_5	X_6 (°)	Extrusion Force (kN)
1	6	20	2	100	0.1	45	241.82
2	6	20	2	150	0.1	45	222.75
3	6	20	2	200	0.1	45	207.46
4	6	20	2	250	0.1	45	185.97
5	6	20	2	300	0.1	45	170.37

Table 10. Variables combination by varying X_5 (friction coefficient).

Simulation	X_1 (mm)	X_2 (mm)	X_3 (mm/s)	X_4 (°C)	X_5	X_6 (°)	Extrusion Force (kN)
1	6	20	2	200	0.030	45	136.63
2	6	20	2	200	0.065	45	198.06
3	6	20	2	200	0.100	45	207.46
4	6	20	2	200	0.135	45	243.50
5	6	20	2	200	0.170	45	276.28

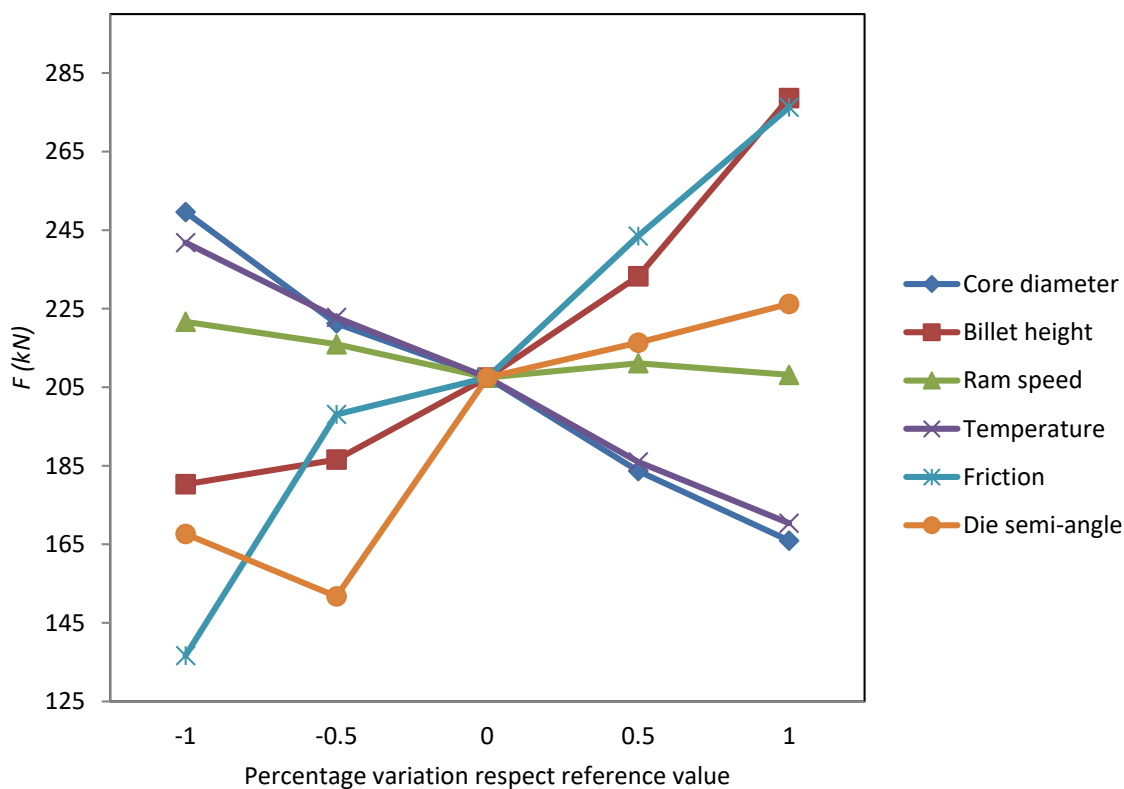
3. Results

3.1. Determination of Most Influential Parameters in the Extrusion Force

After performing the simulations according to the DOE defined in the previous section, the values obtained for the extrusion force are placed in a perturbation chart (Figure 8) in order to check which parameters produce a bigger deviation between the lowest and the highest extrusion force values.

Table 11. Variables combination by varying X_6 (die semi-angle).

Simulation	X_1 (mm)	X_2 (mm)	X_3 (mm/s)	X_4 (°C)	X_5	X_6 (°)	Extrusion Force (kN)
1	6	20	2	200	0.1	15	164.64
2	6	20	2	200	0.1	30	151.71
3	6	20	2	200	0.1	45	207.46
4	6	20	2	200	0.1	60	216.34
5	6	20	2	200	0.1	75	226.21

**Figure 8.** Perturbation chart of the bimetallic extrusion process.

In the perturbation chart shown in Figure 8, it can be verified that the most influential parameters in the extrusion force are billet height, friction, and die semi-angle. However, in the case of the temperature and the core diameter, the difference is not so clear. Therefore, in Figure 9, a percentage variation respect the reference value (level 3) of the extrusion force is shown.

The conclusion is that ram speed and temperature are the less relevant factors in the extrusion force compared to the most influential factors.

In order to classify the rest of the factors, a Taguchi's analysis of variance (ANOVA) [27] is performed. Table 12 shows the Taguchi's orthogonal array for four variables with three levels and Table 13 shows the results for the average values taking into account the criteria "the lower the best" to indicate that the best results occur when the extrusion force is the minimum.

The most relevant factor to obtain a low extrusion force during the process is the die semi-angle followed very close by the friction.

3.2. Analysis of the Influence of the Process Parameters in the Extrusion Force

Once it is clarified in which magnitude the extrusion force is affected by the process parameters, it is time to analyze in which way each parameter affects to the extrusion force. Figure 10 presents the results of the analysis, and they will be discussed below.

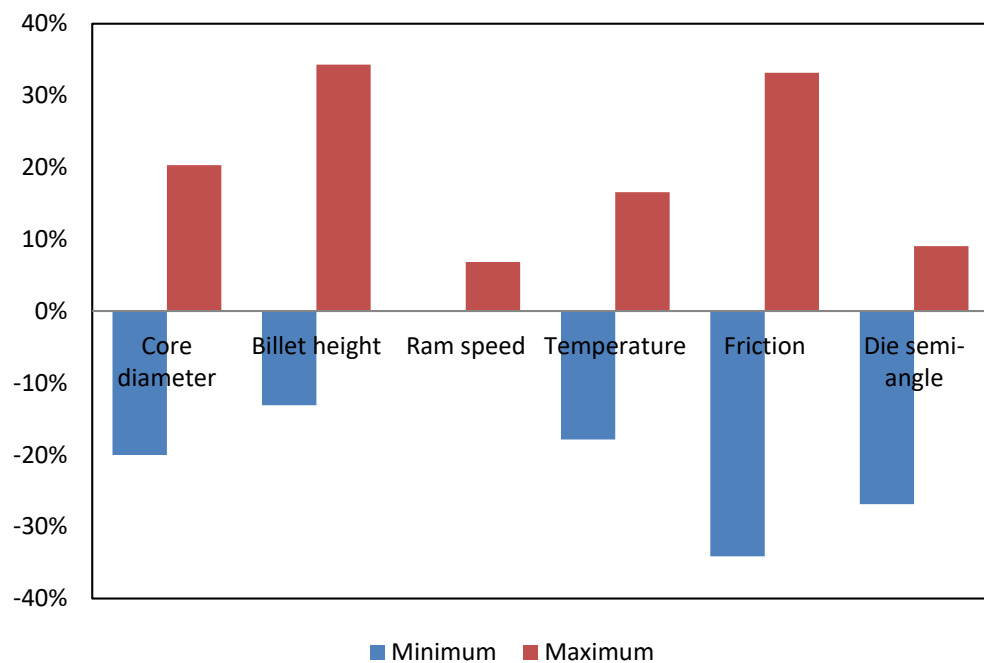


Figure 9. Percentage variation respect the reference value (level 3) of the extrusion force.

Table 12. Taguchi's orthogonal array for extrusion force.

Simulation	Core Diameter (mm)	Friction	Billet Height (mm)	Die Semi-Angle (°)	Extrusion Force (kN)
1	6	0.07	15	30	119.20
2	6	0.10	20	45	207.46
3	6	0.15	25	60	380.79
4	7	0.07	20	60	191.42
5	7	0.10	25	30	161.97
6	7	0.15	15	45	182.98
7	8	0.07	25	45	161.00
8	8	0.10	15	60	157.51
9	8	0.15	20	30	177.18

Table 13. Taguchi's results for the average values for extrusion force (kN).

Level	Core Diameter	Friction	Billet Height	Die Semi-Angle
1	235.80	157.20	153.20	152.80
2	178.80	175.60	192.00	183.80
3	165.20	247.00	234.60	243.20
Delta Classification	70.60	89.80	81.40	90.50
	4	2	3	1

3.2.1. Core Diameter

The influence of the core diameter is inversely proportional to the necessary extrusion force. As the diameter increases, the necessary force decreases as it is shown in Figure 10a.

This result is expected since as we increase the diameter of the core, the internal diameter of the ring decreases, so the volume of Ti6Al4V in the cylinder is smaller. As more force is needed to extrude the Ti6Al4V than for the AZ31B, it is logical to expect that the force necessary to extrude the multi-material cylinder will be less.

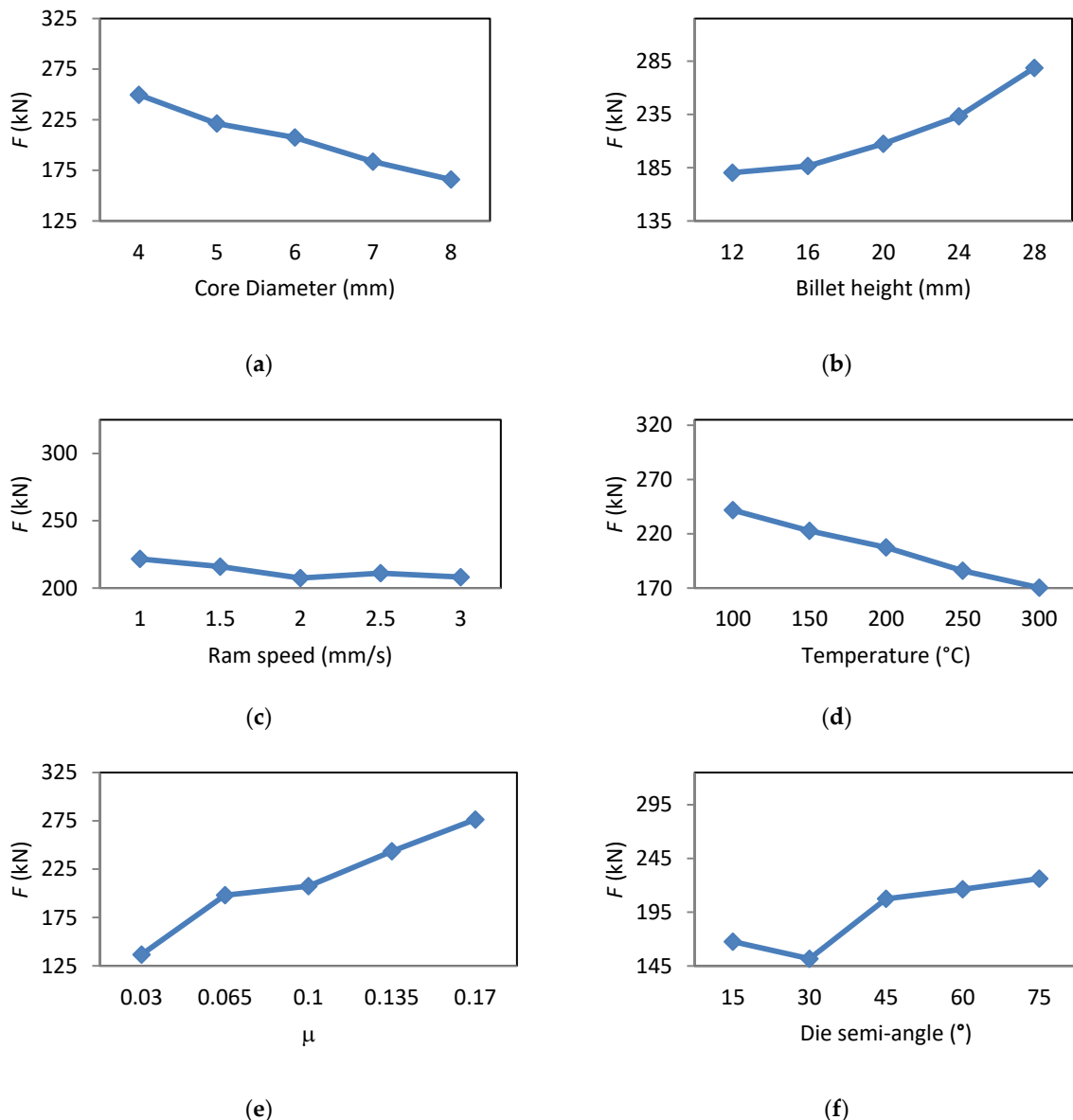


Figure 10. Influence of the parameters on the extrusion force. (a) *Core diameter; (b) *Billet height; (c) *Ram speed; (d) Temperature; (e) *Friction; (f) *Die semi-angle. *Temperature of the process is 200 °C.

3.2.2. Billet Height

Unlike the diameter of the core, as the height increases, the force required to extrude the part increases, as it can be seen in Figure 10b.

This result can be explained because as the height increases, the contact area of the billet with the container increases too; as a consequence, this causes an increase of the energy component due to friction and, therefore, of the total force required.

3.2.3. Ram Speed

The ram speed is linked to the deformation speed that will be imposed to the part during the process and it is the factor that has the least relevance in the extrusion force, resulting in a decrease with the ram speed increase as can be seen in Figure 10c.

This effect can be explained because as the ram speed increases the temperature increases due to the friction in the container/billet interface. This increase of temperature reduces the stress necessary to deform the billet and, thus, the extrusion force is lower and remains practically constant at highest speed.

Another important effect observed is that, as the speed of the die is increased, the maximum effective stress on the core decreases, until it reaches a minimum for $v = 2.5$ mm/s, as shown in Figure 11. This will be of interest in industrial application of extrusion processes because this has a direct influence in the quality of the extrudate.

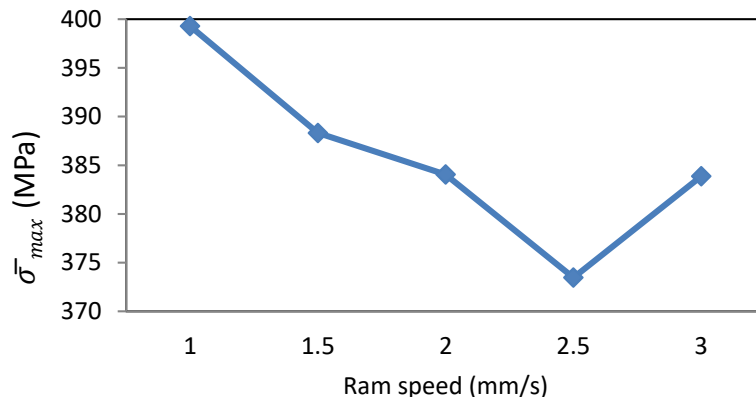


Figure 11. Influence of the ram speed on the core maximum effective stress ($T = 200$ °C).

3.2.4. Temperature

The process temperature has an effect inversely proportional to the extrusion force as shown in the Figure 10d. This relationship was expected by observing the flow curves of AZ31B and Ti6Al4V, because the temperature decreases the flow stress of metallic materials, and it is typically used to increase the formability of these materials. Temperature is the second parameter with the least influence on the extrusion force of the process.

For the entire temperature range, the maximum extrusion force is achieved for a die displacement of 2.88 mm. Furthermore, it is observed in Figure 12 that increasing the temperature decreases the maximum stress on the core.

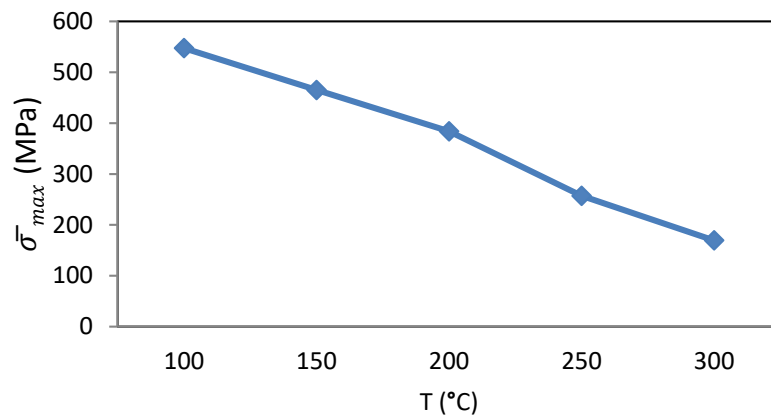


Figure 12. Influence of the temperature on the core maximum effective stress.

Temperature affects the sleeve maximum effective stress in a practically linear way, as shown in Figure 13.

3.2.5. Friction

The friction at the interface between the container and the sleeve is the second most influential factor considered on the extrusion force of the process. In this work, it has been considered that the

ring and core have been assembled with an interference fit, and due to the compression forces that they will suffer during the whole process, the friction between them would be maximum. Even so, in all of the simulations, it can be seen that there is a slip between the two at the beginning of the extrusion, being the part that always slides the AZ31B magnesium alloy. As can be seen in the graph of Figure 10e, as friction increases, the extrusion force necessary to carry out the process increases.

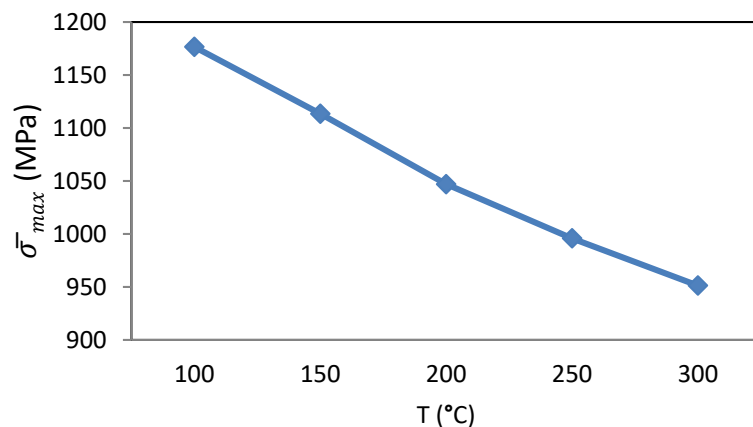


Figure 13. Influence of the temperature on the sleeve maximum effective stress.

Another effect observed on the extruded part is that as friction increases, the maximum effective stress on the core decreases, as shown in Figure 14.

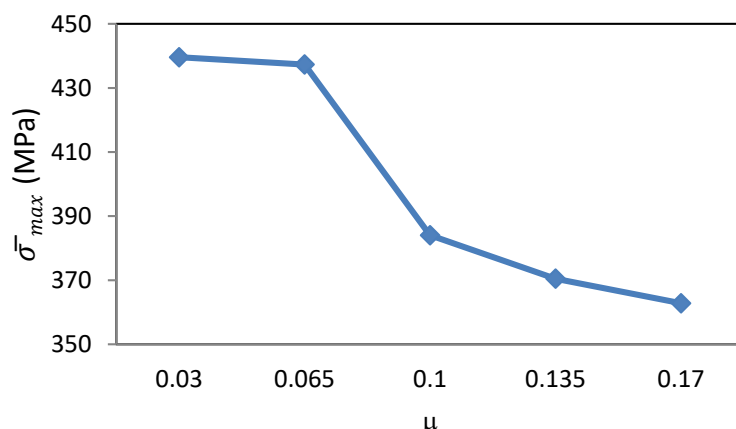


Figure 14. Influence of the friction on the cores maximum effective stress ($T = 200\text{ }^{\circ}\text{C}$).

3.2.6. Die Semi-Angle

Die semi-angle is the most relevant factor to obtain a small extrusion force. The conclusion that can be obtained from the graph in Figure 10f is that there is an optimal value where the extrusion force is minimal; this value has been set at 30° . From this optimal value, the extrusion force increases as the extrusion semi-angle increases or decreases and allows identifying a situation of minimum energy.

3.3. Other Factors Related to the Quality of the Extrudate: Damage Factor

The entire DOE has been done considering the extrusion force as a dependent variable, since this technological parameter is directly related to the power of the extruder to be used and, therefore, will have a direct impact on the investment to be made for the purchase of the equipment; but also, the required forces are close related to the efficiency of the process and, consequently, to the environmental impact of the extrusion process itself. There are other aspects concerning the quality of the final part obtained that can also be analyzed by Finite Element analysis. It is the case of the residual

stresses and the damage induced in the workpiece as a consequence of the forming process. High values of damage could lead to fracture of the part during the component service, so the maximum damage at the core (where inner defects such as chevron cracks can appear in extrusion under specific forming conditions) has been studied in all the configurations.

During the simulations carried out, it was found that the damage induced in the core of the part follows the distribution shown in Figure 15.

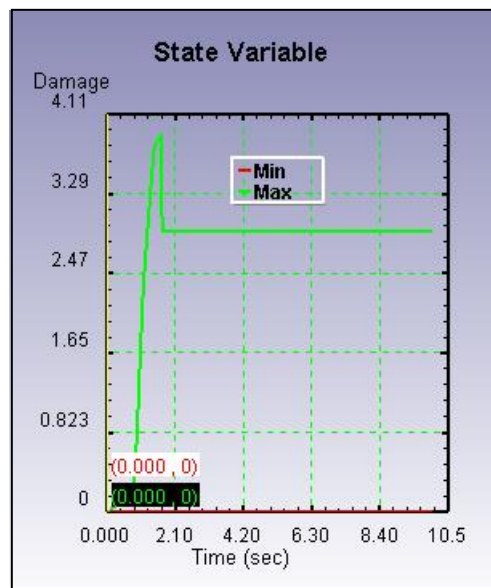


Figure 15. Evolution of damage in the core of the part.

It can be observed that once the damage peak (corresponding to the transient period) is reached, the maximum damage decreases sharply to a value that remains constant throughout the extrusion process, as it reaches a permanent regime.

Taking into account the most influencing factors analyzed, another Taguchi's ANOVA is performed to check their influence in the damage induced in the part. Tables 14 and 15 show the orthogonal array and the results for the average values.

Table 14. Taguchi's orthogonal array for damage factor.

Simulation	Core Diameter (mm)	Friction	Billet Height (mm)	Die Semi-Angle (°)	Damage Factor
1	6	0.07	15	30	0.97
2	6	0.10	20	45	0.76
3	6	0.15	25	60	0.69
4	7	0.07	20	60	1.85
5	7	0.10	25	30	0.53
6	7	0.15	15	45	2.18
7	8	0.07	25	45	2.31
8	8	0.10	15	60	1.62
9	8	0.15	20	30	1.25

Table 15. Taguchi's results for the average values for damage factor.

Level	Core Diameter	Friction	Billet Height	Die Semi-Angle
1	0.81	1.71	1.59	0.92
2	1.52	0.97	1.29	1.75
3	1.73	1.37	1.18	1.39
Delta Classification	0.92	0.74	0.41	0.84
	1	3	4	2

In this case, the order of influence of the factors changes, the core diameter appearing as the most relevant one to obtain a minimum damage value during the process.

3.4. Summary of Most Influential Parameters

According to the results in forces and maximum damage induced in the bimetallic billets, a summary of the most influential parameters in extrusion of these bimetallic components is presented in Table 16.

Table 16. Classification¹ of most influential parameters in extrusion of bimetallic parts (AZ31B core and Ti6Al4V sleeve).

Output Variable	Core Diameter	Friction at Sleeve-Container/Die Interface	Billet Height	Die Semi-Angle
Extrusion force	4	2	3	1
Damage in the core	1	3	4	2

¹ Note: 1—most influential; 4—least influential.

The most influential parameters, considering both criteria (minimum values of forces and damage), are the die semi-angle and friction at the sleeve-container/die interface, so special attention should be paid to obtain favorable interface contact conditions; followed by the geometrical dimensions of the billet, being the billet height more important when paying attention to the minimum forces, and being the core diameter when considering the minimum damage as the most important criterion. These kind of tables are very useful from a practical point of view, as they can be used as guidelines in process design for engineering applications.

As an example of the simulations preformed, Figure 16 shows the effective stress and temperature distribution respectively in the FE model, in different stages of the simulation.

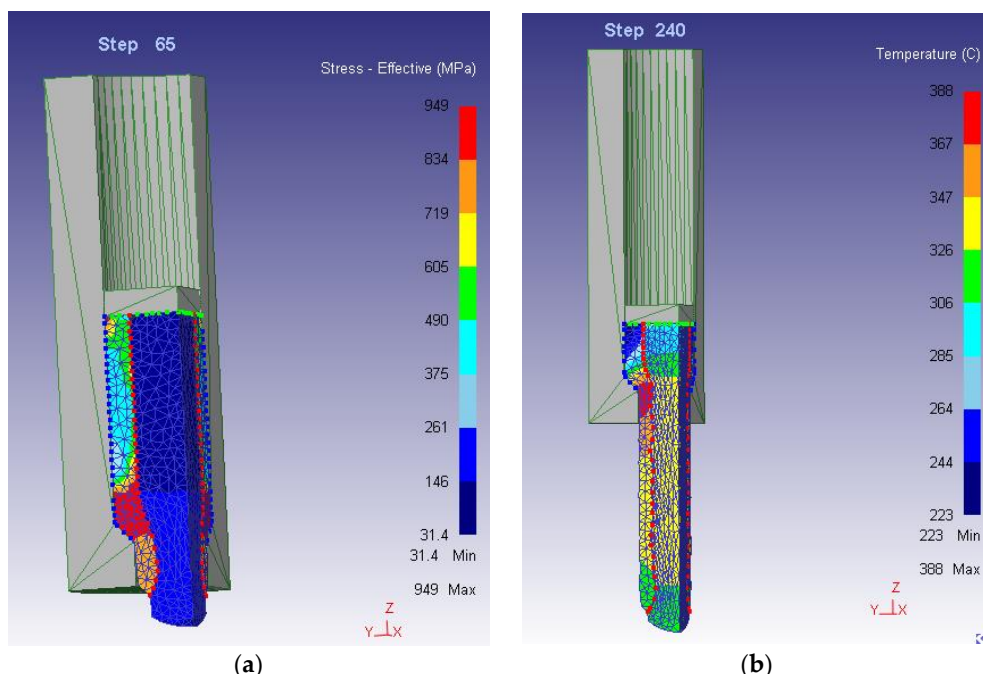


Figure 16. Contour diagrams. (a) Effective stress distribution during co-extrusion process; (b) temperature distribution during co-extrusion process.

4. Conclusions

According to the results presented in this paper, a robust FE model for bimetallic co-extrusion process has been developed. This model represents very accurately the theoretical behavior of a bimetallic cylinder during extrusion process according to Johnson's model.

Using this FE model combined with Taguchi's ANOVA has allowed identifying the most relevant factors in the extrusion force, and in which way this force is affected for each of the factors, as shown in Table 13.

Temperature and ram speed have been revealed as the less influence factors in the extrusion force. Regarding ram speed, it has been seen that the higher it is, the lower is the extrusion force needed until it reaches a minimum value from which the extrusion force remains practically constant.

Die semi-angle has been identified as the most critical factor to reduce the extrusion force while the core diameter is the most relevant one to reduce the damage factor in the core component during the process.

During this study die semi-angle of 30° has been proved as the optimum one to reduce the extrusion force during the process.

Friction is found as one of the most relevant factors for both extrusion force and damage factor; however, a balance in the shape factor (ratio between sleeve external diameter and billet height) is also found as key to obtain an extruded part using the minimum extrusion force and with the minimum damage factor.

Finally, this paper describes how the maximum damage in the core component of the billet is influenced by the parameters process and also the damage factor evolution during the co-extrusion process.

The methodology employed in this paper can also be extended to analyze other technological factors; the results of this paper can potentially be used to improve the efficiency of this kind of extrusion processes and the quality of the extrudates that, along with the use of lightweight materials, can contribute to sustainable production approaches.

Author Contributions: Conceptualization, D.F., A.R.-P., and A.M.C.; methodology, D.F.; formal analysis, D.F., A.R.-P., and A.M.C.; investigation, D.F., A.R.-P., and A.M.C.; resources, A.R.-P. and A.M.C.; writing—original draft preparation, D.F.; writing—review and editing, A.R.-P. and A.M.C.; supervision, A.R.-P. and A.M.C.; project administration, A.R.-P. and A.M.C.; funding acquisition, A.R.-P. and A.M.C. All authors have read and agreed to the published version of the manuscript.

Funding: This research was funded by the Annual Grants Call of the E.T.S.I. Industriales of UNED through the projects of references [2020-ICF04/B] and [2020-ICF04/D].

Acknowledgments: This work has been developed within the framework of the “Doctorate Program in Industrial Technologies” of the UNED. We would like to extend our acknowledgement to the Research Group of the UNED “Industrial Production and Manufacturing Engineering (IPME)”.

Conflicts of Interest: The authors declare no conflict of interest.

References

- European Comission. Horizon 2020 Work Programme 2018–2020 5.ii. Nanotechnologies, Advanced Materials, Biotechnology and Advanced Manufacturing and Processing. Available online: https://ec.europa.eu/research/participants/data/ref/h2020/wp/2018-2020/main/h2020-wp1820-leit-nmp_en.pdf (accessed on 30 October 2019).
- Rodríguez-Panes, A.; Claver, J.; Camacho, A.M. The influence of manufacturing parameters on the mechanical behavior of PLA and ABS pieces manufactured by FDM: A comparative analysis. *Materials* **2018**, *11*, 1333. [[CrossRef](#)] [[PubMed](#)]
- García-Domínguez, A.; Claver, J.; Sebastián, M.A. Optimization methodology for additive manufacturing of customized parts by fused deposition modeling (FDM). Application to a shoe heel. *Polymers* **2020**, *12*, 2119. [[CrossRef](#)] [[PubMed](#)]
- Rodríguez-Prieto, A.; Camacho, A.M.; Sebastián, M.A.; Yanguas-Gil, A. Polymers selection for harsh environments to be processed using additive manufacturing techniques. *IEEE Access* **2018**, *6*, 29899–29911. [[CrossRef](#)]
- García-Domínguez, A.; Claver, J.; Camacho, A.M.; Sebastián, M.A. Considerations on the applicability of test methods for mechanical characterization of materials manufactured by FDM. *Materials* **2020**, *13*, 28. [[CrossRef](#)]
- Negendanka, M.; Mueller, S.; Reimers, W. Coextrusion of Mg–Al macrocomposites. *J. Mater. Process. Technol.* **2012**, *212*, 1954–1962. [[CrossRef](#)]
- Thirumurugan, M.; Anka Rao, S.; Kumaran, S.; Srinivasa Rao, T. Improved ductility in ZM21 magnesium-aluminium macrocomposite produced by co-extrusion. *J. Mater. Process. Technol.* **2011**, *211*, 1637–1642. [[CrossRef](#)]

8. Gall, S.; Müller, S.; Reimers, W. Aluminum coating of magnesium hollow profiles by using the coextrusion process. *Alum. Int. J.* **2009**, *85*, 63–67.
9. Lehmann, T.; Stockmann, M.; Naumann, J. Experimental and numerical investigations of Al/Mg compound specimens under load in an extended temperature range. *FEM Trans.* **2009**, *37*, 1–8.
10. Lapovok, R.; Ng, H.P.; Tomus, D.; Estrin, Y. Bimetallic copper-aluminum tube by severe plastic deformation. *Scr. Materialia* **2012**, *66*, 1081–1084. [[CrossRef](#)]
11. Berski, S.; Dyja, H.; Banaszek, G.; Janik, M. Theoretical analysis of bimetallic rods extrusion process in double reduction die. *J. Mater. Process. Technol.* **2004**, *153–154*, 583–588. [[CrossRef](#)]
12. Kocich, R. Deformation behavior of Al/Cu clad composite during twist channel angular pressing. *Materials* **2020**, *13*, 4047. [[CrossRef](#)] [[PubMed](#)]
13. Rong, W.; Zhang, Y.; Wu, Y.; Chen, Y.; Tang, T.; Peng, L.; Li, D. Fabrication of high-strength Mg-Gd-Zn-Zr alloys via differential-thermal extrusion. *Mater. Charact.* **2017**, *131*, 380–387. [[CrossRef](#)]
14. Alcaraz, J.L.; Gil-Sevillano, J. An analysis of the extrusion of bimetallic tubes by numerical simulation. *Int. J. Mech. Sci.* **1996**, *38*, 157–173. [[CrossRef](#)]
15. Camacho, A.M.; Rodríguez-Prieto, A.; Herrero, J.M.; Aragón, A.M.; Bernal, C.; Lorenzo-Martin, C.; Yanguas-Gil, A.; Martins, P. An experimental and numerical analysis of the compression of bimetallic cylinders. *Materials* **2019**, *12*, 4094. [[CrossRef](#)]
16. Behrens, B.A.; Klose, C.; Chugreev, A.; Heimes, N.; Thürer, S.E.; Uhe, J. A numerical study on co-extrusion to produce coaxial aluminum—Steel compounds with longitudinal weld seams. *Metals* **2018**, *8*, 717. [[CrossRef](#)]
17. Thürer, S.E.; Peddinghaus, J.; Heimes, N.; Bayram, F.C.; Bal, B.; Uhe, J.; Behrens, B.A.; Maier, H.J.; Klose, C. Lateral angular co-extrusion: Geometrical and mechanical properties of compound profiles. *Metals* **2020**, *10*, 1162. [[CrossRef](#)]
18. Avedesiam, M.; Baker, H. *ASM Speciality Handbook. Magnesium and Magnesium Alloys*; ASM International: Novelty, OH, USA, 1999; pp. 3–4.
19. Donachie, M.J. *Titanium. A Technical Guide*; ASM International: Novelty, OH, USA, 1988.
20. Zhang, D.-W.; Ou, H. Relationship between friction parameters in a Coulomb–Tresca friction model for bulk metal forming. *Tribol. Int.* **2016**, *95*, 13–18. [[CrossRef](#)]
21. Li, W.-J.; Zhao, G.-Q.; Ma, X.; Gao, J. Flow stress characteristics of AZ31B magnesium alloy sheet at elevated temperatures. *Int. J. Appl. Phys. Math.* **2012**, *2*, 83–88. [[CrossRef](#)]
22. Cockcroft, M.G.; Latham, D.J. Ductility and the workability of metals. *J. Inst. Met.* **1968**, *96*, 33–39.
23. Stebunox, S.; Vlasov, A.; Biba, N. Prediction of the fracture in cold forging with modified Cockcroft–Latham criterion. *Procedia Manuf.* **2018**, *15*, 519–526. [[CrossRef](#)]
24. Johnson, W. The pressure for the cold extrusion of lubricated rod through square dies of moderate reduction at slow speeds. *J. Inst. Met.* **1957**, *85*, 403–408.
25. Amigo, F.; Camacho, A.M. Reduction of induced central damage in cold extrusion of dual–Phase steel DP800 using double–Pass dies. *Metals* **2017**, *7*, 335. [[CrossRef](#)]
26. García, A.; Claver, J.; Camacho, A.M.; Sebastián, M.A. Comparative analysis of extrusion processes by finite element analysis. *Procedia Eng.* **2015**, *100*, 74–83. [[CrossRef](#)]
27. Gisbert, C.; Bernal, C.; Camacho, A.M. Improved analytical model for the calculation of forging forces during compression of bimetallic axial assemblies. *Procedia Eng.* **2015**, *132*, 298–305. [[CrossRef](#)]
28. Kumar, T.B.; Panda, A.; Kumar Sharma, G.; Johar, A.K.; Kar, S.K.; Boolchandani, D. Taguchi DoE and ANOVA: A systematic perspective for performance optimization of cross-coupled channel length modulation OTA. *AEU Int. J. Electron. Commun.* **2020**, *116*, 153070. [[CrossRef](#)]

Publisher's Note: MDPI stays neutral with regard to jurisdictional claims in published maps and institutional affiliations.



© 2020 by the authors. Licensee MDPI, Basel, Switzerland. This article is an open access article distributed under the terms and conditions of the Creative Commons Attribution (CC BY) license (<http://creativecommons.org/licenses/by/4.0/>).

4.2. Analysis of AZ31B -Ti6Al4V bimetallic extrusion by numerical simulation and Taguchi method

Los indicios de calidad de este artículo se pueden encontrar en el Apéndice B de esta Tesis Doctoral.

4.2.1. Datos de la publicación y factor de impacto

Título	Analysis of AZ31B -Ti6Al4V bimetallic extrusion by numerical simulation and Taguchi method
Autores	Daniel Fernández ; Álvaro Rodríguez-Prieto; Ana María Camacho
Revista	IOP Conference Series: Materials Science and Engineering
ISSN	1757-899X
Editorial	IOP Publishing Ltd
País	United Kingdom
Volumen	1193
Páginas	012080
Fecha	Junio de 2021
doi	https://doi.org/10.1088/1757-899X/1193/1/012080
Factor de impacto	SJR (2021): 0.25

4.2.2. Resumen y copia de la publicación

Este artículo investiga la fuerza de extrusión y el daño inducido durante un proceso de extrusión para fabricar cilindros bimétálicos que combinan un anillo exterior de aleación de titanio (Ti6Al4V) con un núcleo de aleación de magnesio (AZ31B). Se ha realizado un estudio para determinar la distribución del factor de daño a través del proceso de extrusión y cómo este factor junto con la fuerza de extrusión se ven influenciados por los parámetros de fabricación (relación de extrusión, fricción y semi-ángulo de matriz) mediante elementos finitos (FE) simulaciones. Además, se ha realizado un Diseño de Experimentos (DoE) usando matrices ortogonales de Taguchi y un Análisis de Varianza (ANOVA) con el fin de estudiar la influencia de cada parámetro para minimizar la fuerza de extrusión necesaria para realizar el proceso y el daño en el extruido. Los resultados muestran que la distribución del daño en el anillo exterior no sigue ningún patrón, apareciendo en diferentes regiones de forma aleatoria.

Sin embargo, en el núcleo el daño siempre ocurre en la región fuera del contorno del anillo, donde alcanza el valor máximo y luego permanece estacionario durante el resto del proceso. En el núcleo, el daño aumenta con el factor de fricción y es independiente de la reducción de la sección transversal para semi-ángulos de matriz bajos (15°) y alcanza los valores máximos para semi-ángulos de matriz de 60° . En ambos casos, daño y fuerza de extrusión, el factor más relevante para obtener valores mínimos es el semi-ángulo de la matriz.

This paper investigates the extrusion force and damage induced during an extrusion process to manufacture bimetallic cylinders combining a external ring of titanium alloy (Ti6Al4V) with a magnesium alloy core (AZ31B). A study has been carried out to determine the damage factor distribution through the extrusion process and how this factor together with the extrusion force are influenced by the manufacturing parameters (extrusion ratio, friction and die semi-angle) by means of finite element (FE) simulations. Also, a Design of Experiments (DoE) using Taguchi's orthogonal arrangements and an Analysis of Variance (ANOVA) have been performed in order to study the influence of each parameter to minimize the extrusion force needed to perform the process and the damage in the extrudate. The results show that damage distribution in the external ring does not follow any pattern, appearing in different region in a random way. However, in the core the damage always occurs in the region outside the contour of the ring, where it reaches the maximum value and afterwards remains stationary during the rest of the process. In the core, damage increases as friction factor does and it is independent of the cross-section reduction for low die semi-angles (15°) and reaches the maximum values for 60° die semi-angle. In both cases, damage and extrusion force, the more relevant factor to obtain minimum values is the die semi-angle.

4.2.3. Resumen de las aportaciones

En esta publicación el doctorando estuvo a cargo de la definición y desarrollo de los modelos numéricos, la revisión del estado del arte, la metodología empleada y la escritura del artículo. La conceptualización, el análisis formal y la investigación fueron realizadas en conjunto por el doctorando y sus directores de tesis. Por último, las labores de revisión y edición del artículo, administración de recursos del proyecto, supervisión y adquisición de fondos fue llevada a cabo por los directores de tesis.

Analysis of AZ31B – Ti6Al4V bimetallic extrusion by numerical simulation and Taguchi method

D Fernández¹, A Rodríguez¹ and A M Camacho¹

¹ Department of Manufacturing Engineering, Universidad Nacional de Educación a Distancia (UNED), 28040 Madrid, Spain

*Corresponding author: dfernande146@alumno.uned.es

Abstract: This paper investigates the extrusion force and damage induced during an extrusion process to manufacture bimetallic cylinders combining a titanium alloy sleeve (Ti6Al4V) and a magnesium alloy core (AZ31B). A study has been carried out to determine the damage factor distribution through the extrusion process and how this factor together with the extrusion force are influenced by the manufacturing parameters (extrusion ratio, friction and die semi-angle) by means of finite element (FE) simulations. Also, a Taguchi Design of Experiments (DoE) and an Analysis of Variance (ANOVA) have been performed in order to study the influence of each parameter to minimize the extrusion force needed to perform the process and the damage in the extrudate. The results show that damage distribution in the sleeve does not follow any pattern, appearing in different region in a random way. However, in the core the damage always occurs in the region outside the contour of the sleeve, where it reaches the maximum value and afterwards remains stationary during the rest of the process. In the core, damage increases as friction factor does and it is independent of the cross-section reduction for low die semi-angles (15°) and reaches the maximum values for 60° die semi-angle. In both cases, damage and extrusion force, the more relevant factor to obtain minimum values is the die semi-angle.

Keywords: Extrusion, Bimetallic, Finite element method, Damage, Forces.

1. Introduction

Advanced joining and assembly processes of parts with different materials have gained relevance during last years, attracting great interest in sectors such as aerospace and transport due to the possibility of weight reduction which involves saving fuel, reduction of the environmental impact, and, in the case of aerospace industry, to increase the payload in aircraft and satellites. Another interesting aspect of using multi-materials in manufacturing is the possibility to customize the mechanical and thermal properties of the final part to the specific in-service requirements. For all these reasons, multi-material forming and assembly processes were identified as critical research and development area of the EU Horizon 2020 work program 2018–2020 [1].

Co-extrusion process is typically used to produce multi-material cylinders, which will be used as billets to manufacture complex shape components. This is a very complex thermo-mechanical process because of the high pressures and temperatures generated in the interface of both materials due to the plastic deformation and diffusion processes. There are several studies that involve the combination of magnesium alloys with other lightweight alloys, such as aluminium ones. An example given is Negendanka *et al.* [2] who investigated the influence of the die angle on the diffusion layer formation during coextrusion of Mg-core and Al-sleeve. Another relevant study was developed by Thirumurugan



Content from this work may be used under the terms of the [Creative Commons Attribution 3.0 licence](#). Any further distribution of this work must maintain attribution to the author(s) and the title of the work, journal citation and DOI.

et al. [3] and dealt with the manufacturing of an ZM21 magnesium alloy/CP aluminium using direct hot co-extrusion with three different extrusion ratios, while temperature and ram speed remained constant. Gall *et al.* [4] applied FEM simulations to co-extrusion process of bimetallic Al-Mg billets to produce hollow profiles. Unfortunately, there are only a few studies which combine such different metallic alloys in terms of density, yield strength or elastic modules, like Titanium and Magnesium alloys, as the one performed by Behrens *et al.* [5] where an analysis of semi-finished products made of aluminium and steel and manufactured by means of lateral angular co-extrusion (LACE) process was done. Or Fernández *et al.* [6] that determined the most relevant parameters to reduce the extrusion force during a co-extrusion process of bimetallic AZ31B-Ti6Al4V billets. In the other hand, none of these studies are focused in the damage induced in the parts during the co-extrusion process. Induced damage can affect the quality of the final part, its mechanical properties and its in-service performance. This damage estimation is very interesting to define favourable process conditions in order to avoid the combination of parameters that can lead to the onset of fracture. Particularly critical in extrusion is the defect called “chevron cracking” also known as “central burst” because it is an internal defect and it cannot be detected by visual inspection techniques. Again, there are several studies about central bursting in extrusion like the ones carried out by Parghazeh *et al.* [7] predicting the defects in rod extrusion process by means of upper bound analysis method or Reddy *et al.* [8] about obtaining an optimal die profile to reduce the central bursting in axisymmetric extrusion. All these studies are focused in single material extrusion; it is possible to find articles about quality of the final part of a multi-material component after coextrusion process like Berski *et al.* [9], but again damage distribution is barely mentioned. Special mentions are the studies about prevention of core and sleeve fracture of bimetal rods performed by Avitzur *et al.* [10,11] and safety maps in bimetallic extrusions by Alcaraz *et al.* [12] and Amigo *et al.* [13].

This study focuses on forces and damage distribution in coextrusion process of bimetallic AZ31B-Ti6Al4V billet considering the manufacturing parameters die semi-angle, extrusion relation and friction between container and sleeve. An ANOVA was performed in order to establish which of these manufacturing parameters are more significant to reduce the damage but also to minimize the extrusion force required. Cockcroft-Latham criterion [14] has been applied during simulations.

2. Materials and Methods

2.1. Materials, Geometrical Dimensions and Process Parameters

The materials used in the simulations for the bimetallic cylinders are the following:

- Magnesium alloy UNS M11311 (AZ31B) for the core.
- Titanium alloy UNS R56400 (Ti6Al4V) for the sleeve.

The election of these materials bases mainly on the difference in density of both materials, which is almost 4 times higher in titanium alloy.

Main physical and mechanical properties of both materials are listed in table 1 [15-16].

Table 1. Physical and nmechanical properties titanium alloy Ti6Al4V and magnesium alloy AZ31B.

Property	Ti6Al4V	AZ31B
Density (g/cm ³)	4.46	1.74
Tensile strength (MPa)	895	260
Yield strength (MPa)	828	200
Elastic modulus (GPa)	105 – 120	44.80
Poisson’s ratio	0.31	0.35

The initial bimetallic cylinder geometrical dimensions are presented in figure 1.

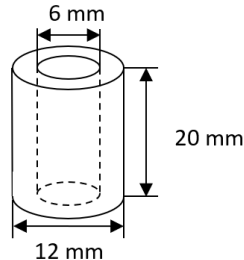


Figure 1. Bimetallic cylinder geometrical dimensions.

2.2. Finite Element Modelling

Finite element simulations have been performed using the commercial finite element software DEFORM3D[®]. In order to reduce computation time, only a quarter of the process was modelled because of axial symmetry of the problem. Sleeve and core were modelled as plastic objects while ram and container were done as rigid ones. The friction model used in all simulations was the shear friction model, which considers a constant friction factor m and it only depends on the shear flow stress k according with equation (1).

$$\tau = m \cdot k \quad (1)$$

Shear friction model is probated more realistic than Coulomb's one in modelling forming operations [17].

The method chose for estimating the damage factor is the normalized Cockcroft and Latham criterion, which is mainly used for predicting damage in metal forming operations [18] because of its simplicity and the accessibility of material data needed for the calculation. This criterion is based on the hypothesis that the accumulation of damages occurs only when at least one of the principal stress components is tensile and it establishes that fracture occurs in a ductile material when the integral in equation (2) reaches a constant value, C , for a given temperature and strain rate. DEFORM3D[®] calculates the damage values during the process by solving the integral in each step

$$\int_0^{\varepsilon_f} \left(\frac{\sigma_{max}}{\sigma_H} \right) d\varepsilon = C \quad (2)$$

where ε is the equivalent plastic strain, ε_f is the equivalent strain to fracture, σ_{max} is the maximum principal stress, σ_H is the stress according to the Huber–Misses hypothesis and C is a constant depending on the material and experimental determined. Materials AZ31B and Ti6Al4V were assumed to be isotropic during all the process. Plastic parts were meshed using 7000 tetrahedral elements and the model was validated by Fernández *et al.* [6] by comparing the simulations results for the extrusion force with the results using Johnson semi-empirical model [19,20].

2.3. Methodology

For this paper only parameters related to the tooling have been taken into account to perform the different simulations. The reason is the direct impact on the design of the container/die and, therefore on the cost of the initial investment. The values considered for temperature, ram speed as well as dimensions of the billet (see figure 1) have been taken from Fernández *et al.* [6] and are the following ones:

- Temperature = 200 °C
- Ram speed = 2 mm/s

Both temperature and ram speed as fixed as an input parameters and heat exchange among parts is allowed during simulations.

The extrusion relation, or reduction relation, has been calculated by equation (3) [21]:

$$R_E = A_0/A_f \quad (3)$$

where A_0 is the initial area and A_f is the final one.

A DoE has been performed using Taguchi method [22] to obtain an orthogonal array for three factors with two levels L4 (2³).

Finally, an ANOVA is used to calculate the signal to noise (S/N) by equation (4) taking into account the condition that the lower the better:

$$S/N = -10 \log [(1/n) \cdot (\Sigma y^2)] \quad (4)$$

where y is the observed data and n the number of observations

Table 2 shows the Taguchi's orthogonal array L4 (2³).

Table 2. Taguchi's orthogonal array for damage factor and extrusion force.

Simulation	Die semi-angle (°)	Friction	R_E	Maximum damage value	Extrusion force (kN)
1	15	0.1	1.44	2.07	82.94
2	15	0.3	1.78	2.51	122.85
3	45	0.1	1.78	0.98	130.35
4	45	0.3	1.44	0.86	164.84

3. Results and discussion

According to simulations, two different damage distributions can be found during the extrusion process. One regarding to titanium alloy sleeve and one for magnesium alloy core.

Damage distribution in the sleeve does not follow any pattern during the forming process, therefore the study will be focused on what happens in the core. Figure 2 shows damage distribution in the core.

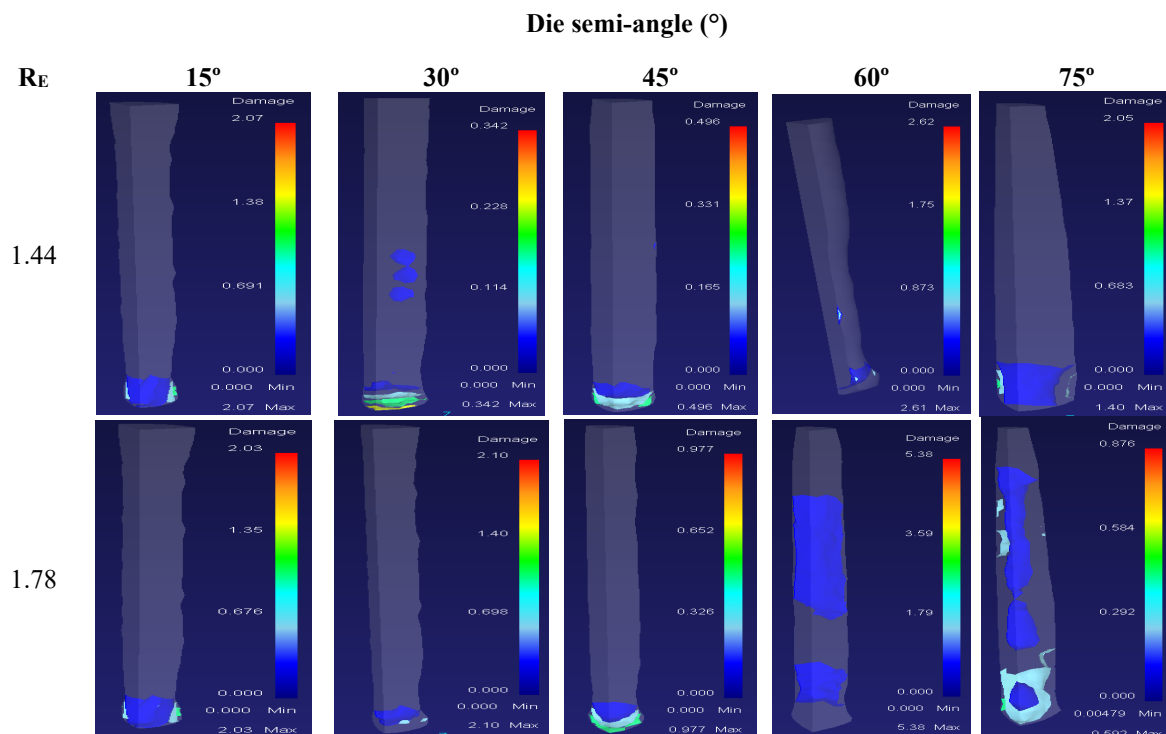


Figure 2. Damage distribution in the core for different R_E at several die semi-angles.

Contrary to what happened in the sleeve, core damage has a defined region of occurrence and its distribution in general (exceptions will be explained later) once it reaches the highest value remains stationary during the rest of the process.

Figure 3 shows the damage evolution during the extrusion process for different die semi-angles and extrusion relations.

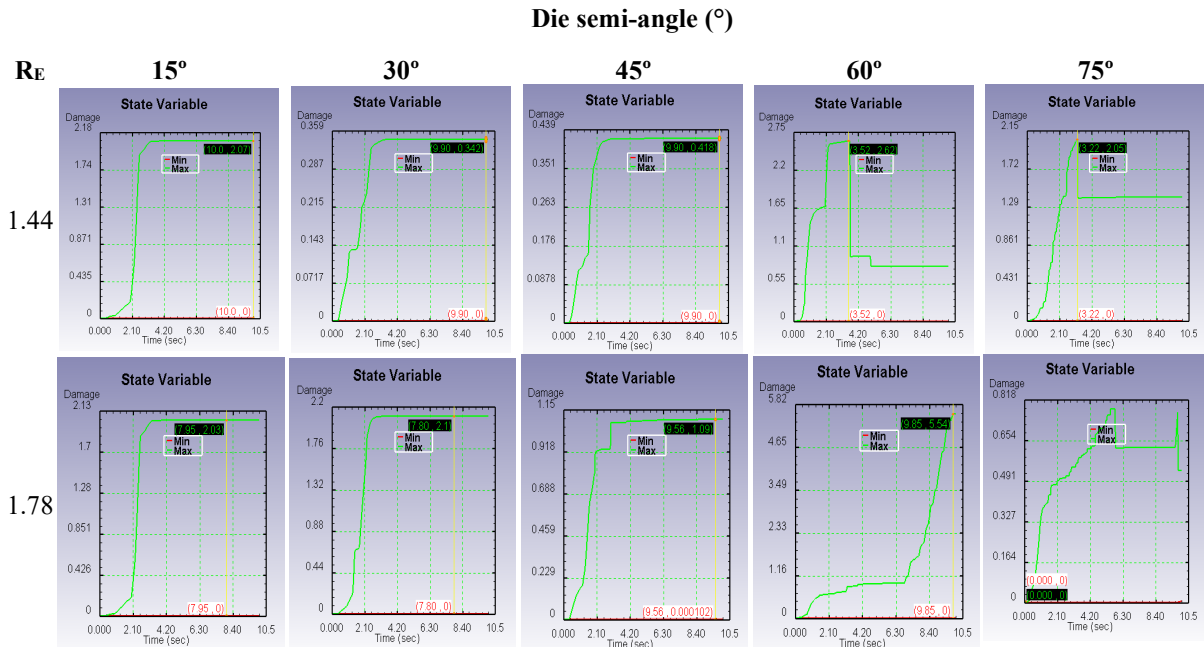


Figure 3. Core damage distribution at different die semi-angles and extrusion relations.

For low extrusion relations and die semi-angles values up to 45° , damage in the core grows very quick during the first steps until it reaches a peak where it remains constant until the end of the process. On the other hand, in this sense, 60° die semi-angle is identified as critical because from this point onwards the damage reaches a peak and an immediate descent until it reaches a permanent regime. The reason behind this can be explained by the dead zone formation for high values of the die semi-angle. Particularly interesting is the case for 60° and $R_E = 1.78$ in figure 2 where the damage increases exponentially, which can mean the formation of the chevron crack. Damage is associated to stress states, mainly because the hydrostatic stress as it's explained in the hydrostatic stress criterion (HSC) that says "whenever hydrostatic stress at a point on the centre line in the deformation zone becomes zero and it is compressive elsewhere, there is a fracture initiation leading to central burst" [8]. Figure 4 shows the damage variation depending of the extrusion relation (R_E) for each die semi-angle.

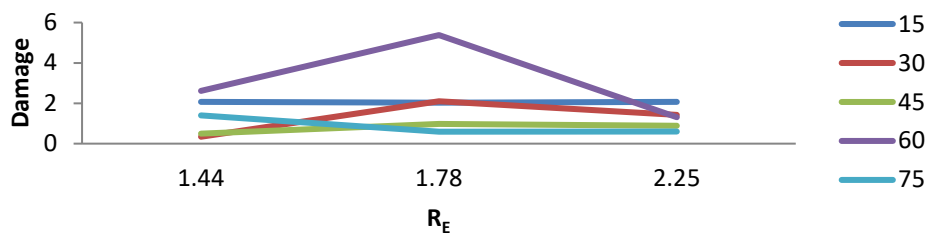


Figure 4. Damage versus extrusion relation at different die semi-angles (°).

This graph reinforces the importance of 60° die semi-angle as critical one. For very low semi-angles, damage factor remains constant independent of extrusion relation, as is the case for 15° . There is a pattern of increase of damage factor with the increase of extrusion relation for semi-angles 30° and 45° . However, from 60° onwards there is no clear relation between damage factor and extrusion relation, as it was mentioned before the most likely cause is the formation of the dead zone for these semi-angle values. Finally, there is not too much variation in damage factor at medium/high die semi-angles for high extrusion relation values. A safety area has been established in figure 5 to ensure that damage values remain as low as possible during the extrusion process.

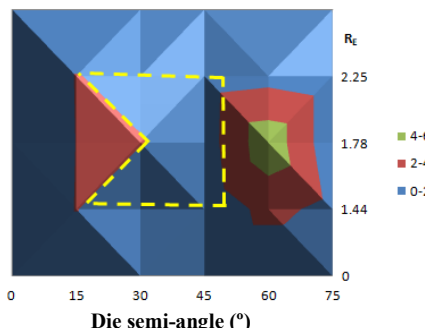


Figure 5. Damage map.

Regarding the influence of the shear friction on the core damage factor, figure 6 shows that, although damage increases as the friction factor does, there are three different regions with their own behaviour. In region I damage increases linearly with a slope of 2, while region II damage remains practically constant and in region III damage increases exponentially reaching between three and four times the values obtained in region I.

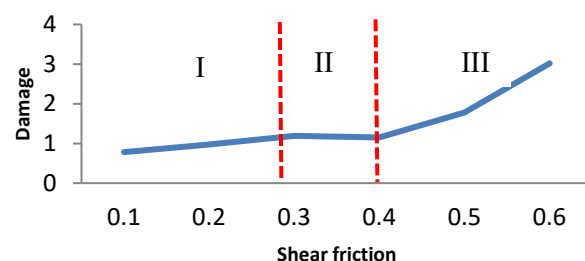


Figure 6. Damage distribution at different shear friction values.

Finally, after applying ANOVA to the orthogonal array showed in table 2, it can be concluded that the most relevant factor to obtain a low damage factor in the core and requires low values for the extrusion force is the die semi-angle, as table 3 and 4 shows.

Table 3. Taguchi's results for the average values of the damage factor and extrusion force.

Level	Damage Factor			Extrusion Force		
	Die semi-angle	Friction	R _E	Die semi-angle	Friction	R _E
1	2.29	1.52	1.46	-7.24	-4.18	-4.00
2	0.92	1.68	1.74	-0.73	-5.46	-5.60
Delta	1.37	0.16	0.28	7.96	1.28	1.60
Classification	1	3	2	1	3	2

Table 4. Taguchi's results for the noise signal values of the damage factor.

Level	Damage Factor			Extrusion Force		
	Die semi-angle	Friction	R _E	Die semi-angle	Friction	R _E
1	-7.24	-4.18	-4.00	-40.41	-40.77	-42.31
2	-0.73	-5.46	-5.60	-43.44	-43.25	-42.05
Delta	7.96	1.28	1.60	3.03	2.48	0.26
Classification	1	3	2	1	2	3

4. Conclusions

According with the results presented in this paper, a robust FE model for AZ31B – Ti6Al4V bimetallic co-extrusion has been used to estimate the induced damage and the extrusion force during the process for different manufacturing parameters while ram speed and temperature are maintained as it is explaining in section 2.3 Methodology. Sleeve damage has been proved as random with no clear zone of appearance or a pattern for the appearance of maximum or minimum values. Core damage is focus in the region outside the contour of the sleeve and for low/medium extrusion relations and angles below of 60° when the damage reaches its maximum value it remains stationary for the rest of the process. Die semi-angle of 60° has been identified as critical because from this value the formation of the dead zone causes random distribution of the damage and in one case (60° and a extrusion reduction of 1.78) a possible chevron crack defect. For low die semi-angles as 15°, damage factor is independent of the extrusion relation. For high extrusion relations damage factor has no significant variation at die semi-angles above 15°. Regarding friction, damage factor increases as the friction coefficient does, reaching a stationary state from values between 0.3 and 0.4. For friction values higher than 0.4 the damage increases exponentially. Finally, the most relevant manufacturing parameter to reduce the damage factor in the core is the die semi-angle as well as to obtain minimum values for the extrusion force which are very useful to reduce the power requirement of the machinery to invest in.

The results of this paper can potentially be used to improve the quality of the extrudates and, along with the use of lightweight materials, can contribute to sustainable production approaches by reducing fuel consumption of the vehicles made of them and thus the environmental impact.

Acknowledgements

This work was developed within the framework of the Doctorate Program in Industrial Technologies of the UNED and was funded by the Annual Grants Call of the E.T.S.I.I. of the UNED via the project References 2021-ICF07 and 2021-ICF08 and by the Innovation Teaching Project of the GID2016-28 focused on “Reliability and Advanced Failure Prognosis applied to the teaching of Materials Technology and Processing”.

References

- [1] European Comission Horizon 2020 Work Programme 2018-2020 5.ii. Nanotechnologies, Advanced Materials, Biotechnology and Advanced Manufacturing and Processing (https://ec.europa.eu/research/participants/data/ref/h2020/wp/2018-2020/main/h2020-wp1820-leit-nmp_en.pdf) accessed 3 March 2021
- [2] Negendanka M, Mueller S and Reimers W 2012 Coextrusion of Mg-Al macrocomposites *Journal of Material Process Technology* **212** (9) pp 1954–1962
- [3] Thirumurugan M, Anka Rao S, Kumaran S and Srinivasa Rao T 2011 Improved ductility in ZM21 magnesium-aluminium macrocomposite produced by co-extrusion *Journal of Material Process Technology* **211** pp 1637–1642
- [4] Gall S, Müller S and Reimers W 2009 Aluminum coating of magnesium hollow profiles by using the coextrusion process *Aluminum International Journal* **85** pp 63–67
- [5] Behrens B A, Klose C, Chugreev A, Heimes N, Thürer S E and Uhe J 2018 A numerical study on co-extrusion to produce coaxial aluminium-steel compounds with longitudinal weld seams

Metals **8** p 717

- [6] Fernández D, Rodríguez-Prieto A and Camacho A M 2020 Effect of Process Parameters and Definition of Favorable Conditions in Multi-material Extrusion of Bimetallic AZ31B-Ti6Al4V Billets *Appl. Sci.* **10** (22) p 8048
- [7] Parghazeh A and Haghigat H 2016 Prediction of central bursting defects in rod extrusion process with upper bound analysis method *Transactions of Nonferrous Metals Society of China* **26** (11) pp 2892–2899.
- [8] Reddy N V, Dixit P M and Lal G K 1996 Central bursting and optimal die profile for axisymmetric extrusion *J. Manuf. Sci. Eng.-Trans. ASME* **118** pp 579–584
- [9] Berski S, Dyja H, Maranda H, Nowaczewski J and Banaszek G 2006 Analysis of quality of bimetallic rod after extrusion process *Journal of Materials Processing Technology* **177** pp 582–586
- [10] Avitzur B, Wu R, Talbert S and Chou Y T 1982 Criterion of the prevention of core fracture during extrusion of bimetal rods ASME *J. Eng. Ind.* **104** p 292
- [11] Avitzur B, Wu R, Talbert S and Chou Y T 1986 Criterion of the prevention of sleeve fracture during extrusion of bimetal rods ASME *J. Eng. Ind.* **108** p 205
- [12] Alcaraz J L and Gil-Sevillano J 1996 Safety maps in bimetallic extrusions *Jornal of Materials Processing Technology* **60** pp 133–140
- [13] Amigo F and Camacho A M 2017 Reduction of induced central damage in cold extrusion of dual-phase steel DP800 using double-pass dies *Metals* **7** (9) p 335
- [14] Cockcroft M G and Latham D J 1968 Ductility and the workability of metals *J. Inst. Metals* **96** pp 33–39
- [15] Avedesiam M and Baker H 1999 *Magnesium and magnesium alloys ASM speciality handbook* (Ohio, USA)
- [16] Donachie M J 1988 *Titanium. A technical guide* ASM International (USA)
- [17] Zhang D W and Ou H 2016 Relationship between parameters in a Coulomb-Tresca friction model for bulk metal forming *Tribol. Int.* **95** pp 13–18
- [18] Stebunox S, Vlasov A and Biba N 2018 Prediction of the fracture in cold forging with modified Cockcroft-Latham criterion *Procedia Manuf* **15** pp 519–526
- [19] Johnson W 1956–1957 The pressure for the cold extrusion of lubricated rod through square dies of moderate reduction at slow speeds *Journal of the Institute of Metals* **85** pp 403–408
- [20] García-Domínguez A, Claver J, Camacho A M and Sebastián M A 2015 Comparative analysis of extrusion processes by finite elements analysis *Procedia Eng* **100** pp 74–83
- [21] M P Groover 2010 *Fundamentals of modern manufacturing* (New Jersey, USA: John Wiley & Sons)
- [22] Gisbert C, Bernal C and Camacho A M 2015 Improved analytical model for the calculation of forging forces during compression of bimetallic axial assemblies *Procedia Eng* **132** pp 298–305
- [23] Scientific Forming Technologies 2017 *DEFORM v11.2 User's Manual* Scientific Forming Technologies Corporation (Columbus Ohio, USA)

4.3. Selection of Die Material and Its Impact on the MultiMaterial Extrusion of Bimetallic AZ31B–Ti6Al4V Components for Aeronautical Applications

Los indicios de calidad de este artículo se pueden encontrar en el Apéndice C de esta Tesis Doctoral.

4.3.1. Datos de la publicación y factor de impacto

Título	Selection of Die Material and Its Impact on the MultiMaterial Extrusion of Bimetallic AZ31B–Ti6Al4V Components for Aeronautical Applications
Autores	Daniel Fernández; Álvaro Rodríguez-Prieto; Ana María Camacho
Revista	Materials
ISSN	1996-1944
Editorial	MDPI
País	Switzerland
Volumen	14 (24)
Páginas	7568
Fecha	9 de diciembre de 2021
doi	https://doi.org/10.3390/ma14247568
Factor de impacto	3.748 (2021); 5-Year Impact Factor: 4.042 (2021) Q1 (18/79) en “Metallurgy & Metallurgical engineering”

4.3.2. Resumen y copia de la publicación

Este trabajo investiga el efecto que genera la selección del material de la matriz empleada en el proceso de fabricación por coextrusión de cilindros bimétálicos formados por un núcleo de aleación de magnesio (AZ31B) y un anillo externo de aleación de titanio (Ti6Al4V). Para ello, se ha desarrollado un modelo robusto en DEFORM3D© usando el método de elementos finitos para analizar la variación en la fuerza de extrusión, la distribución del daño inducido en la pieza y el desgaste utilizando diferentes materiales en la matriz. Los resultados muestran que el material de la matriz es un factor clave que puede causar variaciones de entre el 8 % al 15 % en la fuerza de extrusión, o cambiar el efecto que tienen ciertos parámetros del proceso en las

Capítulo 4. Publicaciones

variables de salida estudiadas; por ejemplo el valor del semi-ángulo óptimo de la matriz con el que se consigue una fuerza de extrusión mínima. La distribución del daño inducido en la pieza extruida también se ve afectado por el material de la matriz, teniendo especial relevancia en el daño resultante en el núcleo. Por último, el desgaste de la matriz es el parámetro más afectado por el material de la misma, no sólo por la diferente dureza de los materiales usados, sino también por las variaciones en la presión normal y la velocidad de deslizamiento en su superficie, encontrándose valores críticos en ciertos parámetros del proceso, como por ejemplo el coeficiente de fricción, para los que la matriz no puede ser utilizada en más de una etapa de conformado debido al fuerte desgaste sufrido. Estos resultados pueden utilizarse potencialmente para mejorar la eficiencia del proceso de extrusión y la calidad de la pieza extruida que, junto con el uso de materiales ligeros, puede contribuir a una producción más sostenible.

This paper investigates the effect generated by the selection of the material of the die used in the co-extrusion manufacturing process of bimetallic cylinders compounded by a magnesium alloy core (AZ31B) and a titanium alloy sleeve (Ti6Al4V). In order to do that, a robust model in DEFORM3D© has been developed using the finite element method to analyze the variation in the extrusion force, the distribution of the induced damage in the part and the tool wear using different die materials. The results show that the material of the die is a key factor that can cause variations in the extrusion force between 8% to 15%, or change the effect that certain process parameters have on the output variables studied, for example the value of the optimum semi-angle of the die with which a minimum extrusion force is achieved. The distribution of the induced damage in the extruded part is also affected by the material of the die, having special relevance in the resulting damage in the core. Finally, the tool wear is the parameter most affected by the die material, not only due to the different hardness of the materials used, but also due to the variations in the normal pressure and the sliding speed on its surface, being critical values in certain process parameters, such as the coefficient of friction for which the die cannot be used for more than once because of the strong wear suffered. These results can potentially be used to improve the efficiency of the extrusion process and the quality of the extruded part which, together with the use of lightweight materials, can contribute to more sustainable production.

4.3.3. Resumen de las aportaciones

En esta publicación el doctorando estuvo a cargo de la definición y desarrollo de los modelos numéricos, la revisión del estado del arte, la metodología empleada y la escritura del artículo. La conceptualización, el análisis formal y la investigación fueron realizadas en conjunto por el doctorando y sus directores de tesis. Por último, las labores de revisión y edición del artículo, administración de recursos del proyecto, supervisión y adquisición de fondos fue llevada a cabo por los directores de tesis.

Article

Selection of Die Material and Its Impact on the Multi-Material Extrusion of Bimetallic AZ31B–Ti6Al4V Components for Aeronautical Applications

Daniel Fernández *, Alvaro Rodríguez-Prieto  and Ana María Camacho 

Department of Manufacturing Engineering, Universidad Nacional de Educación a Distancia (UNED), 28040 Madrid, Spain; alvaro.rodriguez@ind.uned.es (A.R.-P.); amcamacho@ind.uned.es (A.M.C.)

* Correspondence: dfernandez146@alumno.uned.es

Abstract: This paper investigates the effect that the selection of the die material generates on the extrusion process of bimetallic cylindrical billets combining a magnesium alloy core (AZ31B) and a titanium alloy sleeve (Ti6Al4V) of interest in aeronautical applications. A robust finite element model is developed to analyze the variation in the extrusion force, damage distribution, and wear using different die materials. The results show that die material is a key factor to be taken into account in multi-material extrusion processes. The die material selection can cause variations in the extrusion force from 8% up to 15%, changing the effect of the extrusion parameters, for example, optimum die semi-angle. Damage distribution in the extrudate is also affected by die material, mainly in the core. Lastly, die wear is the most affected parameter due to the different hardness of the materials, as well as due to the variations in the normal pressure and sliding velocity, finding critical values in the friction coefficient for which the die cannot be used for more than one forming stage because of the heavy wear suffered. These results can potentially be used to improve the efficiency of this kind of extrusion process and the quality of the extruded part that, along with the use of lightweight materials, can contribute to sustainable production approaches.

Keywords: bimetallic extrusion; multi-material; Ti6Al4V; AZ31B; die material; force; induced damage; wear



Citation: Fernández, D.; Rodríguez-Prieto, A.; Camacho, A.M. Selection of Die Material and Its Impact on the Multi-Material Extrusion of Bimetallic AZ31B–Ti6Al4V Components for Aeronautical Applications. *Materials* **2021**, *14*, 7568. <https://doi.org/10.3390/ma14247568>

Academic Editors: Daoguang He and Francisco Javier Trujillo Vilches

Received: 29 October 2021

Accepted: 3 December 2021

Published: 9 December 2021

Publisher's Note: MDPI stays neutral with regard to jurisdictional claims in published maps and institutional affiliations.



Copyright: © 2021 by the authors. Licensee MDPI, Basel, Switzerland. This article is an open access article distributed under the terms and conditions of the Creative Commons Attribution (CC BY) license (<https://creativecommons.org/licenses/by/4.0/>).

1. Introduction

Multi-material applications for the production of structural elements have gained relevance during recent years thanks to equal or increased performance and lower weight compared to their equivalent single material. Working with multiple materials allows designers to combine the mechanical properties of each material to the specific in-service requirements of the component. A reduction in the weight of the final parts is one of the most relevant characteristics when using these advanced materials, which is a key factor in industries such as aerospace to increase the payload in aircrafts and satellites, saving fuel and reducing the environmental impact.

There are several multi-material manufacturing applications; the most extended in aerospace industry is the use of composite material, with both a thermoplastic and a thermosetting matrix. Moreover, in recent years, additive manufacturing has been developed to reduce tooling costs and manufacture parts with shapes that cannot be achieved using conventional methods. Unfortunately, there are still limitations in the use of these multi-material manufacturing methods such as the high temperature needed for composites and the poor surface finishing of additive manufacturing, as well as the low mechanical properties and lack of airworthiness certifications to be used as primary structural parts in aircrafts.

There are several studies about multi-material formation such as Camacho et al. [1] analyzing the effect of shape factors and different assembly fit tolerances on the ductile

damage and the microstructure resultant in minting of bimetallic cylinders made of a brass UNS C38500 ring and aluminum alloy UNS A92011 center. Additionally, Zhang et al. [2] used hot rolling to manufacture an Al/Mg/Al composite with a trilaminate structure. Alcaraz and Sevillano [3] used finite element (FE) calculations to study the influence of some extrusion variables such as yield stress ratio between the two materials, location of the layers, thickness ratio, and die angle in the bimetallic tubes composed of two different alloys. Chenot et al. [4] analyzed several methods for the multi-body contact problem such as classical multi mesh approach, single-mesh technique, and Euler formulation, reviewing mechanical and numerical formulations and evaluating the elapsed CPU time for each method.

As mentioned above, bimetals allow combining the properties of dissimilar materials. Magnesium alloys have special interest in the aerospace industry due to their high strength-to-weight ratio, but they also present poor corrosion resistance which is a clear limitation for their in-service performance, as stated by Mordike et al. [5]. Titanium alloys are also widely used in aerospace applications because of their high strength-to-weight ratio, great toughness, fatigue resistance at high temperatures, and good resistance to corrosive environments; however, due to the high flow stress at elevated temperatures, these alloys are difficult to fabricate [6,7]. A common process typically used to obtain multi-material billets composed of a sleeve and a cylindrical core is coextrusion. This is a complex thermomechanical process due to the combination of plastic deformation and diffusion in the interface of both materials because of the pressure and temperatures generated. In addition, for joining dissimilar materials, this process gets more complicated because of the different flow stress characteristics of the materials. Most of the studies about multi-material processes have been carried out using aluminum alloys; for example, the study performed by Khosravifard et al. [8] proved that interface bonding can be associated with material flow velocity and local interface temperature in the Al/Cu clad bimetal rod extrusion process. Another interesting study combining Al and Cu was that by Lapovok et al. [9] on the inter-diffusion improvement in the manufacturing of Cu/Al using severe plastic deformation (SVD) methods. Berski et al. [10] analyzed the strain–stress state in bimetallic rods composed of Cu–Al using two different extrusion ratios in a conical die and in double reduction die. Kocich et al. [11] used the method of twist channel angular pressing (TCAP) to analyze the deformation behavior of an Al/Cu clad composite.

Regarding magnesium alloys in multi-material forming processes, Negendanka et al. [12] analyzed the influence of the die angle and different combining techniques of Mg-core and Al-sleeve on the diffusion layer formation. An analysis of the effect of the extrusion ratio while keeping temperature and ram speed constant in a ZM21 magnesium alloy/CP aluminum coextrusion process was performed by Thirumurugan et al. [13]. Gall et al. [14] proposed a finite element method (FEM) simulation together with experiments to study the behavior of bimetallic Al–Mg billets during the coextrusion process. Rong et al. [15] analyzed the effects on microstructure and mechanical properties of an Mg–Gd–Zn–Zr alloy manufactured by differential thermal extrusion. Moreover, some studies using the hydrostatic extrusion process to obtain bimetallic rods have been performed; Osakada et al. [16] carried out an experimental study using Cu–Al composite rods, determining that uniform deformation occurred for low extrusion ratios, whereas copper rod failed by tension at high extrusion ratios. Moreover, the critical extrusion ratio increased as the die angle decreased. Another study using hydrostatic extrusion is that by Lehmann et al. [17] who analyzed the mechanical strength and fracture properties of hydrostatic coextruded Al–Mg compounds. Nevertheless, there are not too many studies combining different metallic alloys such as titanium and magnesium alloys in terms of density, tensile strength, yield strength, and elastic modulus. Behrens et al. [18] performed a lateral angular coextrusion (LACE) to product semifinished products consisting of aluminum and steel, while Fernández et al. [19] analyzed the effect of different extrusion process parameters and determined the most relevant using the Taguchi method. Regarding the LACE process, a very complete study was performed by Thürer et al. [20] to manufacture coaxially reinforced hollow

profiles made of aluminum alloy EN AW-6082 and AISI5120 case-hardening steel 20MnCr5, including the results of shear compression test in the hybrid profiles to measure the shear strength of the bonding area.

This study continues the work mentioned by Fernández et al. [19], but taking into account the material of the die as the driven factor to analyze the effect of the remaining extrusion parameters on the extrusion force, damage, and wear distribution.

2. Materials and Methods

2.1. Materials, Geometrical Dimensions, and Process Parameters

The bimetallic cylinders used in the simulations were made of a titanium alloy UNS R56400 sleeve and a magnesium alloy UNS M11211 core (see Figure 1). These two alloys are widely used in aerospace industry due their excellent properties. The most commercial designations for these alloys (Ti6Al4V and AZ31B, respectively) are used henceforth.

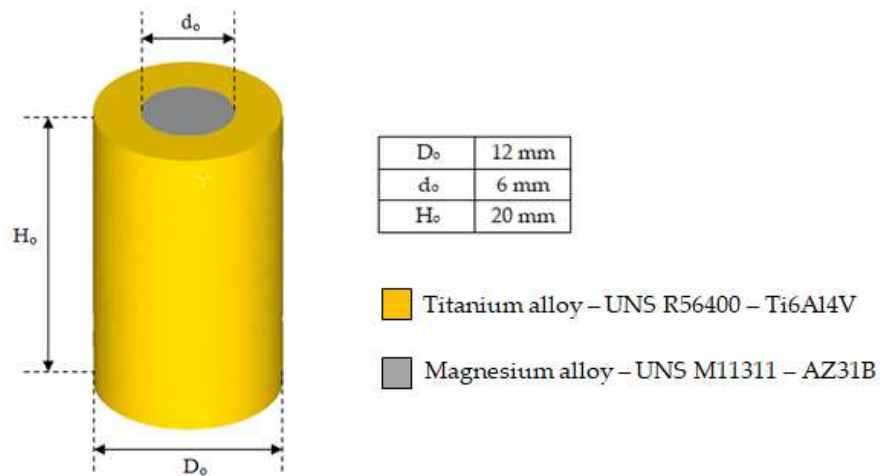


Figure 1. Bimetallic cylinder sketch and initial geometrical dimensions.

The parameters of the extrusion process considered in this work are presented in Figure 2.

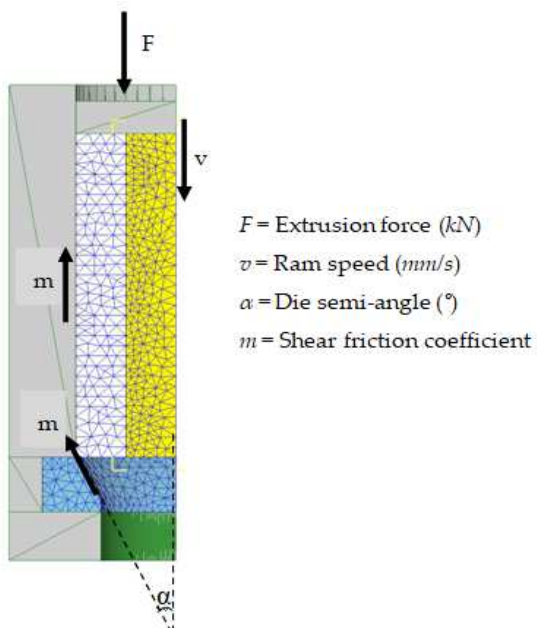


Figure 2. Extrusion process schema.

The chemical compositions were extracted from Daniel et al. [19]; the physical and mechanical properties for AZ31B were obtained from Avedesiam et al. [21], while those for Ti6Al4V were obtained from Donachie [22].

The chemical composition of each steel used to model the die and a comparison of their physical and mechanical properties are listed in Tables 1 and 2. Physical and mechanical properties were extracted from Davis et al. [23], and chemical compositions of H13, 25CrMo4, 53 HRC, AISI3310, and AISI316 were obtained from [24–29], respectively.

Table 1. Chemical composition of die steels.

Material	C (wt.%)	Mn (wt.%)	Si (wt.%)	P (wt.%)	S (wt.%)	Cr (wt.%)	Mo (wt.%)	Ni (wt.%)	N (wt.%)
AISI316	0.08	2	0.75	0–0.045	0.03	16–18	2–3	10–14	0.10
H13	0.32–0.45	0.2–0.5	0.80–1.20	-	-	4.75–5.50	1.10–1.75	0.30 max	-
25CrMo4	0.22–0.29	0.60–0.90	0.10–0.40	-	-	0.90–1.20	0.15–0.30	-	-
AISI3310	0.1	0.45	0.26	-	-	1.51	0.06	3.39	-
53HRC	0.99	0.39	0.16	-	-	1.4	-	1.4	-

Table 2. Physical and mechanical properties of die steels.

Property	AISI316	H13	25CrMo4	AISI3310	53HRC
Density (g/cm ³)	8.03	7.78	7.85	7.83	7.81
Tensile strength (MPa)	550	1990	670	992	1866
Yield strength (MPa)	240	1650	435	579	1800
Elastic modulus (GPa)	210	210	205	200	210
Poisson's ratio	0.3	0.3	0.3	0.3	0.3

Material selection criteria for die components included Young's modulus, hardness of the workpiece material, and availability on the market.

- AISI316 is one of the most used austenitic stainless steels in the world, showing improvements in the corrosion and high-temperature resistance due to the addition of molybdenum.
- H13 is a chromium hot work tool steel, widely used in hot and cold working applications. This tool steel stands out for its high toughness and fatigue resistance.
- 25CrMo4, also known under the classification AISI4130, is a versatile alloy with good overall combination of strength, toughness, fatigue strength, and corrosion resistance. The normal applications for this steel are fittings with a large cross-section and high-stress working conditions such as shafts and gear wheels; it was selected for this study due to its low hardness (48 HRC).
- AISI3310 steel is commonly used in components with a large cross-section requiring high toughness and core strength, such as bearings and gear applications. This was the steel with a high percentage of Ni and the highest hardness (58.22 HRC) in the present study.
- AISI52100 (53HRC) is a high-carbon chromium steel. Because of its combination of strength, hardness, and workability, this steel is particularly useful in bearings, mill rolls, and vehicle parts. This steel was chosen in this study for its high modulus of elasticity (210 GPa) staying constant independently of the temperature.

2.2. Finite Element Modeling

Finite element simulations were performed using the commercial finite element program DEFORM3D© v11.2 [30].

The ram, container, holder, and blocker (extrusion tooling) were modeled as rigid objects. The bimetallic cylinders were modeled as an assembly between two plastic objects (sleeve and core). The die was modeled as an elastic object.

In order to reduce the computation time and the size of the database files, taking into account the axial symmetry of the coextrusion process, only one-quarter of the problem was modeled. Figure 3 shows the whole setup for the simulation.

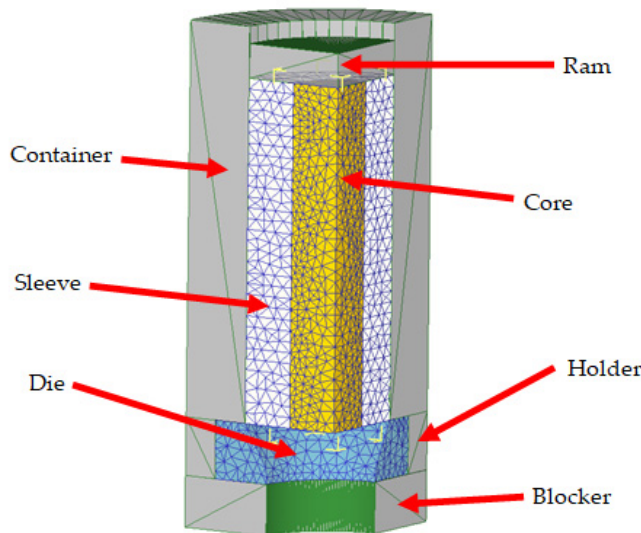


Figure 3. Object set up for simulations.

Considering the heat transfer across the billet, die, and the extrusion tooling, all parts were meshed with tetrahedral elements. The heat transfer coefficient between sleeve and core and between sleeve and die was set to $11 \text{ N}/(\text{s} \cdot \text{mm} \cdot ^\circ\text{C})$, that between extrusion tooling elements and die was set to $5 \text{ N}/(\text{s} \cdot \text{mm} \cdot ^\circ\text{C})$, and that between billet/die/tooling and air was set to $0.02 \text{ N}/(\text{s} \cdot \text{mm} \cdot ^\circ\text{C})$.

The contact conditions among the different objects were also defined. Rigid and elastic objects were considered “masters” (those that deform) and the plastic objects were considered “slaves” (those that are deformed). In the case of the sleeve and core interaction, where both objects are plastic, the titanium alloy was defined as the “master” and the magnesium alloy was defined as the “slave”; due to the assumption that the fitting between these two parts was performed with interference, the friction took the maximum value of 1. In addition, sticking and non-separable conditions were also defined for these objects.

Regarding the die, to avoid movement with respect to the rigid parts, the sticking condition was also defined.

The friction model used in the simulations was the shear model as the range of friction coefficients used in this study was from 0.1 to 0.7; according to Rowe [31] and Leu et al. [32], the upper limit of the Coulomb friction coefficient is 0.577 for von Mises and 0.5 for Tresca criteria. Moreover, this friction model is typically used in metal formation analysis. Materials AZ31B, Ti6Al4V, and die steels were assumed to be isotropic throughout the process.

The normalized Cockcroft and Latham criterion [33] was used to evaluate the damage factor on the extrudate. This method is widely used to predict the damage, mainly in cold formation processes, because of its simplicity and very little material data required for calculations. This criterion is based on the hypothesis that the accumulation of damages occurs only when at least one of the principal stress components is tensile, as represented in Equation (1).

$$\int_0^{\varepsilon_f} \left(\frac{\sigma_{max}}{\sigma_H} \right) d\varepsilon = C, \quad (1)$$

where ε is the equivalent plastic strain, ε_f is the limit fracture strain, σ_{max} is the maximum principal stress, σ_H is the stress according to the Huber–Mises hypothesis, and C is the parameter that is usually called the material constant, and its value is experimental determined.

Damage is associated with stress states, mainly because of hydrostatic stress; according to the hydrostatic stress criterion (HSC), “whenever hydrostatic stress at a point on the center line in the deformation zone becomes zero and it is compressive elsewhere, there is a fracture initiation leading to central burst” [34–36].

The calculus of the wear in the die was performed using Archard’s wear model [37–39]. In this model, the wear depth is directly proportional to the wear coefficient (K), the interface pressure (P), and the sliding velocity (v) between die and billet, and it is inversely proportional to the die hardness (H), according to Equation (2).

$$W = \int K \cdot \frac{P^a \cdot v^b}{H^c} \cdot dt, \quad (2)$$

where a , b , c , and K are experimentally calibrated coefficients; a , b are commonly taken as 1, and $c = 2$ for tool steels. K was taken as 2×10^{-5} .

However, die material behavior (such as hardness and wear coefficient) will change significantly with varying temperature over 400 °C. Therefore, in order to avoid this effect and to use modified Archard’s wear theory to take into account the variations in the values of K and hardness with the temperature, the maximum working temperature used in this study was 300 °C.

2.3. Methodology

The aim of this study was to establish if the material of the die significantly affects to the extrusion force and damage factor values, as well as if their behavior with the different extrusion parameters changes with the material of the die.

The parameters affecting the extrusion process taken into account for this study were the following:

- Ram speed (mm/s) and temperature (°C) as process parameters.
- Die semi-angle (°), shear friction factor, and extrusion ratio (A_0/A_f) as tool parameters.
- Shape factor (H_0/D_0) and diameter ratio (D_0/d_0) as geometric parameters.
- Die material.

H_0 is the initial height of the billet, D_0 is the initial external diameter of the sleeve, d_0 is the initial diameter of the core, and A_0 and A_f are the initial and final area, respectively, of the cross-section of the billet.

The behavior of die wear has not yet been investigated during a multi-material extrusion process. As modeling of the wear was done according to Archard’s model, the parameters taken into account were ram speed, temperature, and friction.

Ram speed may influence the sliding velocity, which is a factor to calculate wear according to Archard’s model; furthermore, an excessive ram speed may cause surface defects to the extrudate such as over-burning, adhesion, and gravure.

Temperature is not in Archard’s wear model [38,39]. The range of temperature considered in this study was below 400 °C; therefore, the friction coefficient and the hardness would remain unaffected. However, the temperature has a direct influence on the metal plasticity, flow resistance, and flow stress curves, and these factors may impact in the die wear because they may affect the normal pressure and sliding velocity.

Although Archard’s wear model does not include direct friction-related factors, the friction parameter has an influence on the material flow and stress distribution of the extrusion die, which may have certain effects on the wear factor.

The design of experiments (DOE) to evaluate the effect of each parameter on the extrusion force and damage factor is shown in Table 3 for the range of extrusion parameters taken in the simulations and in Table 4 for the baseline values of the simulations.

The DOE methodology in this study consisted of varying the parameter to be studied while holding the remainder to their baseline values. Each set of simulations for each parameter was repeated while changing the die material to analyze the behavior of the extrusion force and damage factor with respect to each parameter.

Table 3. Range of extrusion parameters.

Extrusion Parameters	Level					
	1	2	3	4	5	6
Die semi-angle (°)	15	30	45	60	75	90
Billet height (mm)	15	20	25	30	35	-
Core diameter (mm)	2	4	6	8	10	-
Ram speed (mm/s)	1	2	3	4	-	-
Friction	0.1	0.3	0.5	0.7	-	-
Temperature (°C)	100	200	300	-	-	-
Extrusion ratio	1.44	1.78	2.25	-	-	-

Table 4. Values of reference (baseline) for extrusion parameters.

Die Semi-Angle (°)	Billet Height (mm)	Core Diameter (mm)	Ram Speed (mm/s)	Friction	Temperature (°C)	Extrusion Ratio
Baseline	30	20	6	2	0.1	200

The methodology to evaluate the wear on the die was the same but only using ram speed, temperature, and friction as parameters of the study.

3. Results and Discussion

This section is split into three parts covering the effects of the extrusion parameters for each die material on the extrusion force, damage factor, and die wear.

3.1. Effects of the Extrusion Parameters on the Extrusion Force and FE Model Validation

After performing the simulations according to the methodology defined in Section 2.3, the results obtained for each parameter in the baseline are shown in Figure 4.

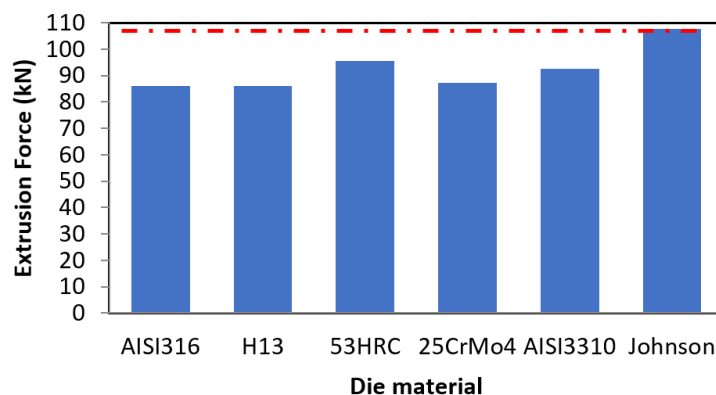


Figure 4. Extrusion force comparison among the different die materials for the baseline conditions and comparison with semi-empirical method of Johnson for FE model validation.

A difference of 9.59 kN can be observed between the highest (53HRC) and the lowest (AISI316) value of the extrusion force, which represents an increase of 11%.

In Figure 4, results from the semiempirical model of Johnson, described in the work of García et al. [40], were included for FE model validation. This method is commonly used as a reference in the analysis of extrusion processes and typically used as an upper limit of the extrusion force in direct extrusion. To this aim, the average yield stress was calculated considering the volume fraction of the AZ31B core and Ti6Al4V ring, proven as valid in the work of Gisbert et al. [41].

The sections below show the effect of the variation of the process parameters on the extrusion force, analyzing if the behavior is the same independent of the die material, as well as the variation in the values of the extrusion force for each material.

3.1.1. Core Diameter

A peak can be observed for the core diameter value of 4 mm; however, after this point, the values of the extrusion force decreased as the core diameter increased, converging to the values of the extrusion force for the different die materials with 8 mm core diameter. Therefore, the effect of this parameter was inversely proportional to the necessary extrusion force for all die materials, as shown in Figure 5.

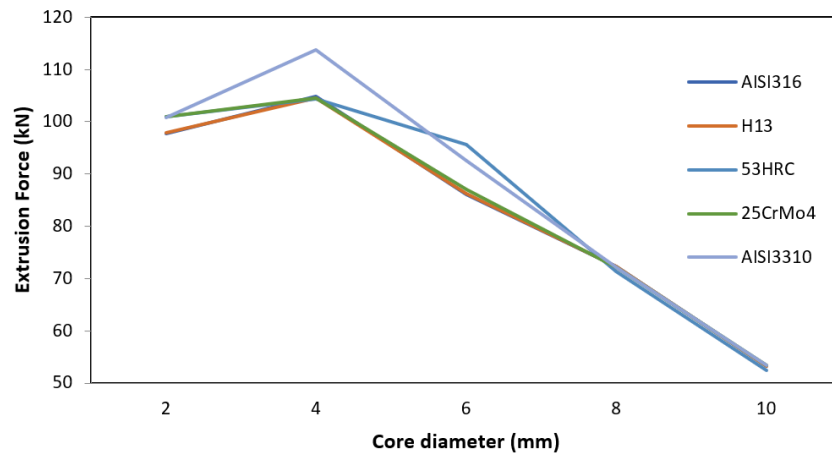


Figure 5. Effect of core diameter on the extrusion force for different die materials.

The maximum difference in the extrusion force among die materials occurred at the baseline. This can be explained by the reduction in volume of Ti6Al4V due to the increment in core diameter. As more force is needed to extrude Ti6Al4V than AZ31B due to the flow curves of each material, if the volume of Ti6Al4V is lower, the force needed will also be lower.

3.1.2. Billet Height

The behavior of the extrusion force with the billet height was completely the opposite with respect to the core diameter. As the billet height increased, the extrusion force increased.

It can be observed in Figure 6 that the biggest increment in extrusion force, measured by the slope of the line, occurred between 25 and 30 mm of billet height (shape factor between 2 and 2.5).

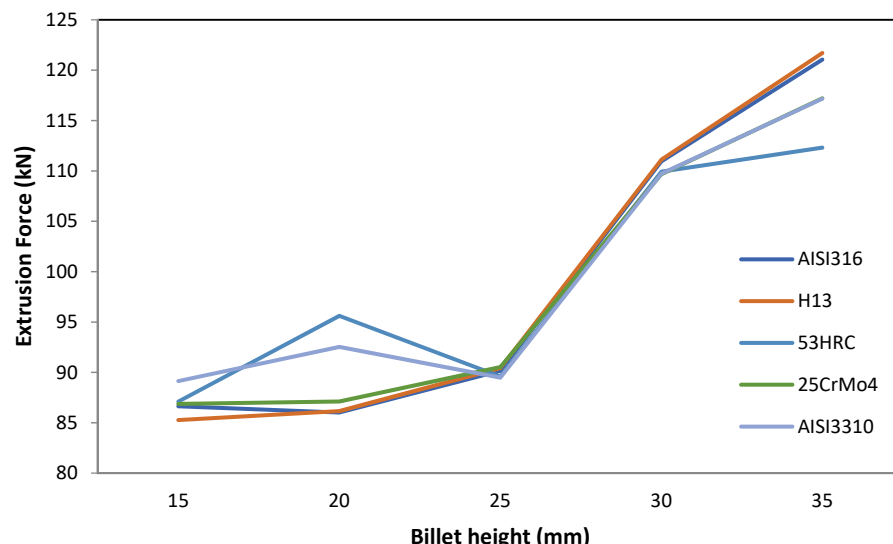


Figure 6. Effect of billet height on the extrusion force for different die materials.

This is because, as the height increases, the contact area of the billet with the container also increases; this causes an increase in the energy component due to friction and, consequently, an increase in the total force required.

3.1.3. Friction

This parameter had the biggest impact on the extrusion force, going from 86.02 kN for the lowest friction factor to 309.40 kN for the highest one. The behavior was similar to the billet height, and the biggest difference in extrusion force among die materials was 28.93 kN (shear friction factor of 0.5) for AISI316 and 53HRC, as shown in Figure 7.

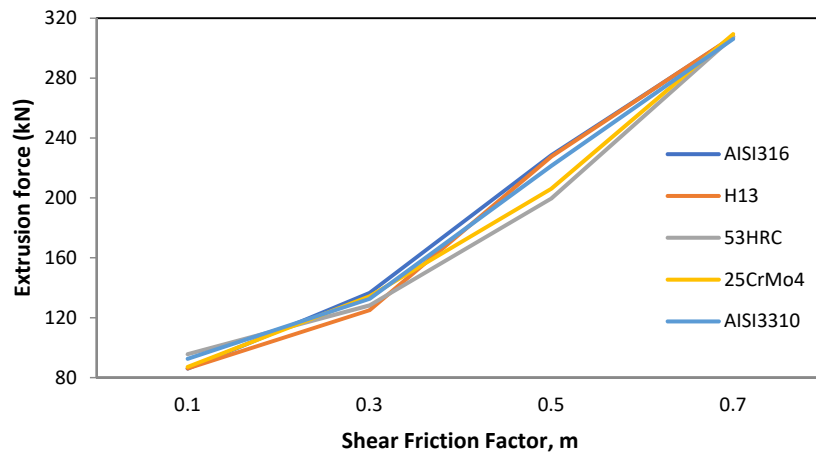


Figure 7. Effect of friction variation on the extrusion force for different die materials.

3.1.4. Extrusion Ratio

The extrusion ratio affects the final cross-section of the billet and, therefore, the shape factor. The expected result is an increase in the extrusion force with the extrusion ratio because, to get a smaller cross-section using the same semi-die angle, the distance the billet has to travel through the die is larger; thus, as with billet height, an increase in the contact area increases causes the component due to friction to increase, along with a logical increment in the extrusion force.

Figure 8 confirms this expectation and highlights the directly proportional relationship between extrusion force and extrusion ratio.

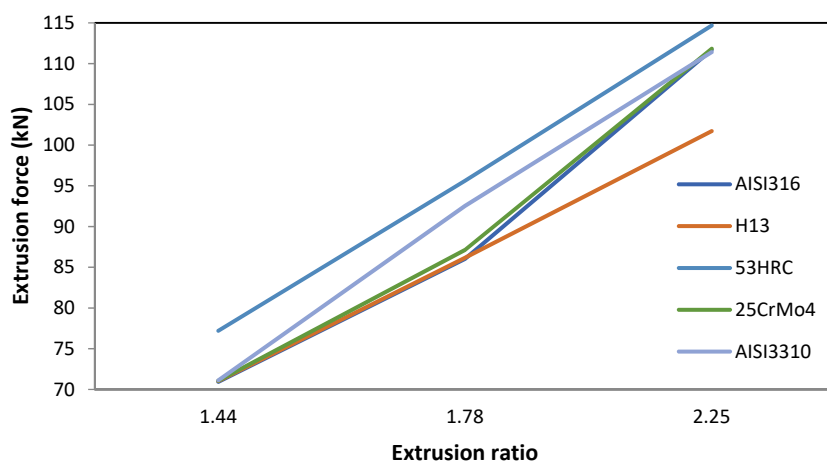


Figure 8. Effect of extrusion ratio variation on the extrusion force for different die materials.

In this case, the biggest difference in the extrusion force with the different die materials occurred at an extrusion ratio of 2.25, with 12.97 kN between 53HRC and H13. In this case, the extrusion force showed an important dependence on the die material.

3.1.5. Ram Speed

The effect of this parameter on the extrusion force is inversely proportional to the extrusion force. This phenomenon occurs because, as the ram speed increases, it also increases the temperature due to the friction in the interface die/billet; accordingly, the stress necessary to deform the billet and, thus, the extrusion force will be lower.

For ram speeds higher than 3 mm/s, the variation in the extrusion force tended to be lower than 2 kN. This is due to the compensation for the increment in temperature, which reduces the stress necessary to achieve a certain strain, and the rise in strain rate involves a higher stress to deform the material.

Figure 9 also shows that the biggest difference in extrusion force among die materials occurred for the lowest value of the ram speed (1 mm/s) between AISI310 and AISI316.

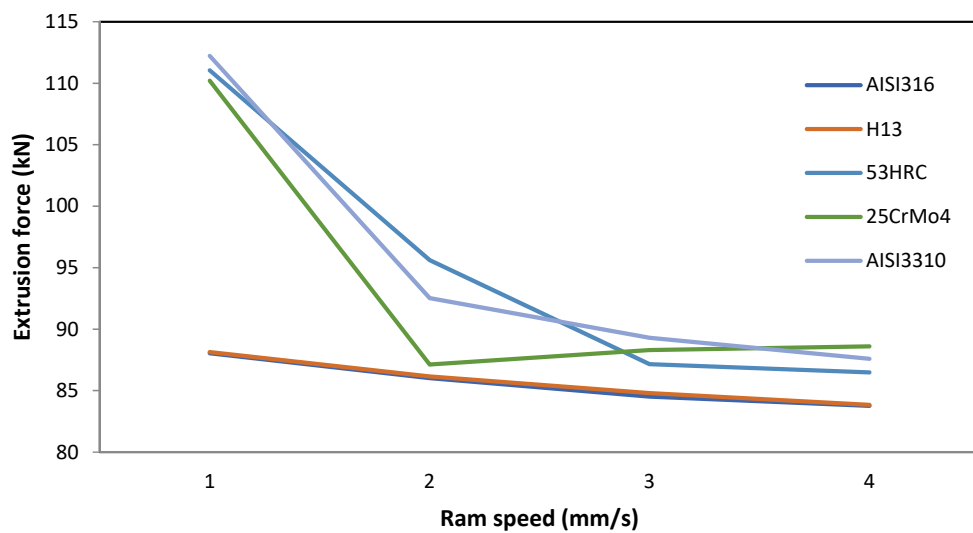


Figure 9. Effect of ram speed variation on the extrusion force for different die materials.

3.1.6. Temperature

The effect of this parameter is similar to that produced by the core diameter and the ram speed. Normally, as the temperature increases, the stress necessary to deform a part is lower in line with material flow stresses.

This effect can be observed in Figure 10, where the biggest difference in the extrusion force values among the different die materials was produced at the baseline value of 200 °C.

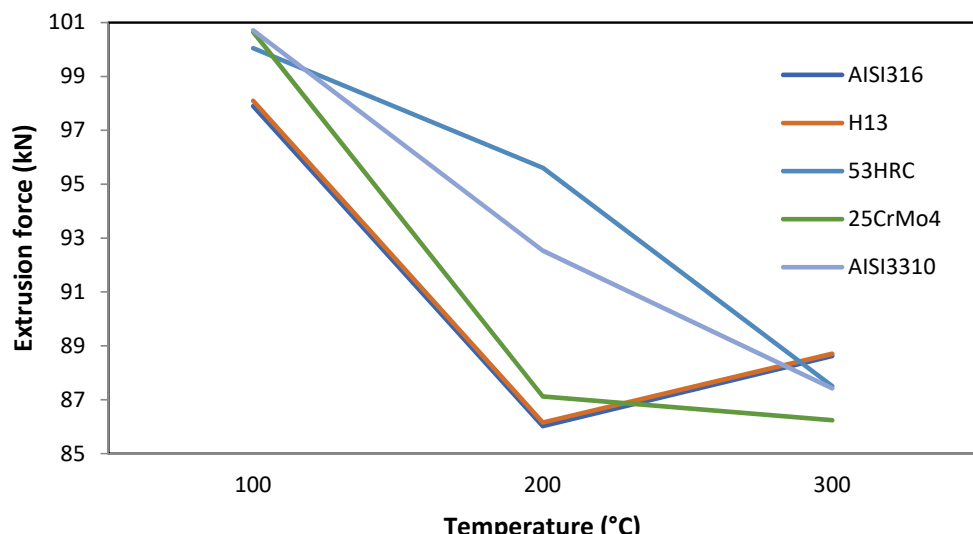


Figure 10. Effect of temperature variation on the extrusion force for different die materials.

Another important phenomenon is that, for the AISI316 and H13 die materials, the extrusion forces increased again at temperatures higher than 200 °C.

3.1.7. Die Semi-Angle

This parameter is most affected by the die material. In extrusion, there is a semi-angle at which the extrusion force needed for the process is the minimum for the same extrusion ratio. This is called the optimum die semi-angle. Thus, at lower or higher semi-angles, the extrusion force will be higher.

This is a matter of balance between the area of contact and the abrupt change in cross-section and, therefore, energy contributions due to friction and internal distortion. For low semi-angles, the area of contact to achieve a certain reduction in area is larger but the change in cross-section occurs more gradually. For higher semi-angles, the opposite is true, producing an abrupt change in the cross-section for a very short distance traveled over the die.

Figure 11 shows that the die optimum semi-angle ranged from 15° for 53HRC to 45° for AISI310.

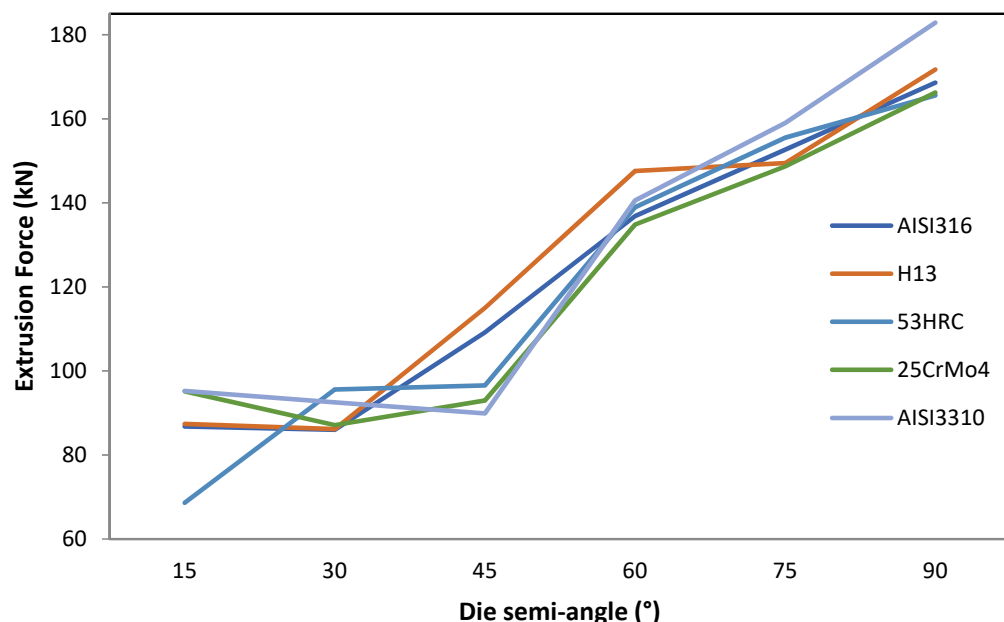


Figure 11. Effect of die semi-angle variation on the extrusion force for different die materials.

It is important to note that the optimum die semi-angle value depended on the material of the die. The greatest deviation of the extrusion force occurred for a die semi-angle of 15° between AISI3310 and 53HRC (26.61 kN).

3.2. Effects of the Extrusion Parameters on the Damage Factor

Another important aspect that can be analyzed by finite element analysis is the damage induced in the workpiece as a consequence of the formation process. This factor is mainly related to the quality of the extrudate since high values of damage can lead to fracture of the part during the component service.

The study of the effect of the different extrusion parameters on the damage factor focused on the core of the billet. After performing the simulations, the results obtained showed that the damage was spread over the entire surface of the ring, whereas the core damage was mainly centered on the same area, extending to the rest of the core only under certain conditions. This area can be observed in Figure 12.

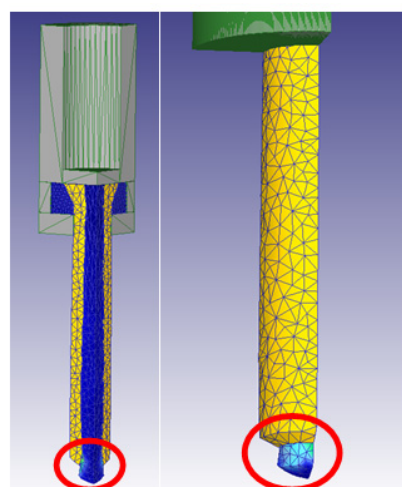


Figure 12. General damage location in the core of the billet.

As all the damage was concentrated in the bottom part of the extrudate, it could be easily removed from the final part. Nevertheless, there were some configurations in which the damage was all over the extrudate. The main parameters mediating this effect were die semi-angle, extrusion ratio, and billet height, whereas parameters such as temperature, ram speed had hardly any influence on the damage.

3.2.1. Die Semi-Angle

This was the most important parameter regarding the damage factor because there was a semi-angle at which the damage spread through the whole extrudate. This critical semi-angle value varied depending on the die material, as can be observed in Figures 13 and 14 for the core and the ring plus core, respectively.

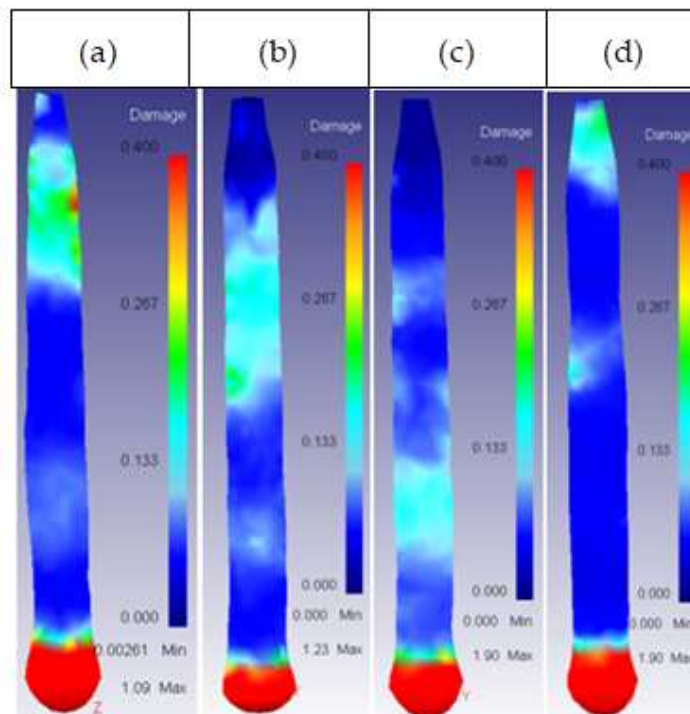


Figure 13. Damage distribution in the core: (a) 53HRC $\alpha = 75^\circ$; (b) 25CrMo4 $\alpha = 75^\circ$; (c) AISI3110 $\alpha = 75^\circ$; (d) H13 $\alpha = 90^\circ$.

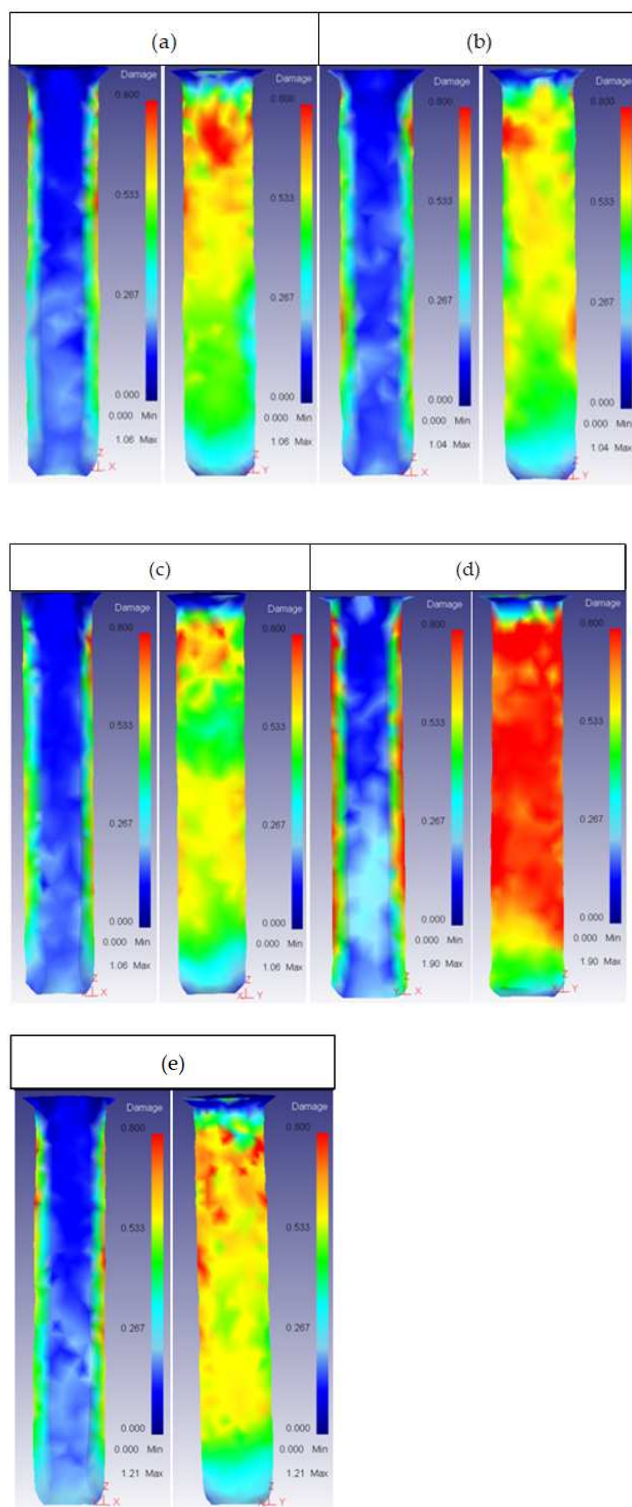


Figure 14. Damage distribution in the ring (inner and outer part): (a) 25CrMo4 $\alpha = 60^\circ$; (b) 53 HRC $\alpha = 60^\circ$; (c) AISI316 $\alpha = 60^\circ$; (d) AISI3110 $\alpha = 75^\circ$; (e) H13 $\alpha = 60^\circ$.

For angles higher than 60° , the damage started increasing in both the ring and the core, spreading across the extrudate. This could cause a crack, affecting the working life of the part. As the extrusion force also increased from 45° in all die material cases, it is recommended to keep the semi-angle between 15° and 45° to obtain the best results.

Lastly, it is important to realize that the damage growth in the ring was not the same in inner and outer part. The die semi-angle barely affected the damage in the inner part.

3.2.2. Extrusion Ratio

The extrusion ratio had a big influence on the damage factor of the ring. In general, for low values of extrusion ratio (1.44), the damage in the inner face of the ring was highest, as shown in Figure 15.

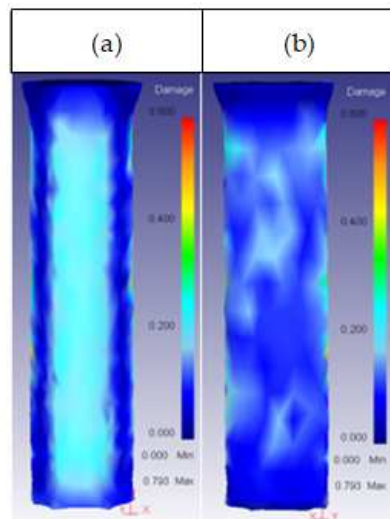


Figure 15. Damage distribution in inner (a) and outer (b) part of the ring for 53HRC $R_E = 1.44$.

For the outer part of the ring, the effect was opposite, whereby increasing the extrusion ratio increased the damage, as shown in Figure 16.

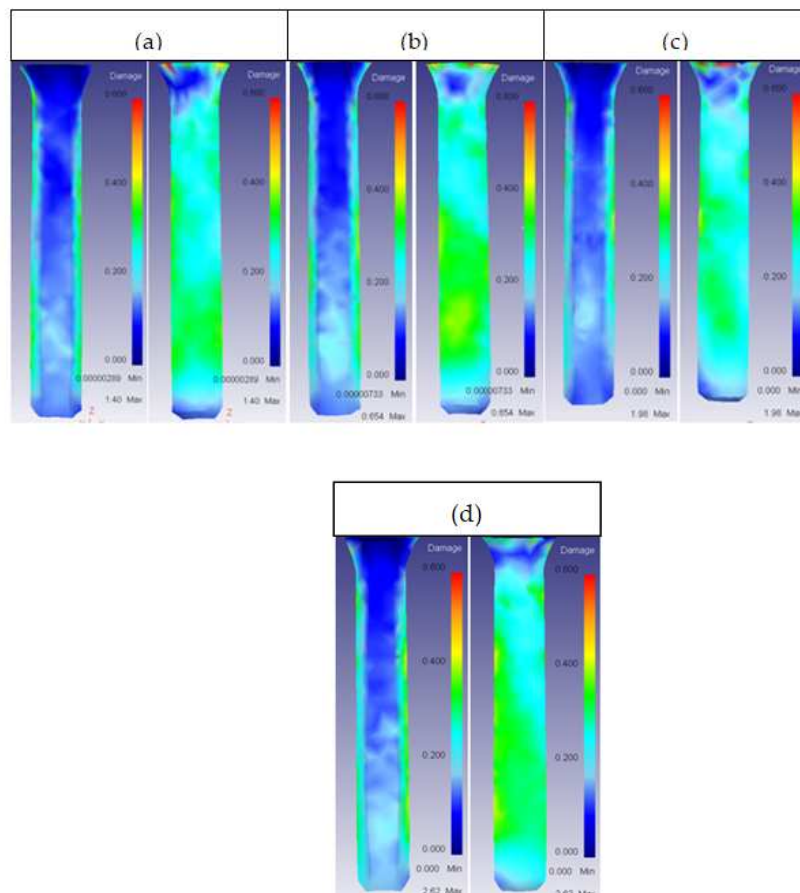


Figure 16. Damage distribution in inner and outer part of the ring: (a) 25CrMo4 $R_E = 2.25$; (b) 53HRC $R_E = 2.25$; (c) AISI3310 $R_E = 2.25$; (d) H13 $R_E = 2.25$.

In the core, the damage generally extended across the surface in contact with the ring, as shown in Figure 17.

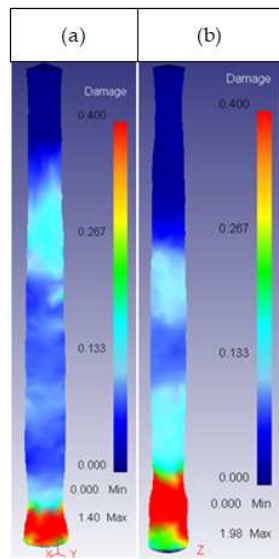


Figure 17. Damage distribution in the core: (a) 25CrMo4 $R_E = 2.25$; (b) AISI3310 $R_E = 2.25$.

3.2.3. Billet Height

This parameter had an effect on the core damage only for high values of height, with a 2.5 shape factor. At this value, the damage started spreading across the core surface, as shown in Figure 18.

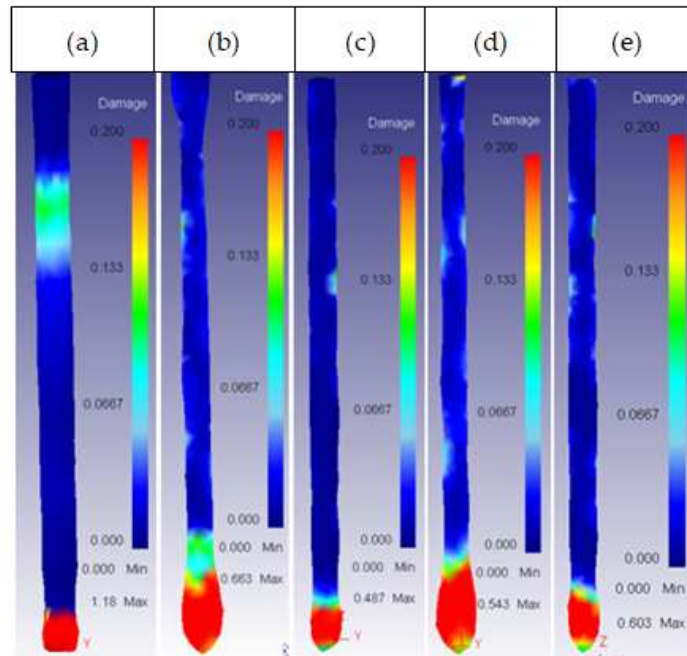


Figure 18. Damage distribution in the core: (a) 25CrMo4 $H_o = 30$ mm; (b) 53HRC $H_o = 35$ mm; (c) AISI316 $H_o = 35$ mm; (d) AISI3110 $H_o = 35$ mm; (e) H13 $H_o = 30$ mm.

In the ring, this parameter most affected the inner part, reaching a maximum damage distribution at 20 mm height; from this point, the damage distribution decreased with the increase in height, as shown in Figure 19.

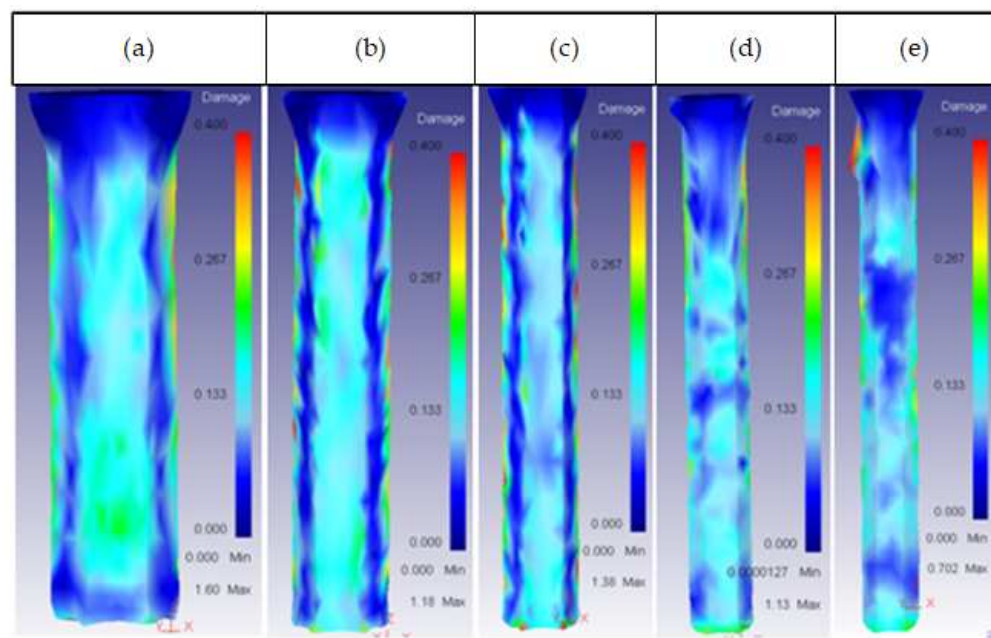


Figure 19. Damage distribution in the inner part of the ring: (a) 25CrMo4 $H_o = 15$ mm; (b) 25CrMo4 $H_o = 20$ mm; (c) 25CrMo4 $H_o = 25$ mm; (d) 25CrMo4 $H_o = 30$ mm; (e) 25CrMo4 $H_o = 35$ mm.

3.2.4. Friction

This parameter only had an effect on the ring part of the billet as it was the only part in direct contact with the container and the die, where the friction factor varied.

The behavior was the same for all the die materials, producing the maximum damage for $m = 0.5$ on the face of the ring in direct contact with the container and the die, while the damage decreased on the inner face with the increase in friction factor, being highest for $m = 0.1$, as shown in Figure 20.

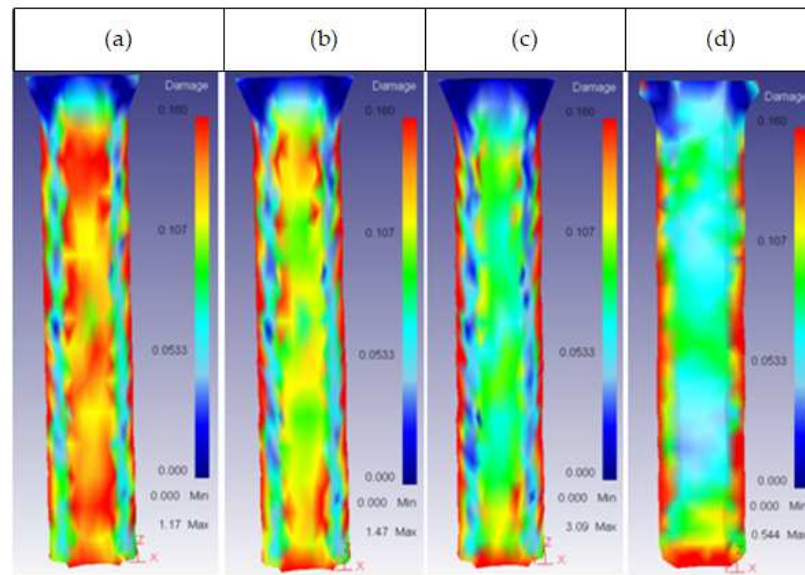


Figure 20. Damage distribution in the inner part of the ring: (a) AISI316 $m = 0.1$; (b) AISI316 $m = 0.3$; (c) AISI316 $m = 0.5$; (d) AISI316 $m = 0.7$.

Lastly, for friction factors higher than 0.5, damage in the ring decreased as shown in Figure 21. This behavior may have been caused by the increase in temperature with friction factor, as the damage factor is calculated by measuring stress and the stress decreased with the increase in the temperature according to the flow stress curves.

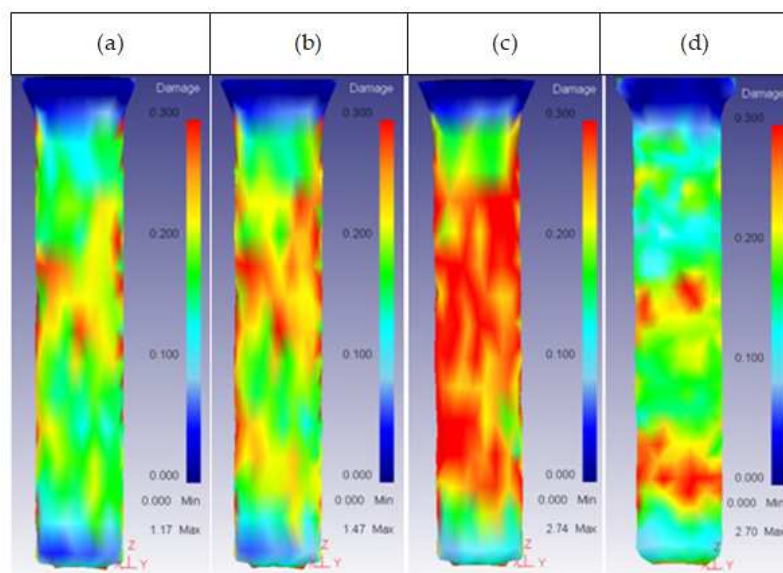


Figure 21. Damage distribution in the outer part of the ring: (a) AISI316 $m = 0.1$; (b) AISI316 $m = 0.3$; (c) AISI316 $m = 0.5$; (d) AISI316 $m = 0.7$.

Figure 22 shows the variation in temperature with friction factors.

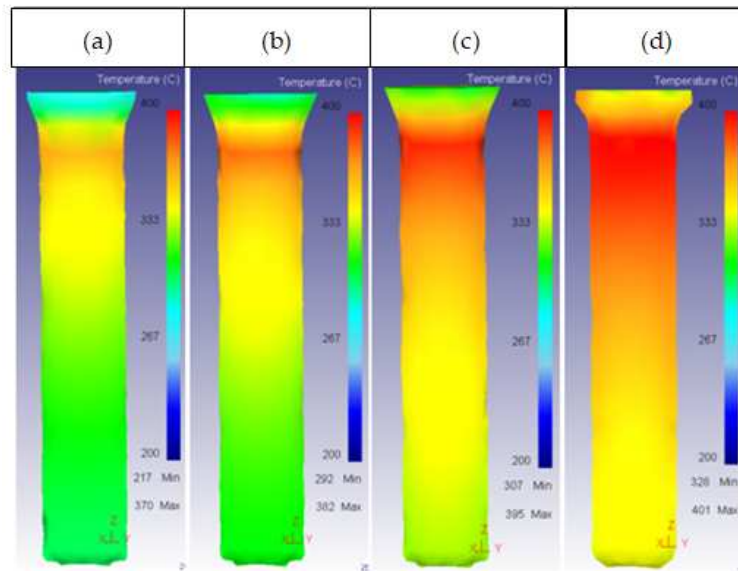


Figure 22. Temperature distribution in the ring: (a) AISI316 $m = 0.1$; (b) AISI316 $m = 0.3$; (c) AISI316 $m = 0.5$; (d) AISI316 $m = 0.7$.

3.2.5. Core Diameter

The effect of this parameter was similar to that of friction, affecting only the ring part of the billet. Both the outer and the inner face showed similar behavior, producing the greatest damage for a core diameter of 10 mm. There was also an optimum value of core diameter, 4 mm, for which the damage distribution was lowest. Therefore, the damage decreased as the core diameter increased until reaching a minimum value, beyond which the damage increased with core diameter.

The main difference in the behavior of the inner and outer face was found for a core diameter value of 2 mm, where the ring showed the second largest damage distribution. All behaviors can be observed in Figures 23 and 24.

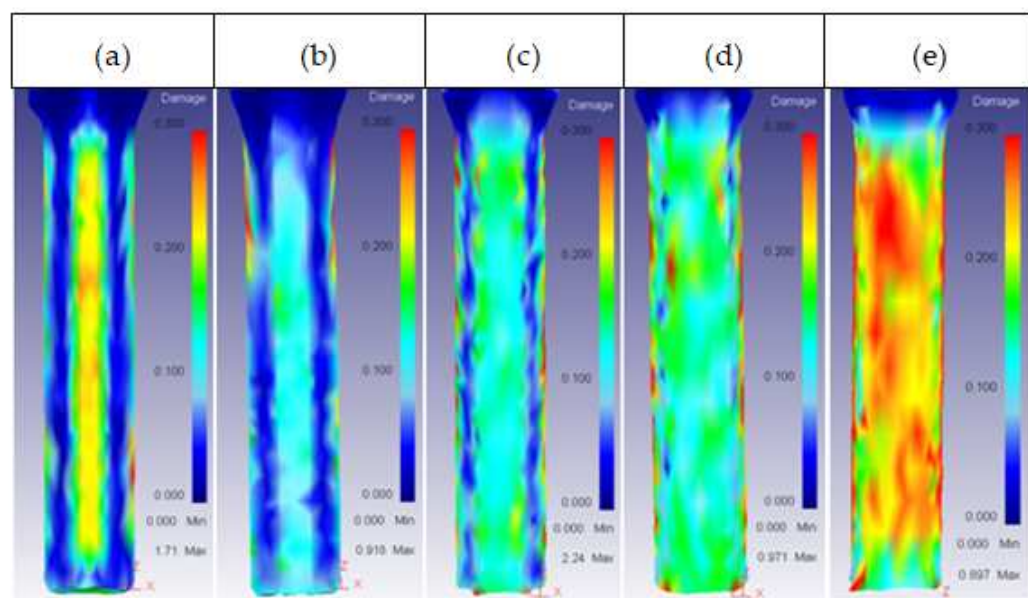


Figure 23. Damage distribution in the inner part of the ring: (a) H13 d = 2 mm; (b) H13 d = 4 mm; (c) H13 d = 6 mm; (d) H13 d = 8 mm; (e) H13 d = 10 mm.

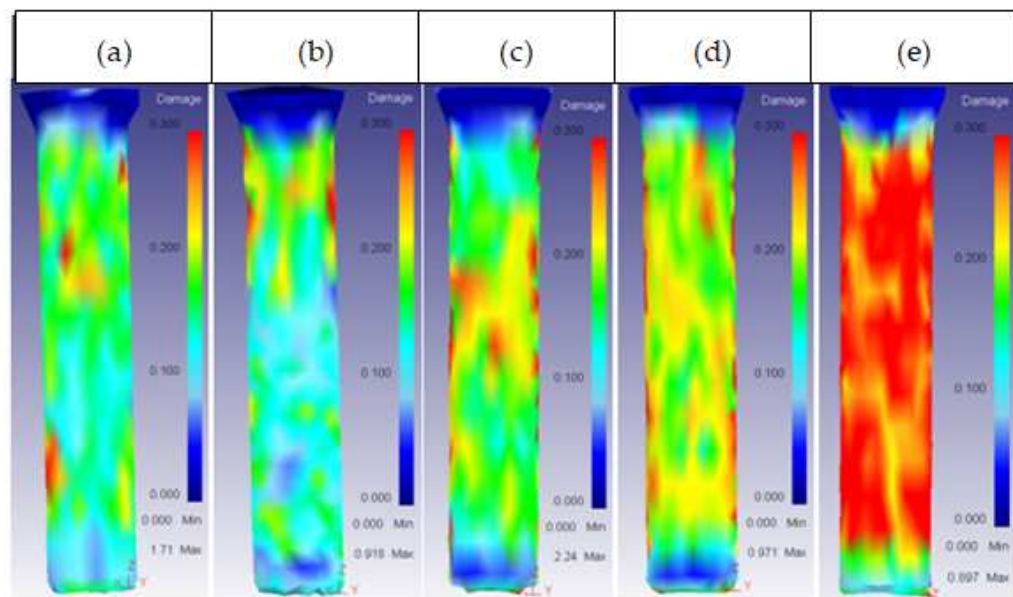


Figure 24. Damage distribution in the outer part of the ring: (a) H13 d = 2 mm; (b) H13 d = 4 mm; (c) H13 d = 6 mm; (d) H13 d = 8 mm; (e) H13 d = 10 mm.

This effect was due to the reduction in thickness of the ring. Larger thicknesses denote low values of the core diameter; thus, the contact area with the core is smaller, which causes an increment in the stress. As the core diameter increases, the contact area also increases, but the reduction in thickness causes the ring to receive more damage during the process.

3.3. Effects of the Extrusion Parameters on the Die Wear

As explained in Section 2, only ram speed, temperature, and friction were considered as relevant parameters to study the wear on the die.

Figure 25 shows the path taken into account to measure the wear variation through the die.

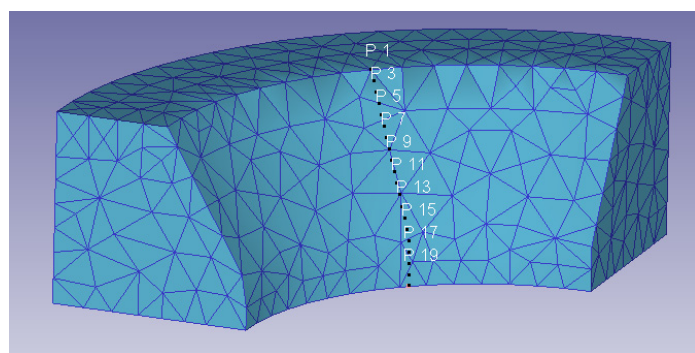


Figure 25. Wear path through the die.

The wear distribution for baseline conditions is presented in Figures 26 and 27.

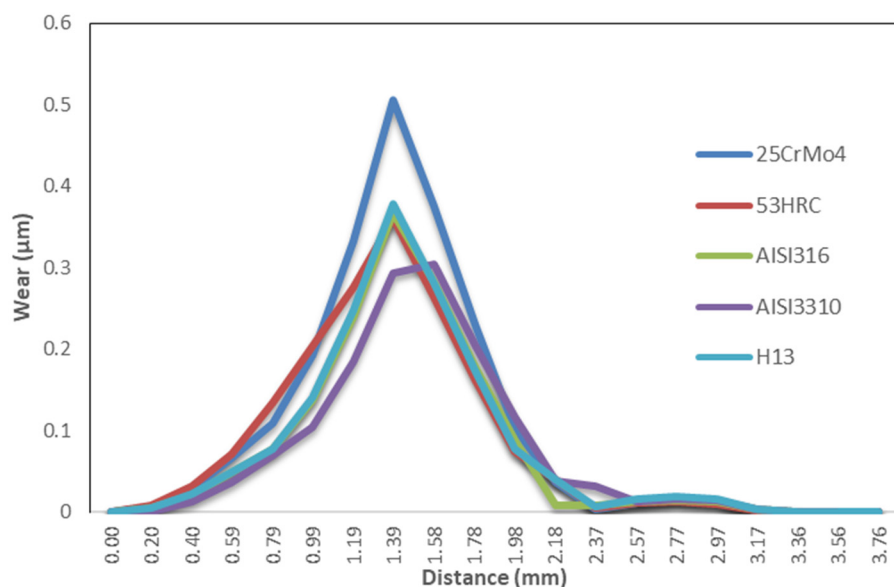


Figure 26. Wear distribution chart through the die for baseline conditions.

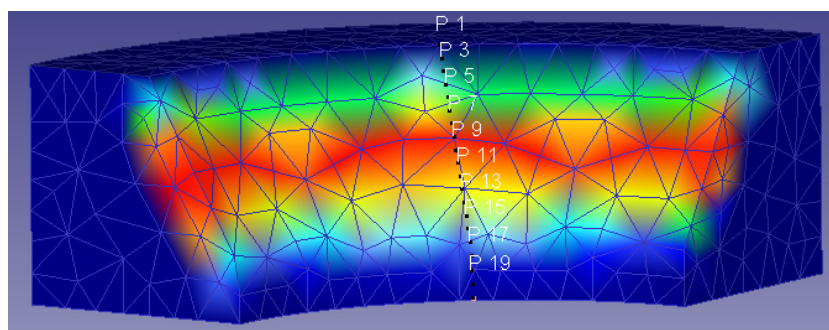


Figure 27. Wear distribution through the die for baseline conditions.

The first conclusion that can be obtained from the chart is that wear distribution was highly dependent on the hardness, as expected, with the highest wear occurring in the die material with the lowest hardness value (25CrMo4; 48).

Secondly, maximum wear values appeared during the first stages of displacement through the die, reaching a peak before the midpoint, after which the wear gradually decreased until it reached the change in section.

The sections below describe how the wear distribution was affected by different extrusion parameters for different die materials.

3.3.1. Ram Speed

Ram speed had almost no impact on the wear distribution for die materials 53HRC and AISI316, as can be observed in Figure 28.

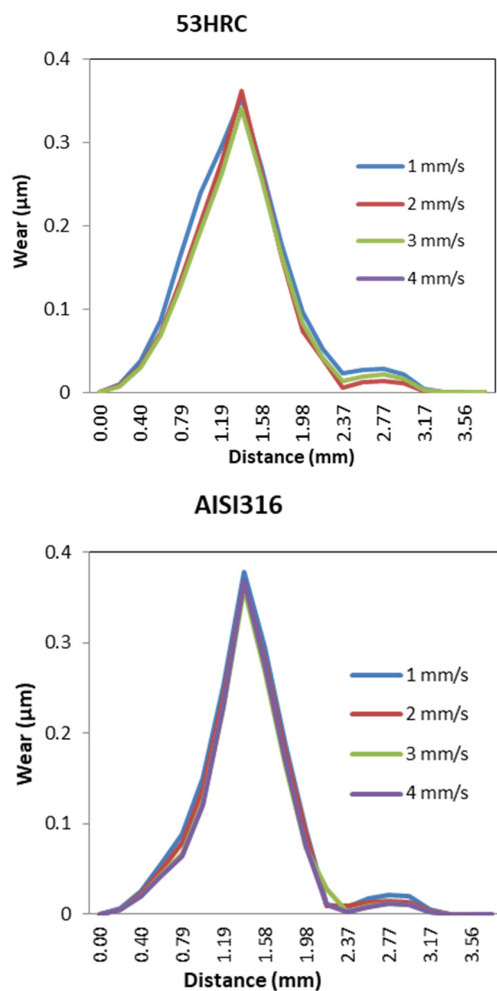


Figure 28. Wear distribution function of ram speed for 53HRC and AISI316 die materials.

The die material most affected by ram speed was AISI3310, which suffered the highest reduction in wear for ram speed values of 4 mm/s, as shown in Figure 29.

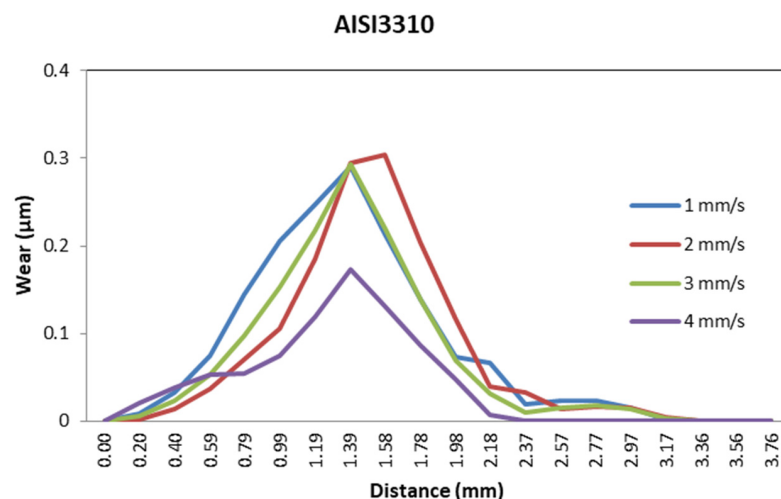


Figure 29. Wear distribution function of ram speed for AISI3310.

A typical behavior in wear distribution for different die materials was characterized by the lowest wear values for ram speeds between 3 and 4 mm/s, as shown in Figure 30.

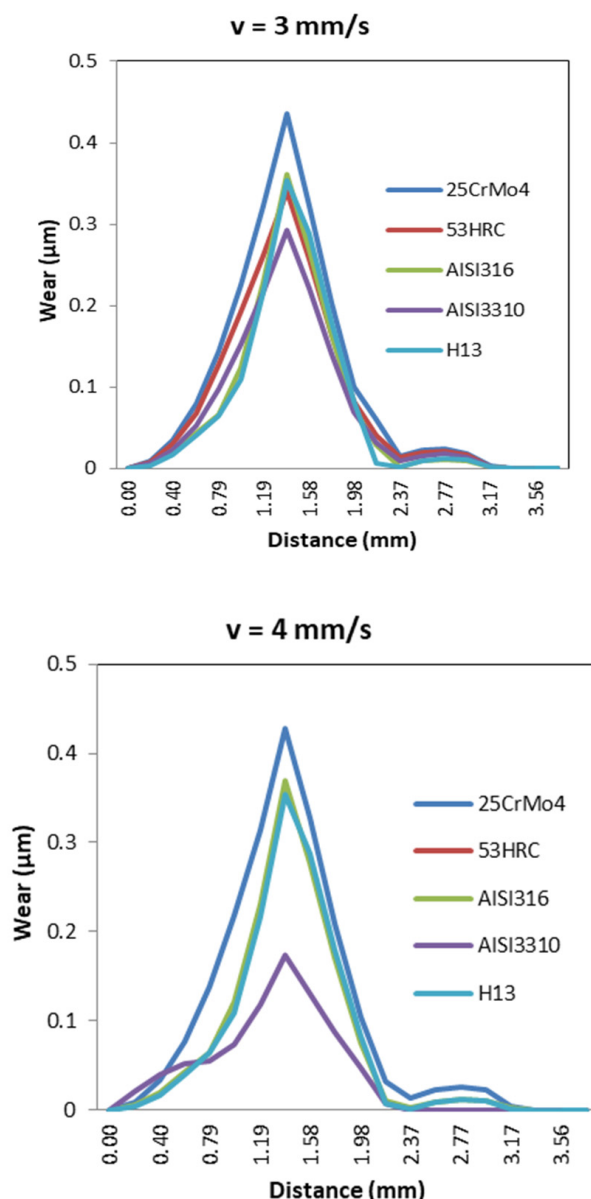


Figure 30. Wear distribution for high values of ram speed for different die materials.

3.3.2. Temperature

Figure 31 shows the effect of temperature. For most die materials considered in this study, the wear decreased as the temperature increased.

As mentioned above, the general behavior is that wear decreased with the increment in temperature, but this was not the same for all the die materials, as can be observed for 53HRC. There were also die materials more sensible to the temperature rise, such as AISI316 and H13, which suffered more wear than the softer AISI3310; however, the tendency changed for high temperatures, with the materials with less wear during the process being AISI316 and H13. Figure 32 shows the general behavior of wear decreasing with the increase in temperature; only three materials are presented because the wear increased for temperatures higher than 200 °C for 53HRC, whereas the wear remained constant from 200 °C for AISI3310.

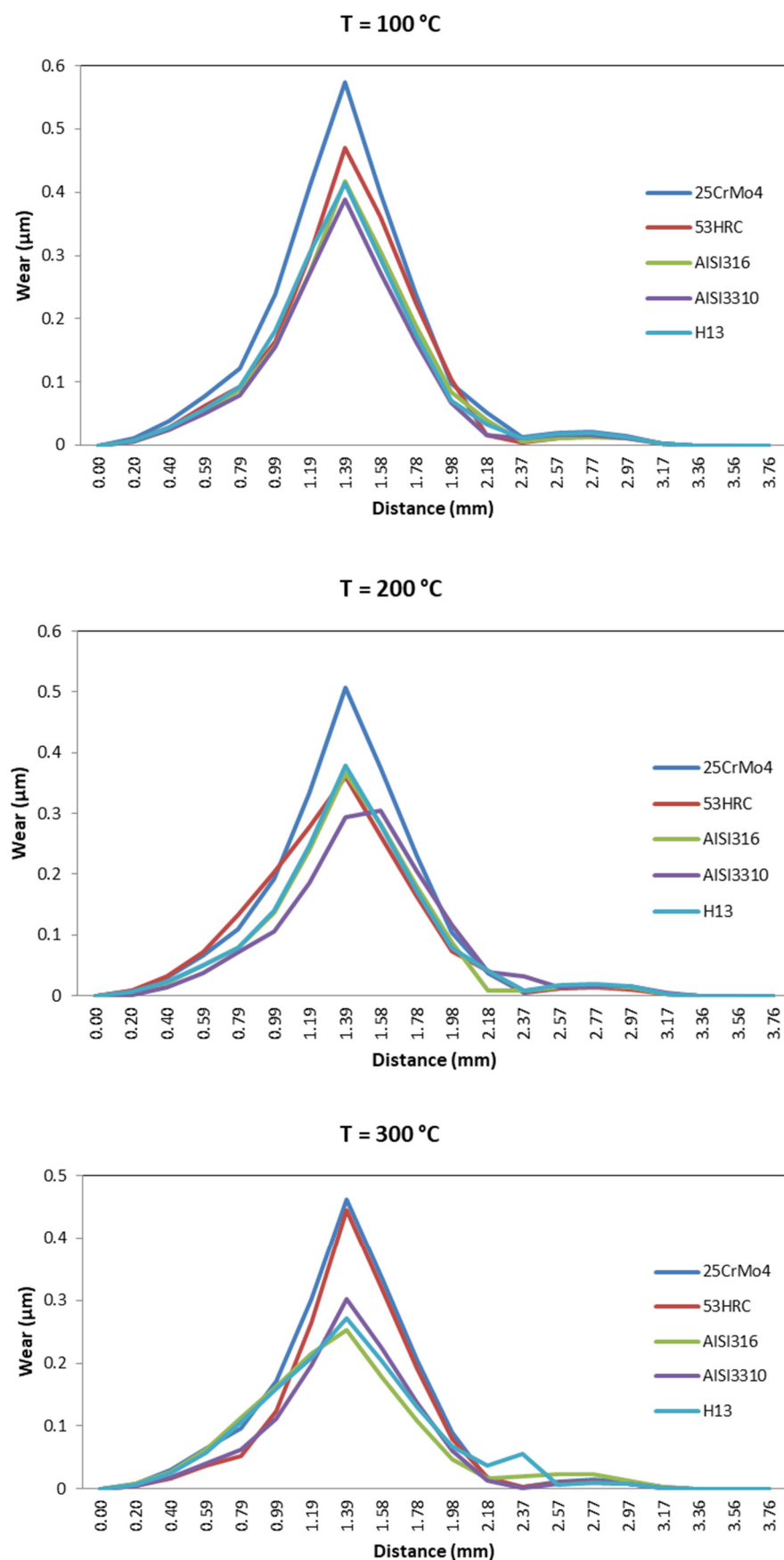


Figure 31. Wear distribution as a function of ram speed for different die materials.

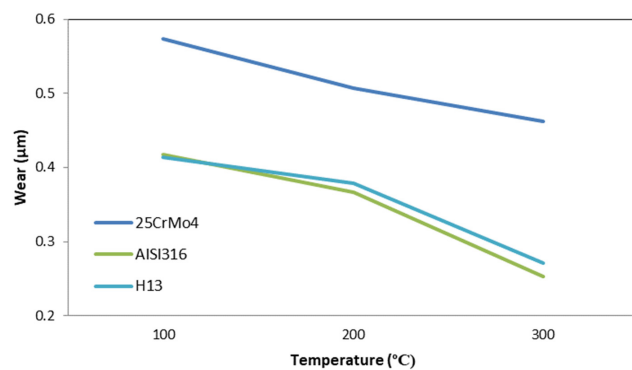


Figure 32. Wear evolution with temperature variation for 25CrMo4, AISI316, and H13.

3.3.3. Friction

The effect of the friction was inversely proportional to the wear distribution in the die. In Figure 33, it can be observed that, as friction increased, the wear distribution decreased. This was due to the reduction in sliding velocity and the increase in temperature produced by increased friction between billet and die.

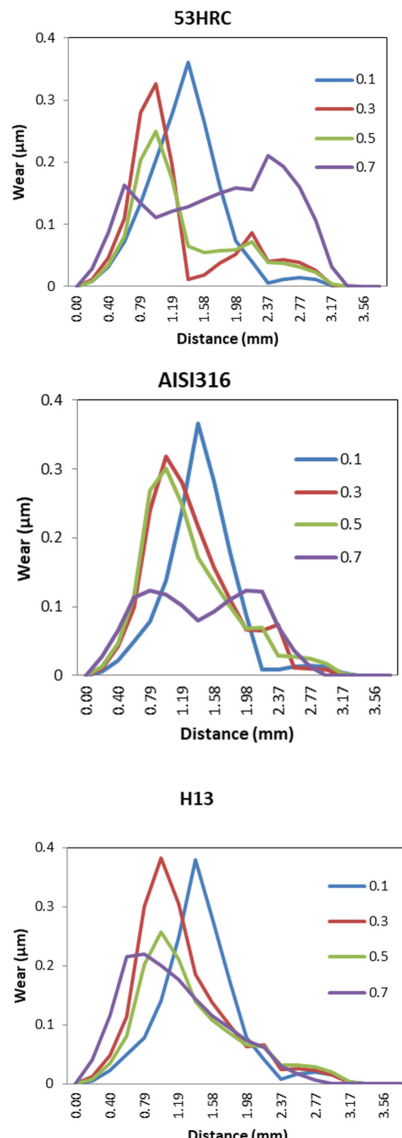


Figure 33. Wear distribution function of friction coefficients for 53HRC, AISI316, and H13.

For 25CrMo4 and AISI310, there were critical values of friction coefficient (0.7 and 0.5, respectively) for which wear exceeded 1 mm. Thus, these dies could only be used once due to the geometrical tolerance of the extrudate.

4. Conclusions

In general, the results obtained in this paper are consistent with experimental findings and previous numerical studies reported in the literature [19,42–45]. Furthermore, experimental studies are planned to validate this numerical approach and provide better insight into the process.

According to the results, it can be concluded that the material of the die is a relevant factor to take into account when defining a multi-material coextrusion process as it has an impact on the effect of process parameters on the extrusion force required, as well as on the distribution of extrudate damage and die wear.

The die semi-angle was the parameter most affected by the die material regarding the extrusion force. Depending on the material chosen, the behavior varied with an effect on the optimum die semi-angle.

The highest difference in the extrusion force value in the same conditions for different die materials occurred at a ram speed of 1 mm/s, where the increment in extrusion force using AISI310 was 27.50% higher than that needed for AISI316.

For the remaining parameters, the extrusion force varied between 8% and 15% of the value of the parameter requiring the lowest force.

Regarding the damage, in most configurations, the core only showed damage in the bottom part of the extrudate, in the region outside the contour of the sleeve which can be easily removed.

The damage distribution, in terms of its behavior and local values, was very similar for the different die materials; nevertheless, there were some critical values for some of the die materials where the damage was spread across the core, being a potential cause of future failure of the final part, e.g., for high values of die semi-angle ($\geq 75^\circ$), extrusion relation (2.25), and billet height (≥ 30 mm). All these values, as well as their distribution across the core, were dependent of the material of the die.

The ring part was the most affected by damage, being distributed cross its entire surface (both inner and outer face). The effect of different process parameters on ring damage was very similar for all die materials studied, and there were only slight variations in the maximum values reached.

Parameters such as temperature and ram speed had no influence on the damage.

Regarding wear distribution in the die, only three parameters were taken into account: ram speed, temperature and friction. Hardness was the most relevant parameter of the die material, whereby 25CrMo4 with the lowest hardness had the highest values of wear at the end of the process.

For 25CrMo4 and AISI310, there were critical values of the friction coefficient at which the wear increased too much for the die to be reused.

Although the effect of these parameters was dependent of the die material, some general rules of behavior can be extracted from the results:

- Ram speed only affects the wear distribution by decreasing it for values higher than or equal to 3 mm/s.
- An increase in temperature implies a reduction in the wear.
- An increase in friction leads to a reduction in wear and a peak shift to the left (i.e., closer than point 1 in Figure 33).

In summary, it can be concluded that, to obtain an optimum coextrusion process for a bimetallic billet, it is necessary to take into account the die material and a proper combination of process parameters to achieve a balance among minimum extrusion force, minimum damage, and wear distribution.

Lastly, taking into account the results obtained in this study, improvements in the model will be implemented to incorporate the microstructure of the die materials to obtain

better relationships between the selection of the die material and the extrusion force and damage. Furthermore, future lines of investigation can be opened, such as reducing the deformation load of titanium alloy due to work under relatively low temperatures or the effect of process parameters on the microstructure on the extrudate.

Author Contributions: Conceptualization, D.F., A.R.-P. and A.M.C.; methodology, D.F.; formal analysis, D.F., A.R.-P. and A.M.C.; investigation, D.F., A.R.-P. and A.M.C.; resources, A.R.-P. and A.M.C.; writing—original draft preparation, D.F.; writing—review and editing, A.R.-P. and A.M.C.; supervision, A.R.-P. and A.M.C.; project administration, A.R.-P. and A.M.C.; funding acquisition, A.R.-P. and A.M.C. All authors have read and agreed to the published version of the manuscript.

Funding: This research was funded by the Annual Grants Call of the E.T.S.I. Industriales of UNED through projects [2021-ICF07] and [2021-ICF08].

Institutional Review Board Statement: Not applicable.

Informed Consent Statement: Not applicable.

Data Availability Statement: Not applicable.

Acknowledgments: This work was developed within the framework of the “Doctorate Program in Industrial Technologies” of the UNED. We would like to extend our acknowledgement to the Research Group of the UNED “Industrial Production and Manufacturing Engineering (IPME)’’.

Conflicts of Interest: The authors declare no conflict of interest.

References

1. Camacho, A.M.; Rodríguez-Prieto, Á.; Herrero, J.M.; Aragón, A.M.; Bernal, C.; Lorenzo-Martin, C.; Yanguas-Gil, Á.; Martins, P.A.F. An Experimental and Numerical Analysis of the Compression of Bimetallic Cylinders. *Materials* **2019**, *12*, 4094. [[CrossRef](#)] [[PubMed](#)]
2. Zhang, X.P.; Yang, T.H.; Liu, J.Q.; Luo, X.F.; Wang, J.T. Mechanical properties of an Al/Mg/Al trilaminated composite fabricated by hot rolling. *J. Mater. Sci.* **2010**, *45*, 3457–3464. [[CrossRef](#)]
3. Alcaraz, J.; Gil-Sevillano, J. An analysis of the extrusion of bimetallic tubes by numerical simulation. *Int. J. Mech. Sci.* **1996**, *38*, 157–173. [[CrossRef](#)]
4. Chenot, J.-L.; Béraudo, C.; Bernacki, M.; Fourment, L. Finite Element Simulation of Multi Material Metal Forming. *Procedia Eng.* **2014**, *81*, 2427–2432. [[CrossRef](#)]
5. Mordike, B.L.; Ebert, T. Magnesium: Properties-applications-potential. *Mater. Sci. Eng. A* **2001**, *302*, 37–45. [[CrossRef](#)]
6. Li, L.X.; Rao, K.P.; Lou, Y.; Peng, D.S. A study on hot extrusion of Ti-6Al-4V using simulations and experiments. *Int. J. Mech. Sci.* **2002**, *44*, 2415–2425. [[CrossRef](#)]
7. Omoniyi, P.; Akinlabi, E.T.; Mahamood, R.M. Heat Treatments of Ti6Al4V Alloys for Industrial Applications: An Overview. In Proceedings of the IOP Conference Series: Materials Science and Engineering, Ota, Nigeria, 10–14 August 2020.
8. Khosravifard, A.; Ebrahimi, R. Investigation of parameters affecting interface strength in Al/Cu clad bimetal rod extrusion process. *Mater. Des.* **2010**, *31*, 493–499. [[CrossRef](#)]
9. Lapovok, R.; Ng, H.P.; Tomus, D.; Estrin, Y. Bimetallic copper-aluminum tube by severe plastic deformation. *Scr. Materialia* **2012**, *66*, 1081–1084. [[CrossRef](#)]
10. Berski, S.; Dyja, H.; Banaszek, G.; Janik, M. Theoretical analysis of bimetallic rods extrusion process in double reduction die. *J. Mater. Process. Technol.* **2004**, *153–154*, 583–588. [[CrossRef](#)]
11. Kocich, R. Deformation Behavior of Al/Cu Clad Composite during Twist Channel Angular Pressing. *Materials* **2020**, *13*, 4047. [[CrossRef](#)] [[PubMed](#)]
12. Negendank, M.; Mueller, S.; Reimers, W. Coextrusion of Mg-Al macrocomposites. *J. Mater. Process. Technol.* **2012**, *212*, 1954–1962. [[CrossRef](#)]
13. Thirumurugan, M.; Rao, S.A.; Kumaran, S.; Rao, T.S. Improved ductility in ZM21 magnesium–aluminium macrocomposite produced by co-extrusion. *J. Mater. Process. Technol.* **2011**, *211*, 1637–1642. [[CrossRef](#)]
14. Gall, S.; Müller, S.; Reimers, W. Aluminum coating of magnesium hollow profiles by using the coextrusion process. *Alum. Int. J.* **2009**, *85*, 63–67.
15. Rong, W.; Zhang, Y.; Wu, Y.; Chen, Y.; Tang, T.; Peng, L.; Li, D. Fabrication of high-strength Mg-Gd-Zn-Zr alloys via differential-thermal extrusion. *Mater. Charact.* **2017**, *131*, 380–387. [[CrossRef](#)]
16. Osakada, K.; Limb, M.; Mellor, P. Hydrostatic extrusion of composite rods with hard cores. *Int. J. Mech. Sci.* **1973**, *15*, 291–307. [[CrossRef](#)]
17. Lehmann, T.; Stockmann, M.; Naumann, J. Experimental and numerical investigations of Al/Mg compound specimens under load in an extended temperature range. *FEM Trans.* **2009**, *37*, 1–8.

18. Behrens, B.-A.; Klose, C.; Chugreev, A.; Heimes, N.; Thürer, S.E.; Uhe, J. A Numerical Study on Co-Extrusion to Produce Coaxial Aluminum-Steel Compounds with Longitudinal Weld Seams. *Metals* **2018**, *8*, 717. [[CrossRef](#)]
19. Fernández, D.; Rodríguez-Prieto, A.; Camacho, A.M. Effect of Process Parameters and Definition of Favorable Conditions in Multi-material Extrusion of Bimetallic AZ31B-Ti6Al4V Billets. *Appl. Sci.* **2020**, *10*, 8048. [[CrossRef](#)]
20. Thürer, S.E.; Peddinghaus, J.; Heimes, N.; Bayram, F.C.; Bal, B.; Uhe, J.; Behrens, B.-A.; Maier, H.J.; Klose, C. Lateral Angular Co-Extrusion: Geometrical and Mechanical Properties of Compound Profiles. *Metals* **2020**, *10*, 1162. [[CrossRef](#)]
21. Avedesiam, M.; Baker, H. *ASM Speciality Handbook. Magnesium and Magnesium Alloys*; ASM International: Geauga County, OH, USA, 1999; pp. 3–4.
22. Donachie, M.J. *Titanium: A Technical Guide*; ASM International: Geauga County, OH, USA, 1988; pp. 5–6.
23. Davis, J.R. *ASM Speciality Handbook—Stainless Steels*; ASM International: Geauga County, OH, USA, 1999.
24. Karmakar, D.; Muvvala, G.; Kumar, A. High-temperature abrasive wear characteristics of H13 steel modified by laser remelting and cladded with Stellite 6 and Stellite 6/30% WC. *Surf. Coat. Technol.* **2021**, *422*, 127498. [[CrossRef](#)]
25. Li, D.; Zhu, Z.; Xiao, S.; Zhang, G.; Lu, Y. Plastic flow behavior based on thermal activation and dynamic constitutive equation of 25CrMo4 steel during impact compression. *Mater. Sci. Eng. A* **2017**, *707*, 459–465. [[CrossRef](#)]
26. Bhandarkar, L.; Behera, M.; Mohanty, P.; Sarangi, S. Experimental investigation and multi-objective optimization of process parameters during machining of AISI 52100 using high performance coated tools. *Measurement* **2021**, *172*, 108842. [[CrossRef](#)]
27. Guo, Y.B.; Wen, Q. A hybrid modelling approach to investigate chip morphology transition with the stagnation effect by cutting edge geometry. *Trans. North Am. Manuf. Res. Inst. SME* **2005**, *33*, 469–476.
28. Bedekar, V.; Voothaluru, R.; Yu, D.; Wong, A.; Galindo-Nava, E.; Gorti, S.B.; An, K.; Hyde, R.S. Effect of nickel on the kinematic stability of retained austenite in carburized bearing steels—In-situ neutron diffraction and crystal plasticity modeling of uniaxial tension tests in AISI 8620, 4320 and 3310 steels. *Int. J. Plast.* **2020**, *131*, 102748. [[CrossRef](#)]
29. Peat, T.; Galloway, A.; Toumpis, A.; Steel, R.; Zhu, W.; Iqbal, N. Enhanced erosion performance of cold spray co-deposited AISI316 MMCs modified by friction stir processing. *Mater. Des.* **2017**, *120*, 22–35. [[CrossRef](#)]
30. Scientific Forming Technologies. *DEFORM v11.2 User’s Manual*; Scientific Forming Technologies Corporation: Columbus, OH, USA, 2017.
31. Rowe, G.W. *Principles of Industrial Metalworking Processes*; Edward Arnold Publishers: London, UK, 1977.
32. Leu, D.-K. A simple dry friction model for metal forming process. *J. Mater. Process. Technol.* **2009**, *209*, 2361–2368. [[CrossRef](#)]
33. Cockcroft, M.G.; Latham, D.J. Ductility and the workability of metals. *J. Inst. Met.* **1968**, *96*, 33–39.
34. Stebunov, S.; Vlasov, A.; Biba, N. Prediction of fracture in cold forging with modified Cockcroft-Latham criterion. *Procedia Manuf.* **2018**, *15*, 519–526. [[CrossRef](#)]
35. Gu, J.; Chen, P. A failure criterion for homogeneous and isotropic materials distinguishing the different effects of hydrostatic tension and compression. *Eur. J. Mech. A Solids* **2018**, *70*, 15–22. [[CrossRef](#)]
36. Amigo, F.J.; Camacho, A.M. Reduction of Induced Central Damage in Cold Extrusion of Dual-Phase Steel DP800 Using Double-Pass Dies. *Metals* **2017**, *7*, 335. [[CrossRef](#)]
37. Zhang, C.; Zhao, G.; Li, T.; Guan, Y.; Chen, H.; Li, P. An Investigation of Die Wear Behavior during Aluminum Alloy 7075 Tube Extrusion. *J. Tribol.* **2012**, *135*, 011602. [[CrossRef](#)]
38. Li, T.; Zhao, G.; Zhang, C.; Guan, Y.; Sun, X.; Li, H. Effect of Process Parameters on Die Wear Behavior of Aluminum Alloy Rod Extrusion. *Mater. Manuf. Process.* **2013**, *28*, 312–318. [[CrossRef](#)]
39. Lepadatu, D.; Hamblin, R.; Kobi, A.; Barreau, A. Statistical investigation of die wear in metal extrusion processes. *Int. J. Adv. Manuf. Technol.* **2005**, *28*, 272–278. [[CrossRef](#)]
40. García-Domínguez, A.; Claver, J.; Camacho, A.M.; Sebastián, M.A. Comparative Analysis of Extrusion Processes by Finite Element Analysis. *Procedia Eng.* **2015**, *100*, 74–83. [[CrossRef](#)]
41. Gisbert, C.; Bernal, C.; Camacho, A. Improved Analytical Model for the Calculation of Forging Forces during Compression of Bimetallic Axial Assemblies. *Procedia Eng.* **2015**, *132*, 298–305. [[CrossRef](#)]
42. Gutovskaya, J.; Solberg, J.K.; Lange, H.I.; Andersen, L.H. Wear of Inconel 718 die during aluminium extrusion—A case study. *Wear* **2004**, *256*, 126–132. [[CrossRef](#)]
43. Jajimoggala, S.; Dhananjay, R.; Lakshmi, V. Shabana Multi-response optimization of hot extrusion process parameters using FEM and Grey relation based Taguchi method. *Mater. Today Proc.* **2019**, *18*, 389–401. [[CrossRef](#)]
44. Moraes, A.L.; Silva, U.S.; Sigwart, H. On the Friction Conditions in FEM Simulations of Cold Extrusion. *Procedia Manuf.* **2020**, *47*, 231–236.
45. Jiayong, S.; Fan, G.; Pengbiao, H.; Ji, Z. Simulation on extrusion process of TiAl alloy. *Intermetallics* **2011**, *19*, 169–174.

4.4. Optimal parameters selection in advanced multimetallic co-extrusion based on independent MCDM analytical approaches and numerical simulation

Los indicios de calidad de este artículo se pueden encontrar en el Apéndice D de esta Tesis Doctoral.

4.4.1. Datos de la publicación y factor de impacto

Título	Optimal parameters selection in advanced multimetallic co-extrusion based on independent MCDM analytical approaches and numerical simulation
Autores	Daniel Fernández; Álvaro Rodríguez-Prieto; Ana María Camacho
Revista	Mathematics
ISSN	2227-7390
Editorial	MDPI
País	Switzerland
Volumen	10 (23)
Páginas	4489
Fecha	28 noviembre 2022
doi	https://doi.org/10.3390/math10234489
Factor de impacto	2.592 (2021); 5-Year Impact Factor: 2.542 (2021) Q1 (21/332) en “Mathematics-Sci”

4.4.2. Resumen y copia de la publicación

En este trabajo se ha desarrollado una metodología de comparación entre diferentes métodos de toma de decisiones multicriterio (MCDM) junto con varios métodos de ponderación de criterios a los resultados obtenidos de las simulaciones realizadas por el método de los elementos finitos mediante el software comercial DEFORM3D®, de un proceso de coextrusión multimaterial para la obtención de cilindros bimetálicos formados por un núcleo de aleación de magnesio (AZ31B) y un anillo externo de aleación de titanio (Ti6Al4V). El objetivo es seleccionar la combinación óptima de parámetros del proceso para cumplir con unos criterios específicos de reducción del daño inducido en la pieza, fuerza de extrusión mínima necesaria para llevar a cabo el proceso y desgaste mínimo de la herramienta empleada, todo ello junto

Capítulo 4. Publicaciones

con una microestructura de grano lo más fina posible. Los resultados revelaron que en tres de los cuatro métodos MCDM estudiados la mejor solución obtenida es la misma independientemente del método de ponderación utilizado, así como que el método VIKOR es el único en el que se obtienen resultados diferentes dependiendo del método de ponderación empleado. La conclusión a que se llegó en este estudio es que la mejor combinación para obtener unos parámetros óptimos en el proceso de fabricación por coextrusión es la formada por el método VIKOR junto con el método de ponderación de la entropía, siendo uno de los factores determinantes para esta elección las condiciones de “ventaja aceptable” y “estabilidad aceptable en el proceso de decisión” que se deben cumplir usando el método VIKOR para confirmar la viabilidad de la solución de compromiso o conjunto de soluciones compromisos recomendadas.

In this work, a comparison methodology has been developed among different multicriteria decision-making methods (MCDM) together with different criteria weighting methods, to the results obtained from the simulations carried out by using the finite element method with the commercial software DEFORM3D®, of a multimaterial co-extrusion process to obtain bimetallic cylinders made up of a magnesium alloy (AZ31B) core and a titanium alloy (Ti6Al4V) sleeve. The objective is to select the optimal process parameters combination to fulfil specific criteria of reduction of damage induced in the part, minimum extrusion force necessary to perform the process and minimum wear of the tool used, all together with a grained microstructure as fine as possible. The results revealed that in three of the four MCDM methods studied, the best solution obtained is the same regardless of the weighting method used, as well as that the VIKOR method is the only one in which different results were obtained depending on the weighting method used. The conclusion reached in this study is that the best combination to obtain optimal parameters in this co-extrusion manufacturing process is the one composed by VIKOR method together with entropy weighting method, being one of the determining factors for this choice the conditions of “acceptable advantage” and “acceptable stability in the decision process” that have to be met when using VIKOR method to confirm the viability of the recommended compromised solution or set of compromised solutions.

4.4.3. Resumen de las aportaciones

En esta publicación el doctorando estuvo a cargo de la definición y desarrollo de los modelos numéricos, la revisión del estado del arte, la metodología empleada y la escritura del artículo. La conceptualización, el análisis formal y la investigación fueron realizadas en conjunto por el

Capítulo 4. Publicaciones

doctorando y sus directores de tesis. Por último, las labores de revisión y edición del artículo, administración de recursos del proyecto, supervisión y adquisición de fondos fue llevada a cabo por los directores de tesis.

Article

Optimal Parameters Selection in Advanced Multi-Metallic Co-Extrusion Based on Independent MCDM Analytical Approaches and Numerical Simulation

Daniel Fernández *, Álvaro Rodríguez-Prieto  and Ana M. Camacho 

Department of Manufacturing Engineering, Universidad Nacional de Educación a Distancia (UNED), 28040 Madrid, Spain

* Correspondence: dfernande146@alumno.uned.es

Abstract: Multi-material co-extrusion is a complex thermo-mechanical forming process used to obtain bimetallic billets. Its complexity is due to the combination of diffusion phenomena in the interface of both materials together with the high temperature and pressure generated and the different flow stress characteristics created by the joining of dissimilar materials. Accordingly, the selection of optimal process parameters becomes key to ensure process feasibility. In this work, a comparison among different multi-criteria decision making (MCDM) methodologies, together with different weighting methods, were applied to the simulation results by using DEFORM3D© software to select the optimal combination of process parameters to fulfil the criteria of minimum damage, extrusion force, and tool wear, together with the maximum reduction in the average grain size.



Citation: Fernández, D.; Rodríguez-Prieto, Á.; Camacho, A.M. Optimal Parameters Selection in Advanced Multi-Metallic Co-Extrusion Based on Independent MCDM Analytical Approaches and Numerical Simulation. *Mathematics* **2022**, *10*, 4489. <https://doi.org/10.3390/math10234489>

Academic Editors: Sambor Guze and Enrico Zio

Received: 19 October 2022

Accepted: 24 November 2022

Published: 28 November 2022

Publisher's Note: MDPI stays neutral with regard to jurisdictional claims in published maps and institutional affiliations.



Copyright: © 2022 by the authors. Licensee MDPI, Basel, Switzerland. This article is an open access article distributed under the terms and conditions of the Creative Commons Attribution (CC BY) license (<https://creativecommons.org/licenses/by/4.0/>).

Keywords: multi-material; co-extrusion; MCDM; titanium; magnesium; FEM

MSC: 90B50

1. Introduction

One of the main problems that arises during part design processes involves balancing weight reduction and the fulfillment of in-service requirements. This problem is especially critical in industries such as aerospace, where the parts work under severe conditions and the reduction of weight is key to obtain the desired performance of the vehicle. Multi-material forming allows designers to combine the mechanical properties of dissimilar materials being the co-extrusion process one of the most highlighted.

Two of the most widely used alloys in the aerospace and automotive industries are titanium alloys, which present excellent mechanical and physical-chemical properties, as well as a good relationship between strength and weight and high corrosion resistance [1], and magnesium alloys, which possess low density and good specific strength [2].

Several studies about the application of multi-material forming processes using these two alloys have been performed over the years. Among those which can be highlighted are the study by Gall et al. [3], which performed Finite Element Method (FEM) simulation together with experiments on Al–Mg billets into hollow profiles during a bimetallic co-extrusion process. Negendanka et al. [4] studied the effect of the die angle on the formation of the diffusion layer during co-extrusion of a bimetallic billet composed by an Mg-core and Al-sleeve. Lehmann et al. [5], by experimenting with hydrostatic, coextruded Al–Mg compounds. However, there are very few studies that explore the combination of titanium and magnesium alloys together. Some of them are, for example, those carried out by Fernández et al. [6,7], who applied ANOVA to determine the influence of the different process parameters together with the effect of the selection of die material on extrusion force and damage during co-extrusion of a Ti₆Al₄V-AZ31B bimetallic billet.

In order to achieve the maximum productivity and the highest performance, proper selection of the process parameters becomes a significant task. Due to the complexity and the number of variables involved, multi objective optimization presents the best approach to obtain a compromise solution for this problem. However, the wide range of Multi-Criteria Decision Making (MCDM) methods, each one with its own pros and cons, makes its choice the first obstacle to overcome, even more when different results can be obtained when applied to the same problem because of the different methods used to determine the weights, scale the objectives, and so on.

The first MCDM method was applied by Pareto in 1896 [8] with his famous 80/20 principle. Another example is Saaty in 1977 [9], who used multi-criteria models to solve problems with conflicting goals. Since 1980, several MCDM methods have been developed and applied to support decision-making in different areas such as supply chain managing contract selection [10], manufacturing process selection [11,12], and material selection [13,14].

From a literature review, is possible to find several examples of applications and even comparisons among MCDM methods regarding the optimization of manufacturing process parameters [15–17], but there is a lack of studies which examine the step before and compare the different weighting methods [18–21] with the MCMD methods, and their effects on the results obtained, being that most of these studies focused on the TOPSIS method [22–25].

This study develops a methodology of comparison between three weighting methods (AHP, Entropy, and Standard Deviation) and their influence on four different MCDM methods (ARAS, TOPSIS, VIKOR, and COPRAS) when applied to a multi-metallic co-extrusion manufacturing process to obtain the optimal parameters under the principle of minimizing the extrusion force, damage, die wear, and grain size. The results of this paper determine the best combination between weighting methods and MCDM, additionally proving that a compromise solution which brings together criteria as disparate as extrusion force, damage, tool wear, and grain size can be reached.

2. Materials and Methods

2.1. Materials, Geometrical Dimensions and Process Parameters

The materials used in this study are a cylindrical sleeve and core made of a titanium alloy UNS R56400 (Ti6Al4V) and magnesium alloy UNS M11211 (AZ31B), respectively.

Figure 1 shows the bimetallic cylinder co-extrusion set up with the initial dimensions.

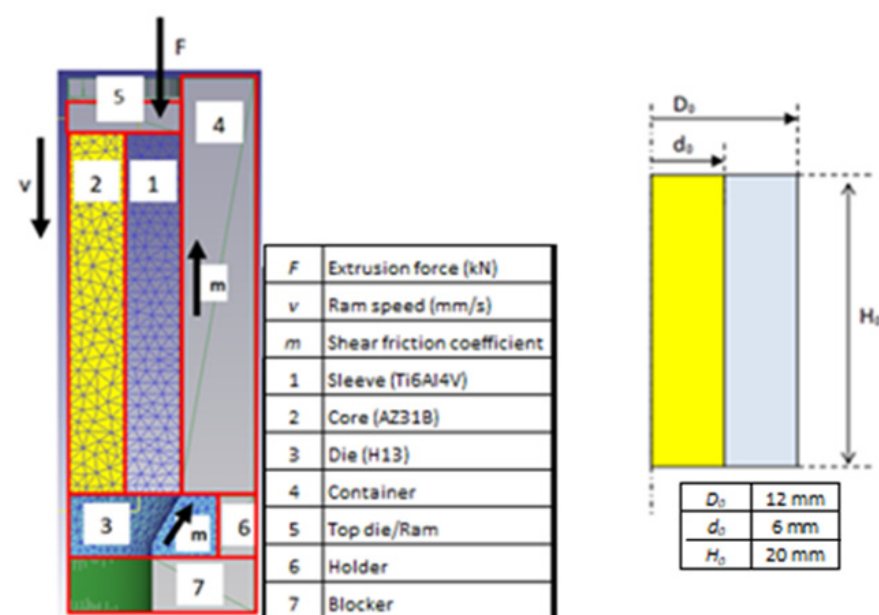


Figure 1. Bimetallic co-extrusion set up and initial billet dimensions.

Chemical compositions, along with the physical and mechanical properties, are shown in Tables 1–4 for the aforementioned materials:

Table 1. Chemical composition of titanium alloy Ti₆Al₄V [26].

Ti (wt.%)	Al (wt.%)	V (wt.%)	Fe (wt.%)	C (wt.%)	O (wt.%)	N (wt.%)	H (wt.%)
Bal.	5.5–6.5	3.5–4.5	0.25	0.08	0.13	0.040	0.012

Table 2. Chemical composition of magnesium alloy AZ31B [27].

Mg (wt.%)	Al (wt.%)	Zn (wt.%)	Mn (wt.%)	Si (wt.%)	Cu (wt.%)	Ca (wt.%)	Fe (wt.%)	Ni (wt.%)
97	2.5–3.5	0.6–1.4	0.20	0.1	0.05	0.04	0.005	0.005

Table 3. Chemical composition of H13 steel [28].

C (wt.%)	Mn (wt.%)	Si (wt.%)	Cr (wt.%)	Mo (wt.%)	Ni (wt.%)
0.32–0.45	0.2–0.5	0.80–1.20	4.75–5.50	1.10–1.75	0.30 max

Table 4. Physical and mechanical properties of the titanium alloy Ti₆Al₄V and magnesium alloy AZ31B [26–29].

Property	AZ31B	Ti ₆ Al ₄ V	H13
Density (g/cm ³)	1.74	4.46	7.78
Tensile strength (MPa)	260	895	1990
Yield strength (MPa)	200	828	1650
Elastic modulus (GPa)	44.80	110	210
Poisson's ratio	0.35	0.31	0.3

The parameters affecting the extrusion process considered for this study were the following:

- Ram speed (mm/s) and temperature (°C) as process parameters.
- Die semi-angle (°), shear friction factor, and extrusion ratio (A_0/A_f) as tool parameters.
- Shape factor (H_0/D_0) and diameter ratio (D_0/d_0) as geometric parameters.

Where, A_0 and A_f are the initial and final areas of the cross-section of the billet, D_0 and d_0 are the initial external diameter and internal diameter of the sleeve, and H_0 is the initial billet height.

2.2. Finite Element Modeling and Simulation Preparation

Commercial software DEFORM3D© (v11.2) [30] was used to perform the finite element simulations.

The ram, container, holder, and blocker (extrusion tooling) were modeled as rigid objects. The bimetallic cylinders were modeled as an assembly between two plastic objects (sleeve and core). The die was modeled as an elastic object. All parts were meshed with 7000 tetrahedral elements.

In order to reduce the computation time and the size of the database files, and considering the axial symmetry of the co-extrusion process, only one quarter of the problem was modeled.

Ti₆Al₄V was modeled by using Johnson-Cook constitutive equations [31], and for modeling AZ31B, the exponential model defined by Wen-juan et al. (2012) [32] was used.

The normalized Cockcroft and Latham criterion [33], together with the hydrostatic stress criterion (HSC) [34–36], are used to evaluate the damage factor on the extrudate.

Finally, in order to evaluate the wear of the die and the dynamic recrystallization the Archad's model [37–39] and the Johnson–Mehl–Avrami–Kolmogorov (JMAK) model [40,41], respectively, were implemented in the simulations.

2.3. Weighting Methods

The weights of the criteria show their importance. These methods are clustered in three categories. Subjective weighting methods are when the criteria weights are determined dependent of the preferences of decision makers, stakeholders, customer requirements, etc. Objective weighting methods are based on initial data or decision matrix with no involvement of the actors mentioned before. Finally, hybrid weighting methods are a combination of subjective and objective methods, taking features of both methods. Figure 2 shows the weighting methods classification, as well as some example of each.

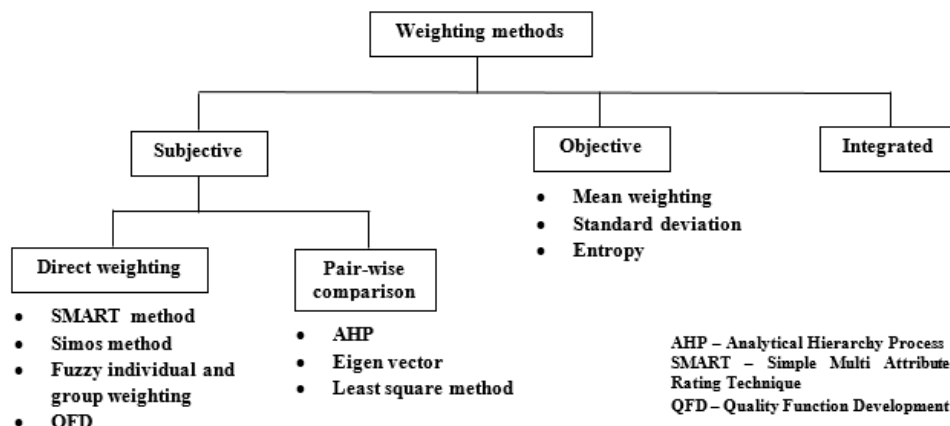


Figure 2. Weighting methods classification.

2.3.1. AHP Method

Analytic Hierarchy Process (AHP) was produced by Thomas L. Saaty in the 1970s [42,43]. It is a structured technique for organizing and analysing complex decisions, based on mathematics and psychology. In this study, AHP is applied to assign weights to the different criteria (extrusion force, damage, tool wear, Ti6Al4V grain size, and AZ31B grain size).

A paired comparison matrix has to be generated by assigning values based on the 9-point Saaty rating scale to the different criteria, as shown in Table 5:

Table 5. The Saaty rating scale [9].

Scale	Numerical Rating	Reciprocal
Extremely preferred	9	1/9
Very strong to extreme	8	1/8
Very strongly preferred	7	1/7
Strongly to very strongly	6	1/6
Strongly preferred	5	1/5
Moderately to strongly	4	1/4
Moderately preferred	3	1/3
Equally to moderately	2	1/2
Equally preferred	1	1

With these values, the $n \times n$ pairwise matrix A is generated, as follows:

$$A = \begin{bmatrix} 1 & a_{12} & \cdots & a_{1n} \\ a_{21} & 1 & \cdots & a_{2n} \\ \vdots & \cdots & \ddots & \vdots \\ a_{n1} & a_{n2} & \cdots & 1 \end{bmatrix}$$

The values a_{ij} represent the strength of agreement of i th element respect to j th element. Being a condition that all the values in the diagonal takes value 1 and $a_{ij} = 1/a_{ji}$, where $i, j = 1, 2 \dots n$.

The next step is to obtain the normalized matrix. The Equation (1) is applied:

$$N_{ij} = \frac{a_{ij}}{\sum_{i=1}^n a_{ij}} \text{ for } i \text{ and } j = 1 \dots n. \quad (1)$$

Obtaining this matrix:

$$A^* = [\sum_{i=1}^n a_{i1} \quad \cdots \quad \sum_{i=1}^n a_{in}] = [A_1^* \dots A_n^*]$$

$$N = \begin{bmatrix} N_{12} & N_{12} & \cdots & N_{1n} \\ \vdots & \cdots & \ddots & \vdots \\ N_{n1} & N_{n2} & \cdots & N_{nn} \end{bmatrix}$$

A first check can be done at this point to ensure that the method is well applied. If the summation of all the elements of each column is equal to 1 then the normalized matrix is correct.

Then, a column matrix composed by the summation of the elements of each row of the normalized matrix can be obtained:

$$N^* = \begin{bmatrix} \sum_{j=1}^J N_{1j} \\ \vdots \\ \sum_{j=1}^n N_{nj} \end{bmatrix} = \begin{bmatrix} N_1^* \\ \vdots \\ N_n^* \end{bmatrix}$$

Finally, the weights for each criteria are obtained by using Equation (2):

$$W_j = \frac{N_j^*}{\sum N_j^*} \quad (2)$$

A final check is needed to validate the consistency of the measurement scales during the assessment process used to produce matrix A . The recommendation is to calculate the maximal eigenvalue λ_{max} , as shown in Equation (3):

$$\lambda_{max} = \sum (A_i * W_j) \text{ for } i \text{ and } j = 1 \dots n. \quad (3)$$

The consistency index (CI) can be calculated accordingly with Equation (4):

$$CI = \frac{\lambda_{max} - n}{n - 1} \quad (4)$$

where, n is the dimension of pairwise matrix.

The consistency ratio (CR) is used as a guidance value to check for conformity. Equation (5) shows how it can be obtained:

$$CR = \frac{CI}{RI} \quad (5)$$

where, RI is the random index, which is obtained from Table 6, depending on the dimension (n) of our pairwise matrix:

Table 6. Random index values as function of dimension of our pairwise matrix [9].

n	1	2	3	4	5	6	7	8
CI	0.00	0.00	0.58	0.90	1.12	1.24	1.32	1.41

The threshold for the *CR* value is 0.1. If this condition is fulfilled, then the importance degree evaluation criteria is assumed to be rational.

2.3.2. Entropy Method

The entropy method [44] is classified within the category of objective weighting methods. It was first proposed by C.E. Shannon in 1948 and is applicable when the data of the decision matrix are known. Entropy is a measure of randomness and disorder in the universe.

First of all, it is necessary to perform the normalization of the arrays of the decision matrix (performance indices) to obtain the project outcomes p_{ij} using Equation (6). Being the decision matrix D :

$$D = \begin{bmatrix} x_{11} & \cdots & x_{1n} \\ \vdots & \ddots & \vdots \\ x_{m1} & \cdots & x_{mn} \end{bmatrix}$$

$$p_{ij} = \frac{x_{ij}}{\sum_{i=1}^m x_{ij}} \quad (6)$$

where, n is the number of criteria and m corresponds with the number of alternatives.

Starting from this normalized matrix, the entropy measure of project outcomes is obtained by means of Equation (7).

$$E_j = -k * \sum_{i=1}^m p_{ij} * \ln(p_{ij}) \quad (7)$$

with $k = 1/\ln(m)$.

The objective weight-based definition is given by Equation (8).

$$w_j = \frac{1 - E_j}{\sum_{j=1}^n (1 - E_j)} \quad (8)$$

2.3.3. Standard Deviation (SD) Method

The SD method [45] is grouped as an objective weighting method and consists of establishing weights based on the standard deviations of the different alternatives from the target.

In order to do that, a normalized matrix is created from the decision matrix D , taking into account the beneficial and non-beneficial criteria in accordance with Equation (9) for beneficial and (10) for non-beneficial.

$$D = \begin{bmatrix} x_{11} & \cdots & x_{1n} \\ \vdots & \ddots & \vdots \\ x_{m1} & \cdots & x_{mn} \end{bmatrix}$$

$$F_{ij} = \frac{x_{ij} - \min(x_{ij})}{\max(x_{ij}) - \min(x_{ij})} \quad (9)$$

$$F_{ij} = \frac{\max(x_{ij}) - x_{ij}}{\max(x_{ij}) - \min(x_{ij})} \quad (10)$$

where, n is the number of criteria and m the number of alternatives.

Then SD is calculated, as shown in Equation (11):

$$\sigma_j = \sqrt{\frac{\sum_{i=1}^m (F_{ij} - \bar{F}_j)^2}{m}} \quad (11)$$

where, \bar{F}_j is the mean value of each column.

Finally, weights are calculated for each criterion using Equation (12):

$$W_i = \frac{\sigma_j}{\sum_{j=1}^J \sigma_j} \quad (12)$$

2.4. MCDM Methods

MCDM methods can be classified in two main groups, according to Hwang and Yoon (1981) [46]: Multi-attribute decision making (MADM) and Multi-objective decision making (MODM).

MADM methods are used to solve discrete problems while MODM are applied towards the resolution of continuous problems. This study is focused on MADM.

MADM can be also clustered depending on the initial information (determinist, stochastic, or uncertain) or depending on the groups of decision makers (single or several groups), but the most common classifications are the ones proposed by Hajkowicz–Collins (2007) [47] and De Brito–Evers (2016) [48]:

- Scoring Methods (COPRAS).
- Distance-based methods (VIKOR and TOPSIS).
- Pair wise comparison methods (AHP).
- Utility/Value methods (ARAS)

2.4.1. ARAS

The Additive Ratio Assessment (ARAS) [17,49] is a method used to select the best alternatives among those given by considering quantitative measurements and utility theory, which determines the relative efficiency. The weight criteria will be those obtained by the methods mentioned before (AHP, Standard Deviation, and Entropy).

In the first step of this method, the definition of the beneficial and non-beneficial criteria of the objective functions is required. After this, the decision matrix can be produced using the following equation, where each column of the matrix represents one of the criteria to be evaluated:

$$D = \begin{bmatrix} x_{11} & \cdots & x_{1n} \\ \vdots & \ddots & \vdots \\ x_{m1} & \cdots & x_{mn} \end{bmatrix}$$

where, m is the number of alternatives and n is the number of criteria. Typically, this decision matrix is not symmetrical because the number of criteria is less than the number of experimental cases performed.

At this point, normalization is needed to continue, since the variety and unit of the output value differs from the others. By applying a normalization process, the original score is converted into a comparable score by means of Equation (13) for beneficial criteria, and by means of Equations (14) and (15) for non-beneficial criteria:

$$N_{ij} = \frac{x_{ij}}{\sum_{i=0}^m x_{ij}} \quad (13)$$

$$x_{ij}^* = \frac{1}{x_{ij}} \quad (14)$$

$$N_{ij} = \frac{x_{ij}^*}{\sum_{i=0}^m x_{ij}^*} \quad (15)$$

The weight factor matrix (W) is obtained from the multiplication of the normalized value of N and its respective weight factor (previously obtained with AHP, Standard Deviation, and Entropy methods), as Equation (16) shows:

$$W_{ij} = N_{ij} * W_j \quad (16)$$

In order to calculate the degree of utility, first it is necessary to get the optimality function (S_i) for the i^{th} alternative, according to Equation (17):

$$S_i = \sum_{j=1}^n W_{ij}; i = 0 \dots m. \quad (17)$$

Finally, the degree of utility (K_i) is determined by the comparison made between each S_i , with the most efficient one (S_0) obtained in the previous step, as can be seen in Equation (18):

$$K_i = \frac{S_i}{S_0} \quad (18)$$

The alternatives are ranked by their value of K_i in an increasing sequence, with the highest value being the best alternative.

2.4.2. TOPSIS

TOPSIS [50,51] is the acronym for Technique for Order Preference by Similarity to Ideal Solution and is a MCDM method initially proposed by Hwang and Yoon in 1981. The concept behind this method is that the best option would be the one closest to the ideal solution, and at the same time, the most remote to the anti-ideal solution.

The first step is to determine the objectives to identify the pertinent evaluation criteria and to define if the objective for each criterion is maximized or minimized. Then, a decision matrix (D) is formulated (same as in the ARAS method).

$$D = \begin{bmatrix} x_{11} & \cdots & x_{1n} \\ \vdots & \ddots & \vdots \\ x_{m1} & \cdots & x_{mn} \end{bmatrix}$$

The method used to obtain the normalized matrix is slightly different from ARAS, as shown in Equation (19):

$$R_{ij} = \frac{x_{ij}}{\sqrt{\sum x_{ij}^2}}; i = 1 \dots m; j = 1 \dots n. \quad (19)$$

To build the weight-normalized matrix, it is necessary to assign the weights previously calculated by the AHP, SDM, and Entropy methods to the different criteria and then multiply each element of the normalized matrix, as shown in Equation (20):

$$V_{ij} = w_j * R_{ij} \quad (20)$$

Before obtaining the Euclidian distance with the ideal (A^+) and anti-ideal (A^-) solutions, it is required to determine which are the elements of these A^+ and A^- , depending on whether the criteria is to maximize (J) or minimize (J^*), according to Equation (21):

$$A^+ = \{V_1^+ \dots V_n^+\} ; \text{ Where } V_j^+ = \{\max(V_{ij}) \text{ if } j \in J; \min(V_{ij}) \text{ if } j \in J^*\} \quad (21)$$

$$A^- = \{V_1^- \dots V_n^-\} ; \text{ Where } V_j^- = \{\min(V_{ij}) \text{ if } j \in J; \max(V_{ij}) \text{ if } j \in J^*\}$$

Euclidian distance is obtained by Equations (22) and (23):

$$S_i^+ = \sqrt{\sum_{j=1}^n (V_j^+ - V_{ij})^2} \quad (22)$$

$$S_i^- = \sqrt{\sum_{j=1}^n (V_j^- - V_{ij})^2} \quad (23)$$

with $i = 1 \dots m$.

Finally, to settle the relative closeness to the ideal solution, Equation (24) is used:

$$C_i^+ = \frac{S_i^-}{S_i^+ + S_i^-} \quad (24)$$

Now, based on the values obtained, sort the criteria from the highest C_i^+ for the best solution to the lowest C_i^+ for the worst.

2.4.3. VIKOR

The VIKOR method [52,53] is a MCDM originally developed by Serafim Opricovic in 1980 and is an acronym for Serbian VIseKriterijumska Optimizacija I Kompromisno Resenje, which means Multi-criteria Optimization and Compromise Solution.

This methodology is based on the same concept as TOPSIS, which assumes that a compromise solution is acceptable for conflict resolution. The difference of VIKOR in respect to TOPSIS is the addition of a validation step before the compromise solution is declared feasible.

The method begins with the definition of the criteria to be evaluated and the determination of whether the objective is to maximize or minimize each criterion. With this information, the decision matrix (D) is built.

$$D = \begin{bmatrix} x_{11} & \cdots & x_{1n} \\ \vdots & \ddots & \vdots \\ x_{m1} & \cdots & x_{mn} \end{bmatrix}$$

At this point, the best f_b^* and worst f_b^- for each criterion is rated according to the values of the decision matrix.

$f_b^* = \max(x_{ib})$ $f_b^- = \min(x_{ib})$ Whether the objective is to maximize the criteria.

$f_b^* = \min(x_{ib})$ $f_b^- = \max(x_{ib})$ Whether the objective is to minimize the criteria.

Where, $b = 1 \dots m$, with m being the number of criteria taken into account and $i = 1 \dots n$, where n is the number of the alternatives considered.

Equations (25) and (26) are used to calculate the Utility measure (S_j) and Regret measure (R_j):

$$S_j = \sum_{b=1}^m W_b * \left[\frac{f_b^* - f_{ij}}{f_b^* - f_b^-} \right] \quad (25)$$

$$R_j = \max \left[W_b * \left[\frac{f_b^* - f_{ij}}{f_b^* - f_b^-} \right] \right] \quad (26)$$

where, W_b are the weight values obtained by the AHP, Entropy, and Standard Deviation methods explained before.

With these data, the index Q can be obtained by means of Equation (27):

$$Q_a = v * \frac{S_j - S^*}{S^- - S^*} + (1 - v) * \frac{R_j - R^*}{R^- - R^*} \quad (27)$$

where:

$$\begin{aligned} S^- &= \max(S_j) \\ S^* &= \min(S_j) \\ R^- &= \max(R_j) \\ R^* &= \min(R_j) \end{aligned}$$

v is a parameter that represents the type of voting used during the process. The rule states that $v > 0.5$ means “vote by majority rule”, $v = 0.5$ “vote by consensus”, and $v < 0.5$ “with vote”.

The best alternative solution is the one with the lowest Q_a value, and it can be recommended if the following conditions are satisfied:

The “acceptable advantage” condition means that $Q(a'') - Q(a') \geq DQ$. With a'' being the alternative with eth second position in the ranking list by Q_a , and a' the first one. DQ is defined by Equation (28):

$$DQ = \frac{1}{(n - 1)} \quad (28)$$

where, n is the number of alternatives.

Finally, the “Acceptable stability in decision making” condition implies that the a' alternative must also be the best ranked in S_j and/or R_j . If one of these conditions is not fulfilled, then a set of compromise solutions is proposed.

2.4.4. COPRAS

The COmplex PRoportional ASsessment [54,55] is a MCDM method developed by Zavadskas in 1994, which assumes direct and proportional dependences of the significance and utility degree of the available alternatives under the presence of mutually conflicting criteria.

It is a compensatory method, and as with TOPSIS and VIKOR, it also considers both the ideal and the ideal-worst solutions to solve the problem.

COPRAS begins with the definition of the decision matrix (D), and the normalization of this D , according to Equation (29):

$$D = \begin{bmatrix} x_{11} & \cdots & x_{1n} \\ \vdots & \ddots & \vdots \\ x_{m1} & \cdots & x_{mn} \end{bmatrix}$$

$$N_{ij} = \frac{x_{ij}}{\sum_{i=0}^m x_{ij}} \quad (29)$$

where, m is the number of alternatives.

The weighted normalized decision matrix is obtained by multiplying N_{ij} by the weights from the AHP, Entropy, and Standard Deviation methods, as Equation (30) shows:

$$y_{ij} = N_{ij} * W_j \quad (30)$$

At this point, the beneficial and non-beneficial criteria need to be separated, and then they are summed, as indicated by Equations (31) and (32):

$$S_{+i} = \sum_{j=1}^n y_{+ij} \quad (31)$$

$$S_{-i} = \sum_{j=1}^n y_{-ij} \quad (32)$$

With n being the number of criteria taken into account.

Then, the relative significance of the alternatives is determined by Equation (33):

$$Q_i = S_{+i} + \frac{S_{-min} * \sum_{i=1}^m S_{-i}}{S_{-i} * \sum_{i=1}^m (S_{-min}/S_{-i})} \quad (33)$$

where, $S_{-min} = \min(S_{-i})$.

Finally, the quantitative utility (U_i) is calculated by Equation (34) and the alternatives are sorted by the highest U_i percentage value.

$$U_i = \left[\frac{Q_i}{Q_{max}} \right] * 100\% \quad (34)$$

where, $Q_{max} = \max(Q_i)$.

2.5. Methodology

A methodology to compare MCDM methods based on weight assignment to select the optimum process parameters values is presented in this paper. Both weighting and MCDM methods have been selected based on ease of application, results in earlier works, and their popularity. The weighting methods selected are AHP, Entropy, and Standard Deviation, while the MCDM methods are ARAS, TOPSIS, VIKOR, and COPRAS. The methodology steps are shown in Figure 3.

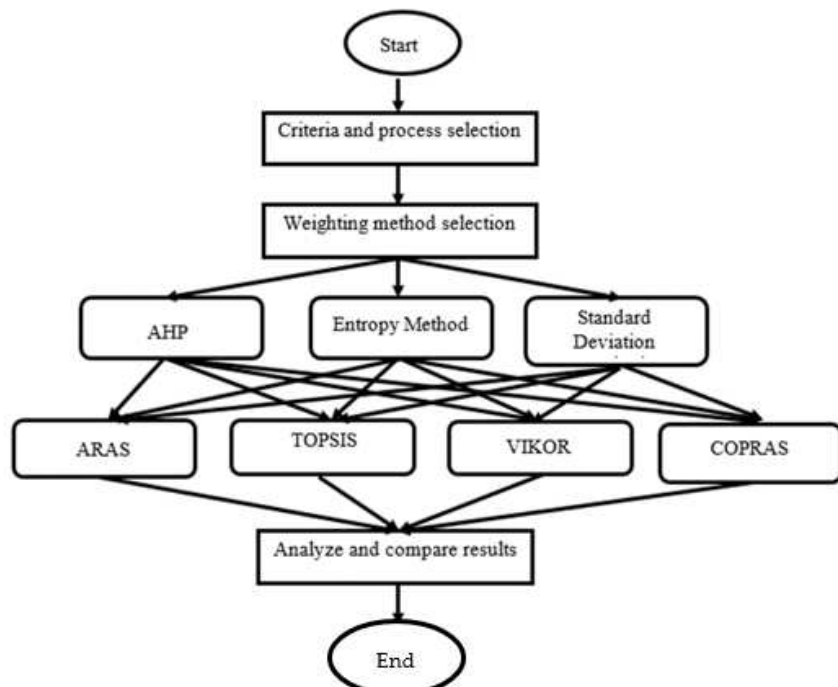


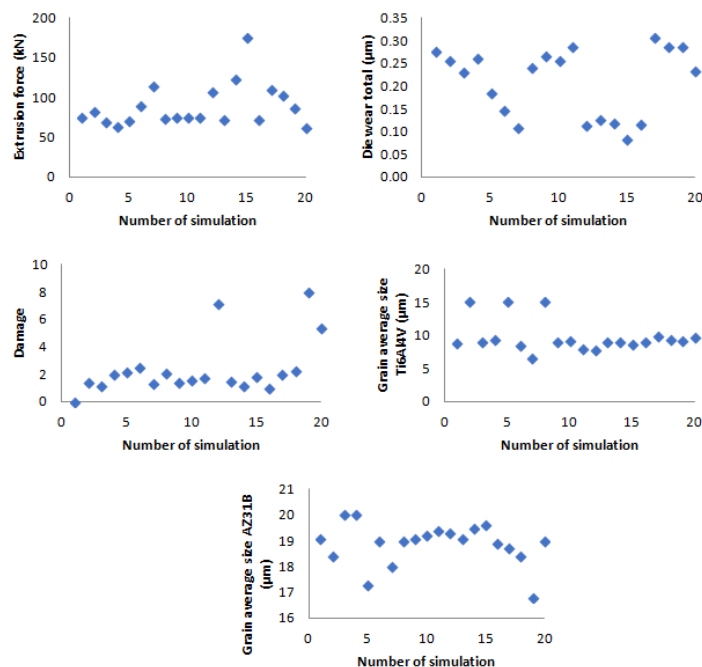
Figure 3. Steps of the methodology.

3. Results

In this paper, a set of simulations of a multi-material co-extrusion process have been performed by using commercial software DEFORM3D© (v11.2), followed by application and comparison of diverse MCDM and weighting methods to establish the optimal process parameters. Table 7 and Figure 4 show the list of simulations carried out in the present work with the process parameters used and the results obtained by each of them.

Table 7. List of simulations with extrusion process parameters.

Number of Simulation	Temperature (°C)	Die Semi-Angle (°)	Ram Speed (mm/s)	Extrusion Ratio (A_o/A_f)	Friction	Billet Height (mm)	Core Diameter (mm)
1	350	30	2	1.78	0.10	20	6
2	300	30	2	1.78	0.10	20	6
3	400	30	2	1.78	0.10	20	6
4	450	30	2	1.78	0.10	20	6
5	350	15	2	1.78	0.10	20	6
6	350	45	2	1.78	0.10	20	6
7	350	60	2	1.78	0.10	20	6
8	350	30	1	1.78	0.10	20	6
9	350	30	3	1.78	0.10	20	6
10	350	30	4	1.78	0.10	20	6
11	350	30	2	1.44	0.10	20	6
12	350	30	2	2.25	0.10	20	6
13	350	30	2	1.78	0.05	20	6
14	350	30	2	1.78	0.30	20	6
15	350	30	2	1.78	0.50	20	6
16	350	30	2	1.78	0.10	15	6
17	350	30	2	1.78	0.10	25	6
18	350	30	2	1.78	0.10	30	6
19	350	30	2	1.78	0.10	20	4
20	350	30	2	1.78	0.10	20	8

**Figure 4.** Plot charts of the different co-extrusion criteria obtained during simulations.

3.1. Weighting Methods

In this section, the different weighting methods explained before are applied and compared. For the AHP method, the pairwise matrix is built, as shown in Table 8:

Table 8. AHP pairwise matrix.

Criteria	Extrusion Force	Damage	Tool Wear	Grain Average Size Ti	Grain Average Size Mg
Extrusion Force	1.00	0.33	5.00	3.00	3.00
Damage	3.00	1.00	7.00	5.00	5.00
Tool wear	0.20	0.14	1.00	0.33	0.33
Grain average size Ti	0.33	0.20	3.00	1.00	3.00
Grain average size Mg	0.33	0.20	3.00	0.33	1.00
Total	4.86	1.87	19.00	9.66	12.33

In this pairwise matrix, the order of significance is found to be Damage > Extrusion force > Grain average size Ti > Grain average size Mg > Tool wear. The reasons are as follows:

- Damage is considered the most important factor due to the fact that a high value could mean a central burst or chevron cracking occurrence. In this case, a deeper analysis of the hydrostatic stress using the HSC has to be performed.
- Extrusion force is a factor that can limit the characteristics of the machine to be used. If a high value is required, a more complex machine is needed to perform the process.
- Grain average size is recommended to be as small as possible to enhance the mechanical properties of the final part. The results of simulation AZ31B show a smaller range of variation in the grain size, which is why Ti₆Al₄V is considered moderately preferred.
- Tool wear is an economic factor. The less wear in each extrusion, the longer the change time of the die.

Then, the normalized matrix is obtained:

0.20547945	0.17766497	0.26315789	0.31034483	0.24324324
0.61643836	0.53299492	0.36842105	0.51724138	0.40540541
0.04109589	0.07614213	0.05263158	0.03448276	0.02702703
0.06849315	0.10659898	0.15789474	0.10344828	0.24324324
0.06849315	0.10659898	0.15789474	0.03448276	0.08108108

The weights are calculated from the normalized matrix and shown in Table 9:

Table 9. AHP weights.

	Extrusion Force (kN)	Die Wear Total (μm)	Damage	Grain Average Size Ti ₆ Al ₄ V (μm)	Grain Average Size AZ31B (μm)
In %	0.24 24.00%	0.04 4.63%	0.48 48.81%	0.13 13.59%	0.08 8.97%

Finally, the consistency ratio is calculated to verify the assumptions taken in the pairwise matrix. In order to do that, the following parameters are calculated:

$$\lambda_{\max} = 5.38$$

$$CI = 0.09$$

$$RI = 1.12$$

$$CR = 0.08$$

The condition $CR < 0.1$ is fulfilled.

For the Entropy method, the normalized matrix is:

0.04238881	0.06597512	0.02842942	0.04546156	0.05055585
0.04663699	0.06099129	0.02385686	0.07714065	0.04870302
0.03916851	0.05496847	0.03936382	0.04628439	0.05293806
0.03568236	0.06225345	0.04274354	0.04834148	0.05293806
0.03976735	0.04418737	0.05109344	0.07714065	0.04579142
0.05053058	0.03514114	0.02624254	0.04309591	0.05029116
0.06410506	0.02586695	0.04234592	0.03432762	0.04764426
0.04159751	0.05770154	0.02862823	0.07714065	0.05029116
0.04230461	0.06371716	0.03240557	0.04628439	0.05055585
0.04217691	0.06142081	0.03518887	0.04679866	0.05082054
0.0419384	0.06847687	0.14274354	0.04062741	0.05134992
0.06025291	0.02717757	0.03081511	0.04011314	0.05108523
0.04062679	0.03013044	0.02326044	0.04628439	0.05055585
0.06965068	0.02848820	0.03677932	0.04649010	0.05161461
0.09860600	0.01949619	0.02067594	0.04443302	0.0518793
0.04078153	0.02798574	0.03956262	0.04587298	0.05002647
0.06235858	0.07319051	0.04512922	0.05044999	0.04949709
0.05784159	0.06833866	0.1584493	0.04787863	0.04870302
0.04885389	0.06853062	0.10735586	0.04690152	0.04446797
0.03473095	0.05596188	0.04493042	0.04983286	0.05029116

Then, the entropy array (E_j) is calculated:

$$E_j = [0.98691712 \ 0.97765503 \ 0.92705489 \ 0.99129917 \ 0.99970911]$$

The weights are presented in Table 10:

Table 10. Entropy method weights.

	Extrusion Force (kN)	Die Wear Total (μm)	Damage	Grain Average Size Ti6Al4V (μm)	Grain Average Size AZ31B (μm)
In %	0.11 11.15%	0.19 19.04%	0.62 62.15%	0.07 7.41%	2.47×10^{-3} 0.25%

For the SD method, the decision matrix is:

	74.99224	0.00027495	1.43	8.84	19.10
	82.50792	0.00025418	1.20	15.00	18.40
	69.29504	0.00022908	1.98	9.00	20.00
	63.12752	0.00025944	2.15	9.40	20.00
	70.35448	0.00018415	2.57	15.00	17.30
	89.39628	0.00014645	1.32	8.38	19.00
	113.4116	0.0001078	2.13	6.50	18.00
	73.59232	0.00024047	1.44	15.00	19.00
	74.84328	0.00026554	1.63	9.00	19.10
	74.61736	0.00025597	1.77	9.10	19.20
	74.19540	0.00028538	7.18	7.90	19.40
	106.59656	0.00011326	1.55	7.80	19.30
	71.874960	0.00012557	1.17	9.00	19.10
	123.22264	0.00011872	1.85	9.04	19.50
	174.44900	0.00008125	1.04	8.64	19.60
	72.14872	0.00011663	1.99	8.92	18.90
	110.32180	0.00030502	2.27	9.81	18.70
	102.33056	0.0002848	7.97	9.31	18.40
	86.42996	0.00028560	5.40	9.12	16.80
	61.44432	0.00023322	2.26	9.69	19.00
Max	174.4490	0.00030502	7.97	15.00	20.00
Min	61.44432	0.00008125	1.04	6.50	16.80

The normalized matrix is obtained considering that all criteria are clustered as non-beneficial, because the objective is to minimize all these outcomes from the co-extrusion process.

0.88011187	0.13437905	0.94372294	0.72470588	0.28125
0.81360418	0.22719757	0.97691198	0.00	0.50
0.93052748	0.33936631	0.86435786	0.70588235	0.00
0.98510504	0.20369129	0.83982684	0.65882353	0.00
0.92115229	0.54015284	0.77922078	0.00	0.84375
0.75264777	0.70862940	0.95959596	0.77882353	0.3125
0.54013161	0.88135139	0.84271284	1.00	0.625
0.89250003	0.28846584	0.94227994	0.00	0.3125
0.88143004	0.17643116	0.91486291	0.70588235	0.28125
0.88342925	0.21919828	0.89466089	0.69411765	0.25
0.88716326	0.08778657	0.11399711	0.83529412	0.1875
0.6004392	0.8569424	0.92640693	0.84705882	0.21875
0.90769727	0.80194843	0.98124098	0.70588235	0.28125
0.45331185	0.8325334	0.88311688	0.70117647	0.15625
0.00	1.00	1.00	0.74823529	0.125
0.90527472	0.84189123	0.86291486	0.71529412	0.34375
0.56747384	0.00	0.82251082	0.61058824	0.40625
0.63818985	0.09036064	0.00	0.66941176	0.50
0.7788973	0.08678554	0.37085137	0.69176471	1.00
1.00	0.32086517	0.82395382	0.62470588	0.3125

After calculating the standard deviation for each column, the following array is obtained:
 $\sigma = [0.23896758 \ 0.33516811 \ 0.28284746 \ 0.2810343 \ 0.25080053]$

The resultant weights are shown in Table 11:

Table 11. Standard Deviation method weights.

	Extrusion Force (kN)	Die Wear Total (μm)	Damage	Grain Average Size Ti6Al4V (μm)	Grain Average Size AZ31B (μm)
In %	0.17 17.21%	0.24 24.13%	0.20 20.37%	0.20 20.24%	0.18 18.06%

The weighting process results comparison among these three methods is shown in Table 12:

Table 12. Standard Deviation method weights.

	Extrusion Force (kN)	Die Wear Total (μm)	Damage	Grain Average Size Ti6Al4V (μm)	Grain Average Size AZ31B (μm)
AHP	24.00%	4.63%	48.81%	13.59%	8.97%
Entropy	11.15%	19.04%	62.15%	7.41%	0.25%
Standard Variation	17.21%	20.37%	24.13%	20.24%	18.06%

3.2. MCDM Methods

This section presents the results obtained after applying the MCDM methods explained in this paper. To avoid being redundant, only the numbers for weighting values obtained by AHP methods will be shown. For the Entropy and SD methods, only the final results will be presented.

All the methods share the same Decision matrix (D):

74.99224	0.000274950	1.43	8.84	19.10
82.50792	0.000254180	1.20	15.00	18.40
69.29504	0.000229080	1.98	9.00	20.00
63.12752	0.000259440	2.15	9.40	20.00
70.35448	0.000184150	2.57	15.00	17.30
89.39628	0.000146450	1.32	8.38	19.00
113.4116	0.000107800	2.13	6.50	18.00
73.59232	0.000240470	1.44	15.00	19.00
74.84328	0.000265540	1.63	9.00	19.10
74.61736	0.000255970	1.77	9.10	19.20
74.1954	0.000285376	7.18	7.90	19.40
106.59656	0.000113262	1.55	7.80	19.30
71.87496	0.000125568	1.17	9.00	19.10
123.22264	0.000118724	1.85	9.04	19.50
174.449	0.000081250	1.04	8.64	19.60
72.14872	0.000116630	1.99	8.92	18.90
110.3218	0.000305020	2.27	9.81	18.70
102.33056	0.000284800	7.97	9.31	18.40
86.42996	0.000285600	5.40	9.12	16.80
61.44432	0.000233220	2.26	9.69	19.00

The first MCDM method to be applied is ARAS.

As explained before, all the criteria are considered non-beneficial; therefore, before calculating, the normalized matrix needs to be obtained x_{ij}^* :

0.01333471	3637.02491	0.6993007	0.11312217	0.05235602
0.01212005	3934.21984	0.83333333	0.06666667	0.05434783
0.01443105	4365.28724	0.50505051	0.11111111	0.05
0.01584095	3854.45575	0.46511628	0.10638298	0.05
0.01421374	5430.35569	0.38910506	0.06666667	0.05780347
0.01118615	6828.26903	0.75757576	0.11933174	0.05263158
0.00881744	9276.43785	0.46948357	0.15384615	0.05555556
0.01358837	4158.52289	0.69444444	0.06666667	0.05263158
0.01336125	3765.91097	0.61349693	0.11111111	0.05235602
0.01340171	3906.70782	0.56497175	0.10989011	0.05208333
0.01347792	3504.14891	0.13927577	0.12658228	0.05154639
0.00938117	8829.08654	0.64516129	0.12820513	0.05181347
0.01391305	7963.81244	0.85470085	0.11111111	0.05235602
0.00811539	8422.8968	0.54054054	0.11061947	0.05128205
0.00573233	12307.6923	0.96153846	0.11574074	0.05102041
0.01386026	8574.1233	0.50251256	0.11210762	0.05291005
0.00906439	3278.47354	0.44052863	0.10193680	0.05347594
0.00977225	3511.23596	0.12547051	0.10741139	0.05434783
0.01157006	3501.40056	0.18518519	0.10964912	0.05952381
0.01627490	4287.79693	0.44247788	0.10319917	0.05263158
Optimal value (OV)	0.0162749	12307.6923	0.96153846	0.15384615
				0.05952381

With these values, the normalized matrix is obtained:

	0.05173867	32.78369954	0.71314958	0.28840608	0.21459583
	0.04702577	35.46257844	0.84983659	0.16996732	0.2227598
	0.05599244	39.3481674	0.51505248	0.28327886	0.20493902
	0.06146287	34.74359462	0.47432740	0.27122444	0.20493902
	0.05514928	48.9485647	0.39681086	0.16996732	0.23692372
	0.04340224	61.54918531	0.77257871	0.30423744	0.21572528
	0.03421166	83.61668079	0.47878117	0.39223227	0.22771002
	0.05272287	37.4844188	0.70819715	0.16996732	0.21572528
	0.05184164	33.94546279	0.62564657	0.28327886	0.21459583
	0.05199861	35.21458838	0.57616040	0.28016591	0.21347814
	0.05229433	31.58597145	0.14203397	0.32272275	0.21127734
	0.03639891	79.58431061	0.65793800	0.32686023	0.21237204
	0.05398262	71.78483522	0.87162727	0.28327886	0.21459583
	0.03148771	75.92296577	0.55124535	0.28202542	0.21019386
	0.02224145	110.9400392	0.98058068	0.29508215	0.20912144
	0.05377779	77.28610296	0.51246427	0.28581948	0.21686668
	0.03516983	29.55176116	0.44925282	0.25988886	0.21918611
	0.03791632	31.64985319	0.12795532	0.27384638	0.2227598
	0.04489183	31.56119814	0.18885257	0.27955151	0.24397502
	0.06314658	38.64967922	0.45124066	0.26310730	0.21572528
OV	0.06314658	110.9400392	0.98058068	0.39223227	0.24397502

The normalized weighted matrix is calculated by multiplying the weights obtained before by the normalized matrix.

	0.01241615	16.00173107	0.03300162	0.03920468	0.01925142
	0.01128515	17.30929246	0.03932693	0.02310462	0.01998381
	0.01343696	19.20584930	0.02383451	0.0385077	0.01838511
	0.01474974	16.95835630	0.02194992	0.03686908	0.01838511
	0.01323462	23.89180537	0.01836277	0.02310462	0.02125446
	0.01041559	30.04217110	0.03575176	0.04135672	0.01935275
	0.00821005	40.81332058	0.02215602	0.05331836	0.0204279
	0.01265233	18.29615319	0.03277244	0.02310462	0.01935275
	0.01244086	16.56878797	0.02895234	0.03850770	0.01925142
	0.01247853	17.18824846	0.02666233	0.03808454	0.01915115
	0.01254949	15.41711972	0.00657275	0.04386954	0.01895372
	0.00873494	38.8451198	0.03044666	0.04443197	0.01905193
	0.01295465	35.03819411	0.04033532	0.0385077	0.01925142
	0.00755636	37.05801656	0.02550936	0.03833732	0.01885652
	0.00533746	54.14985795	0.04537723	0.04011219	0.01876031
	0.01290549	37.72336413	0.02371473	0.03885306	0.01945514
	0.00843999	14.42422123	0.02078957	0.03532817	0.01966322
	0.00909909	15.44830042	0.00592124	0.03722549	0.01998381
	0.01077305	15.40502787	0.00873932	0.03800102	0.02188703
	0.01515379	18.86491707	0.02088156	0.03576567	0.01935275
OV	0.01515379	54.14985795	0.04537723	0.05331836	0.02188703

To calculate the degree of utility (K_i), it is necessary to obtain the optimality function (S_i):

	16.1056049	
	17.402993	
	19.3000136	
	17.0503101	
	23.9677618	
	30.1490479	
	40.9174329	
	18.3840353	
	16.6679403	
	17.284625	
	15.4990652	
	38.9477853	
	35.1492432	
	37.1482761	
	54.2594451	
	37.8182926	
	14.5084422	
	15.5205301	
	15.4844283	
	18.9560708	
OV	54.2855944	

Finally, K_i is obtained and the results are sorted by highest value:

0.29668285
0.32058216
0.35552735
0.31408535
0.44151238
0.55537843
0.75374385
0.33865403
0.30704168
0.31840169
0.28550973
0.71746079
0.64748749
0.68431186
0.99951830
0.69665430
0.26726137
0.28590513
0.28524010
0.34919155

For AHP weighted values, the best alternative is number 15. In Tables 13 and 14 below, there is a comparison with the results obtained by using the weight values of the other methods.

Table 13. Best alternative comparison among weighting methods for process parameters using ARAS.

	Temperature (°C)	Die Semi-Angle (°)	Ram Speed (mm/s)	Extrusion Ratio (Ao/Af)	Friction	Billet Height (mm)	Core Diameter (mm)
AHP	350.00	30.00	2.00	1.78	0.50	20.00	6.00
Entropy	350.00	30.00	2.00	1.78	0.50	20.00	6.00
SD	350.00	30.00	2.00	1.78	0.50	20.00	6.00

Table 14. Best alternative comparison among weighting methods for process criteria using ARAS.

	Extrusion Force (kN)	Die Wear Total (μm)	Damage	Grain Average Size Ti6Al4V (μm)	Grain Average Size AZ31B (μm)
AHP	174.45	8.12×10^{-5}	1.04	8.64	19.60
Entropy	174.45	8.12×10^{-5}	1.04	8.64	19.60
SD	174.45	8.12×10^{-5}	1.04	8.64	19.60

In the case of the ARAS method, it can be verified that independent of the weight criterion, the best extrusion parameter combination is number 15.

The next MCDM method to be studied is TOPSIS. As with the ARAS method, the starting point is the decision matrix D .

The first difference is the method used to calculate the normalized matrix. With the TOPSIS method, Equation (19) is used:

$$R_{ij} = \frac{x_{ij}}{\sqrt{\sum x_{ij}^2}}$$

Consequently, the normalized matrix obtained is different from the one obtained by using ARAS.

0.18169569	0.27841399	0.10124168	0.19771981	0.22589903
0.19990512	0.25738231	0.08495806	0.33549741	0.21762001
0.16789217	0.23196609	0.14018079	0.20129845	0.23654349
0.15294913	0.26270858	0.15221652	0.21024504	0.23654349
0.17045904	0.18647003	0.18195184	0.33549741	0.20461012
0.21659466	0.14829507	0.09345386	0.18743122	0.22471631
0.27478041	0.10915813	0.15080055	0.14538221	0.21288914
0.17830388	0.24349959	0.10194967	0.33549741	0.22471631
0.18133478	0.26888543	0.11540136	0.20129845	0.22589903
0.18078740	0.25919486	0.12531313	0.2035351	0.22708175
0.17976505	0.28897134	0.50833237	0.1766953	0.22944718
0.25826852	0.11468894	0.10973749	0.17445865	0.22826446
0.17414295	0.12714998	0.08283411	0.20129845	0.22589903
0.29855118	0.12021976	0.13097700	0.20219311	0.23062990
0.42266547	0.08227364	0.07363032	0.19324651	0.23181262
0.17480623	0.11809938	0.14088878	0.19950913	0.22353359
0.26729426	0.30886283	0.16071232	0.21941531	0.22116816
0.24793260	0.28838808	0.56426310	0.20823206	0.21762001
0.20940768	0.28919816	0.38231126	0.20398243	0.19869653
0.14887097	0.23615825	0.16000434	0.21673133	0.22471631

From normalized decision matrix, the weighted one is obtained by multiplying each column by the weight associated to the correspondent criteria.

0.04360298	0.01288385	0.04941609	0.02687718	0.02026543
0.04797285	0.01191059	0.04146805	0.04560607	0.01952272
0.04029044	0.01073443	0.06842228	0.02736364	0.02122035
0.03670444	0.01215707	0.07429692	0.0285798	0.02122035
0.04090643	0.00862906	0.08881073	0.04560607	0.0183556
0.05197797	0.00686248	0.04561485	0.02547859	0.02015933
0.06594127	0.00505139	0.07360578	0.01976263	0.01909831
0.04278902	0.01126816	0.04976166	0.04560607	0.02015933
0.04351637	0.01244291	0.05632743	0.02736364	0.02026543
0.04338501	0.01199447	0.06116537	0.02766768	0.02037154
0.04313967	0.01337240	0.24811715	0.02401920	0.02058374
0.06197878	0.00530733	0.05356289	0.02371516	0.02047764
0.04179049	0.00588398	0.04043135	0.02736364	0.02026543
0.07164574	0.005556327	0.06392991	0.02748526	0.02068984
0.10143045	0.00380728	0.03593897	0.0262691	0.02079594
0.04194966	0.00546515	0.06876784	0.02712041	0.02005323
0.06414476	0.0142929	0.07844372	0.02982637	0.01984103
0.05949839	0.01334541	0.27541694	0.02830617	0.01952272
0.05025325	0.0133829	0.18660621	0.02772849	0.01782509
0.03572577	0.01092843	0.07809815	0.02946152	0.02015933
A⁺	0.10143045	0.0142929	0.27541694	0.04560607
A⁻	0.03572577	0.00380728	0.03593897	0.01976263
				0.01782509

Then, the distance to the ideal solution (A^+) and anti-ideal solution (A^-) is calculated:

D_j^+	D_j^-
0.01956117	0.23403861
0.03028185	0.23999658
0.03454403	0.21663412
0.04038909	0.21197447
0.05927627	0.19627868
0.02012987	0.23604237
0.04832116	0.20674868
0.03114406	0.23317247
0.02479289	0.22735737
0.02882775	0.22271237
0.21258354	0.06789948
0.03201143	0.22657484
0.01118059	0.2432685
0.04631054	0.21451981
0.06609285	0.24048647
0.03432669	0.2160158
0.05319383	0.20109593
0.24100142	0.04540224
0.15187762	0.10410771
0.04390472	0.20862622

The last step is to obtain the closeness to the ideal solution and sort the values from highest to lowest.

0.05935214
0.06486590
0.05441376
0.05349463
0.05015999
0.06046750
0.05273535
0.06163134
0.05732822
0.05602110
0.01904465
0.05858914
0.06189945
0.05595327
0.07372818
0.05407793
0.05113664
0.01300337
0.02665005
0.05268458

Using the AHP weights, the best alternative solution is again number 15. After applying the weights from the Entropy and SD methods, the results obtained are shown in Tables 15 and 16.

Table 15. Best alternative comparison among weighting methods for process parameters using TOPSIS.

	Temperature (°C)	Die Semi-Angle (°)	Ram Speed (mm/s)	Extrusion Ratio (Ao/Af)	Friction	Billet Height (mm)	Core Diameter (mm)
AHP	350.00	30.00	2.00	1.78	0.50	20.00	6.00
Entropy	350.00	30.00	2.00	1.78	0.50	20.00	6.00
SD	350.00	30.00	2.00	1.78	0.50	20.00	6.00

Table 16. Best alternative comparison among weighting methods for process criteria using TOPSIS.

	Extrusion Force (kN)	Die Wear Total (μm)	Damage	Grain Average Size Ti6Al4V (μm)	Grain Average Size AZ31B (μm)
AHP	174.45	8.12×10^{-5}	1.04	8.64	19.60
Entropy	174.45	8.12×10^{-5}	1.04	8.64	19.60
SD	174.45	8.12×10^{-5}	1.04	8.64	19.60

The TOPSIS results are aligned with the ARAS ones. In both cases, the best alternative is number 15, independent of the weighting method used.

After obtaining the same results with the ARAS and TOPSIS methods, it is needed to check what happened with the other two pending MCDM methods. Let us start by VIKOR.

In VIKOR, the best f_b^* and worst f_b^- values for each criteria are obtained directly from decision matrix D .

74.99224	0.00027495	1.43	8.84	19.10
82.50792	0.00025418	1.20	15.00	18.40
69.29504	0.00022908	1.98	9.00	20.00
63.12752	0.00025944	2.15	9.40	20.00
70.35448	0.00018415	2.57	15.00	17.30
89.39628	0.00014645	1.32	8.38	19.00
113.4116	0.00010780	2.13	6.50	18.00
73.59232	0.00024047	1.44	15.00	19.00
74.84328	0.00026554	1.63	9.00	19.10
74.61736	0.00025597	1.77	9.10	19.20
74.1954	0.000285376	7.18	7.90	19.40
106.59656	0.000113262	1.55	7.80	19.30
71.87496	0.000125568	1.17	9.00	19.10
123.22264	0.000118724	1.85	9.04	19.50
174.449	0.00008125	1.04	8.64	19.60
72.14872	0.00011663	1.99	8.92	18.90
110.3218	0.00030502	2.27	9.81	18.70
102.33056	0.0002848	7.97	9.31	18.40
86.42996	0.0002856	5.4	9.12	16.80
61.44432	0.00023322	2.26	9.69	19.00
f_i^*	61.44432	0.00008125	1.04	6.50
f_i^-	174.449	0.00030502	7.97	15.00

Utility measure (S_j) and Regret measure (R_j) are obtained:

	S_i		R_i
	0.19819819		0.06447916
	0.27255304		0.13593568
	0.24314147		0.08971014
	0.25469310		0.08971014
	0.29791683		0.13593568
	0.18430526		0.06167572
	0.22626210		0.11035833
	0.28450908		0.13593568
	0.21258124		0.06447916
	0.22438568		0.06728261
	0.59702892		0.43245821
	0.22930296		0.09588583
	0.14493217		0.06447916
	0.31230722		0.13119317
	0.35269826		0.23997808
	0.19453387		0.06691129
	0.34290553		0.10379680
	0.70681489		0.48810022
	0.44430736		0.30708759
	0.23004732		0.08592818
S^*	0.14493217	R^*	0.06167572
S^-	0.70681489	R^-	0.48810022

Using the values S^* , S^- , R^* and R^- together with the assumption of vote by consensus ($v = 0.5$), the index Q is calculated:

0.05068674
0.20063820
0.12026455
0.13054395
0.22320856
0.03503675
0.12945502
0.21127747
0.06348572
0.07727723
0.83706275
0.11519138
0.00328715
0.23045330
0.39395059
0.05027775
0.22555831
1.00
0.55415898
0.10417802

In VIKOR, the index Q is ranked from the lowest to the highest value, therefore the best alternative solution should be number 13. However, before recommending this alternative as the best compromise solution, the conditions of “Acceptable advantages” and “Acceptable stability in decision making” have to be fulfilled.

In this case, $DQ = 0.05263158$ due to the number of alternatives is 20. Then:

$$Q(2) - Q(1) = 0.0317496$$

$$Q(3) - Q(1) = 0.0469906$$

$$Q(4) - Q(1) = 0.04739959$$

$$Q(5) - Q(1) = 0.06019857 > DQ$$

$$Q(1) = S^*$$

As only the second condition is fulfilled, a set of compromise solutions is presented. These results were obtained using AHP weights. Next, the same process is performed, but using the weights from the Entropy and SD methods, and the results are compared in Tables 17 and 18:

Table 17. Best alternative comparison among weighting methods for process parameters using VIKOR.

	Temperature (°C)	Die Semi-Angle (°)	Ram Speed (mm/s)	Extrusion Ratio (Ao/Af)	Friction	Billet Height (mm)	Core Diameter (mm)
AHP	350.00	30.00	2.00	1.78	0.05	20.00	6.00
Entropy	350.00	30.00	2.00	1.78	0.05	20.00	6.00
SD	350.00	60.00	2.00	1.78	0.10	20.00	6.00

Table 18. Best alternative comparison among weighting methods for process criteria using VIKOR.

	Extrusion Force (kN)	Die Wear Total (μm)	Damage	Grain Average Size Ti6Al4V (μm)	Grain Average Size AZ31B (μm)
AHP	71.87	1.25×10^{-4}	1.17	9.00	19.10
Entropy	71.87	1.25×10^{-4}	1.17	9.00	19.10
SD	113.41	1.07×10^{-4}	2.13	6.50	18.00

Entropy weights lead to the same results as the AHP ones, stating the best alternative solution is number 13, but only fulfilling the condition of “Acceptable stability in decision making”. In the case of the SD method, the results are different, and the best compromise solution is number 7, which, in addition, fulfills the two conditions for Q index; however, it is the one with the highest value of damage, which is the criteria considered the most relevant, followed by extrusion force and Ti₆Al₄V grain size. In the case of alternative 7, a deeper analysis using the HSC method is recommended to verify the integrity of the final part.

The last method to be analyzed is COPRAS. The normalization matrix is obtained by using Equation (29):

$$N_{ij} = \frac{x_{ij}}{\sum_{i=0}^m x_{ij}}$$

0.04238881	0.06597512	0.02842942	0.04546156	0.05055585
0.04663699	0.06099129	0.02385686	0.07714065	0.04870302
0.03916851	0.05496847	0.03936382	0.04628439	0.05293806
0.03568236	0.06225345	0.04274354	0.04834148	0.05293806
0.03976735	0.04418737	0.05109344	0.07714065	0.04579142
0.05053058	0.03514114	0.02624254	0.04309591	0.05029116
0.06410506	0.02586695	0.04234592	0.03342762	0.04764426
0.04159751	0.05770154	0.02862823	0.07714065	0.05029116
0.04230461	0.06371716	0.03240557	0.04628439	0.05055585
0.04217691	0.06142081	0.03518887	0.04679866	0.05082054
0.04193840	0.06847687	0.14274354	0.04062741	0.05134992
0.06025291	0.02717757	0.03081511	0.04011314	0.05108523
0.04062679	0.03013044	0.02326044	0.04628439	0.05055585
0.06965068	0.02848820	0.03677932	0.04649010	0.05161461
0.09860600	0.01949619	0.02067594	0.04443302	0.0518793
0.04078153	0.02798574	0.03956262	0.04587298	0.05002647
0.06235858	0.07319051	0.04512922	0.05044999	0.04949709
0.05784159	0.06833866	0.1584493	0.04787863	0.04870302
0.04885389	0.06853062	0.10735586	0.04690152	0.04446797
0.03473095	0.05596188	0.04493042	0.04983286	0.05029116

Next, the weighted matrix is calculated by multiplying the normalized one by the weights obtained before:

0.01017238	0.00305306	0.01387641	0.00617985	0.00453537
0.01119185	0.00282243	0.01164454	0.01048617	0.00436915
0.00939958	0.00254371	0.01921349	0.00629170	0.00474908
0.00856298	0.00288083	0.02086313	0.00657133	0.00474908
0.00954329	0.00204481	0.02493872	0.01048617	0.00410796
0.01212623	0.00162619	0.01280899	0.00585827	0.00451163
0.01538381	0.00119702	0.02066906	0.00454401	0.00427417
0.00998249	0.00267019	0.01397345	0.01048617	0.00451163
0.01015218	0.00294857	0.01581716	0.00629170	0.00453537
0.01012153	0.0028423	0.01717569	0.00636161	0.00455912
0.01006430	0.00316883	0.06967315	0.00552271	0.00460661
0.01445938	0.00125767	0.01504086	0.00545281	0.00458286
0.00974954	0.00139431	0.01135342	0.00629170	0.00453537
0.01671464	0.00131832	0.01795200	0.00631966	0.00463035
0.02366328	0.0009022	0.01009193	0.00604003	0.00465451
0.00978667	0.00129506	0.01931053	0.00623577	0.00448788
0.01496469	0.00338696	0.02202758	0.00685795	0.00444039
0.01388071	0.00316243	0.07733914	0.00650841	0.00436915
0.01172386	0.00317131	0.05240042	0.00637559	0.00398923
0.00833467	0.00258968	0.02193055	0.00677406	0.00451163

As all the criteria are considered to be non-beneficial. Only S_{-i} , according to Equation (28), has to be calculated:

$$S_{-i} = \sum_{j=1}^n y_{-ij}$$

Finally, the relative significance of alternatives (Q_i) and quantitative utility (U_i) are determined:

Q_i	U_i
0.06051591	88.1198594
0.05648730	82.2536226
0.05423380	78.9722039
0.05245640	76.3840570
0.04476706	65.1872727
0.06196732	90.2333220
0.04967724	72.3372077
0.05498123	80.0605711
0.05758046	83.8454203
0.05573600	81.1596231
0.02459848	35.8189210
0.05610036	81.6901852
0.06867454	100.00
0.04875969	71.0011115
0.05046210	73.4800694
0.05566054	81.0497473
0.04428486	64.4851229
0.02174176	31.6591243
0.02946848	42.9103388
0.05184648	75.4959312

Ranking U_i from highest to lowest value, the best alternative using COPRAS combined with AHP weighting method is number 13; the same obtained by VIKOR. In Tables 19 and 20, a comparison of combining the Entropy and SD weighting methods with COPRAS is shown:

Table 19. Best alternative comparison among weighting methods for process parameters using COPRAS.

	Temperature (°C)	Die Semi-Angle (°)	Ram Speed (mm/s)	Extrusion Ratio (Ao/Af)	Friction	Billet Height (mm)	Core Diameter (mm)
AHP	350.00	30.00	2.00	1.78	0.05	20.00	6.00
Entropy	350.00	30.00	2.00	1.78	0.05	20.00	6.00
SD	350.00	30.00	2.00	1.78	0.05	20.00	6.00

Table 20. Best alternative comparison among weighting methods for process criteria using COPRAS.

	Extrusion Force (kN)	Die Wear Total (μm)	Damage	Grain Average Size Ti6Al4V (μm)	Grain Average Size AZ31B (μm)
AHP	71.87	1.25×10^{-4}	1.17	9.00	19.10
Entropy	71.87	1.25×10^{-4}	1.17	9.00	19.10
SD	71.87	1.25×10^{-4}	1.17	9.00	19.10

The results after applying the three weighting methods confirm that the best alternative is number 13; no matter which weighting method is used, the best alternative is the same in all cases.

4. Discussion

The main novelty of this paper is the comparison of four different MCDM methods together with three weighting methods to check the grade of influence of choosing a particular weighting method on the final result, and also to evaluate which of the MCDM methods applied fits better in obtaining the optimal process parameters to meet specific criteria to manufacture a bimetallic billet of dissimilar materials by co-extrusion.

The results reveal that in three of the four MCDM methods studied, the best solution obtained is the same, independent of the weighting method used. This becomes especially relevant when observing the great difference in weights obtained for the damage criteria between AHP and SD, the grain size criteria between Entropy and SD, or the total wear among AHP, Entropy, and SD. It must be taken into account that the Entropy and SD methods are independent of previous experience and only consider the current results of the different experiments, while AHP is supported by customer needs or design characteristics. In addition, the AHP method needs a validation to check the consistency of the pairwise comparison matrix.

Regarding the MCDM methods, it has been seen that they are aligned two by two; on one side, ARAS and TOPSIS, and on the other side, VIKOR and COPRAS. It is also relevant to take into account that TOPSIS and VIKOR are both distance-based methods (see Section 2.4) and, therefore, the results they obtain should be similar. Comparing these methods by complexity, TOPSIS can be considered more complex than ARAS because it needs to calculate the Euclidian distances from the ideal and non-ideal solution, and VIKOR is more complex than COPRAS because COPRAS performs a final validation before recommending the best compromise solution.

VIKOR is the only method that obtains different results depending on the weighing method used, leading to the result that alternative 7 is the optimal one when applied together with the SD method.

Table 21 shows a summary of the best alternative for each MCDM method depending on the weighting method applied.

Table 21. Best alternative comparison for each MCDM together with weighting method.

	ARAS	TOPSIS	VIKOR	COPRAS
AHP	Alternative 15	Alternative 15	Alternative 13	Alternative 13
Entropy	Alternative 15	Alternative 15	Alternative 13	Alternative 13
SD	Alternative 15	Alternative 15	Alternative 7	Alternative 13

A comparison among all the alternative solutions has been made in Table 22 to evaluate which can be considered as optimal. After studying the values obtained for each criterion, our conclusion is that the alternative with the best balance among all the criteria considered is number 13.

Table 22. Best alternative comparison for process criteria.

	Extrusion Force (kN)	Die Wear Total (μm)	Damage	Grain Average Size Ti6Al4V (μm)	Grain Average Size AZ31B (μm)
Alternative 7	113.41	1.07×10^{-4}	2.13	6.50	18.00
Alternative 13	71.87	1.25×10^{-4}	1.17	9.00	19.10
Alternative 15	174.45	8.12×10^{-5}	1.04	8.64	19.60

In summary, it could be said that both VIKOR and COPRAS are the recommended MCDM methods from the point of view of calculation results. The COPRAS method also

obtained the same result independent of the weighting method chosen and it is simpler than VIKOR, considering the computing mechanism. Secondly, the VIKOR method implements two conditions to be fulfilled to confirm the compromise solution or set of compromise solutions; these conditions increase the complexity of application of this method but also provide a security check of the alternative chosen. Finally, the methodology recommended to obtain the optimal manufacturing parameters in a multi-material co-extrusion process is VIKOR together with the Entropy weighting method. Even when considering that is VIKOR a more complex process than COPRAS, the determining factors are the “Acceptable advantages” and “Acceptable stability in decision making” conditions to confirm the compromise solution or set of compromise solutions to be recommended.

In future work, this methodology can be extended to other multi-material manufacturing processes.

Author Contributions: Conceptualization, D.F., Á.R.-P. and A.M.C.; methodology, D.F.; formal analysis, D.F., Á.R.-P. and A.M.C.; investigation, D.F., Á.R.-P. and A.M.C.; resources, Á.R.-P. and A.M.C.; writing—original draft preparation, D.F.; writing—review and editing, Á.R.-P. and A.M.C.; supervision, Á.R.-P. and A.M.C.; project administration, Á.R.-P. and A.M.C.; funding acquisition, Á.R.-P. and A.M.C. All authors have read and agreed to the published version of the manuscript.

Funding: This research was funded within the framework of the “Doctorate Program in Industrial Technologies” of the UNED and it has been funded by the Annual Grants Call of the E.T.S.I. Industriales of UNED through the projects 2021-ICF07 and 2022-ETSII-UNED-01, as well as by the project 2021V-/TAJOV/006 (awarded in the UNED Research Projects call named “Young Talents 2021”).

Data Availability Statement: The raw/processed data required to reproduce these findings cannot be shared at this time as the data also form part of an ongoing study.

Acknowledgments: We would like to extend our acknowledgement to the Research Group of the UNED “Industrial Production and Manufacturing Engineering (IPME)” and the Industrial Research Group “Advanced Failure Prognosis for Engineering Applications”.

Conflicts of Interest: The authors declare no conflict of interest. The funders had no role in the design of the study; in the collection, analyses, or interpretation of data; in the writing of the manuscript; or in the decision to publish the results.

References

1. Bermudo, C.; Andersson, T.; Svensson, D.; Trujillo, F.J.; Martín-Béjar, S.; Sevilla, L. Modeling of the fracture energy on the finite element simulation in Ti₆Al₄V alloy machining. *Sci. Rep.* **2021**, *11*, 18490. [[CrossRef](#)] [[PubMed](#)]
2. Sheng, L.Y.; Du, B.N.; Hu, Z.Y.; Qiao, Y.X.; Xiao, Z.P.; Wang, B.J.; Xu, D.K.; Zheng, Y.F.; Xi, T.F. Effects of annealing treatment on microstructure and tensile behaviour of the Mg-Zn-Y-Nd alloy. *J. Magnes. Alloys* **2020**, *8*, 601–613. [[CrossRef](#)]
3. Gall, S.; Müller, S.; Reimers, W. Aluminum coating of magnesium hollow profiles by using the co-extrusion process. *Alum. Int. J.* **2009**, *85*, 63–67.
4. Negendanka, M.; Mueller, S.; Reimers, W. Co-extrusion of Mg-Al macrocomposites. *J. Mater. Process. Technol.* **2021**, *212*, 1954–1962. [[CrossRef](#)]
5. Lehmann, T.; Stockmann, M.; Naumann, J. Experimental and numerical investigations of Al/Mg compound specimens under load in an extended temperature range. *FEM Trans.* **2009**, *37*, 1–8.
6. Fernández, D.; Rodríguez-Prieto, A.; Camacho, A.M. Effect of Process Parameters and Definition of Favorable Conditions in Multi-material Extrusion of Bimetallic AZ31B-Ti₆Al₄V Billets. *Appl. Sci.* **2020**, *10*, 8048. [[CrossRef](#)]
7. Fernández, D.; Rodríguez-Prieto, A.; Camacho, A.M. Selection of Die Material and Its Impact on the Multi-Material Extrusion of Bimetallic AZ31B-Ti₆Al₄V Components for Aeronautical Applications. *Materials* **2021**, *4*, 7568. [[CrossRef](#)] [[PubMed](#)]
8. Rebello, C.M.; Martins, M.A.F.; Santana, D.D.; Rodrigues, A.E.; Loureiro, J.M.; Ribeiro, A.M.; Nogueira, I.B.R. From a Pareto Front to Pareto Regions: A Novel Standpoint for Multiobjective Optimization. *Mathematics* **2021**, *9*, 3152. [[CrossRef](#)]
9. Saaty, T.L. A scaling method for priorities in hierarchical structures. *J. Math. Psychol.* **1977**, *15*, 234–281. [[CrossRef](#)]
10. Karbassi Yazdi, A.; Tan, Y.; Spulbar, C.; Birau, R.; Alfaro, J. An Approach for Supply Chain Management Contract Selection in the Oil and Gas Industry: Combination of Uncertainty and Multi-Criteria Decision-Making Methods. *Mathematics* **2022**, *10*, 3230. [[CrossRef](#)]
11. Dohale, V.; Akarte, M.; Gupta, S.; Verma, V. Additive Manufacturing Process Selection Using MCDM. In *Advances in Mechanical Engineering*; Kalamkar, V., Monkova, K., Eds.; Lecture Notes in Mechanical Engineering; Springer: Singapore, 2021.
12. Ghaleb, A.M.; Kaid, H.; Alsamhan, A.; Mian, S.H.; Hidri, L. Hindawi Assessment and Comparison of Various MCDM Approaches in the Selection of Manufacturing Process. *Adv. Mater. Sci. Eng.* **2020**, *2020*, 4039253. [[CrossRef](#)]

13. Jajimoggala, S. Decision Making Model for Material Selection Using a Hybrd MCDM Technique. *Int. J. Appl. Decis. Sci.* **2013**, *6*, 144–159.
14. Rodríguez-Prieto, A.; Camacho, A.M.; Sebastián, M.A. Multi-criteria materials selection for extreme operating conditions base on a multi-objective analysis of irradiation embrittlement and hot cracking prediction models. *Int. J. Mech. Mater. Des.* **2018**, *14*, 617–634. [[CrossRef](#)]
15. Madic, M.; Antucheviciene, J.; Radovanovic, M.; Petkovic, D. Determination of Manufacturing Process Conditions by Using MCDM Methods: Application in Laser Cutting. *Eng. Econ.* **2016**, *27*, 144–150. [[CrossRef](#)]
16. Jajimoggala, S.; Krishna, M.; Syed, K. Selection of optimal hot extrusion process parameters for AA6061 using hybrid MCDM technique. *Mater. Today Proc.* **2019**, *18*, 278–290. [[CrossRef](#)]
17. Singaravel, B.; Shankar, D.P.; Prasanna, L. Application of MCDM Method for the Selection of Optimum Process Parameters in Turning Process. *Mater. Today Proc.* **2018**, *5*, 13464–13471. [[CrossRef](#)]
18. Zardari, N.H.; Ahmed, K.; Shirazi, S.M.; Yusop, Z.B. *Weighting Methods and Their Effects on Multi-Criteria Decision Making Models Outcomes in Water Resources Management*; Springer Briefs in Water Sciences and Technology; Springer: Cham, Switzerland, 2005.
19. Odu, G.O. Weighting Methods for Multi-Criteria Decision Making Technique. *J. Appl. Sci. Environ. Manag.* **2019**, *23*, 1449–1457. [[CrossRef](#)]
20. Keshavarz-Ghorabae, M.; Amiri, M.; Zavadskas, E.K.; Turskis, Z.; Antucheviciene, J. Determination of Objective Weights Using a New Method Based on the Removal Effects of Criteria (MEREC). *Symmetry* **2021**, *13*, 525. [[CrossRef](#)]
21. Kao, C. Weight determination for consistently ranking alternatives in multiple criteria decision analysis. *Appl. Math. Model.* **2010**, *34*, 1779–1787. [[CrossRef](#)]
22. Freeman, J.; Chen, T. Green supplier selection using an AHP-Entropy-TOPSIS framework. *Supply Chain Manag.* **2015**, *20*, 327–340. [[CrossRef](#)]
23. Du, Y.; Zheng, Y.; Wu, G.; Tang, Y. Decision-making method of heavy-duty machine tool remanufacturing based on AHP-entropy weight and extension theory. *J. Clean. Prod.* **2020**, *252*, 119607. [[CrossRef](#)]
24. Vinodh, S.; Prasanna, M.; Prakash, N.H. Integrated Fuzzy AHP-TOPSIS for selecting the best plastic recycling methods. A case study. *Appl. Math. Model.* **2014**, *38*, 4662–4672. [[CrossRef](#)]
25. Chen, C.-H. A novel multi-criteria decision-making model for building material supplier selection based on Entropy-AHP weighted TOPSIS. *Entropy* **2020**, *22*, 259. [[CrossRef](#)]
26. Donachie, M.J. *Titanium: A Technical Guide*; ASM International: Novelty, OH, USA, 1988.
27. Avedesiam, M.; Baker, H. *ASM Speciality Handbook: Magnesium and Magnesium Alloys*; ASM International: Novelty, OH, USA, 1999.
28. Karmakar, D.; Muvvala, G.; Kumar, A. High-temperature abrasive wear characteristics of H13 steel modified by laser remelting and cladded with Stellite 6 and Stellite 6/30% WC. *Surf. Coat. Technol.* **2021**, *422*, 127498. [[CrossRef](#)]
29. Davis, J.R. *ASM Speciality Handbook—Stainless Steels*; ASM International: Novelty, OH, USA, 1999.
30. Scientific Forming Technologies. *DEFORM v11.2 User's Manual*; Scientific Forming Technologies Corporation: Columbus, OH, USA, 2017.
31. Wang, F.; Zhao, J.; Zhu, N.; Li, Z. A comparative study on Johnson—Cook constitutive modelling for Ti₆Al₄V alloy using automated ball indentation (ABI) technique. *J. Alloys Compd.* **2015**, *633*, 220–228. [[CrossRef](#)]
32. Li, W.; Zhao, G.; Ma, X.; Gao, J. Flow Stress Characteristics of AZ31B Magnesium Alloy Sheet at Elevated Temperatures. *Int. J. Appl. Phys. Math.* **2012**, *2*, 83–88. [[CrossRef](#)]
33. Cockcroft, M.G.; Latham, D.J. Ductility and the workability of metals. *J. Inst. Met.* **1968**, *96*, 33–39.
34. Camacho, A.M.; González, C.; Rubio, E.M.; Sebastián, M.A. Influence of geometrical conditions on central burst appearance in axisymmetrical drawing processes. *J. Mater. Process. Technol.* **2006**, *177*, 304–306. [[CrossRef](#)]
35. Ko, D.C.; Kim, B.M. The prediction of central burst defects in extrusion and wire drawing. *J. Mater. Process. Technol.* **2000**, *102*, 19–24. [[CrossRef](#)]
36. Venkata, N.; Dixit, P.M.; Lal, G.K. Ductile fracture criteria and its prediction in axisymmetric drawing. *Int. J. Mach. Tools Manuf.* **2000**, *40*, 95–111. [[CrossRef](#)]
37. Zhang, C.; Zhao, G.; Li, T.; Guan, Y.; Chen, H.; Li, P. An Investigation of Die Wear Behavior during Aluminum Alloy 7075 Tube Extrusion. *J. Tribol.* **2012**, *135*, 011602. [[CrossRef](#)]
38. Li, T.; Zhao, G.; Zhang, C.; Guan, Y.; Sun, X.; Li, H. Effect of Process Parameters on Die Wear Behavior of Aluminum Alloy Rod Extrusion. *Mater. Manuf. Process.* **2013**, *28*, 312–318. [[CrossRef](#)]
39. Lepadatu, D.; Hambli, R.; Kobi, A.; Barreau, A. Statistical investigation of die wear in metal extrusion processes. *Int. J. Adv. Manuf. Technol.* **2005**, *28*, 272–278. [[CrossRef](#)]
40. Xu, X.; Zhang, J.; Outeiro, J.; Xu, B.; Zhao, W. Multiscale simulation of grain refinement induced by dynamic recrystallization of Ti6Al4V alloy during high speed machining. *J. Mater. Process. Technol.* **2020**, *286*, 116834. [[CrossRef](#)]
41. Zhang, D.; Hu, H.; Pan, F.; Yang, M.; Zhang, J. Numerical and physical simulation of new SPD method combining extrusion and equal channel angular pressing for AZ31 magnesium alloy. *Trans. Nonferrous Met. Soc. China* **2010**, *20*, 478–483. [[CrossRef](#)]
42. Saaty, T.L. *Multicriteria Decision Making: The Analytic Hierarchy Process*; McGraw-Hill: New York, NY, USA, 1980.
43. Pant, S.; Kumar, A.; Ram, M.; Klochkov, Y.; Sharma, H.K. Consistency Indices in Analytic Hierarchy Process: A Review. *Mathematics* **2022**, *10*, 1206. [[CrossRef](#)]

44. Sałabun, W.; Watróbski, J.; Shekhovtsov, A. Are MCDA methods benchmarkable? A comparative study of TOPSIS, VIKOR, COPRAS, and PROMETHEE II Methods. *Symmetry* **2020**, *12*, 1549. [[CrossRef](#)]
45. Narayananamoorthy, S.; Annapoorni, V.; Kalaiselvan, S.; Kang, D. Hybrid Hesitant Fuzzy Multi-Criteria Decision Making Method: A Symmetric Analysis of the Selection of the Best Water Distribution System. *Symmetry* **2020**, *12*, 2096. [[CrossRef](#)]
46. Hwang, C.L.; Yoon, K. *Multiple Attribute Decision Making: Methods and Applications*; Springer: Berlin/Heidelberg, Germany, 1981.
47. Hajkowicz, S.; Collins, K. A review of multiple criteria analysis for water resource planning and management. *Water Resour. Manag.* **2007**, *21*, 1553–1566. [[CrossRef](#)]
48. De Brito, M.M.; Evers, M. Multi-criteria decision-making for flood risk management: A survey of the current state of the art. *Nat. Hazards Earth Syst. Sci.* **2016**, *16*, 1019–1033. [[CrossRef](#)]
49. Zavadskas, E.K.; Turskis, Z. A new additive ratio assessment (ARAS) method in multicriteria decision-making. *Technol. Econ. Dev. Econ.* **2010**, *16*, 159–172. [[CrossRef](#)]
50. Behzadian, M.; Otaghsara, S.K.; Yazdani, M.; Ignatius, J. A state-of-the-art survey of TOPSIS applications. *Expert Syst. Appl.* **2012**, *39*, 13051–13069. [[CrossRef](#)]
51. Wang, C.-N.; Yang, C.-Y.; Cheng, H.-C. Fuzzy Multi-Criteria Decision-Making Model for Supplier Evaluation and Selection in a Wind Power Plant Project. *Mathematics* **2019**, *7*, 417. [[CrossRef](#)]
52. Opricovic, S.; Tzeng, G.H. Compromise solution by MCDM methods: A comparative analysis of VIKOR and TOPSIS. *Eur. J. Oper. Res.* **2004**, *156*, 445–455. [[CrossRef](#)]
53. Chang, S.-C.; Chang, H.-H.; Lu, M.-T. Evaluating Industry 4.0 Technology Application in SMEs: Using a Hybrid MCDM Approach. *Mathematics* **2021**, *9*, 414. [[CrossRef](#)]
54. Zavadskas, E.K.; Kaklauskas, A.; Peldschus, F.; Turskis, Z. Multi-attribute assessment of road design solutions by using the COPRAS method. *Balt. J. Road Bridge Eng.* **2007**, *2*, 195–203.
55. Vinogradova, I. Multi-Attribute Decision-Making Methods as a Part of Mathematical Optimization. *Mathematics* **2019**, *7*, 915. [[CrossRef](#)]

Capítulo 4. Publicaciones

Capítulo 5. Conclusiones y desarrollos futuros

En esta Tesis Doctoral se ha desarrollado un modelo robusto por elementos finitos en el que se han incorporado aspectos como el daño, el desgaste de la herramienta e, incluso, una predicción de la microestructura resultante por recristalización dinámica; así como una metodología de optimización de los parámetros del proceso en función de las características finales que se quieren obtener en la pieza combinada con métodos estadísticos y de toma de decisiones multicriterio.

5.1. Conclusiones generales

Se pueden extraer las siguientes conclusiones generales de las publicaciones que conforman esta Tesis Doctoral:

- El conformado multmaterial es una buena alternativa al uso de materiales compuestos tanto por la reducción del peso como por no tener tantas limitaciones en el rango de temperaturas de trabajo, así como una menor inversión inicial en los equipos de fabricación.
- Los procesos de simulación por elementos finitos son claves en el marco de la Industria 4.0 por su capacidad de predecir la viabilidad y eficiencia de un proceso, permitiendo optimizar parámetros de procesado, sin necesidad de consumir materiales, energía, horas de trabajo y, en general, los costes productivos recurrentes.
- Es posible generar un modelo por elementos finitos en el que se combinen dos aleaciones tan distintas como son las de titanio y magnesio [65-68].
- Métodos de diseño de experimentos como el de las matrices ortogonales de Taguchi junto con la aplicación de métodos estadísticos como el análisis de la varianza, son esenciales para determinar los parámetros más influyentes en el proceso [65, 66].
- Los parámetros más influyentes en un proceso dependen directamente de la variable o variables de salida que sean de interés, siendo necesario llegar a una solución de compromiso cuando se traten de optimizar más de una variable de salida [65-68].
- El daño se distribuye de forma distinta en el anillo de titanio que en el núcleo de magnesio, estando en este último concentrado la mayoría de las veces en la parte inferior del cilindro, lo cual no es un problema ya que se desechará para obtener la pieza final [65-67].
- Los métodos de decisión multicriterio junto con los métodos de ponderación ayudan a obtener esa solución de compromiso mencionada anteriormente [68].

- El material de la matriz usada durante la coextrusión afecta, no sólo al desgaste de la misma, sino a otras variables de salida como lo son el daño y la fuerza de extrusión. Por lo que es necesario tenerlo en cuenta durante la optimización del proceso [67].
- Una forma de mejorar las propiedades mecánicas resultantes de la pieza final es mediante el refinamiento de grano, por lo que para analizar la calidad del producto es necesario implementar un modelo de predicción de la microestructura en el modelo de elementos finitos [68].
- La distribución del daño, así como el tamaño de grano, son distintas en las partes interior y exterior del anillo [68].

5.2. Conclusiones particulares

De cada uno de los trabajos publicados, se pueden extraer las siguientes conclusiones particulares:

- La temperatura y la velocidad del pistón son los factores que menos influencia tienen en la fuerza de extrusión. Además, a mayor velocidad del pistón menor es la fuerza de extrusión requerida, llegando a un mínimo a partir del cual, por mucho que se aumente la velocidad, esta no afecta a la fuerza [65].
- El parámetro que más afecta a la fuerza de extrusión es el semi-ángulo de la matriz, siendo el valor óptimo de 30° . Mientras que el diámetro del núcleo es el parámetro que más afecta al daño [65].
- Es necesario alcanzar un equilibrio en el factor de forma (relación altura/diámetro), ya a mayor altura del cilindro se necesita una mayor fuerza de extrusión, mientras que un mayor diámetro del núcleo implica un aumento del daño producido [65].
- Hay valores críticos del semi-ángulo de la matriz ($\geq 75^\circ$), relación de extrusión (2,25) y altura del cilindro (≥ 30 mm) para los que el daño se extiende por todo el núcleo y es causa potencial de un futuro fallo de la pieza [66].
- Para valores pequeños del semi-ángulo de la matriz (15°) el factor de daño es independiente de la relación de extrusión [66].
- El factor de daño aumenta conforme aumenta el coeficiente de fricción, sin embargo alcance un valor constante para coeficientes entre 0,3 y 0,4 [66].
- El valor de 0,4 en el coeficiente de fricción se puede considerar crítico pues a partir de este punto conforme aumente la fricción el daño se incrementará exponencialmente

alcanzando valores entre 3 y 4 veces superiores a los obtenidos en el intervalo de 0,1 a 0,4 [66].

- Para factores de forma (H_0/D_0) de 1,66 y relaciones altas de extrusión (2,25), el semi-ángulo de la matriz no tiene apenas influencia en el factor de daño [66].
- La temperatura y la velocidad del pistón no tienen apenas influencia en el daño [65, 66].
- La mayor variación en la fuerza de extrusión respecto al material de la matriz se produce para una velocidad de pistón de 1 mm/s, donde se necesita una fuerza de extrusión un 27,50% mayor para la matriz fabricada con AISI3310, que la que necesita el mismo proceso usando una matriz fabricada con AISI316 [67].
- El parámetro más afectado por la variación del material de la matriz es el semi-ángulo de la matriz, cuyo valor óptimo puede cambiar en función del material elegido [67].
- Para matrices fabricadas con 53HRC y AISI316, la velocidad del pistón no tiene efecto en el desgaste. Sin embargo para matrices de AISI3310, altas velocidades del pistón (≥ 4 mm/s) producen una reducción significativa del desgaste [67].
- Como regla general, el desgaste disminuye con el aumento de temperatura. Sin embargo, hay materiales más sensibles a este parámetro como el AISI316 y H13 que a temperaturas inferiores a 300°C tienen un desgaste mayor que el AISI3310, que es el de mayor dureza [67].
- Se ha demostrado que la fricción es un factor determinante para disminuir el desgaste de la matriz, ya que los menores valores de desgaste se producen para altos valores del coeficiente de fricción ($\geq 0,5$) [67].
- El método de ponderación utilizado para priorizar una variable de salida respecto a otra no tiene una gran relevancia, ya que se ha demostrado que los resultados obtenidos son los mismos en tres de los cuatro MCDM estudiados [68].
- Atendiendo a la complejidad de cálculo y la validación de la solución obtenida, así como que es el único MCDM en el que se obtienen distintos resultados en función del método de ponderación utilizado, se ha optado por el método VIKOR junto con el método de ponderación de la entropía como la mejor opción para obtener los valores de los parámetros del proceso que optimicen las cuatro variables de salida consideradas durante esta Tesis (mínima fuerza de extrusión, mínimo daño inducido en la pieza, mínimo desgaste de la matriz y menor tamaño final de grano) [68].

5.3. Desarrollos futuros

Como trabajos futuros se proponen las siguientes líneas de investigación:

- Extender el modelo a la extrusión indirecta y, sobre todo por su aplicación a conformado superplástico, a la ECAE (Equal Channel Angular Extrusion) y comparar los resultados obtenidos con los de la extrusión directa.
- Extender el modelo a otros procesos de conformado por deformación plástica, siendo de especial interés el conformado por laminación y el conformado por forja para obtener piezas con formas más complejas.
- Incorporar un modelo de fractura que ayude a establecer los límites durante el proceso de conformado.
- Aplicar la metodología a otros materiales avanzados de interés tecnológico para la obtención de piezas multmaterial.
- Incorporar ensayos experimentales en la metodología que complementen el estudio numérico.

Capítulo 6. Otras aportaciones científicas derivadas de la Tesis Doctoral

6.1. Contribuciones en congresos internacionales

Congreso: **9th Manufacturing Engineering Society International Conference (MESIC'09).**

Entidad organizadora: Sociedad de Ingeniería de Fabricación (SIF) y Universidad de Oviedo.

Carácter: Internacional.

Lugar de celebración: Gijón (España).

Fecha: 23 – 24 – 25 de junio de 2021.

Título: Analysis of AZ31B-Ti₆Al₄V bimetallic extrusion by numerical simulation and Taguchi method.

Autores: Daniel Fernández Martín; Álvaro Rodríguez-Prieto; Ana María Camacho López.

Tipo de participación: póster.

Publicación: Book of Abstracts. ISBN: 978-84-09-29229-5.

Congreso: **4th International Conference on Materials Design and Applications (MDA2022).**

Entidad organizadora: Faculdade de Engenharia da Universidade do Porto (FEUP).

Carácter: Internacional.

Lugar de celebración: Oporto (Portugal).

Fecha: 7 – 8 de julio de 2022

Título: Numerical modelling and analysis of microstructural evolution in multimaterial co-extrusion of bimetallic Ti₆Al₄V-AZ31B billets.

Autores: Daniel Fernández Martín; Álvaro Rodríguez-Prieto; Ana María Camacho López.

Tipo de participación: póster.

Publicación: Book of Abstracts. ISBN: 978-98-99-10127-2.

Capítulo 7. Referencias

Capítulo 7. Referencias

1. Khodadad Motarjemi, A.; Koçak, M; Venzke, V. Mechanical and fracture characterization of a bi-material steel plate. *International Journal of Pressure Vessels and Piping* **2002**, Volume 79, Issue 3, pp. 181-191. ISSN 0308-0161.
 DOI: [https://doi.org/10.1016/S0308-0161\(02\)00012-1](https://doi.org/10.1016/S0308-0161(02)00012-1).
2. European Comission Horizon 2020 Work Programme 2018-2020 5.ii. Nanotechnologies, Advanced Materials, Biotechnology and Advanced Manufacturing and Processing. Available online: https://ec.europa.eu/research/participants/data/ref/h2020/wp/2018-2020/main/h2020-wp1820-leit-nmp_en.pdf (accessed on 30 October 2019)
3. Rodríguez-Panes, A.; Claver, J.; Camacho, A.M. The influence of manufacturing parameters on the mechanical behavior of PLA and ABS pieces manufactured by FDM: A comparative analysis. *Materials* **2018**, *11*, 1333.
 DOI: <https://doi.org/10.3390/ma11081333>
4. García-Domínguez, A.; Claver, J.; Sebastián, M.A. Optimization methodology for additive manufacturing of customized parts by fused deposition modeling (FDM). Application to a shoe heel. *Polymers* **2020**, *12*, 2119.
 DOI: <https://doi.org/10.3390/polym12092119>.
5. Rodríguez-Prieto, A.; Camacho, A.M.; Sebastián, M.A.; Yanguas-Gil, A. Polymers selection for harsh environments to be processed using additive manufacturing techniques. *IEEE Access* **2018**, *6*, 29899–29911.
 DOI: <https://doi.org/10.1109/ACCESS.2018.2844360>.
6. García-Domínguez, A.; Claver, J.; Camacho, A.M.; Sebastián, M.A. Considerations on the applicability of test methods for mechanical characterization of materials manufactured by FDM. *Materials* **2020**, *13*, 28.
 DOI: <https://doi.org/10.3390/ma13010028>.
7. Camacho, A.M.; Rodríguez-Prieto, Á.; Herrero, J.M.; Aragón, A.M.; Bernal, C.; Lorenzo-Martin, C.; Yanguas-Gil, Á.; Martins, P.A.F. An Experimental and numerical analysis of the compression of bimetallic cylinders. *Materials* **2019**, *12*, 4094.
 DOI: <https://doi.org/10.3390/ma12244094>.
8. Zhang, X.P.; Yang, T.H.; Liu, J.Q.; Luo, X.F.; Wang, J.T. Mechanical properties of an Al/Mg/Al trilaminated composite fabricated by hot rolling. *J. Mater. Sci.* **2010**, *45*, 3457–3464.
 DOI: <https://doi.org/10.1007/s10853-010-4373-z>.
9. Alcaraz, J.; Gil-Sevillano, J. An analysis of the extrusion of bimetallic tubes by numerical simulation. *Int. J. Mech. Sci.* **1996**, *38*, 157–173.
 DOI: [https://doi.org/10.1016/0020-7403\(95\)00044-x](https://doi.org/10.1016/0020-7403(95)00044-x).
10. Chenot, J.-L.; Béraudo, C.; Bernacki, M.; Fourment, L. Finite Element simulation of multi material metal forming. *Procedia Eng.* **2014**, *81*, 2427–2432.
 DOI: <https://doi.org/10.1016/j.proeng.2014.10.345>.
11. Abdelkader, W.B.; Bahloul, R.; Arfa, H. Numerical investigation of the influence of some parameters in SPIF process on the forming forces and thickness distributions of a bimetallic sheet CP-Titanium/Low-carbon steel compared to an individual layer. *Procedia Manufacturing* **2020**, *47*, pp. 1319-1327.
 DOI: <https://doi.org/10.1016/j.promfg.2020.04.252>.
12. Negendanka, M.; Mueller, S.; Reimers, W. Coextrusion of Mg–Al macrocomposites. *J. Mater. Process. Technol.* **2012**, *212*, 1954–1962.
 DOI: <https://doi.org/10.1016/j.jmatprotec.2012.04.023>.
13. Khosravifard, A.; Ebrahimi, R. Investigation of parameters affecting interface strength in Al/Cu clad bimetal rod extrusion process. *Mater. Des.* **2010**, *31*, 493–499.
 DOI: <https://doi.org/10.1016/j.matdes.2009.06.026>.

Capítulo 7. Referencias

14. Lapovok, R.; Ng, H.P.; Tomus, D.; Estrin, Y. Bimetallic copper-aluminum tube by severe plastic deformation. *Scr. Materialia* **2012**, *66*, 1081–1084.
DOI: <http://doi.org/10.1016/j.scriptamat.2012.03.004>.
15. Berski, S.; Dyja, H.; Banaszek, G.; Janik, M. Theoretical analysis of bimetallic rods extrusion process in double reduction die. *J. Mater. Process. Technol.* **2004**, *153–154*, 583–588.
DOI: <http://doi.org/10.1016/j.jmatprotec.2004.04.052>.
16. Kocich, R. Deformation behavior of Al/Cu clad composite during twist channel angular pressing. *Materials* **2020**, *13*, 4047.
DOI: <http://doi.org/10.3390/ma13184047>.
17. Thirumurugan, M.; Rao, S.A.; Kumaran, S.; Rao, T.S. Improved ductility in ZM21 magnesium–aluminium macrocomposite produced by co-extrusion. *J. Mater. Process. Technol.* **2011**, *211*, 1637–1642.
DOI: <http://doi.org/10.1016/j.jmatprotec.2011.05.005>.
18. Gall, S.; Müller, S.; Reimers, W. Aluminum coating of magnesium hollow profiles by using the coextrusion process. *Alum. Int. J.* **2009**, *85*, 63–67.
19. Rong, W.; Zhang, Y.; Wu, Y.; Chen, Y.; Tang, T.; Peng, L.; Li, D. Fabrication of high-strength Mg-Gd-Zn-Zr alloys via differential-thermal extrusion. *Mater. Charact.* **2017**, *131*, 380–387. DOI: <http://doi.org/10.1016/j.matchar.2017.07.031>.
20. Osakada, K.; Limb, M.; Mellor, P. Hydrostatic extrusion of composite rods with hard cores. *Int. J. Mech. Sci.* **1973**, *15*, 291–307,
DOI: [http://doi.org/10.1016/0020-7403\(73\)90011-8](http://doi.org/10.1016/0020-7403(73)90011-8).
21. Lehmann, T.; Stockmann, M.; Naumann, J. Experimental and numerical investigations of Al/Mg compound specimens under load in an extended temperature range. *FEM Trans.* **2009**, *37*, 1–8.
22. Behrens, B.-A.; Klose, C.; Chugreev, A.; Heimes, N.; Thürer, S.E.; Uhe, J. A Numerical study on co-extrusion to produce coaxial aluminum-steel compounds with longitudinal weld seams. *Metals* **2018**, *8*, 717.
DOI: <http://doi.org/10.3390/met8090717>.
23. Thürer, S.E.; Peddinghaus, J.; Heimes, N.; Bayram, F.C.; Bal, B.; Uhe, J.; Behrens, B.-A.; Maier, H.J.; Klose, C. Lateral angular co-extrusion: geometrical and mechanical properties of compound profiles. *Metals* **2020**, *10*, 1162.
DOI: <http://doi.org/10.3390/met10091162>.
24. Sheng, L. Y., Du, B. N., Hu, Z. Y., Qiao, Y. X., Xiao, Z. P., Wang, B. J., Xu, D. K., Zheng, Y. F. & Xi, T. F. Effects of annealing treatment on microstructure and tensile behaviour of the Mg-Zn-Y-Nd alloy. *Journal of Magnesium Alloys* **2020**, *8*, 601–613.
DOI: <https://doi.org/10.1016/j.jma.2019.07.011>.
25. Wang, J., Li, T., Li, H. X., Ma, Y. Z., Zhao, K. N., Yang, C. L. & Zhang, J. S. Effect of trace Ni addition on microstructure, mechanical and corrosion properties of the extruded Mg-Gd-Y-Zr-Ni alloys for dissolvable fracturing tools. *Journal of Magnesium Alloys* **2021**, *9*, 1632–1643. DOI: <https://doi.org/10.1016/j.jma.2020.08.019>.
26. Mordike, B.L.; Ebert, T. Magnesium: Properties-applications-potential. *Mater. Sci. Eng. A* **2001**, *302*, 37–45.
DOI: [https://doi.org/10.1016/S0921-5093\(00\)01351-4](https://doi.org/10.1016/S0921-5093(00)01351-4).
27. Luo , Q., Li, J., Li, B., Liu, B., Shao, H. & Li, Q. Kinetics in Mg-based hydrogen storage materials: Enhancement and mechanism. *Journal of Magnesium Alloys* **2019**, *7* (1), 58–71.
DOI: <https://doi.org/10.1016/j.jma.2018.12.001>.
28. Li, S., Yang, X., Hou, J. & Du, W. A review on thermal conductivity of magnesium and its alloy. *Journal of Magnesium Alloys* **2020**, *8* (1), 78–90.
DOI: <https://doi.org/10.1016/j.jma.2019.08.002>.

Capítulo 7. Referencias

29. Rokhlin L.L. Magnesium alloys containing rare earth metals. *Taylor & Francis 1st Edition 2003*.
 DOI: <https://doi.org/10.1201/9781482265163>.
30. Zhou, B., Wu, D., Chen, R. S. & Han E-h. Enhanced tensile properties in an Mg-6Gd-3Y-0.5Zr alloy due to hot isostatic pressing (HIP). *J. Mater. Sci. Technol.* **2019**, 35 (9): 1860-1868.
 DOI: <https://doi.org/10.1016/j.jmst.2019.05.006>.
31. Z Zhang, F., Wang, Y., Duan, Y., Wang, K., Wang, Y. & Zhang, W. Precipitation processes during the peak-aged and over-aged stages in an Mg-Gd-Y-Zr alloy. *J. Alloys Compd.* **2019**, 788: 541-548 (2019).
 DOI: <https://doi.org/10.1016/j.jallcom.2019.02.203>.
32. Li, L.X.; Rao, K.P.; Lou, Y.; Peng, D.S. A study on hot extrusion of Ti-6Al-4V using simulations and experiments. *Int. J. Mech. Sci.* **2002**, 44, 2415–2425.
 DOI: [https://doi.org/10.1016/S0020-7403\(02\)00173-X](https://doi.org/10.1016/S0020-7403(02)00173-X).
33. Omoniyi, P.; Akinlabi, E.T.; Mahamood, R.M. Heat Treatments of Ti6Al4V alloys for industrial applications: an overview. In *Proceedings of the IOP Conference Series: Materials Science and Engineering*, Ota, Nigeria, 10–14 August **2020**.
 DOI: <https://doi.org/10.1088/1757-899X/1107/1/012094>.
34. Bermudo, C., Andersson, T., Svensson, D., Trujillo, F. J., Martín-Béjar, S. & Sevilla, L. Modeling of the fracture energy on the finite element simulation in Ti₆Al₄V alloy machining. *Scientific Reports* **2021**, 11, 18490.
 DOI: <https://doi.org/10.1038/s41598-021-98041-5>.
35. Cockcroft, M.G.; Latham, D.J. Ductility and the workability of metals. *J. Inst. Met.* **1968**, 96, 33–39.
36. Stebunov, S.; Vlasov, A.; Biba, N. Prediction of fracture in cold forging with modified Cockcroft-Latham criterion. *Procedia Manuf.* **2018**, 15, 519–526.
 DOI: <https://doi.org/10.1016/j.promfg.2018.07.264>.
37. Gu, J.; Chen, P. A failure criterion for homogeneous and isotropic materials distinguishing the different effects of hydrostatic tension and compression. *Eur. J. Mech. A Solids* **2018**, 70, 15–22.
 DOI: <http://doi.org/10.1016/j.euromechsol.2018.01.013>.
38. Amigo, F.J.; Camacho, A.M. Reduction of induced central damage in cold extrusion of dual-phase steel DP800 using double-pass dies. *Metals* **2017**, 7, 335.
 DOI: <https://doi.org/10.3390/met7090335>.
39. Zhang, C.; Zhao, G.; Li, T.; Guan, Y.; Chen, H.; Li, P. An investigation of die wear behavior during aluminum alloy 7075 tube extrusion. *J. Tribol.* **2012**, 135, 011602.
 DOI: <https://doi.org/10.1115/1.4023081>.
40. Li, T.; Zhao, G.; Zhang, C.; Guan, Y.; Sun, X.; Li, H. Effect of process parameters on die wear behavior of aluminum alloy rod extrusion. *Mater. Manuf. Process.* **2013**, 28, 312–318.
 DOI: <https://doi.org/10.1080/10426914.2012.675536>.
41. Lepadatu, D.; Hamblin, R.; Kobi, A.; Barreau, A. Statistical investigation of die wear in metal extrusion processes. *Int. J. Adv. Manuf. Technol.* **2005**, 28, 272–278.
 DOI: <https://doi.org/10.1007/s00170-004-2362-6>.
42. Song, H. R., Kim Y. S. & Nam, W. J. Mechanical properties of ultrafine grained 5052 Al alloy produced by accumulative roll-bonding and cryogenic rolling. *J. Metal Mater Inter* **2006**, 12 (1), 7-13 (2006).
 DOI: <https://doi.org/10.1007/BF03027516>.
43. Rotella, G., Dillon O.W., Umbrello, D., Settineri, L. & Jawahir, I.S. Finite element modeling of microstructural changes in turning of AA7075-T651 Alloy. *J. Manuf. Process.* **2013**, 15, 87–95.

Capítulo 7. Referencias

- DOI: <https://doi.org/10.1016/j.jmapro.2012.09.005>.
44. Xiang, X., Zhang, J., Outeiro, J., Binbin, X. & Wanhua, Z. Multiscale simulation of grain refinement induced by dynamic recrystallization of Ti₆Al₄V alloy during high speed machining. *J. of Materials Processing Tech.* **2020**, 286, 116834.
 DOI: <https://doi.org/10.1016/j.jmatprotec.2020.116834>.
45. Ding-fei, Z., Hong-jun, H., Fu-sheng, P., Ming-bo, Y. & Jun-ping, Z. Numerical and physical simulation of new SPD method combining extrusion and equal channel angular pressing for AZ31 magnesium alloy. *Trans. Nonferrous Met. Soc. China* **2010**, 20, 478-483.
 DOI: [https://doi.org/10.1016/S1003-6326\(09\)60165-5](https://doi.org/10.1016/S1003-6326(09)60165-5).
46. Yuan, M., He, C., Zhao, J., Yang, H., Song, Y., Lei, B., Qian, X., Dong, Z., Li, Q., Jiang, B. & Pan, F. Microstructure evolution and mechanical properties of the Mg-Sm-Gd-Zn-Zr alloy during extrusion. *Journal of Materials Research and Technology* **2021**, 15, 2518-2528.
 DOI: <https://doi.org/10.1016/j.jmrt.2021.09.080>.
47. Liu, X.Q., Qoap, X.G., Pei, R.S., Chi, Y.Q., Yuan, L. & Zheng, M.Y. Role of the extrusion rate on the microstructure and tensile properties evolution of ultrahigh-strength low-alloy Mg-1.0Al-1.0Ca-0.4Mn (wt.%) alloy. *Journal of Magnesium and Alloys* **2021**.
 DOI: <http://doi.org/10.1016/j.jma.2021.05.010>.
48. Duan, X. & Sheppard, T. Simulation and control of microstructure evolution during hot extrusion of hard aluminum alloys. *Materials Science and Engineering* **2003**, A351, pp. 282-292.
49. Pareto, V. Cours d'economie politique. Tome premier. *The Economic Journal* **1896**, volumen 6, número 2, pp. 249-253.
 DOI: <http://doi.org/10.2307/2956507>.
50. Saaty, T.L. A scaling method for priorities in hierarchical structures. *J. Math. Psychology* **1977**, 15 (3), pp.234-281.
 DOI: [https://doi.org/10.1016/0022-2496\(77\)90033-5](https://doi.org/10.1016/0022-2496(77)90033-5).
51. Karbassi Yazdi, A.; Tan, Y.; Spulbar, C.; Birau, R.; Alfaro, J. An approach for supply chain management contract selection in the oil and gas industry: combination of uncertainty and multiCriteria decision-making methods. *Mathematics* **2022**, 10 (18), 3230.
 DOI: <https://doi.org/10.3390/math10183230>.
52. Dohale, V., Akarte, M., Gupta, S., Verma, V. Additive manufacturing process selection using MCDM. In: Kalamkar, V., Monkova, K. (eds) *Advances in Mechanical Engineering*. Lecture Notes in Mechanical Engineering. Springer, Singapore **2021**, pp. 601 – 609.
 DOI: https://doi.org/10.1007/978-981-15-3639-7_72.
53. Ghaleb, A.M.; Kaid, H.; Alsamhan, A.; Mian, S.H.; Hidri, L. Assessment and comparison of various MCDM approaches in the selection of manufacturing process. *Advances in Materials Science and Engineering* **2020**, Article ID 4039253, 16 pages.
 DOI: <https://doi.org/10.1155/2020/4039253>.
54. Jajimoggala, S. Decision making model for material selection using a hybrd MCDM technique. *International Journal of Applied Decision Sciences* **2013**, ISSN: 1755-8085, Vol. 6, Issue 2, pp.144-159.
 DOI: <https://doi.org/10.1504/IJADS.2013.053273>.
55. Rodríguez-Prieto, A.; Camacho, A.M.; Sebastián, M.A. Multicriteria materials selection for extreme operating conditions base on a multiobjective analysis of irradiation embrittlement and hot cracking prediction models. *Int. J. Mech. Mater Des* **2018**, 14, pp.617-634.
 DOI: <https://doi.org/10.1007/s10999-017-9393-2>.
56. Madic *et al.* Determination of manufacturing process conditions by using MCDM methods: application in laser cutting, *Engineering economics* **2016**, 27 (2), pp.144–150.
 DOI: <https://doi.org/10.5755/J01.EE.27.2.13428>.

Capítulo 7. Referencias

57. Jajimoggala, S.; Krishna, M.; Syed, K. Selection of optimal hot extrusion process parameters for AA6061 using hybrid MCDM technique. *Materials Today: Proceedings* **2019**, 18, pp.278-290.
DOI: <https://doi.org/10.1016/j.matpr.2019.06.302>.
58. Singaravel, B.; Shankar, D.P.; Prasanna, L. Application of MCDM method for the selection of optimum process parameters in turning process. *Materials Today: Proceedings* **2018**, 5, pp.13464-13471.
DOI: <https://doi.org/10.1016/j.matpr.2018.02.341>.
59. Zardari, N.H; Ahmed, K; Shirazi, S.M; Yusop, Z.B. Weighting methods and their effects on multicriteria decision making models outcomes in water resources management. *Springer International Publishing* **2014**, (Verlag) Switzerland, ISBN 978-3-319-12585-5, p. 191.
60. Department of Mechanical Engineering, Faculty of Engineering, Delta State University, Abraka, Oleh Campus, 331107, Nigeria. Weighting methods for multicriteria decision making technique. *J. Appl. Sci. Environ. Manage* **2019**, Vol. 23 (8) pp.1449-1457.
DOI: <https://doi.org/10.4314/jasem.v23i8.7>.
61. Freeman, J.; Chen, T. Green supplier selection using an AHP-Entropy-TOPSIS framework. *Supply Chain Manag. Int. J.* **2015**, 20, pp.327-340.
DOI: <https://doi.org/10.1108/SCM-04-2014-0142>.
62. Vinodh, S; Prasanna, M; Prakash, N. H. Integrated Fuzzy AHP-TOPSIS for selecting the best plastic recycling methods. A case study. *Applied Mathematics Modeling* **2014**, 38 (19 – 20), pp.4662-4672.
DOI: <https://doi.org/10.1016/j.apm.2014.03.007>.
63. Chen, C.-H. A novel multicriteria decision-making model for building material supplier selection based on Entropy-AHP weighted TOPSIS. *Entropy* **2020**, 22, 259.
DOI: <https://doi.org/10.3390/e22020259>.
64. Scientific Forming Technologies. *DEFORM v11.2 user's manual*; *Scientific Forming Technologies Corporation*, Columbus, OH, USA, **2017**.
65. Fernández, D.; Rodríguez-Prieto, A.; Camacho, A.M. Effect of process parameters and definition of favorable conditions in multimaterial extrusion of bimetallic AZ31B–Ti6Al4V billets. *Appl. Sci.* **2020**, 10, 8048.
DOI: <http://doi.org/10.3390/app10228048>.
66. Fernández, D.; Rodríguez-Prieto, A.; Camacho, A.M. Analysis of AZ31B -Ti6Al4V bimetallic extrusion by numerical simulation and Taguchi method. *IOP Conference Series Materials Science and Engineering*. **2021**. 1193. 012080; pp. 1-8.
DOI: <http://doi.org/10.1088/1757-899X/1193/1/012080>.
67. Fernández, D., Rodríguez-Prieto, A.; Camacho, A.M. Selection of die material and its impact on the multimaterial extrusion of bimetallic AZ31B- Ti6Al4V components for aeronautical applications. *Materials* **2021**, 14 (24), 7568.
DOI: <https://doi.org/10.3390/ma14247568>.
68. Fernández, D.; Rodríguez-Prieto, A.; Camacho, A.M. Optimal parameters selection in advanced multi-metallic co-extrusion based on independent MCDM analytical approaches and numerical simulation. *Mathematics* **2022**, 10, 4489.
DOI: <http://doi.org/10.3390/math10234489>.
69. Rowe, G.W. *Principles of Industrial Metalworking Processes*; Edward Arnold Publishers: London, UK, **1977**.
70. Leu, D.-K. A simple dry friction model for metal forming process. *J. Mater. Process. Technol.* **2009**, 209, 2361–2368.
DOI: <http://doi.org/10.1016/j.jmatprotec.2008.05.027>.

Capítulo 7. Referencias

71. Rodríguez Prieto, J.; Larsson, S.; Carbonell, J.; Jonsén, P. Dislocation density based flow stress model applied to the PFEM simulation of orthogonal cutting processes of Ti-6Al-4V. *Materials* **2020**, 13, 1979.
DOI: <http://doi.org/10.3390/ma13081979>.
72. Wen – juan, L.; Guo – Qun, Z.; Xin – Wu, M.; Jun, G. Flow Stress Characteristics of AZ31B Magnesium Alloy Sheet at Elevated Temperatures. *International Journal of Applied Physics and Mathematics* **2012**, Vol. 2, Issue 2, pp.83–88.
DOI: <https://doi.org/10.7763/IJAPM.2012.V2.59>.
73. García-Domínguez, A., Claver, J., Camacho, A.M. & Sebastián, M.A. Comparative analysis of extrusion processes by finite element analysis. *Procedia Engineering* **2015**, 100, 74-83.
DOI: <https://doi.org/10.1016/j.proeng.2015.01.344>.
74. Gisbert, C., Bernal, C. & Camacho, A.M. Improved analytical model for the calculation of forging forces during compression of bimetallic axial assemblies. *Procedia Engineering* **2015**, 132, pp.298-305.
DOI: <https://doi.org/10.1016/j.proeng.2015.12.498>.
75. Naranjo-Palacios, F., Rios-Lira, A.R., Pantoja -Pacheco, Y.V., Tapia-Esquivias, M. Diseños ortogonales de Taguchi fraccionados. *Ingeniería Investigación y Tecnología* **2020**, 02 (21), pp.1-12.
DOI: <https://doi.org/10.22201/fi.25940732e.2020.21n2.011>.
76. Fisher, R.A. The arrangement of field experiments. *Journal of the Ministry of Agriculture of Great Britain* **1926**, 33, pp. 503-513.
DOI: <https://doi.org/10.23637/rothamsted.8v61q>.
77. Hwang, C. L.; Yoon, K. Multiple attribute decision making: methods and applications. *CRC Press Taylor & Francis Group*, 6000 Broken Sound Parkway NW, Suite 300, Boca Ratón, Fl. 33487-2742, **1981**.
78. Hajkowicz, S.; Collins, K. A review of multiple criteria analysis for water resource planning and management. *Water Resour. Manag.* **2007**, 21, pp.1553–1566.
DOI: <https://doi.org/10.1007/s11269-006-9112-5>.
79. De Brito, M. M.; Evers, M. Multicriteria decision-making for flood risk management: A survey of the current state of the art. *Nat. Hazards Earth Syst. Sci.* **2016**, 16, pp.1019–1033. DOI: <https://doi.org/10.5194/nhess-16-1019-2016>.
80. Zavadskas, E.K.; Turskis, Z. A new additive ratio assessment (ARAS) method in multicriteria decision-making. *Technological and Economic Development of Economy* **2010**, 16 (2), pp 159-172.
DOI: <https://doi.org/10.3846/tede.2010.10>.
81. Behzadian, M.; Otaghara, S.K.; Yazdani, M.; Ignatius, J. A state-of the-art survey of TOPSIS applications. *Expert Syst. Appl.* **2012**, 39, pp.13051–13069.
DOI: <https://doi.org/10.1016/j.eswa.2012.05.056>.
82. Wang, C.-N.; Yang, C.-Y.; Cheng, H.-C. Fuzzy multicriteria decision-making model for supplier evaluation and selection in a wind power plant project. *Mathematics* **2019**, 7, 417.
DOI: <https://doi.org/10.3390/math7050417>.
83. Opricovic, S.; Tzeng, G.H. Compromise solution by MCDM methods: a comparative analysis of VIKOR and TOPSIS. *Eur. J. Oper. Res.* **2004**, 156, pp.445–455.
DOI: [https://doi.org/10.1016/S0377-2217\(03\)00020-1](https://doi.org/10.1016/S0377-2217(03)00020-1).
84. Chang, S.-C.; Chang, H.-H.; Lu, M.-T. Evaluating industry 4.0 technology application in SMEs: using a hybrid MCDM approach. *Mathematics* **2021**, 9, 414.
DOI: <https://doi.org/10.3390/math9040414>.

Capítulo 7. Referencias

85. Zavadskas, E.K.; Kaklauskas, A.; Peldschus, F.; Turskis, Z. Multiattribute assessment of road design solutions by using the COPRAS method. *Balt. J. Road Bridge Eng.* **2007**, 2, pp.195–203.
86. Vinogradova, I. Multiattribute decision-making methods as a part of mathematical optimization. *Mathematics* **2019**, 7, 915.
DOI: <https://doi.org/10.3390/math7100915>.

Apéndices

Apéndice A. Indicios de calidad del artículo “Effect of Process Parameters and Definition of Favorable Conditions in MultiMaterial Extrusion of Bimetallic AZ31B–Ti6Al4V Billets”

Applied Sciences- Basel

 Open Access since 2011

ISSN

N/A

EISSN

2076-3417

JCR ABBREVIATION

APPL SCI-BASEL

ISO ABBREVIATION

Appl. Sci.-Basel

Journal information

EDITION

Science Citation Index
Expanded (SCIE)

CATEGORY

CHEMISTRY,
MULTIDISCIPLINARY - SCIE

MATERIALS SCIENCE,
MULTIDISCIPLINARY - SCIE

PHYSICS, APPLIED - SCIE

ENGINEERING,
MULTIDISCIPLINARY - SCIE

LANGUAGES

English

REGION

SWITZERLAND

1ST ELECTRONIC JCR YEAR

2014

Publisher information

PUBLISHER

MDPI

ADDRESS

ST ALBAN-ANLAGE
66, CH-4052 BASEL,
SWITZERLAND

PUBLICATION FREQUENCY

24 issues/year

2021 JOURNAL IMPACT FACTOR

JOURNAL IMPACT FACTOR WITHOUT SELF CITATIONS

2.838

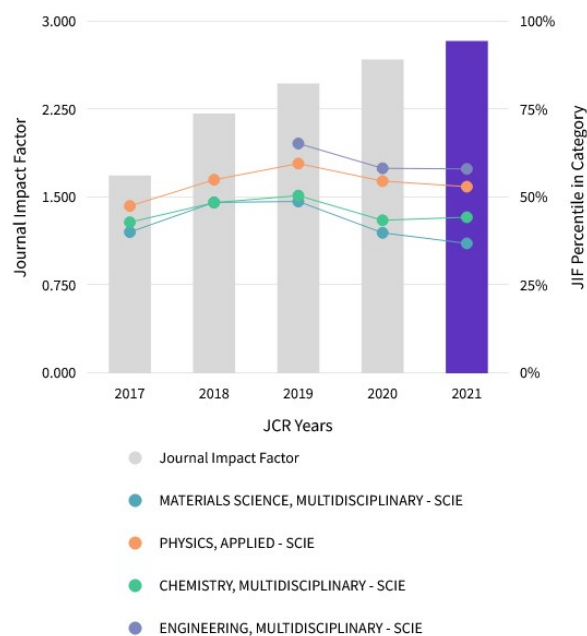
2.468

[View calculation](#)

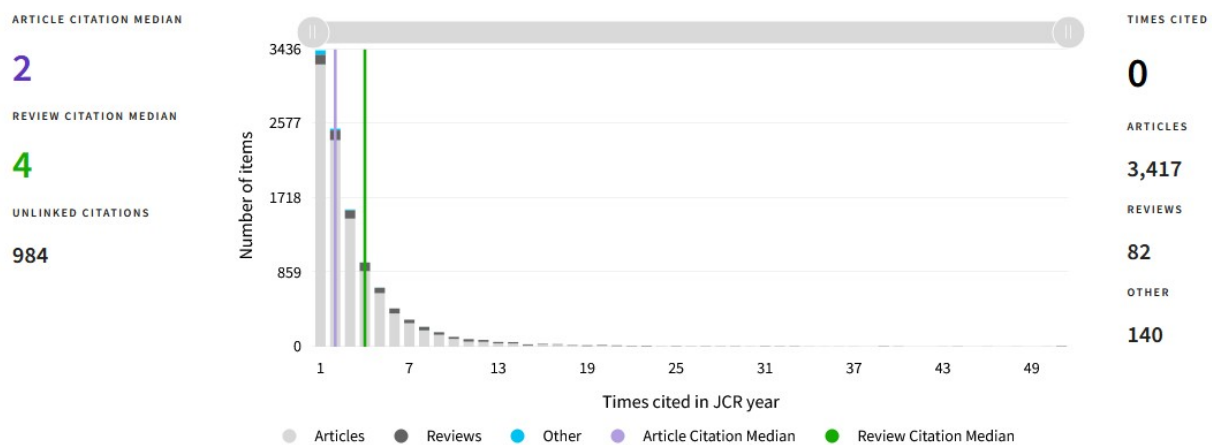
[View calculation](#)

Journal Impact Factor Trend 2021

 Export



Apéndices



Calculation X

5 Year Impact Factor is calculated using the following metrics:

$$\frac{\text{Citations in 2021 to items published in [2016-2020] (55,075)}}{\text{Number of citable items in [2016-2020] (18,854)}} = \frac{55,075}{18,854} = 2.921$$

CATEGORY
ENGINEERING, MULTIDISCIPLINARY
63/175

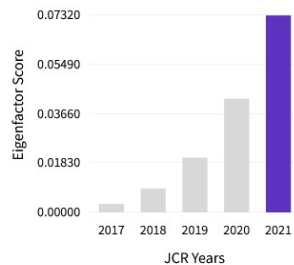
JCR YEAR	JCI RANK	JCI QUARTILE	JCI PERCENTILE	
2021	63/175	Q2	64.29	<div style="width: 64.29%; background-color: #800080;"></div>
2020	55/170	Q2	67.94	<div style="width: 67.94%; background-color: #cccccc;"></div>
2019	57/169	Q2	66.57	<div style="width: 66.57%; background-color: #cccccc;"></div>
2018	56/168	Q2	66.96	<div style="width: 66.96%; background-color: #cccccc;"></div>
2017	69/168	Q2	59.23	<div style="width: 59.23%; background-color: #cccccc;"></div>

Apéndices

Eigenfactor Score

0.07320

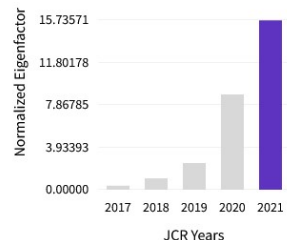
The Eigenfactor Score is a reflection of the density of the network of citations around the journal using 5 years of cited content as cited by the Current Year. It considers both the number of citations and the source of those citations, so that highly cited sources will influence the network more than less cited sources. The Eigenfactor calculation does not include journal self-citations. [Learn more](#)



Normalized Eigenfactor

15.73571

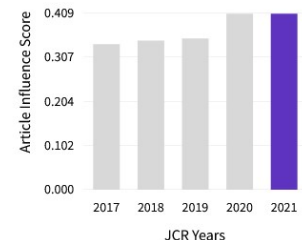
The Normalized Eigenfactor Score is the Eigenfactor score normalized, by rescaling the total number of journals in the JCR each year, so that the average journal has a score of 1. Journals can then be compared and influence measured by their score relative to 1. [Learn more](#)



Article influence score

0.409

The Article Influence Score normalizes the Eigenfactor Score according to the cumulative size of the cited journal across the prior five years. The mean Article Influence Score for each article is 1.00. A score greater than 1.00 indicates that each article in the journal has above-average influence. [Learn more](#)

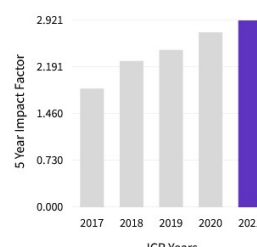


5 Year Impact Factor

2.921

[View Calculation](#)

The 5-year Impact Factor is the average number of times articles from the journal published in the past five years have been cited in the JCR year. It is calculated by dividing the number of citations in the JCR year by the total number of articles published in the five previous years.

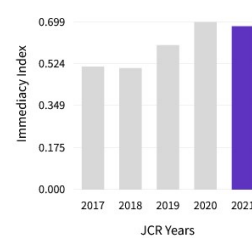


Immediacy Index

0.681

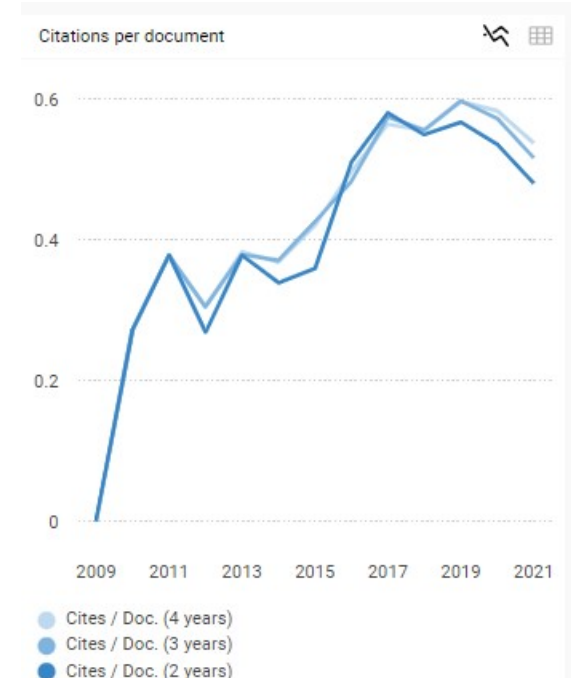
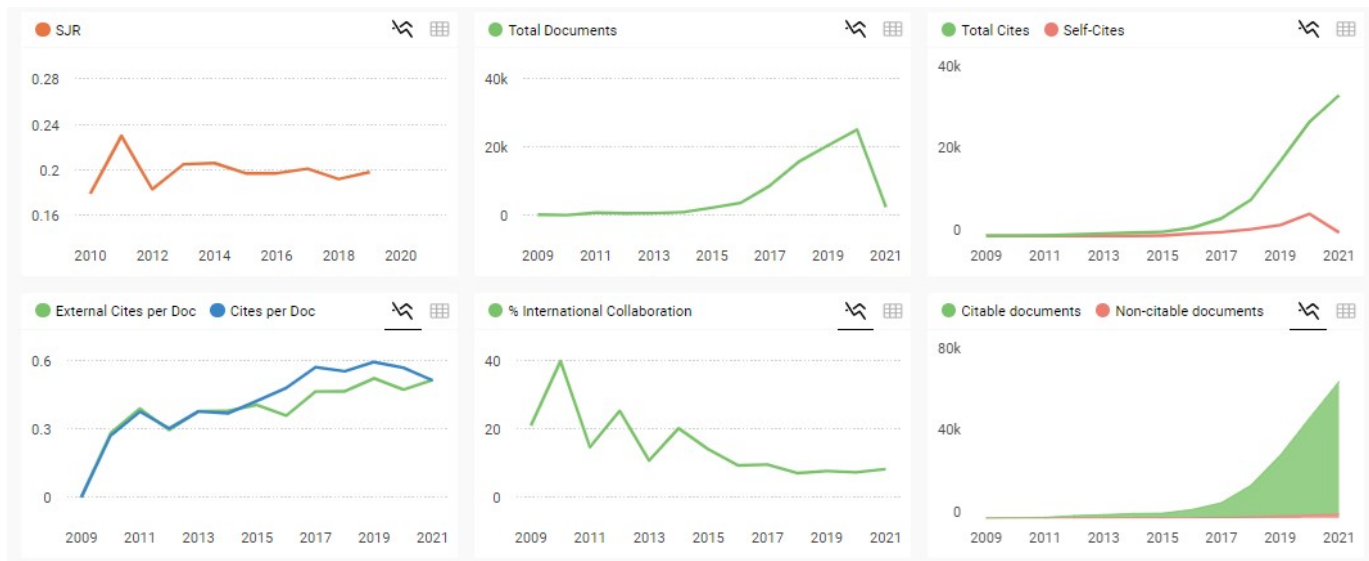
[View Calculation](#)

The Immediacy Index is the count of citations in the current year to the journal that reference content in this same year. Journals that have a consistently high Immediacy Index attract citations rapidly. [Learn more](#)



Apéndices

Apéndice B. Indicios de calidad del artículo “Analysis of AZ31B-Ti6Al4V Bimetallic extrusion by numerical simulation and Taguchi method”



Apéndices

Apéndice C. Indicios de calidad del artículo “Selection of Die Material and Its Impact on the MultiMaterial Extrusion of Bimetallic AZ31B–Ti6Al4V Components for Aeronautical Applications”

Materials

 Open Access since 2008

ISSN

N/A

EISSN

1996-1944

JCR ABBREVIATION

MATERIALS

ISO ABBREVIATION

Materials

Journal information

EDITION

Science Citation Index
Expanded (SCIE)

CATEGORY

METALLURGY &
METALLURGICAL
ENGINEERING - SCIE

MATERIALS SCIENCE,
MULTIDISCIPLINARY - SCIE

PHYSICS, CONDENSED
MATTER - SCIE

CHEMISTRY, PHYSICAL - SCIE

PHYSICS, APPLIED - SCIE

LANGUAGES

English

REGION

SWITZERLAND

1ST ELECTRONIC JCR YEAR

2011

Publisher information

PUBLISHER

MDPI

ADDRESS

ST ALBAN-ANLAGE
66, CH-4052 BASEL,
SWITZERLAND

PUBLICATION FREQUENCY

24 issues/year

2021 JOURNAL IMPACT FACTOR

3.748

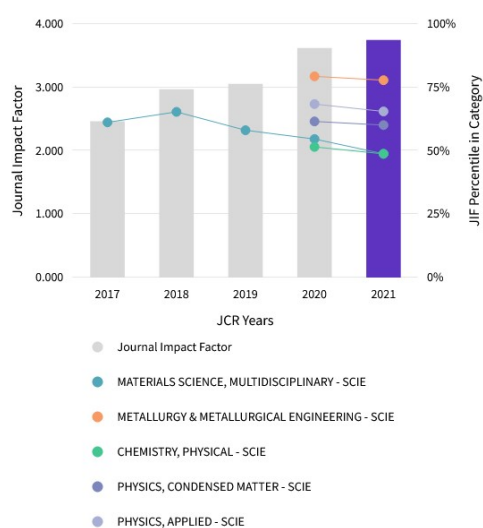
[View calculation](#)

3.188

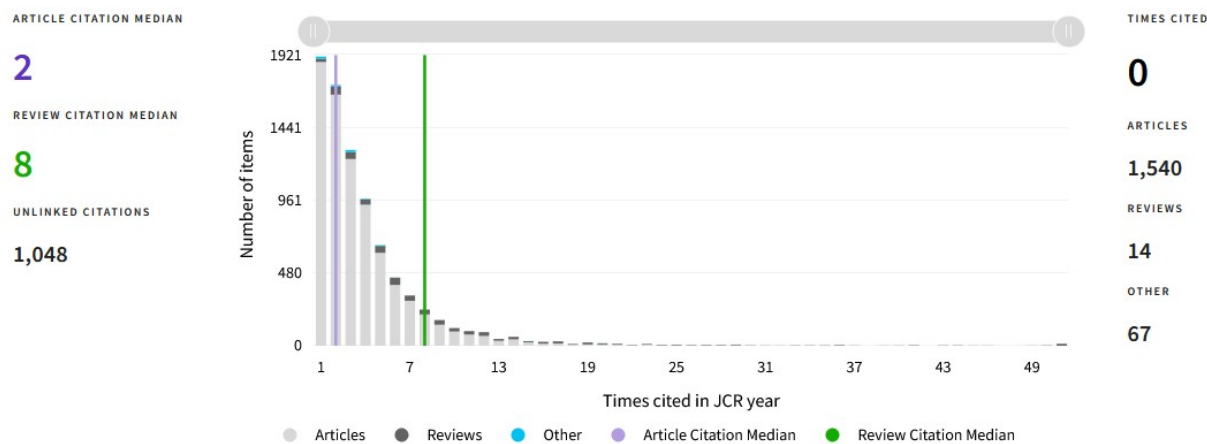
[View calculation](#)

Journal Impact Factor Trend 2021

[Export](#)



Apéndices



Calculation

X

5 Year Impact Factor is calculated using the following metrics:

$$\frac{\text{Citations in 2021 to items published in [2016-2020] (60,534)}}{\text{Number of citable items in [2016-2020] (14,975)}} = \frac{60,534}{14,975} = 4.042$$

CATEGORY
METALLURGY & METALLURGICAL ENGINEERING
21/91

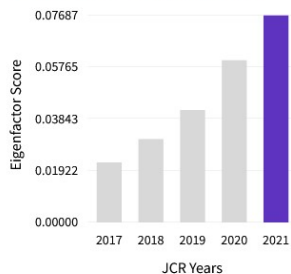
JCR YEAR	JCI RANK	JCI QUARTILE	JCI PERCENTILE	
2021	21/91	Q1	77.47	
2020	18/90	Q1	80.56	
2019	19/89	Q1	79.21	
2018	19/88	Q1	78.98	
2017	26/86	Q2	70.35	

Apéndices

Eigenfactor Score

0.07687

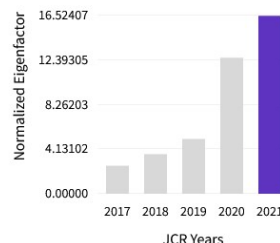
The Eigenfactor Score is a reflection of the density of the network of citations around the journal using 5 years of cited content as cited by the Current Year. It considers both the number of citations and the source of those citations, so that highly cited sources will influence the network more than less cited sources. The Eigenfactor calculation does not include journal self-citations. [Learn more](#)



Normalized Eigenfactor

16.52407

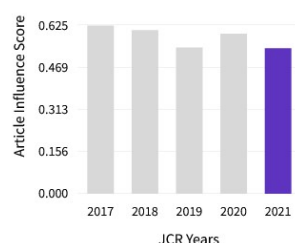
The Normalized Eigenfactor Score is the Eigenfactor score normalized, by rescaling the total number of journals in the JCR each year, so that the average journal has a score of 1. Journals can then be compared and influence measured by their score relative to 1. [Learn more](#)



Article influence score

0.541

The Article Influence Score normalizes the Eigenfactor Score according to the cumulative size of the cited journal across the prior five years. The mean Article Influence Score for each article is 1.00. A score greater than 1.00 indicates that each article in the journal has above-average influence. [Learn more](#)

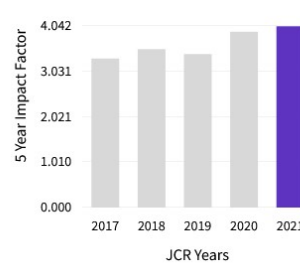


5 Year Impact Factor

4.042

[View Calculation](#)

The 5-year Impact Factor is the average number of times articles from the journal published in the past five years have been cited in the JCR year. It is calculated by dividing the number of citations in the JCR year by the total number of articles published in the five previous years.

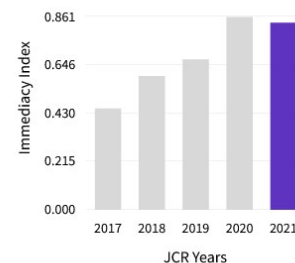


Immediacy Index

0.835

[View Calculation](#)

The Immediacy Index is the count of citations in the current year to the journal that reference content in this same year. Journals that have a consistently high Immediacy Index attract citations rapidly. [Learn more](#)



Apéndices

Apéndice D. Indicios de calidad del artículo “Optimal parameters selection in advanced multimetallic co-extrusion based on independent MCDM analytical approaches and numerical simulation”

Mathematics

 Open Access since 2013

ISSN

N/A

EISSN

2227-7390

JCR ABBREVIATION

MATHEMATICS-BASEL

ISO ABBREVIATION

Mathematics

Journal information

EDITION

Science Citation Index
Expanded (SCIE)

CATEGORY

MATHEMATICS - SCIE

LANGUAGES

English

REGION

SWITZERLAND

1ST ELECTRONIC JCR YEAR

2018

Publisher information

PUBLISHER

MDPI

ADDRESS

ST ALBAN-ANLAGE
66, CH-4052 BASEL,
SWITZERLAND

PUBLICATION FREQUENCY

24 issues/year

2021 JOURNAL IMPACT FACTOR

2.592

[View calculation](#)

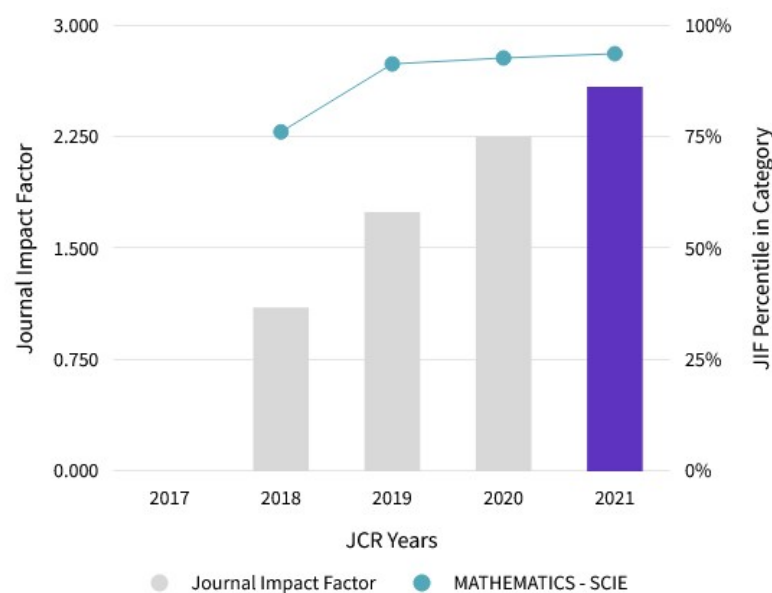
JOURNAL IMPACT FACTOR WITHOUT SELF CITATIONS

2.206

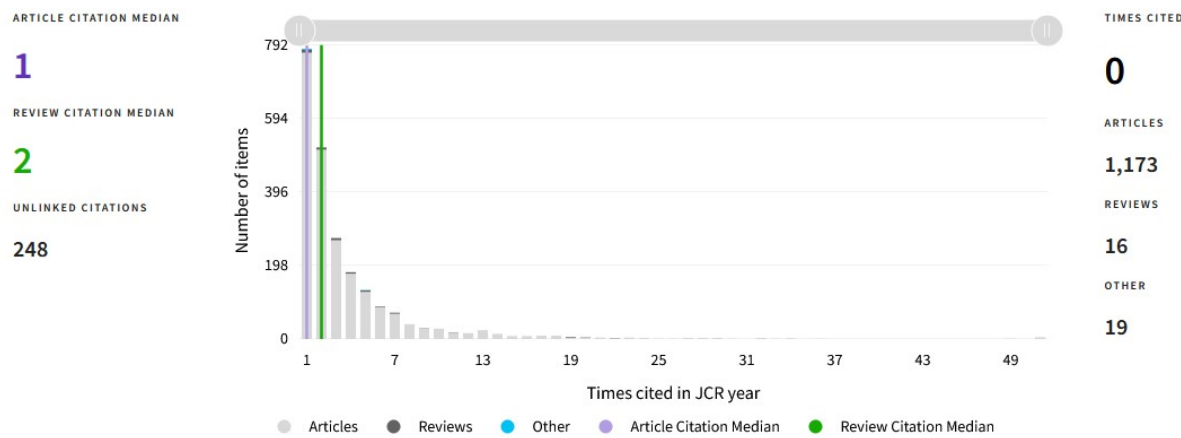
[View calculation](#)

Journal Impact Factor Trend 2021

[Export](#)



Apéndices



Calculation ×

5 Year Impact Factor is calculated using the following metrics:

$$\frac{\text{Citations in 2021 to items published in [2016-2020] (10,068)}}{\text{Number of citable items in [2016-2020] (3,961)}} = \frac{10,068}{3,961} = 2.542$$

CATEGORY
MATHEMATICS
21/333

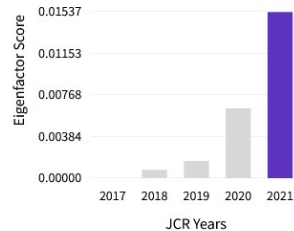
JCR YEAR	JIF RANK	JIF QUARTILE	JIF PERCENTILE
2021	21/333	Q1	93.84
2020	24/330	Q1	92.88
2019	28/325	Q1	91.54
2018	75/314	Q1	76.27

Apéndices

Eigenfactor Score

0.01537

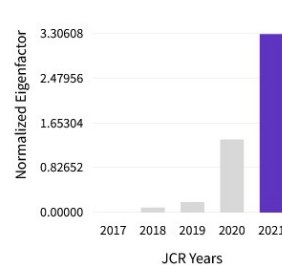
The Eigenfactor Score is a reflection of the density of the network of citations around the journal using 5 years of cited content as cited by the Current Year. It considers both the number of citations and the source of those citations, so that highly cited sources will influence the network more than less cited sources. The Eigenfactor calculation does not include journal self-citations. [Learn more](#)



Normalized Eigenfactor

3.30608

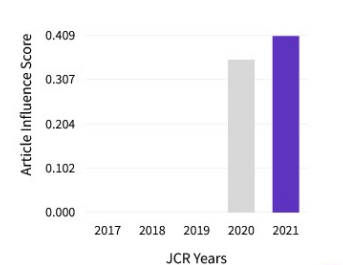
The Normalized Eigenfactor Score is the Eigenfactor score normalized, by rescaling the total number of journals in the JCR each year, so that the average journal has a score of 1. Journals can then be compared and influence measured by their score relative to 1. [Learn more](#)



Article influence score

0.409

The Article Influence Score normalizes the Eigenfactor Score according to the cumulative size of the cited journal across the prior five years. The mean Article Influence Score for each article is 1.00. A score greater than 1.00 indicates that each article in the journal has above-average influence. [Learn more](#)

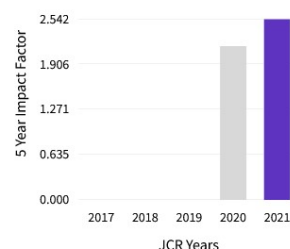


5 Year Impact Factor

2.542

[View Calculation](#)

The 5-year Impact Factor is the average number of times articles from the journal published in the past five years have been cited in the JCR year. It is calculated by dividing the number of citations in the JCR year by the total number of articles published in the five previous years.

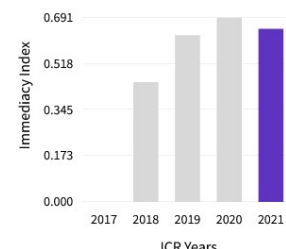


Immediacy Index

0.650

[View Calculation](#)

The Immediacy Index is the count of citations in the current year to the journal that reference content in this same year. Journals that have a consistently high Immediacy Index attract citations rapidly. [Learn more](#)



Apéndices

Apéndice E. Extracto del libro de resúmenes del “9th Manufacturing Engineering Society International Conference (MESIC’09)”



Merging complex information in high speed broaching operations in order to obtain a robust machining process.
A. del Olmo, G. Martínez de Pisón, L. Sastoques, A. Fernández, A. Calleja, L.N. López de Lacalle

Analysis of AZ31B – Ti6Al4V bimetallic extrusion by numerical simulation and Taguchi method.
D. Fernández, A. Rodríguez, A.M. Camacho

Numerical Analysis of Necking in Stretch-Bending based on Modified Maximum Force Criteria.
D. Morales, M. Borrego, J.A. López, A.J. Martínez, G. Centeno, C. Vallellano

Three-dimensional numerical analysis of tubular adhesive joints under torsional loads.
T.J.S. Oliveira, R.D.S.G. Campilho, M.G. Cardoso

Modelling adhesively-bonded T-joints by a meshless method.
I. Sánchez, L. Ramalho, R. Campilho, J. Belinha

Investigation of ball burnishing process using vibration and acoustic emission sensors.
I. Fernandez, E. Velazquez, J. Marques, J. Lluma, R. Jerez, J.A. Travieso

Investigation of Defects in Roll Contacts of Machine Elements with Acoustic Emission and Unsupervised Machine Learning.
J. Hillenbrand, J. Detry, J. Fleischer

A device to reduce positioning errors due to the machine tool compliance.
A. Noriega, F.J. Campa

Design of a machine to rectify ceramic tiles for laboratory tests.
J. Serrano, J.V. Abellán, G.M Bruscas

Superfinishing robotic cell to automate belt polishing process on critical aeronautical components.
M. Gonzalez, A. Rodriguez, O. Pereira, L.N. López de Lacalle

Control Strategies Comparison for a Multi-stage Assembly System using Simulation.
S. Benavent, P. Rosado, F. Romero, J.V. Abellán

Design and Construction of a Test Bench for the Manufacture and On-machine Non-contact Inspection of Parts Obtained by Fused Filament Fabrication.
F. Peña, C. Fernández, G. Valiño, B.J. Álvarez, J.C. Rico, S. Mateos

Contact Image Sensor Integration in Fused Filament Fabrication Machines for Layer Inspection.
F. Peña, J.C. Rico, G. Valiño, P. Fernández, V.M. Meana, P. Zapico

Topology optimization and additive manufacturing applied to a camera bracket for a 3U Cubesat.
M. Serrano, I. González, E.M. Andrés

Analysis of AZ31B – Ti6Al4V bimetallic extrusion by numerical simulation and Taguchi method

D. Fernández⁽¹⁾, A. Rodríguez, A.M. Camacho

⁽¹⁾Department of Manufacturing Engineering, Universidad Nacional de Educación a Distancia (UNED), 28040 Madrid, Spain; dfernande146@alumno.uned.es; alvaro.rodriguez@ind.uned.es; amcamacho@ind.uned.es

Keywords: Extrusion; light alloys; bimetallic; FEM; Taguchi.

1. Introduction

Light alloys, and more recently, multi-material components are attracting great interest in sectors such as aerospace and transport. In this study, the direct extrusion of a bimetallic cylinder with a magnesium alloy AZ31B core and a titanium alloy Ti6Al4V sleeve has been analyzed by means of finite element (FE) simulation; special attention has been paid to the forces required and the effects associated to technological factors such as friction and geometrical conditions; the aim is to determine the most relevant parameters of the process and their influence when processing this kind of multi-material by extrusion, combining the design of experiments (DOE) technique and analysis of variance (ANOVA).

2. Methodology

A FE model with DEFORM 3D has been developed to analyse the influence of the process parameters in the extrusion process of this kind of bimetallic components. The mesh is presented in Figure 1.

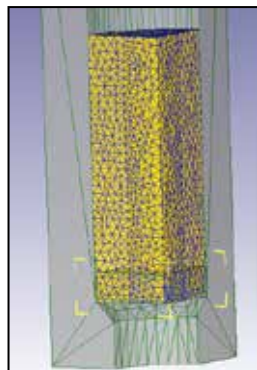


Figure 1. Initial FE mesh of bimetallic extrusion

The FE model validation has been performed comparing the simulations results for the extrusion force with the results obtained by Johnson's semi-empirical model [1,2]. Once the model is validated, the main process parameters are identified using an Ishikawa's chart and a design of experiments (DOE) methodology to quantify their influence in the required extrusion forces. Finally, Taguchi's analysis of variance (ANOVA) is applied in order to classify these parameters from the most to the less relevant in the variation of the extrusion force.

3. Results

The figure 2 shows some of the results after performing the Taguchi's ANOVA on DOE results.

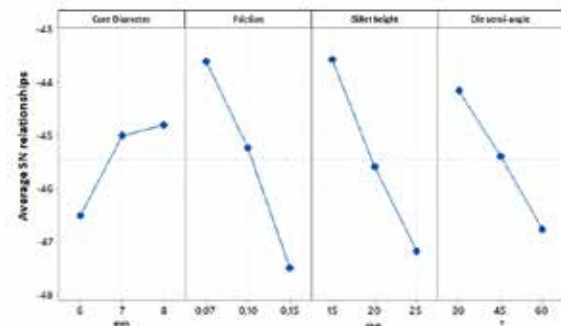


Figure 2. Main effects for SN relationships chart

4. Conclusions

A robust finite element model has been developed and validated to analyse extrusion of bimetallic components. The most influential parameter is the friction at the container/die-sleeve interface, so special attention should be paid to obtain favourable interfaces contact conditions by means of suitable lubricants, for example; followed by the geometrical dimensions of the billet, being the billet height more important than the diameter of the core.

5. Acknowledgements

The authors acknowledge the Industrial Production and Manufacturing Engineering (IPME) Research Group and the funds provided by the Annual Grant Call of the Industrial Engineering School-UNED through the projects REF 2020-ICF04/B and REF2020-ICF04/D and by the Innovation Project of the GID2016-28 on "Reliability and Advanced Failure Prognosis in industrial applications".

6. References

- [1] W. Johnson. *The pressure for the cold extrusion of lubricated rod through square dies of moderate reduction at slow speeds*. Journal of the Institute of Metals 85 (1956-1957): 403-408.
- [2] F.J. Amigo, A.M. Camacho. *Reduction of induced central damage in cold extrusion of dual-phase steel DP800 using double-pass dies*. Metals, 7 (2017): 1-18.

Apéndice F. Extracto del libro de resúmenes del “4th International Conference on Materials Design and Applications (MDA2022).”

- 63** Surface preparation, adhesive bonding and mechanical testing of non-crimp CFRP composite laminates (**MDA22_1**)
T Gao (University of Waterloo, Canada), M Alfano
- 64** Numerical and experimental study of laser welding procedure for joining fibre reinforced polymers (**MDA22_95**)
LRR Silva, EAS Marques (INEGI, Portugal), RJC Carbas, LFM da Silva
- 65** Adhesive type effect on adhesively-bonded aluminium T-joints (**MDA22_58**)
JPM Lopes, RDSG Campilho (Instituto Politécnico do Porto, Portugal), RJB Rocha, IJ Sánchez-Arce
- 66** The interaction of mode mixity and temperature on the S-N response of an epoxy adhesive (**MDA22_36**)
FVBC Lopes, A Akhavan-Safar (INEGI, Portugal), RJC Carbas, EAS Marques, R Goyal, J Jennings, LFM da Silva
- 67** Mode I fatigue threshold energy assessment of different adhesives: Effects of temperature (**MDA22_37**)
D Santos, A Akhavan-Safar (INEGI, Portugal), EAS Marques, RJC Carbas, LFM da Silva
- 68 Session 4B – Composites II**
(Chair: AT Marques, RJC Carbas)
- 69** The effect of angle plies on the strength of hybrid composite laminates (**MDA22_118**)
F Ramezani (INEGI, Portugal), RJC Carbas, EAS Marques, LFM da Silva
- 70** Thermal properties of geopolymmer composites containing microencapsulated phase change materials (**MDA22_17**)
K Pławecka (Cracow University of Technology, Poland), A Bąk, P Bazan, M Łach
- 71** Hydroxiapatite modified with defects and dopants: Modeling and experimental data (**MDA22_19**)
VS Bystrov (Russian Academy of Sciences, Russia), EV Paramonova, NV Bulina
- 72** Static analysis of axially FG straight beams on generalized Winkler foundation via mixed FEM (**MDA22_20**)
Y Bab (Istanbul Technical University, Turkey), M Ermis, A Kutlu, N Eratlı, MH Omurtag
- 73** Development of Mg-based metal matrix biomedical composites for ACL fixation by reinforcing with rare earth oxide and hydroxyapatite- A mechanical, corrosion and microstructural perspective (**MDA22_21**)
D Aggarwal (Thapar Institute of Engineering and Technology, India), V Kumar, S Sharma
- 75** Increased post-breakage strength of point-fixed laminated glass with locally embedded woven steel mesh (**MDA22_109**)
M Kozłowski (Silesian University of Technology, Poland), D Wasik, K Zemla

76 Metals

- 77** Poster 1
Numerical modelling and analysis of microstructural evolution in multi-material co-extrusion of bimetallic Ti6Al4V-AZ31B billets (**MDA22_42**)
D Fernández (UNED, Spain), A Rodríguez-Prieto, AM Camacho
- 78** Poster 2
Electrochemical evaluation of magnetron sputtering thin-films to prevent hydrogen damage in steel substrates (**MDA22_52**)
R Gonzalez (UNED, Spain), A Rodriguez-Prieto, AM Camacho
- 79** Poster 3
Influence of milling time on phase composition and product structure of Mg-Zn-Ca-Ag alloys obtained by mechanical synthesis (**MDA22_72**)
M Karolus (University of Silesia, Poland), S Lesz (Silesian University of Technology, Poland), A Gabryś
- 80** Poster 4
Mechanical and wear properties of multilayer graphene reinforced Ti-6Al-4V composites fabricated by spark plasma sintering (**MDA22_103**)
D Sharma (Thapar Institute of Engineering and Technology, India), V kumar, S Singh

- 81** Poster 5
Effect of the molding material on the roughness of the castings (**MDA22_114**)
AB Moreira (University of Porto, Portugal), J Freitas, D Teixeira, LMM Ribeiro, MF Vieira

82 Polymers

- 83** Poster 6
Phenomenological modeling of the ductile fracture of polycarbonate (**MDA22_89**)
MM Kasaei (INEGI, Portugal), EAS Marques, RJC Carbas, LFM da Silva
- 84** Poster 7
PMMA lens arrays for micro concentrator solar cells produced by hot embossing (**MDA22_115**)
BMC Oliveira, MN Silva Jr, RF Santos, M Alves, S Sadewasser, EW Sequeiros (LAETA/INEGI, Portugal)

17:40	The interaction of mode mixity and temperature on the S-N response of an epoxy adhesive (MDA22_36) FVBC Lopes, A Akhavan-Safar (INEGI, Portugal), RJC Carbas, EAS Marques, R Goyal, J Jennings, LFM da Silva	Development of Mg-based metal matrix biomedical composites for ACL fixation by reinforcing with rare earth oxide and hydroxyapatite- A mechanical, corrosion and microstructural perspective (MDA22_21) D Aggarwal (Thapar Institute of Engineering and Technology, India), V Kumar, S Sharma
18:00	Mode I fatigue threshold energy assessment of different adhesives: Effects of temperature (MDA22_37) D Santos, A Akhavan-Safar (INEGI, Portugal), EAS Marques, RJC Carbas, LFM da Silva	Increased post-breakage strength of point-fixed laminated glass with locally embedded woven steel mesh (MDA22_109) M Kozłowski (Silesian University of Technology, Poland), D Wasik, K Zemla
19:00	Poster session and RECEPTION (Coffee Lounge)	
Metals		
Poster 1	Numerical modelling and analysis of microstructural evolution in multi-material co-extrusion of bimetallic Ti6Al4V-AZ31B billets (MDA22_42)	D Fernández (UNED, Spain), A Rodríguez-Prieto, AM Camacho
Poster 2	Electrochemical evaluation of magnetron sputtering thin-films to prevent hydrogen damage in steel substrates (MDA22_52)	R Gonzalez (UNED, Spain), A Rodríguez-Prieto, AM Camacho
Poster 3	Influence of milling time on phase composition and product structure of Mg-Zn-Ca-Ag alloys obtained by mechanical synthesis (MDA22_72)	M Karolus (University of Silesia, Poland), S Lesz (Silesian University of Technology, Poland), A Gabrys
Poster 4	Mechanical and wear properties of multilayer graphene reinforced Ti-6Al-4V composites fabricated by spark plasma sintering (MDA22_103)	D Sharma (Thapar Institute of Engineering and Technology, India), V Kumar, S Singh
Poster 5	Effect of the molding material on the roughness of the castings (MDA22_114)	AB Moreira (University of Porto, Portugal), J Freitas, D Teixeira, LMM Ribeiro, MF Vieira
Polymers		
Poster 6	Phenomenological modeling of the ductile fracture of polycarbonate (MDA22_89)	MM Kasaei (INEGI, Portugal), EAS Marques, RJC Carbas, LFM da Silva
Poster 7	PMMA lens arrays for micro concentrator solar cells produced by hot embossing (MDA22_115)	BMC Oliveira, MN Silva Jr, RF Santos, M Alves, S Sadewasser, EW Sequeiros (LAETA/INEGI, Portugal)
Composites		
Poster 8	Application of laser heating to increase of adhesion of chosen hard composite coatings to replaceable cutting inserts made of sintered carbides (MDA22_49)	MJ Kupczyk (Poznan University of Technology, Poland)
Poster 9	The use of a super-hard boron nitride composite c-BN+h-BN with increased resistance to brittle cracking for anti-wear coatings (MDA22_50)	MJ Kupczyk (Poznan University of Technology, Poland)
Poster 10	Modelling of the axial strain distribution in graphene flakes for graphene/SU-8/PMMA nanocomposite under thermomechanical load (MDA22_53)	RK Vladova (Bulgarian Academy of Sciences, Bulgaria), TS Petrova, EG Kirilova, AG Apostolov, BH Boyadjiev, TV Rangelov
Poster 11	Effect of cross-section configuration on CF-PEEK overmolded grid reinforcements (MDA22_75)	CJ Rodríguez-Mondéjar (UNED, Spain), A Rodríguez-Prieto, AM Camacho
Poster 12	Application of finite element method and lattice discrete particle modeling for an novel ultra high performance self compacting mortar comprised of recycled steel fiber and equilibrium catalyst (MDA22_101)	H Abdolpour (University of Science and Technology, Poland), P Niewiadomski, Ł Sadowski, GL Sherzer, YF Alghalandis
Poster 13	Proposal of acoustical materials made recycling used cigarette filters (MDA22_111)	CM González, VG Escobar (University of Extremadura, Spain), MJA Caballero, MLD Martín-Merás, GR Gozalo, CJP Sánchez, CO Caraballo, RM Sanz, JC del Río
Poster 14	Vibration response of functionally graded material sandwich plates with elliptical cut-outs and geometric imperfections under mixed boundary conditions (MDA22_113)	D Singh (Shiv Nadar University, India), A Gupta
Joining		
Poster 15	Study of the ultrasonic welding of a polycarbonate-glass fiber laminate (MDA22_14)	A Pirondi (Università di Parma, Italia), P Palmiero, L Marchini, M Bercella

Numerical modelling and analysis of microstructural evolution in multi-material co-extrusion of bimetallic Ti6Al4V-AZ31B billets

D Fernández, A Rodríguez-Prieto, AM Camacho

Department of Manufacturing Engineering, UNED, Juan del Rosal 12, Madrid, Spain.

This paper aims to model and analyse the effect of the multi-material co-extrusion process parameters on microstructure in bimetallic Ti6Al4V-AZ31B billets, paying special attention to the grain refinement resultant. The Johnson-Mehl-Avrami-Kolmogorov (JMAK) [1, 2] equation has been implemented in the Finite Element (FE) model in DEFORM-3D to simulate dynamic recrystallization and predict the final grain size. Temperature, ram speed, extrusion ratio, die semi-angle and shape factor have been taken as main parameters within co-extrusion process to evaluate their influence on the volume fraction of dynamic recrystallization.

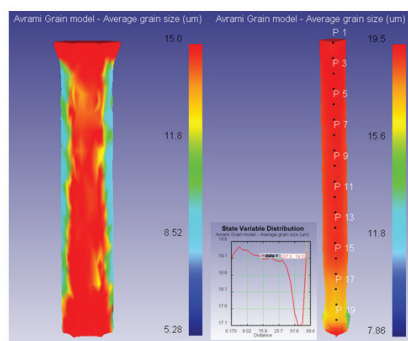


Fig.1 Average grain size distribution in ring - Ti6Al4V (left) and core - AZ31B (right)

The results show that co-extrusion parameters have a direct impact in the grain size distribution and refinement of the final part, being specially interested the non uniform distribution on the ring part.

- [1] X. Xiang, J. Zhang, J. Outeiro, X. Binbin and Z. Wanhu, J. of Materials Processing Tech, 286, 116834 (2020).
- [2] Z. Ding-fei, H. Hong-jun, P. Fu-sheng, Y. Ming-bo and Z. Jun-ping, Trans. Nonferrous Met. Soc. China 20, 478-483 (2010).